ANNUAL SUBSCRIPTION, TWELVE DOLLARS, NEW RATE,
EFFECTIVE JANUARY 1, 1931.

Physics Lib.

DEC 26 1930

VOLUME 36 SECOND SERIES NUMBER 12

THE PHYSICAL REVIEW

A JOURNAL OF EXPERIMENTAL AND THEORETICAL PHYSICS

CONDUCTED BY

THE

AMERICAN PHYSICAL SOCIETY

BOARD OF EDITORS

Managing Editor JOHN T. TATE, University of Minnesota, Minneapolis
I. S. BOWEN, R. S. MULLIKEN, H. D. SMYTH, E. U. CONDON, C. J. DAVISSON,
F. K. RICHTMYER, K. F. HERZFELD, A. W. HULL, F. W. LOOMIS

DECEMBER 15, 1930

Polarization of the Continuous X-Rays from Single Electron Impacts — BALEBAIL DASANNACHARYA 1675

Spectrum of the Radiation from a High Potential X-Ray Tube — C. C. LAURITSEN 1680

Multiple Scattering in the Compton Effect — JESSE W. M. DUMOND 1685

Design and Technique of Operation of a Double Crystal Spectrometer — JESSE W. M. DUMOND AND ARCHER HOYT 1702

Value of e/m by Deflection Experiments — G. E. UHLENBECK AND L. A. YOUNG 1721

Relativistic Wave Mechanics of Electrons Deflected by a Magnetic Field — MILTON S. PLESSET 1728

Hyperfine Structure of S and P Terms of Two Electron Atoms with Special Reference to Li^+ — G. BREIT AND F. W. DOERMANN 1732

Thermoanalysis of Metal Single Crystals and a New Thermoelectric Effect of Bismuth Crystals Grown in Magnetic Fields — ALEXANDER GOETZ AND MAURICE F. HASLER 1752

Second Virial Coefficient for Gases: a Critical Comparison between Theoretical and Experimental Results — HENRY MARGENAU 1782

Temperature Equilibrium in a Static Gravitational Field — RICHARD C. TOLMAN AND PAUL EHRENFEST 1791

Letters to the Editor — 1799

The Inner Potential of a Copper Crystal, *H. E. Farnsworth*—1799; Differences in the Absorption Spectrum of Benzene in the Liquid and Vapor State, *E. D. McAlister and H. J. Unger*—1799; Relative Intensities in Hyperfine Structure Multiplets, *H. E. White*—1800. The Vibrational and Rotational Analysis of the S_2 Bands, *S. M. Naude and Andrew Christy*—1801; Erratum—1802.

Index to Volume 36 — 1803

PUBLISHED BY THE AMERICAN PHYSICAL SOCIETY
PUBLICATION OFFICES: 450-454 AHNAIP STREET, MENASHA, WIS.
EDITORIAL OFFICES: MINNEAPOLIS, MINN.

THE AMERICAN PHYSICAL SOCIETY

OFFICERS OF THE SOCIETY

President:	HENRY G. GALE	University of Chicago, Chicago, Ill.
Vice-President:	W. F. G. SWANN	Bartol Research Foundation, Philadelphia, Pa.
Secretary:	W. L. SEVERINGHAUS	Columbia University, New York City
Treasurer:	G. B. PEGRAM	Columbia University, New York City
Editor:	JOHN T. TATE	University of Minnesota, Minneapolis, Minn.
Local Secretary for the Pacific Coast:	L. B. LOEB	University of California, Berkeley, Calif.

THE PHYSICAL REVIEW

Published by the American Physical Society at 450 Ahnaip St., Menasha, Wis. Executive office: University of Minnesota, Minneapolis, Minn. Two volumes annually, twelve issues per volume.

First series. From July 1, 1893, to January 1, 1913, the REVIEW was conducted by Edward L. Nicholas, Ernest Merritt and Frederick Bedell, with the financial support of Cornell University. The first four volumes were issued annually; subsequent volumes, semi-annually; thirty-five volumes in all.

Second series. On January 1, 1913, the REVIEW was transferred to the American Physical Society as announced on the first page of the new series which was then begun. Since then it has been conducted by a Board of Editors elected by the Society. Semi-annual volumes begin in January and July. Since July 1, 1929, the REVIEW has been issued twice a month.

Contributors are referred to page 2 of the advertisements for further information.

Annual subscription, throughout the Postal Union, $10.00 in advance.

Single copies of current volumes, $.60.

General index, 1893-1920, $4.00, in advance.

Back Volumes, $6.00 per volume; Back Numbers, $1.00 per copy for issues prior to July 1, 1929 (Vols. 1-33), $.60 per copy for issues subsequent thereto. Postage is free if remittance accompanies order; otherwise postage is extra. No bound volumes can be supplied. The REVIEW offers to purchase a limited number of First Series, Vol. 1, No. 1 (at $2.00 each); Second Series, Vol. 7, No. 1, January 1916; Vol. 7, No. 2, February 1916; Vol. 7, No. 4, April 1916; and Vol. 7, No. 5, May 1916 (at $2.00 each).

Advertisements. Rates will be supplied by the Editor on request. Copy for each number must be received at Minneapolis two weeks prior to the dates of issue; old copy is used until new copy is received. Send electrotypes direct to the printers, George Banta Publishing Co., Menasha, Wis.

Discount of ten percent is allowed subscription agencies and members of the American Physical Society.

Changes of Address and Complaints of failure to receive the REVIEW, in the case of members of the Physical Society, should be addressed to the Treasurer; in the case of other subscribers to 450 Ahnaip St., Menasha, Wis.; or to the Editor. New copies can be sent free in response to complaint of non-delivery only if notice of non-delivery is received within three months of date of issue.

Editorial Correspondence should be addressed to the PHYSICAL REVIEW, University of Minnesota, Minneapolis, Minn.

Entered at the postoffice at Menasha, Wis., as second class matter.
Acceptance for mailing at special rate of postage provided for in section 1103, Act of October 3, 1917, authorized September 6, 1926.

Second Series *December 15, 1930* *Vol. 36, No. 12*

THE
PHYSICAL REVIEW

POLARIZATION OF THE CONTINUOUS X-RAYS FROM SINGLE ELECTRON IMPACTS[1]

By Balebail Dasannacharya
Ryerson Physical Laboratory
University of Chicago

(Received November 8, 1930)

Abstract

Experiments are described on the polarization of continuous x-rays from targets of aluminum sheets varying in the thickness from 6 to 250×10^{-6} cm. The velocities of the exciting electrons corresponded to voltages from 27 to 57 kilovolts. It was found that the polarization increased exponentially with decreasing thicknesses, suggesting perhaps a nearly complete polarization for a thickness of about 6×10^{-6} cm. The polarization diminished with an increase in the velocity of the exciting electrons.

The theory of the polarization of continuous x-rays developed by Sugiura seems to be in conformity with the experimental results obtained in the experiments described below.

THE old problem of the radiation due to the stoppage of electrons, attacked by Stokes and J. J. Thomson immediately after Röntgen's discovery of the x-rays, was extended by Sommerfeld[2] by the methods of the classical theory. Recently Sommerfeld[3] extended his previous work by applying the mathematical methods of wave-mechanics to cases where the electrons were stopped in a single process (very thin anticathodes).

This new theory was well supported by the measurements of Kulenkampff[4] on the angular distribution of the radiation produced in an aluminum target of thickness 6.5×10^{-5} cm. The intensity in the forward direction of motion of electrons was from these experiments extrapolated to be zero. Duane[5] working with mercury vapour found that the intensities I_l in the forward direction and I_t at right angles were in the ratio of 1 to about 5.5. Defining the percent polarization as $(I_t-I_l/I_t+I_l)\times100$, this might be interpreted as a polarization of 70 percent. Sommerfeld consequently made a generalized assumption according to which only those electron beams emerging from the target with zero velocity should give rise to complete polarization, i.e., the radiation corresponding to the short wave-length limit of the continuous spectrum should be completely polarized.

[1] A short account was given at the Chicago meeting of the American Physical Society, Nov. 27, 1929. Phys. Rev. **35**, 129 (1930).

[2] A. Sommerfeld, Phys. Zeits. **10**, 969 (1909).

[3] A. Sommerfeld, Proc. Nat. Acad. Sci. **15**, 393 (1929).

[4] H. Kulenkampff Ann. d. Physik **87**, 597 (1928).

[5] W. Duane Proc. Nat. Acad. Sci. **14**, 450 (1928).

P. Kirkpatrick[6] calculated from his experiments with a thick tungsten anticathode a polarization of 11 percent for the short wave-length limit with a thick tungsten target. P. A. Ross[7] using a method of balanced double filters obtained nearly complete polarization at the short wave-length limit with a thick tungsten target. Wagner and Ott[8] reflected x-rays coming normal to the direction of the electron stream at the surface of a crystal and observed the intensity of the radiation thus reflected in directions along and at right angles to that of the electron beam. They found a maximum polarization of 47.5 for the short wave-length limit. Thus results so far recorded fail to show any general agreement.

It appeared therefore desirable to make some direct measurements on the polarization of continuous x-rays from thin targets, like aluminum foils of various thicknesses, with electrons accelerated by different potential drops.

Apparatus

An electron stream (see Fig. 1) from a hot spiral cathode fitted with a focussing cup passes through two openings A and B, both of which form a single element and are earthed. The distance between A and B is 5 cm. The

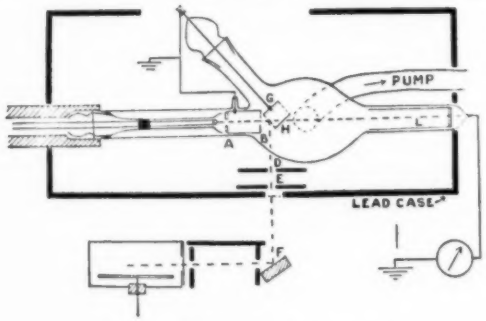

Fig. 1. Diagram of apparatus.

opening A is in the molybdenum disk facing the electron stream. B is in an iron sheet welded into the cylinder which carries the molybdenum. A centimeter behind B the electron beam meets the aluminum foils stretched across two rings G and H. The beam after passing through the aluminum passes without striking the sides of the lower ring H into a hollow cylinder L and through a miliammeter to the earth. Circular openings D and E in lead sheets are so placed and are of such a size as to prevent x-rays formed at B from falling on the graphite block F. The effectiveness of the shielding was tested by observing the effect on the readings of the electrometer when the aluminum foils between G and H were rotated away from the path of the electron beam. Further, when an aluminum foil is in the path of the electron beam, it easily gets punctured at the place where the beam meets the foil. The size of this puncture, about 4 mm in diameter, and the place where it occurs, gives good indication of the path of the beam in the foil system GH.

[6] P. Kirkpatrick, Phys. Rev. **22,** 226 (1923).
[7] P. A. Ross, J. Opt. Soc. Am. **16,** 375 and 433; Phys. Rev. **28,** 425 (1926).
[8] E. Wagner and P. Ott, Ann. d. Physik **85,** 425 (1928).

Pinhole photographs were also made for further confirmation. The openings in the diaphragms in front of the ionization chamber on a Bragg spectrograph were one square centimeter.

In order to avoid charge developing on the inside walls of the x-ray tube, and deflecting the electron beam, the inside surface from A to the end of the tube at L was platinized with platinum paint. Before the paint was heated it was nearly completely removed from that part of the wall through which the x-rays passed to the graphite F, in order to prevent any filtering action of the x-rays by the platinum layer.

The ionization current was measured in a Compton electrometer worked at a deflection of the reflected spot of about 30,000 mm per volt, with the scale at a distance of 2 meters from the mirror. The current from a transformer was rectified through a kenetron before being admitted into the x-ray tube.

Experimental Results

The intensities I_l and I_t of the x-ray beam emerging from the graphite along the direction of the electron beam and at right angles to the same were

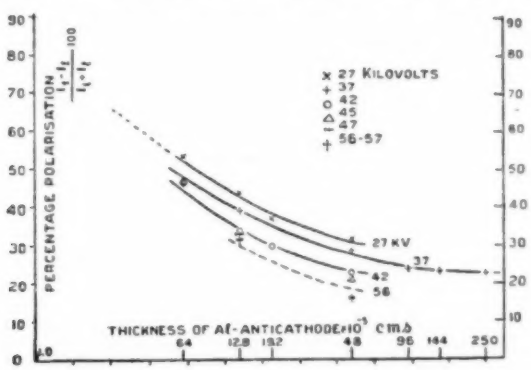

Fig. 2.

measured. Correction due to stray radiation when there was no aluminum foil in the path of the electron beam at C was found negligible. The thickness of the aluminum foils or plates varied from 6.4 to 250×10^{-5} cm. For the thinnest aluminum foil my obligations are due to Dr. Kulenkampff. These foils were stretched between the rings G and H, fastened with a paint made of fine aluminum powder and a little varnish dried over hot air.

The experiments of June 23rd (see Table I) showed that the polarization increased with the diminution of thickness as well as by a diminution of the accelerating voltage of the electrons. The value for 57 KV seems rather too low and that for 45 KV rather too high. The effect of voltage and thickness seems however to be unmistakable. The experiments of October 18 were carried out with one of the thinnest foils used previously, nearly 48.0×10^{-5} cm, and three others. The effects of voltage and thickness (see Fig. 2) are here more clearly marked.

A rough extrapolation for smaller thicknesses indicates that complete polarization may result for a thickness of about 6×10^{-6} cm. This thickness

TABLE I.

Date	Accelerating potential in kilovolts.	Thickness of the aluminum plates, in 10^{-6} cm	Percentage polarization $(I_t-I_l)/(I_t+I_l)\times 100$
June 23, 1929	37 ...	250 ...	... 22.2
		144 ...	... 22.3
		96 ...	... 23.7
		48 ...	... 28.5
	45 ...	48 ...	... 26.3
	57 ...	48 ...	... 16.3 (?)
Oct. 18, 1929	27 ...	48 ...	... 31.5
		19.2 ...	... 37.1
		12.8 ...	... 43.5
		6.4 ...	... 53.0
	37 ...	12.8 ...	... 39.0
		6.4 ...	... 46.2
	42 ...	48.0 ...	... 22.5
		19.2 ...	... 29.8
		12.8 ...	... 33.8
		6.4 ...	... 46.7
	56 ...	12.8 ...	... 31.5
	47 ...	12.8 ...	... 33.0

happens to be about the same as that (4×10^{-6} cm) for which the electron keeps its initial direction of motion, as calculated from theories of the diffusion of electrons through matter[9] for an average accelerating potential of 34 KV. According to the diffusion theory, however, the length of path along which the electron keeps its initial direction should increase with increase in speed, which would mean greater polarization for greater electron speeds. Since this is contrary to the results of the present experiments, it would appear that the approximate agreement between the length of the undeviated path and the thickness for complete polarization is probably fortuitous.

According to Sugiura,[10] who has recently developed a theory of the production of continuous x-rays somewhat on the lines followed by Sommerfeld, one should expect that the polarization at right angles to the direction of motion of the electron beam even for vanishing thickness of the target to be incomplete. The polarization should be greater for rays corresponding to electrons of smaller speed, a result which is in keeping with the findings of our present experiment.

It is interesting to note that Kulenkampff[11] has recorded a value of 45 percent for the polarization with electron beams of 36 KV presumably for the thickness of aluminum the same as the least one in our present experiment.

[9] Handb. d. Exptl. Physik, Kathodenstrahlen by Lenard and Becker pages 333, 379. Akad. Verl. Buchh., Leipzig, 1927.

[10] Sugiura Sci. Papers I. P. C. R. **11**, 251–290 (1929).

[11] H. Kulenkampff, Phys. Zeits. **30**, 513 (1929).

Our value for the same is 47.5, within errors of experiment the same as the value obtained by Kulenkampff.

Duane[12] did not find any great difference between the polarizations with jets of mercury vapour as anticathode, the density of the vapour being varied from one to four. On an average the polarization decreased from 51.4 to 48.6, a result not contradicting our own findings, though Duane is inclined to believe that the difference perhaps is not very much greater than the experimental errors. Secondly, it may be that in Duane's experiment we are nearly at the maximum of polarization; or it may also be that in the case of mercury the change of polarization with thickness is small. Thirdly, a comparison of Duane's value (taking it to be nearly the maximum for mercury) with our own for Al extrapolated to smaller thicknesses than actually used, would lead us to suppose that an increase in the atomic number of the anticathode would result in a decrease in the polarization.

This last result as well as results of Duane just referred to would be hard to reconcile with the almost perfect polarization obtained by Ross[13] with his double filter method, and using thick tungsten as anticathode. Perhaps the balancing of Ross's filters, which may have been perfect, or the error in the same inappreciable, when the differences are large, would cease to be so when the difference to be obtained is about of the order of the inaccuracy. As against Ross,[7] Wagner and Ott[8] using platinum as anticathode could get only 47.5 as the polarization for the short wave-length limit.

A Rough Picture of the Production of Polarization in Continuous X-Rays

The polarization may depend on the following:

(1). Initial direction of the impinging electron.

(2). Its final direction, and probably also on,

(3). The atomic number of the material of the anticathode, and

(4). Electron configuration round the nucleus.

If the energy of the impinging electron is completely utilized in the production of the continuous x-ray, as would be the case for radiation at the short wave-length limit of the spectrum, and consequently (2) is negligible and if (3) and (4) should happen to be negligible too, the polarization may be complete. On the other hand, as we come to frequencies smaller than the limiting one, we may think of them as being produced by electrons leaving the atom with appreciable speeds in directions which however are arbitrary. Consequently (2) becomes increasingly appreciable so that the electric vector would deviate progressively from the initial direction. If we are to account for more complete polarization for smaller velocities, we have to assume that the probability is greater that an electron of a smaller speed would emerge from the atmosphere of an atom with comparatively greater loss of energy.

I wish to thank Professor A. H. Compton for suggesting the problem, for his continued encouragement and for his kindness in permitting me to work in his laboratory as a visiting foreign guest of the University.

[12] W. Duane, Proc. Nat. Acad. Sci. **15,** 805 (1929).

[13] P. A. Ross, J. Opt. Soc. Am. **16,** 375 and 433. Phys. Rev. **28,** 425 (1926)

SPECTRUM OF THE RADIATION FROM A HIGH POTENTIAL X-RAY TUBE

By C. C. Lauritsen
California Institute of Technology
Pasadena

(Received November 7, 1930)

Abstract

A spectrograph of the Seemann type has been constructed for the purpose of investigating the radiation from the high potential x-ray tube at the California Institute. A typical spectrogram obtained with 600 kilovolts on the tube is presented. The photometer record shows a continuous spectrum with its maximum intensity at about 200 kilovolts and a short wave-length limit in the neighborhood of 600 kilovolts. The range covered is roughly from 100 to 20 x-units. It is proposed to use the apparatus for determining absorption coefficients by photographing the spectrum of radiation which has passed through an absorbing screen. No anomalies of any kind have been observed so far.

Apparatus

THE high potential x-ray tube at the California Institute of Technology has recently been rebuilt and equipped with a hot cathode and a tungsten target. A description of the tube and its housing has been presented by Lauritsen and Cassen.[1] The tube in its present form operates satisfactorily at 600 kilovolts and it has been deemed advisable to investigate the available radiation before attempting to go to higher potentials.

In order to investigate the region of the x-ray spectrum from approximately 150 kilovolts and up, a crystal spectrograph was constructed following the principle described by Seemann,[2] Siegbahn[3] and others. High precision cannot be expected with any reasonable time of exposure by this method since the whole of this region of the spectrum lies within an angle of less than one degree and thick slits are required because of the great penetrating power of the hard radiation. On the other hand, the method is convenient and sufficiently precise for the approximate determination of the short wave-length limit as well as of the general distribution of intensity in the spectrum. Also, if any prominent lines, bands or absorption edges or other unexpected irregularities exist in this region, they should be found most conveniently by this method.

The spectrograph consists essentially of a vertical slit 0.9 mm wide in a lead block 4 cm thick, in front of which a rock-salt crystal is placed. The crystal, slit and photographic plate are all rigidly mounted on a long arm which may be rotated through an angle of one degree on each side of the center, the rotation taking place about an axis through the vertical center line of the slit. Since the focal spot has the appearance of a thin horizontal

[1] C. C. Lauritsen and B. Cassen, Phys. Rev. **36**, 988 (1930).
[2] Seemann, Phys. Zeits. **18**, 242 (1917).
[3] M. Siegbahn, Phil. Mag. **2**, 639 (1919).

disk approximately 5 mm in diameter, it is clear that radiation will reach the central planes of the crystal under all angles from zero to 50 minutes, provided that the distance from the focal spot to the crystal does not exceed 35 cm and that the spectrograph arm is set at an angle of 25 minutes on either side of the center line through the focal spot and the slit. Under these conditions the undeviated part of the light will produce an image of the focal spot as seen through the slit, the whole of the image being located on one side of and adjacent to the center line of the photographic plate. The reflected portion of the light will appear as a spectrum on the other side of the center line. The short wave-length limit is thus given by the distance from the center line to the edge of the continuous spectrum, and lines of equal wave-length are parallel to the center line. Since different wave-lengths originate from different lateral regions of the focal spot and since the intensity is not absolutely uniform throughout the whole of the area, it is not possible to obtain the intensity distribution in the spectrum directly with any degree of precision. Correction can, however, be made for this lack of uniformity

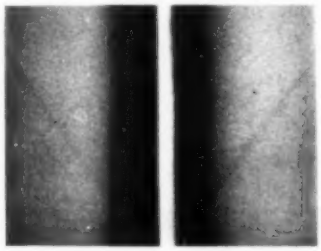

Fig. 1. Double spectrum 600 kv peak.

if the direct beam is reduced by means of a filter to an intensity comparable to the intensity of the spectrum. This is so because the direct beam is a true image of the focal spot and the spectrum is a specular image of the direct beam, except for the wave-length selectivity, and there appears to be no good reason why the radiation from different parts of the target should differ appreciably in hardness if the intensity is the same.

The photographic plate is placed 107.5 cm from the center of the slit. In spite of this comparatively great length, the resolution is not high on account of the wide slit, but it is sufficient for the present purpose.

In order to determine the exact zero on the photographic plate it is most convenient to photograph both right and left hand spectrum on the same plate. This is done by adjusting the spectrograph as described except that the direct image is blocked out completely by a heavy lead screen while one spectrum is being photographed. The spectrograph arm is then rotated into position on the opposite side of the center line and the direct image which now appears on the part of the plate which has been exposed is blocked off. The second exposure thus gives a spectrum on the part of the plate which was covered up during the first exposure. The result is two spectra which are symmetrical with respect to the center line or true zero. Fig. 1 is a positive reproduction of a double spectrum taken in this manner.

A dark line may be seen running diagonally through the spectrum in each of the spectra of Fig. 1. The origin of this line becomes apparent if we consider the geometry of the arrangement. The spectrum shown is due to reflection from vertical (100) planes of the rock-salt crystal, but if the crystal is adjusted so that the horizontal (100) planes are parallel to a horizontal plane through the focal spot and some part of the photographic plate, then it is clear that from each point of the target there will be a ray of a given wave-length which will make the same angle with the horizontal as with the vertical planes. The intensity of this ray will therefore be divided between the spectrum shown and a spectrum which falls above, below, or within the direct image.

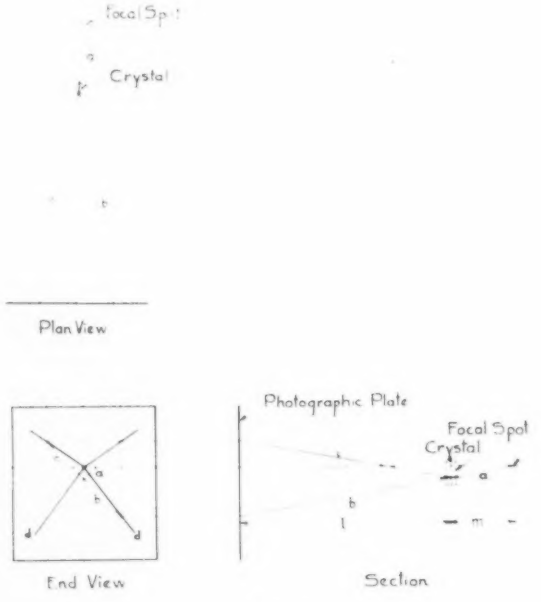

Fig. 2.

This second spectrum is of the type first obtained by Rutherford and Andrade and differs from the first in that the resolution is slightly less. The paths of a ray are shown by the lines a, b and c in Fig. 2, and the heavy lines d in the end view are the intersections with the photographic plate of all the rays which fulfill the foregoing condition. It is readily seen from the figure that the angle between the lines d and the vertical center line is given by

$$\tan\theta = \frac{b}{a+b}.$$

In the present case, this gives

$$\tan\theta = \frac{107.5}{142.5} = 0.755;\ \theta = 37.05^\circ$$

which agrees with the angles made by the dark lines in Fig. 1 with the center line.

The intensity distribution was obtained by means of a recording microphotometer. In Fig. 3 the galvanometer deflections obtained from the photometer records are plotted as ordinates against distance as abscissas. The tube was operated at 600 kilovolts peak and, as indicated in the graph, the short wave-length limit corresponds closely to this value. The maximum intensity occurs somewhat below one half of this potential, as might be expected since the tube is operated with alternating current and a "thick"

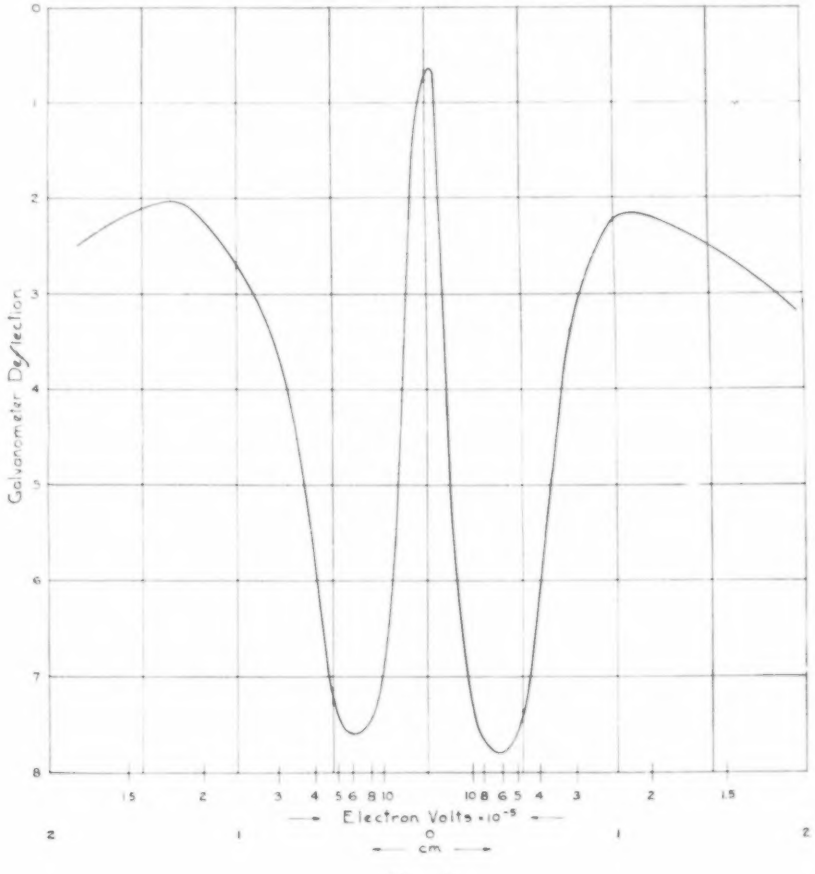

Fig. 3.

target is used. It should be noted, however, that the softer radiation is decreased somewhat in passing through both the 6 mm steel wall of the tube and the crystal. The lack of symmetry which is apparent in the graph is due partly to the aforementioned non-uniformity of the focal spot and partly to a slight difference in exposure.

Results

From the photograph as well as from the photometer record we may conclude that, within the limits of the resolution used, there are no unexpected irregularities in the spectrum from tungsten in the region covered.

At the present time work is in progress to determine as accurately as possible how the spectrum is modified by different absorbers. The right half of Fig. 4 shows the spectrum after passing through lead screens. One screen, 0.28 in. thick, covers the whole image, and in addition the central portion is covered by a second screen 0.14 in. thick. The direct beam was decreased to a suitable intensity by a steel block 2 in. thick.

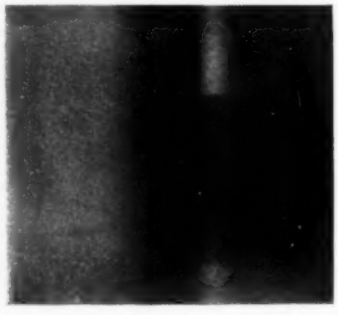

Fig. 4. Left, direct image. Right, spectrum.

The photometer records of spectra taken in this way show accurately how the spectrum is modified by any given absorber and it should therefore be possible to obtain from a single pair of records the absorption coefficient as a function of the wave-length.

If nuclear absorption levels or other unexpected irregularities exist in this region of the spectrum, they should be readily detected by this method. The spectra obtained so far and also the modifications due to absorbing screens of aluminum, iron, copper and lead are roughly what would be expected. There is no indication of any sudden changes in intensity with wave-length.

MULTIPLE SCATTERING IN THE COMPTON EFFECT

By Jesse W. M. Dumond
California Institute of Technology, Pasadena

(Received November 5, 1930)

Abstract

In the experimental study of the spectral distribution of x-radiation scattered by light elements it has always, up to the present, been assumed that multiple scattering could be neglected. Recent improvements in experimental technique however make it possible to suppose that multiple (especially double) scattering may now be detectable from large scattering bodies. Multiple scattering may (1) affect the breadth of the modified line, (2) change the structure of the modified line, (3) distort the background in such a way as to render measurements of shift unreliable. It is therefore valuable to analyze the effect of multiple scattering in case some of the recent mutually discordant experimental results may be explained and harmonized in this way.

Assuming initially monochromatic radiation, scattering of any degree of multiplicity contributes a spectral band whose wave-length limits are here determined and discussed. The Breit, Compton, Jauncey formula taking polarization into account is adopted for the purposes of calculation of modified intensity. The results are thus fairly accurate for hard radiation scattered from very light elements. For softer radiation modified scattering at small scattering angles is greatly reduced below the values given by the Breit, Compton, Jauncey formula and unmodified scattering appears. The effect of this on the results of this paper is discussed in a qualitative way.

The case of double scattering from a spherical scatterer is computed in complete detail and a formula for the ratio of double to single scattering is derived. Curves of the spectral distributions due to double scattering are shown. The dependence of the total doubly scattered intensity on the primary scattering angle is plotted.

The natural width of the modified line is neglected throughout these calculations. Absorption in the scatterer is also neglected. The ratio of double to single scattering for a spherical scatterer observed under any given angle is proportional to the radius of the scatterer (neglecting absorption) and is given by

$$\frac{\text{Doubly scattered energy}}{\text{Singly scattered energy}}=\frac{9}{32}\sigma r R(\theta) \text{ where}$$

σ is the linear scattering coefficient for the material of the scattering sphere, r the radius of the sphere, θ the angle under which single scattering occurs. $R(\theta)$ never differs greatly from 2.5.

Triple scattering is negligible in comparison to single scattering.

Twice modified doubly scattered radiation may contribute a faint asymmetric line or edge at the shifted position

$$\Delta\lambda=2(h/mc)(1+\cos\tfrac{1}{2}\theta)$$

For hard radiation when the Thompson formula (with Breit correction) applies with fair accuracy to modified scattering alone twice modified doubly scattered radiation contributes a spectral band of breadth

$$4(h/mc)\cos\tfrac{1}{2}\theta$$

Once modified doubly scattered radiation may cause a slight broadening of the Compton line except in regions near $\theta=0$ and $\theta=180°$.

Introduction

IN THE experimental study of scattered x-radiation it is impossible completely to eliminate multiple scattering. X-radiation whose direction is defined more or less closely within some solid angle $\delta\Omega_1$ is incident upon a scattering body. The apparatus (a spectrograph, ionization spectrometer or what not) is arranged so as to receive scattered radiation whose direction again is more or less closely defined within some solid angle $\delta\Omega_2$. The angle θ between the initial and final directions has thus assignable limits of inhomogeneity and is called the angle of primary scattering. A ray cannot be prevented, however, from suffering any number of scattering processes between its entry along the first direction and its exit along the last. It is the purpose of this paper to discuss theoretically the effect of such processes on the spectral distribution of the scattered radiation. The path of a multiply scattered ray is a broken line (in space) of $(M+1)$ straight segments, where M is the multiplicity of the scattering. The first and last segments have the fixed directions of the incident and scattered beams just mentioned. The other segments will be called *intermediate rays*. Their directions may be any whatever. In double scattering there is but one intermediate ray. The directions of the entry, exit and intermediate rays are to be plotted upon a sphere of unit radius by means of unit vectors originating at the center of the sphere and terminating on its surface. These vectors have the respective directions of propagation of the radiation along entry, exit and intermediate rays for their directions. The terminii of these vectors thus locate $M+1$ points on the surface of the sphere and represent the $(M+1)$ directions taken by the M-tuply scattered ray. The first and last of these points are fixed upon the sphere and separated by the angle of primary scattering θ. The remaining $(M-1)$ points may have any position on the entire surface of the sphere. The problem of M-tuple scattering thus involves the $(2M-2)$ degrees of freedom of these points.

Each process of scattering splits an initially monochromatic ray into modified and unmodified components as regards wave-length. The modified ray suffers an increase of wave-length given by $\Delta\lambda = h/mc(1-\cos\theta_i)$ where θ_i is the angle of scattering. There exist therefore $(M+1)$ cases in m-tuple scattering for the ray may be *scattered* M times but only *modified* 0, 1, 2, 3, etc. up to M times. Thus in double scattering the ray may be scattered twice without modifications, or modified at the first scattering but not at the second, or modified at the second scattering but not at the first, or modified twice successively. The two cases of singly modified doubly scattered radiation will be identical.

Unfortunately the law governing the partition of the scattered radiation between modified and unmodified rays is complicated and not very well known. For sufficiently hard radiation scattered by sufficiently light atoms however the unmodified radiation is negligible at nearly all scattering angles. In this paper only this limiting case will be discussed analytically in detail and therefore the total shift of the original wave-length will be the sum of all the separate shifts occurring at the successive scattering processes. The breadth of the shifted line will be neglected.

Wave-Length Limits of Multiply Scattered Radiation

It is immediately possible to make the following obvious generalizations if M is both the number of scatterings and the number of shifts of a given ray:

1. When M is odd the maximum shift occurs for a primary scattering angle of $\theta = 180°$.
2. When M is even the maximum shift occurs for $\theta = 0°$.
3. Minimum shift for any multiplicity is always zero and always occurs at a primary scattering angle $\theta = 0$.
4. Maximum shift is always $2M(h/mc)$ where M is the multiplicity of scattering.

Double Scattering

Referring to Fig. 1, on the sphere, A is the direction of the entry ray, B the direction of the intermediate ray and C the direction of the scattered ray. The arc AC measures the fixed primary scattering angle θ and is bi-

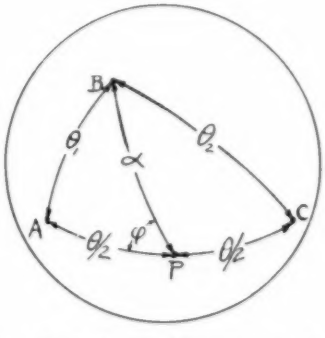

Fig. 1. Illustrating spherical coordinate system (α, ϕ) appropriate to the problem of double scattering.

sected at P. P is taken as the pole of a system of spherical polar coordinates (α, ϕ) which describe the location of the intermediate ray B whose two degrees of freedom are the independant variables of the problem.

That such a system of coordinates (α,ϕ) is appropriate to the problem will be seen from the following considerations:

The total shift

$$\Delta\lambda = \frac{h}{mc}\{2 - (\cos\theta_1 + \cos\theta_2)\} \tag{1}$$

If the letters $\boldsymbol{A}$, $\boldsymbol{B}$ and $\boldsymbol{C}$ represent unit vectors, then

$$\begin{aligned}\Delta\lambda &= h/mc\{2 - (\boldsymbol{A}\cdot\boldsymbol{B} + \boldsymbol{B}\cdot\boldsymbol{C})\}\\ &= h/mc\{2 - \boldsymbol{B}\cdot(\boldsymbol{A} + \boldsymbol{C})\}\\ &= 2h/mc(1 - \cos\tfrac{1}{2}\theta\cos\alpha) \qquad (2)\\ &(\text{since}\,|\,\boldsymbol{A} + \boldsymbol{C}\,| = 2\cos\tfrac{1}{2}\theta)\end{aligned}$$

Hence regions of constant total shift $\Delta\lambda$ correspond to directions of B lying in zones on the sphere described about P as a pole.

Wave-Length Limits of Doubly Scattered Doubly Shifted Radiation

Since cos α may range from 1 to -1, doubly scattered radiation may have a range of shifts defined by the inequalities

$$2h/mc(1 - \cos \tfrac{1}{2}\theta) < \Delta\lambda < 2h/mc(1 + \cos \tfrac{1}{2}\theta) \qquad (3)$$

The limits of this range are evidently equidistant from the point $\Delta\lambda = 2h/mc$ and the total spectral width of the range is $4h/mc \cos \frac{1}{2}\theta$. Thus for a primary scattering angle of zero degrees double scattering contributes shifted radiation over a range of shifts from zero to $4h/mc$ while for a primary scattering angle of 180° double scattering contributes shifted radiation falling exactly at $2h/mc$ and extending over no range whatever. It is convenient to describe the spectral distributions caused by double scattering in terms of a variable x, which is defined as $x = (\Delta\lambda)/(2h/mc)$. This variable which is proportional to the shift in wave-lengths is a pure number.

The Law Governing Intensity of Scattering

In order to compute the distribution of intensity due to double scattering over the range determined for any particular primary scattering angle, some law must be adopted to express the scattered intensity as a function of the angle of scattering and of the polarization of the radiation. Kallman and Mark[1] have shown in a beautiful experiment that both shifted and unshifted radiations are completely polarized by scattering at 90°. In double scattering therefore the beam becomes partially polarized in the first scattering process and this fact is of importance in determining the intensity of scattering in the second scattering process.

We therefore assume in this computation that each scattering process gives modified radiation having the intensity and polarization dictated by the classical Thompson theory of scattering and then apply the Breit correction to this by multiplying by a factor $(1+\alpha \text{ vers } \theta_1)^{-3}$ $(1+\alpha \text{ vers } \theta_2)^{-3}$ (c.f. Compton "X-Rays and Electrons" pp. 304–305). Fortunately $(1+\alpha \text{ vers } \theta_1)^{-3}$ $(1+\alpha \text{ vers } \theta_2)^{-3}$ can be replaced by $(\lambda_0/\lambda_1)^3$ $(\lambda_1/\lambda_2)^3$ and hence by $(\lambda_0/\lambda_2)^3$ where λ_0 is the primary wave-length, λ_1 the wave-length after the first scattering, and λ_2 the wave-length after the second scattering. It is thus a very fortunate fact that the Breit correction factor depends only on the ratio of the initial and final wave-lengths in double scattering and not at all on the intermediate wave-length. Thus after the doubly scattered spectral distribution has been computed by the classical Thompson formula and the distribution is obtained as a function of $\Delta\lambda$ or x the Breit correction can be applied to the curves by simply multiplying each ordinate by the ratio $(\lambda_0/\lambda_2)^3$ applicable to its abscissa.

The above outlined method should give fairly accurate results for hard radiation and light scattering atoms where the presence of unmodified radiation and diminished modified radiation for small scattering angles can be neglected.

[1] Kallman and Mark, "Uber einige Eigenschaften der Comptonstrahlung Zeits. f. Physik 36, 120–142 (1926).

Unfortunately the case of say Mo$K\alpha$ radiation scattered by graphite is not such a one. The author has not succeeded in obtaining an analytic solution for double scattering rigorously applicable to this case taking account of the unmodified scattering and diminished modified scattering. Moreover the really great analytical difficulties incident to such a solution seem scarcely worth overcoming as a good qualitative idea of the spectral intensity distribution can be obtained by a rough examination of the effect of reduced modified scattering on the case which is here solved.

The shape of the scattering body also plays a part in determining the spectral distribution of doubly scattered radiation. It is of course practically impossible to take account of this factor and accordingly the solution here given can again only be applied to real cases qualitatively. In order to construct an ideal case in which the shape of the scatterer does not complicate the analysis we consider first only one electron at the center of a spherical scattering body. This electron receives primary radiation along the direction A and scatters in various directions B to all the other electrons in the scatterer which in turn scatter the radiation along the exit direction C. It is the spectral distribution of this radiation as affected by two wave-length modifications which we propose to investigate. Subsequently the reasoning is readily extended to initial scattering by *all* the electrons in the spherical scattering body.

Computation of Spectral Distributions Due to Double Scattering

Referring to Fig. 2, let E_{n1} and E_{a1} be the primary component electric intensities E_{n1} being normal to the plane of the first angle of scattering θ_1

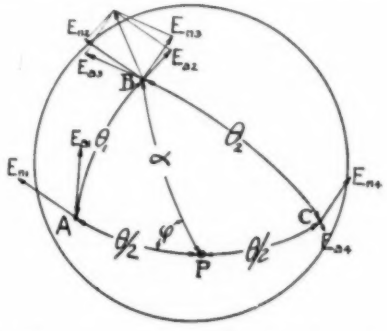

Fig. 2. Illustrating the components of the electric vector of the incident, intermediate and exit rays.

and E_{a1} parallel to that plane. At a distance r_1 from the first scattering electron along the intermediate direction B the scattered radiation will have electric components E_{n2} and E_{a2} again normal and parallel respectively to the plane of θ_1 given by the Thompson classical theory as:

$$E_{n2} = -\frac{E_{n1}e^2}{r_1mc^2} \tag{4}$$

$$E_{a2} = -\frac{E_{a1}e^2}{r_1mc^2}\cos\theta_1. \tag{5}$$

Let B represent the supplement of the angle B of the spherical triangle $A\ B\ C$. We now resolve the electric vector whose components are E_{n2} and E_{a2} along two new directions normal and parallel respectively to the plane of the second angle of scattering θ_2 and obtain E_{n3} and E_{a3}

$$E_{n3} = E_{n2}\cos B + E_{a2}\sin B \tag{6}$$

$$E_{a3} = E_{a2}\cos B - E_{n2}\sin B. \tag{7}$$

The scattered radiation having these components E_{n3} and E_{a3} is now scattered again by an electron at distance r_1 from the first, the new scattering angle being θ_2. At distance r_2 from the second scattering electron along the direction C the doubly scattered radiation will have electric components E_{n4} and E_{a4}

$$E_{n4} = -\frac{E_{n3}e^2}{r_2mc^2} \tag{8}$$

$$E_{a4} = -\frac{E_{a3}e^2}{r_2mc^2}\cos\theta_2. \tag{9}$$

We now express E_{n4} and E_{a4} in terms of E_{n1} and E_{a1} and evaluate the square of the final electric intensity E_4^2

$$\begin{aligned} E_4^2 = E_{n4}^2 + E_{a4}^2 = \frac{e^8}{r_1^2r_2^2m^4c^8}\big[&E_{n1}^2\cos^2 B + E_{a1}^2\cos^2\theta_1\sin^2 B \\ &+ 2E_{n1}E_{a1}\cos B\sin B\cos\theta_1 + \cos^2\theta_2(E_{a1}^2\cos^2\theta_1\cos^2 B \\ &+ E_{n1}^2\sin^2 B - 2E_{a1}E_{n1}\cos\theta_1\cos B\sin B)\big]. \end{aligned} \tag{10}$$

For unpolarized primary radiation we average over all possible orientations of E_1 about the primary beam giving all orientations equal weights. This means that $\{E_{n1}^2\} = \{E_{a1}^2\} = \frac{1}{2}E_1^2$ and $\{E_{n1}E_{a1}\} = 0$, the curly bracket here being used to indicate the average. The average doubly scattered intensity is then given by

$$\begin{aligned} \{E_4^2\} = \frac{1}{2}E_1^2\frac{e^8}{r_1^2r_2^2m^4c^8}\big[&\cos^2 B \\ &+ (\cos^2\theta_1 + \cos^2\theta_2)\sin^2 B + \cos^2\theta_1\cos^2\theta_2\cos^2 B\big] \end{aligned} \tag{11}$$

Now from a well-known formula applying to spherical triangles we can express B in terms of θ_1, θ_2, and θ

$$\cos B = \frac{\cos\theta - \cos\theta_1\cos\theta_2}{\sin\theta_1\sin\theta_2}. \tag{12}$$

By appropriate substitutions employing this formula we obtain the doubly scattered intensity in terms of θ_1, θ_2 and θ as

$$\begin{aligned} \{E_4^2\} = \frac{1}{2}E_1^2\frac{e^8}{r_1^2r_2^2m^4c^8}\big[&\cos^2\theta_1 + \cos^2\theta_2 \\ &+ \cos^2\theta - 2\cos\theta\cos\theta_1\cos\theta_2 + \cos^2\theta_1\cos^2\theta_2\big]. \end{aligned} \tag{13}$$

We now transform this to an expression in α and ϕ the spherical coordinates of our problem by the use of the relations from spherical trigonometry

$$\cos\theta_1 = \cos\alpha\cos\tfrac{1}{2}\theta + \sin\alpha\sin\tfrac{1}{2}\theta\cos\phi \tag{14}$$

$$\cos\theta_2 = \cos\alpha\cos\tfrac{1}{2}\theta - \sin\alpha\sin\tfrac{1}{2}\theta\cos\phi. \tag{15}$$

This gives

$$\begin{aligned}\{E_4^2\} = \frac{1}{2}E_1^2\frac{e^8}{r_1^2r_2^2m^4c^8}\,[&2\cos^2\alpha\cos^2\tfrac{1}{2}\theta + 2\sin^2\alpha\sin^2\tfrac{1}{2}\theta\cos^2\phi + \cos^2\theta \\ &- 2\cos\theta\cos^2\alpha\cos^2\tfrac{1}{2}\theta + 2\cos\theta\sin^2\alpha\sin^2\tfrac{1}{2}\theta\cos^2\phi \\ &+ (\cos^2\alpha\cos^2\tfrac{1}{2}\theta - \sin^2\alpha\sin^2\tfrac{1}{2}\theta\cos^2\phi)^2\,]\end{aligned} \tag{16}$$

or:

$$I_4 = \frac{1}{2}I_1\frac{e^8}{r_1^2r_2^2m^4c^8}[y(\alpha,\theta,\phi)]. \tag{17}$$

I_4 is the doubly scattered intensity. It is the energy per cm.^{2} per second at a distance r_2 from the second scattering electron which in turn is at a distance r_1 from the first scattering electron.

The exit ray is confined to some solid angle $\Delta\Omega_3$ by the construction of the apparatus for studying the scattered radiation. If we multiply the last expression by the area $r_2^2\Delta\Omega_3$ we obtain the *energy* scattered per second into the solid angle $\Delta\Omega_3$

$$I_4r_2^2\Delta\Omega_3 = \frac{1}{2}I_1\frac{e^8\Delta\Omega}{r_1^2m^4c^8}[y(\alpha,\theta,\phi)]. \tag{18}$$

Consider now a spherical shell of radius r_1 and thickness dr_1 described about the first scattering electron as a center. Let the volume density of electrons in the scatterer be ρ. In the solid angle between α and $\alpha+d\alpha$, ϕ and $\phi+d\phi$ there will be $\rho r_1^2\sin\alpha\,dr_1d\alpha d\phi$ electrons. The energy per second entering the solid angle $\Delta\Omega_3$ due to all the electrons just mentioned will be

$$I_4r_2^2\Delta\Omega_3\rho r_1^2\sin\alpha dr_1d\alpha d\phi = \frac{1}{2}I_1\frac{e^8\Delta\Omega_3\rho dr_1}{m^4c^8}[y(\alpha,\phi,\theta)\sin\alpha d\alpha d\phi]. \tag{19}$$

Integrating this from $r=0$ to $r=r$, the distance from the first scattering electron to the furthermost electron in the body in the direction (α,ϕ), we have

$$\frac{1}{2}I_1\frac{e^8\Delta\Omega_3\rho r_{\alpha\phi}}{m^4c^8}[y(\alpha,\phi,\theta)\sin\alpha d\alpha d\phi]. \tag{20}$$

The total shift after two scatterings is independant of ϕ as has already been pointed out. We therefore obtain the total energy going into a zone between α and $\alpha+d\alpha$, all of which contributes to one and the same shifted position in the doubly scattered spectrum by integrating around the zone

from $\phi=0$ to $\phi=2\pi$. We thus obtain the energy per second passing out through the solid angle $\Delta\Omega_3$ after first scattering by one electron at the center of the *spherical* scattering body of radius, r, and then scattering by all other electrons in the body between the cones of half angle α and $\alpha+d\alpha$. It is

$$\frac{1}{2}I_1\frac{e^8\Delta\Omega_3\rho r}{m^4c^8}[y(\alpha, d\alpha, \theta)] = \frac{1}{2}I_1\frac{e^8\Delta\Omega_3\rho r}{m^4c^8}\Big[2\pi(2-2\cos\theta)\cos^2\alpha\cos^2\tfrac{1}{2}\theta + \pi(2+2\cos\theta)\sin^2\alpha\sin^2\tfrac{1}{2}\theta + 2\pi\cos^2\theta + 2\pi(\cos^2\alpha\cos^2\tfrac{1}{2}\theta)^2 - 2\pi\cos^2\alpha\cos^2\tfrac{1}{2}\theta\sin^2\alpha\sin^2\tfrac{1}{2}\theta + \frac{3}{4}\pi(\sin^2\alpha\sin^2\tfrac{1}{2}\theta)^2\Big]\sin\alpha d\alpha. \tag{21}$$

We must now transform this expression to one in terms of x and dx the independant variable used to express the shift in the description of spectral distribution. $x=(\Delta\lambda)/(2h/mc)$. The shift is given by

$$\Delta\lambda = 2h/mc(1-\cos\tfrac{1}{2}\theta\cos\alpha)$$

hence

$$x = (1-\cos\tfrac{1}{2}\theta\cos\alpha) \tag{22}$$

$$dx = \cos\tfrac{1}{2}\theta\sin\alpha d\alpha \tag{23}$$

$$\sin\alpha d\alpha = dx/\cos\tfrac{1}{2}\theta \tag{24}$$

$$\cos^2\alpha = \frac{(1-x)^2}{\cos^2\frac{1}{2}\theta};\quad \sin^2\alpha\sin^2\tfrac{1}{2}\theta = \sin^2\tfrac{1}{2}\theta - (1-x)^2\tan^2\tfrac{1}{2}\theta.$$

Making these substitutions we obtain the total energy per second in the spectral region between x and $x+dx$; it is

$$I_4dx = \frac{1}{2}I_1\frac{\pi e^8\Delta\Omega_3\rho r}{m^4c^8}[y(x,\theta)]dx = \frac{1}{2}I_1\frac{e^8\Delta\Omega_3\rho r\pi}{m^4c^8}\Big[\Big(2\cos^2\theta + \sin^2\theta + \frac{3}{4}\sin^4\tfrac{1}{2}\theta\Big) + \Big(2\sin^2\tfrac{1}{2}\theta - \frac{3}{2}\sin^2\tfrac{1}{2}\theta\tan^2\tfrac{1}{2}\theta\Big)(1-x)^2 + \Big(2+2\tan^2\tfrac{1}{2}\theta + \frac{3}{4}\tan^4\tfrac{1}{2}\theta\Big)(1-x)^4\Big]\frac{dx}{\cos\frac{1}{2}\theta}. \tag{25}$$

This expression refers to one electron only at the center of the spherical scattering body as the first scattering agent. This same electron will by *single scattering* into the solid exit angle $\Delta\Omega_3$ scatter energy

$$I_2 = \frac{1}{2}I_1\frac{e^4\Delta\Omega_3}{m^2c^4}(1+\cos^2\theta). \tag{26}$$

The ratio of double to single scattering is then

$$\frac{I_4}{I_2}dx = \pi\frac{e^4\rho r}{m^2c^4}\frac{[y(x,\theta)]}{1+\cos^2\theta}dx \tag{27}$$

but the "scattering coefficient" is;

$$\sigma = \frac{8}{3}\pi\frac{e^4\rho}{m^2c^4}$$

$$\frac{I_4}{I_2}dx = \frac{3}{8}\sigma r\frac{[y(x,\theta)]}{1+\cos^2\theta}dx. \tag{28}$$

The ratio of total doubly scattered energy to singly scattered energy is

$$\frac{\int_{1-\cos 1/2\theta}^{1+\cos 1/2\theta} I_4 dx}{I_2} = \frac{3}{8}\sigma r\frac{\int[y(x,\theta)]dx}{1+\cos^2\theta} = \frac{3}{8}\sigma rR. \tag{29}$$

Evaluating the integral in this expression we obtain the ratio of double to single scattering, it is

$$\frac{3}{8}\sigma r\frac{1}{1+\cos^2\theta}\left[2A + \frac{2}{3}B\cos^2\tfrac{1}{2}\theta + \frac{2}{5}C\cos^4\tfrac{1}{2}\theta\right] \tag{30}$$

where $A = (2\cos^2\theta + \sin^2\theta + \frac{3}{4}\sin^4\frac{1}{2}\theta)$

$B = (2\sin^2\frac{1}{2}\theta - \frac{3}{2}\sin^2\frac{1}{2}\theta\tan^2\frac{1}{2}\theta)$

$C = (2 + 2\tan^2\frac{1}{2}\theta + \frac{3}{4}\tan^4\frac{1}{2}\theta)$

Both values of the bracket in the last expression and values of R are plotted in Fig. 3.

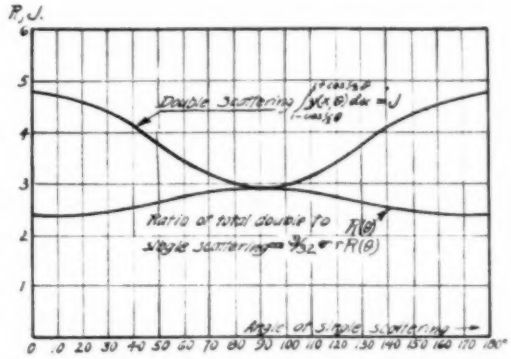
R, J.
6
5
4
3
2
1
Double Scattering
Ratio of total double to single scattering = 3/2 rR(θ)
Angle of single scattering →
0 10 20 30 40 50 60 70 80 90 100 110 120 130 140 150 160 170 180°

Fig. 3. Curves of the integral in Eq. (29) and also of the ratio R in that equation.

For scattering from the *central* electron in the spherical scatterer to all other electrons, the value of $r_{a\phi}$ is the radius r of the spherical scatterer. For initial scattering from *all* electrons in the scatterer however an average[2] value of $\{r_{a\phi}\} = \frac{3}{4}r$ must be taken. To obtain this we average the distance along any fixed arbitrary direction from each elementary volume in the spherical scatterer to the boundary of the sphere throughout the entire volume. Taking as volume elements of the sphere the space between two coaxial cylinders of radii r' and $r'+dr'$ with axis through the center of the

[2] The bracket { } is used to denote "average value."

sphere, the average distance in question is given by $1/(4/3)\pi r^3 \int_0^r (r^2 - r'^2) 4\pi r' dr' = \frac{3}{4}r$. Now $\sigma = 0.4$ per cm for Mo radiation scattered from graphite.

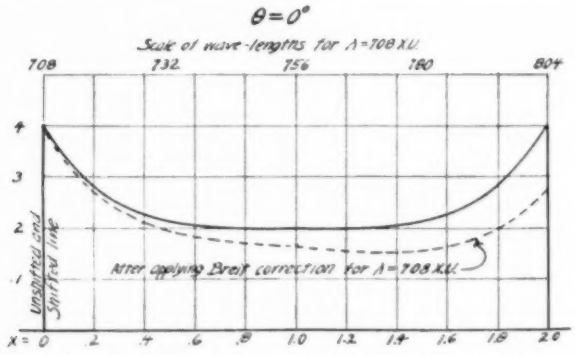

Fig. 4. Spectral distribution due to doubly modified double scattering for primary scattering angle of zero degrees.

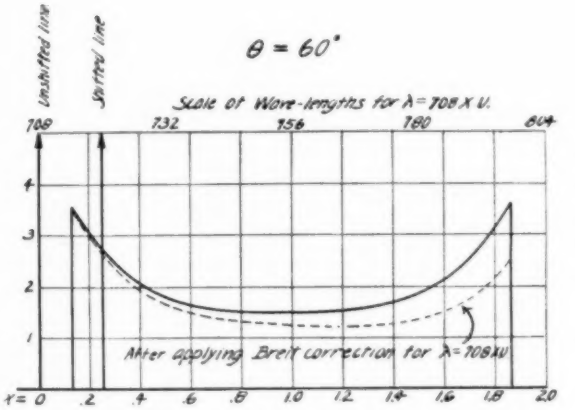

Fig. 5. Spectral distribution due to doubly modified double scattering for primary scattering angle of 60°.

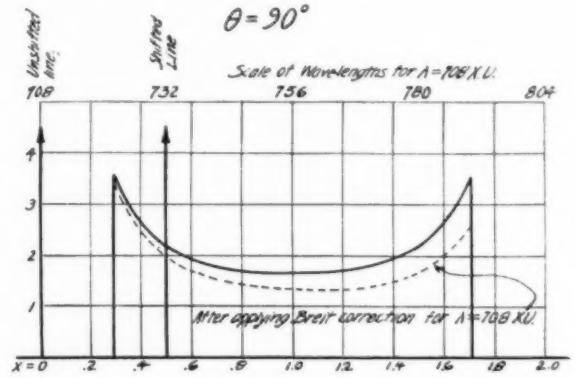

Fig. 6. Spectral distribution due to doubly modified double scattering for primary scattering angle of 90°.

It appears from Fig. 3 that R never differs very greatly from 2.5. The ratio then of total double scattering to single scattering for a spherical carbon

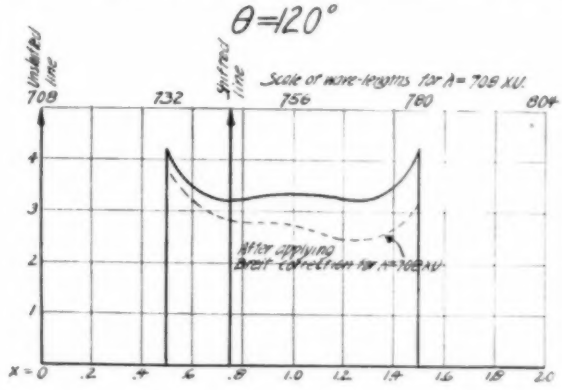

Fig. 7. Spectral distribution due to doubly modified double scattering for primary scattering angle of 120°.

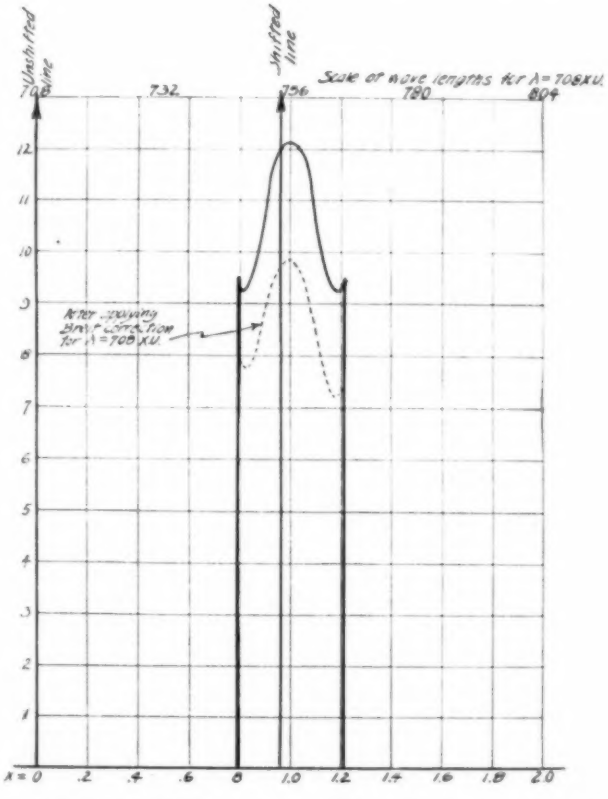

Fig. 8. Spectral distribution due to doubly modified double scattering for primary scattering angle of 156°.

scatterer 0.5 cm in radius scattering Mo radiation is about 0.140. This would increase in direct proportion to the radius of the spherical scatterer were it not for absorption. Except at $\theta = 180°$ however the doubly scattered energy is distributed over a considerable wave-length band.

The spectral distribution of double scattering is obtained from expression (25) for scattering angles θ between initial and final beams of 8°, 60°, 90°, 120°, 156° and 180°. These are exhibited in Figures 4 to 9. The curves both without and with the Breit correction computed for MoK radiation are shown. An interesting feature of these curves occurs when the angle of single scattering is 180°. At this angle the spectral distribution, due to doubly

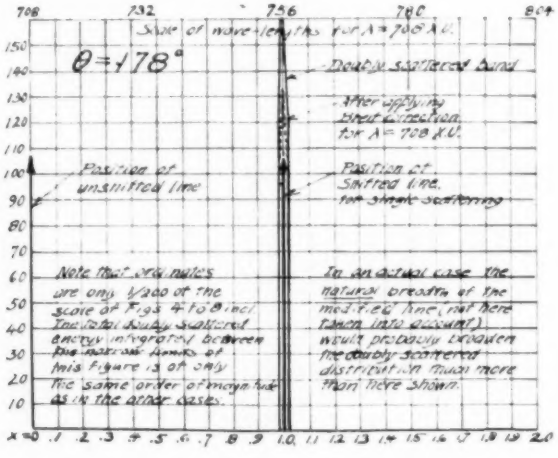
708
732
756
780
804
θ=178°
Doubly scattered band
Position of unmodified line
Position of Shifted line for single scattering
Note that wave lengths are only 1/200 of the scale of Figs 4 to 8 incl. The total doubly scattered energy integrated between the same limits of this figure is of the same order of magnitude as in the other cases.
In an actual case the natural breadth of the mod. shifted line, not here taken into account, would probably broaden the doubly scattered distribution much more than here shown.
x=0 .1 .2 .3 .4 .5 .6 .7 .8 .9 1.0 1.1 1.2 1.3 1.4 1.5 1.6 1.7 1.8 1.9 2.0

Fig. 9. Spectral distribution (with reduced ordinate scale) of doubly modified double scattering for primary scattering angle of 178°.

shifted scattering, narrows down to a sharp line (neglecting the natural breadth of the Compton shifted line itself). The presence of the term $(\cos \frac{1}{2}\theta)^{-1}$ in the expression (25) makes that expression indefinitely large for $\theta = 180°$. The energy associated with double scattering corresponding to the area under this infinitesimally narrow infinitely tall curve is of course finite.

Qualitative Discussion of the Effect of Unmodified and Decreased Modified Scattering

Scattering of x-radiation of intermediate hardness (e.g. MoK radiation scattered by graphite) is of two well-known types; modified and unmodified. The total scattered energy follows the Thompson classical law with the Breit correction to a fair degree of approximation except at small scattering angles where the phenomenon of excess scattering occurs. Excess scattering is without doubt a phenomenon of interference of scattered x-radiation and applies therefore only to unmodified scattering (since modified scattering is incoherent). The total scattered energy is divided between the modified and unmodified types in proportions that depend on the scattering angle. Unfortunately the exact analytic form of this dependence is unknown. It is

doubtless very complex since it depends in an intimate way on the mechanics of the scattering atom. Jauncey has treated the problem theoretically for an approximate Bohr atom model. In Fig. 10 the work of Ross and Woo relative to MoK radiation scattered from graphite is collected in one curve showing the ratio of modified scattered radiation to unmodified scattered radiation as a function of scattering angle. Fig. 11 shows Hewlett's observations on total scattering. Applying the ratio of the previous curve to this we

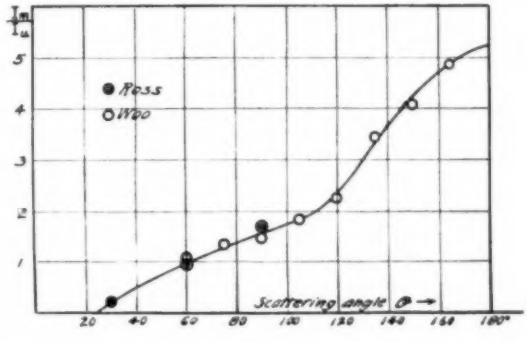

Fig. 10. Combined observations of P. A. Ross and Y. H. Woo of the ratio of modified to unmodified scattered intensity as a function of scattering angle.

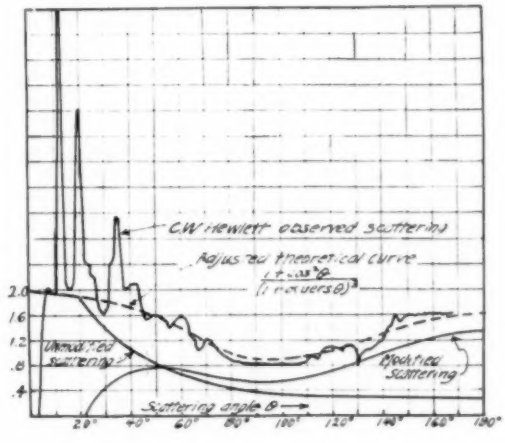

Fig. 11. Hewlett's observations of total scattering and the partition of this into modified and unmodified types in accord with Fig. 10.

obtain the two other curves which give the modified and unmodified scattered energies as a function of scattering angle. Note that below 90° modified scattering diminishes rapidly and disappears completely at about 20°. In this same region unmodified scattering becomes very strong.

To take account analytically of the effect of these phenomena on double scattering would doubtless be an extremely difficult task and one which would certainly not be warranted at present by the utility of its results. The main purpose of the present investigation is to obtain a qualitative idea

of the effect of double scattering regarded as an unavoidable impurity in the experimental study of single scattering. In this paper therefore we discuss only in a brief qualitative way the effect of excess unmodified scattering and diminished modified scattering on the results we have already obtained.

Once Modified Double Scattering

Referring to Fig. 12 to which the same nomenclature of entry, exit and intermediate beams (respectively A, C, B) applies as before we obtain a rough approximation to the effect of once unmodified and once modified doubly scattered radiation by noting that the bulk of unmodified scattering will occur in the region of excess single scattering for θ_1 represented by the heavy shading around A. The zones of constant shift however are now no longer described around the bisector point P as before but around C the exit direction since the shift now occurs wholly in the second scattering process and depends only on θ_2. From these considerations it is evident that

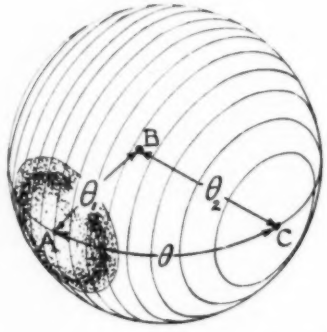

Fig. 12. Coordinate system for double scattering, unmodified at angle θ_1 but modified at angle θ_2.

the only cases of importance are those where the intermediate ray point, B, lies in the shaded regions of excess unmodified scattering. The zones of constant shift have been so spaced in the drawing that they represent equal increments of shift. One can see immediately that the greatest intensity in the spectral distribution of once modified doubly scattered radiation occurs closely adjacent to and about symmetrically on either side of the position of the modified line for single scattering, and that there will also be a considerable contribution between these two positions. Since excess unmodified scattering has been observed to be many times as strong as ordinary unmodified scattering, there is just a chance that some of the observed excess breadth of the modified Compton line may be attributed to this effect. This argument however will not apply to explain the breadth of the Compton line for primary scattering angles of nearly 180° because here the entire shaded region is included in a very small range of shifts. Singly modified double scattering will be absent near $\theta=0°$ because in this case when B is in the shaded area θ will have values for which modified scattering is practically absent. If then the effect in question is the sole cause of the observed

excess breadth of the Compton line we should expect this excess breadth to be least for small and large angles of primary scattering, θ, and greatest for $\theta = 90°$.

Twice Modified Double Scattering

The effect of decreased modified scattering at small angles on the already derived spectral distributions of twice modified doubly scattered radiation occurs principally in the left hand portions of the curves. We can approximate the facts roughly by imagining circles each about 45° in radius described about A and also C from which the point B is supposed to be excluded (see Fig. 13). For scattering angles, θ, up to 90° these excluded regions will lie entirely in the low shift hemisphere. We conclude then that the right hand halves of the curves, Figs. 4 to 6 inclusive, will remain practically unchanged and that the left hand halves will diminish monotonically as we pass to the left, vanishing almost completely at their left extremities.

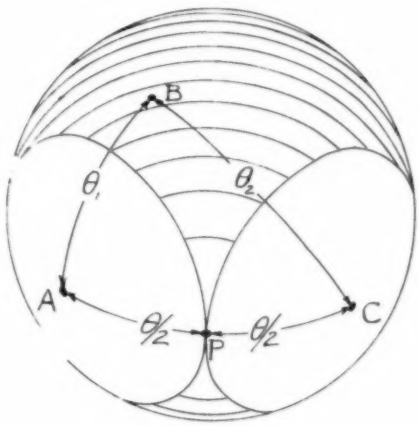

Fig. 13. Coordinate system for doubly modified double scattering taking into account the absence of modified scattering at small angles.

For scattering angles θ greater than 90° as the circles of exclusion move out of the low shift hemisphere into the high shift hemisphere, it is evident that energy will reappear in the left extremity of the spectral distributions and the suppressed portion of our curves will displace toward the right. The left hand regions or regions of low shift will however always be more depressed than the right hand regions of great shift. Fig. 14 shows the spectral distributions to be expected from the preceeding discussion.

Summary of Conclusions

1. The ratio of double to single scattering for a spherical scatterer is proportional to the radius of the scatterer (neglecting absorption) and is given by the formula

$$\frac{\text{Doubly scattered energy}}{\text{Singly scattered energy}} = \frac{9}{32}\sigma r R(\theta)$$

in which the $R(\theta)$ is greatest for about $\theta = 90°$ and has minima at $\theta = 0$ and $\theta = 180°$, the latter being the smaller (Fig. 3). R never differs greatly from 2.5.

2. For MoK radiation scattered by a sphere of graphite 1 cm in diameter double scattering is about 14% of single scattering (neglecting absorption).

3. From the last it seems probable that in most experiments the effect of triple and higher multiplicities of scattering can be completely neglected.

4. Once modified doubly scattered radiation may account for a slight broadening of the Compton line except in regions near $\theta = 0$ and 180°.

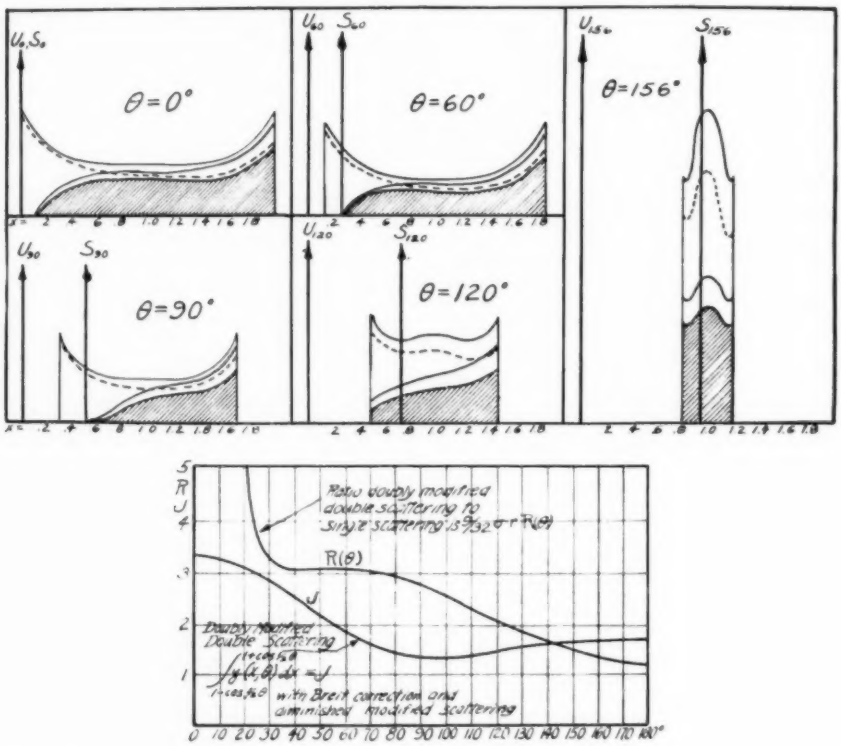

Fig. 14. Spectral distributions due to doubly modified double scattering corrected for diminished modified scattering at small angles (shaded curves). The two curves $R(\theta)$ and J are the same quantities as those shown in Fig. 3 after application of the Breit correction and correction for diminished modified scattering at small angles.

5. Twice modified doubly scattered radiation when corrected qualitatively for diminished modified scattering at small angles may contribute a faint asymmetric line or edge in the position

$$\Delta\lambda = 2\frac{h}{mc}(1 + \cos \tfrac{1}{2}\theta)$$

6. For hard radiation where the Thompson formula with the Breit correction applies with fair accuracy to modified scattering alone, twice modified doubly scattered radiation contributes a spectral band of breadth

$$4\frac{h}{mc}\cos \tfrac{1}{2}\theta$$

List of Symbols

$\Delta\Omega$, $\delta\Omega$—Solid angle measured in steradians.

θ—The angle of single scattering.

θ_1—The first angle of double scattering.

θ_2—The second angle of double scattering.

M—The multiplicity of scattering.

λ_0—The wave-length of the primary radiation.

λ_1, λ_2—The wave-lengths after first and second scatterings.

h—Planck's constant.

m—The mass of the electron.

c—The velocity of light.

$\boldsymbol{A}$, $\boldsymbol{B}$, $\boldsymbol{C}$—Unit vectors representing the directions of the entry, intermediate, and exit rays in double scattering. (Fig. 2).

α, ϕ—The colatitude and longitude angles of the spherical polar coordinates of reference in double scattering. (Fig. 2.)

$x=(\Delta\lambda)/(2h/mc)$—wave-length variable used for convenience in describing spectral distributions due to double scattering.

$E_{n1}E_{a1}E_{n2}E_{a2}E_{n3}E_{a3}E_{n4}E_{a4}$—components of the electric intensity in the radiation. The subscript, n, indicates the component normal to the plane of one scattering angle while the subscript, a, indicates the component parallel to that plane. The subscript 1 refers to the initial beam and the first scattering angle, subscript 2 refers to the intermediate beam and the first scattering angle, 3 to the intermediate beam and the second scattering angle, 4 to the final or exit beam and the second scattering angle. See Fig. 2.

B—The dihedral angle between the planes of θ_1 and θ_2. (Fig. 2.)

r_1—The distance from the point of first scattering to the point of second scattering.

r_2—The distance from the point of second scattering to the point of observation.

r—The radius of the spherical scattering body.

σ—The scattering coefficient for the material of the scatterer and the radiation used.

DESIGN AND TECHNIQUE OF OPERATION OF A DOUBLE CRYSTAL SPECTROMETER

By Jesse W. M. DuMond and Archer Hoyt
California Institute of Technology, Pasadena

(Received November 8, 1930)

Abstract

The double crystal x-ray spectrometer is distinctly different in principle from the single crystal spectrometer and calls therefore for a completely new design rather than an adaptation of single spectrometer design. One such new design is described in this paper. Emphasis is laid on the fact that the wave-length selected by the process of two successive crystal reflections in any prescribed orders depends solely on the dihedral angle between the crystals. The advantages of rotating both crystals in equal and opposite directions with respect to a plane through their axes of rotation are pointed out and a spectrometer designed to accomplish this is described. In this spectrometer the turning of a single shaft drives the two crystals, the spectrometer as a whole and the x-ray tube, at the proper angular rates about the proper centers to insure that the x-ray beam will at all times remain centered on the crystal faces and the window of the stationary ion chamber. It is pointed out that spurious fluctuations may be introduced in spectral curves by the x-ray beam migrating across small steps in the cleavage surface reflecting the radiation. Description of design covers design of spectrometer and turning mechanisms, the tube housing, lead shields, the detecting system consisting of an ion chamber with internal grid of special design to minimize natural leak and a Hoffmann vacuum electrometer connected to it through a short evacuated shield. Description of operating technique covers optical method of accurately orienting the crystal faces, methods of aligning the tube, precautions to eliminate background.

THE Double crystal x-ray spectrometer first used in this country by A. H. Compton was developed by Bergen Davis[1] and his collaborators and has been very thoroughly investigated on the theoretical side by Schwarzschild[2] and on the experimental side by S. K. Allison[3] and others.[4] Its field of applicability seems to fall into two classes. First it may be used to study the properties of the crystals themselves (reflecting power, lattice perfections, etc.[5]) Secondly it may be used as an x-ray spectrometer for exploring spectra (satellites, fine structure line breadths, Compton effect, etc.)[6] In the development stage it was natural not to differentiate sharply in the design of double spectrometers for these different classes of work. It was also perfectly natural to adapt the general features of single crystal spectrometer design to the

[1] Bergen Davis, Phys. Rev. **17,** 608 (1921), Phys. Rev. **27,** 18 (1926), Phys. Rev. **32,** 331 (1928).

[2] Schwarzschild, Phys. Rev. **32,** 162 (1928).

[3] Allison, Phys. Rev. **34,** 176 (1929), **35,** 1476 (1930).

[4] Ehrenberg and Mark, Zeits. f. Physik **42,** 807 (1927).

[5] Davis & Purks, Phys. Rev. **34,** 181 (1929).

[6] DuMond & Hoyt, Phys. Rev. **36,** 799 (1930), Bearden, Phys. Rev. **36,** 791 (1930), Richtmyer & Taylor, Phys. Rev. **36,** 1044, (1930).

double spectrometer. The authors feel however that now that so much is known about the possibilities and applications of this instrument the time has come to design it on its own merits in such a way as best to accomplish some particular function.

The double spectrometer here described was developed for the second of the above mentioned uses—the study of x-ray spectra. It is designed to be used entirely in the antiparallel positions (n, n) (Allison's notation)[7] though slight modifications would permit "straddling two different orders."

The authors feel that much of the apparent complexity arising in connection with the double spectrometer comes from the introduction of such artificial frames of reference as the axis of rotation of the pivots supporting the crystals, or the axis of the slits which latter in the double spectrometer play an entirely different role from the slits of a single spectrometer.

The Important Thing is The Dihedral Angle Between The Crystals

It is of cardinal importance to note just what is measured in using the double spectrometer. A beam of x-rays reflected from a cleavage face of a

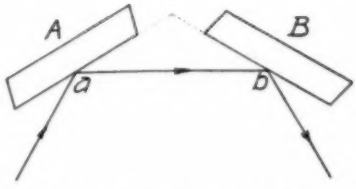

Fig. 1. Symmetrical ray selected by the bicrystalline reflection.

calcite crystal falls upon the face of a second calcite crystal and is again reflected into an ionization chamber. One or both of these crystals is turned slightly about an axis in the plane of the reflecting face and the ionization currents in the ion chamber are plotted as a function of the rocking angles of the crystal. For any given angle setting the two successive calcite reflections select out of the entire x-ray spectrum an exceedingly sharply defined narrow region of wave-lengths.

Precisely what angle determines the wave-length selected by the double x-ray reflection? Is it the angle through which one crystal rotates with respect to the slit system? Obviously not, since the horizontal slit width has nothing to do with the resolution of the double spectrometer. Neither do the pivots about which the crystals rotate constitute in any sense the system of reference with respect to which the rotation must be measured which determines the selected wave-length. The authors wish to emphasize most strongly that *the important thing is the dihedral angle formed by the two crystal faces themselves.* Let us consider for simplicity the case of first order reflection from two similar calcites in the anti-parallel position (1, 1). Fig. 1 represents the dihedral angle formed by the two crystals. Obviously the only rays which can be reflected twice selectively in the first order by both crystals are the

[7] Allison & Williams, Phys. Rev. **35**, 149 (1930).

symmetrical rays which make the same glancing angle at crystal A as at crystal B. A symmetrical ray, ab, is shown in Fig. 1 passing from crystal A to crystal B.

Define a plane *normal to the dihedral angle* formed by the crystal faces which for brevity and in accord with other writers we will call the "horizontal plane," (plane of the paper in Fig. 1). Now the ray, a, b, need not be parallel to the "horizontal plane" in order that it shall make equal glancing angles at each crystal and therefore be reflected. Such a ray oblique to the horizontal plane will in accord with Davis' terminology be said to have an angle of vertical divergence namely the angle α of obliquity with the horizontal plane. The projection of such an oblique ray will in Fig. 1 still be represented by the line, a, b, but the ray will in space actually suffer reflection at both crystals under a smaller glancing angle than rays which are not oblique. See Fig. 2.

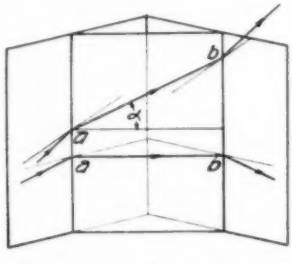

Fig. 2. Horizontal and oblique symmetrical rays.

We can assert then that the glancing angle (Bragg angle) *selected by the process of the double selective reflection* is half of the supplement of the dihedral angle between the crystal faces for horizontal rays and less than this for oblique rays. The band of wave-lengths selected then by the double reflection has a sharp limit on the long wave-length side determined only by the dihedral angle between the crystals. The band selected can be made as narrow as one pleases by limiting the vertical divergence.

Nothing in the above argument is made to depend on or refer to the pivots or axes of rotation of the crystals. It is of course obviously desirable that these axes of rotation should be parallel to the edge of the dihedral angle formed by the two crystal faces in order readily to permit the measurement of that dihedral angle and also to maintain the "horizontal ray" in a permanently fixed position with respect to the frame of the apparatus as the crystals rotate. The pivots, however, have nothing at all to do with the selective action of the double reflection and the dihedral angle between the crystals has everything to do with it. If this very fundamental fact is remembered all uncertainty as to the effect of various errors of alignment, etc., will vanish.

Band Pass Filter Width

The theoretical spectral intensity curve of the wave-length band selected from a uniform or "flat" spectral energy distribution by the double crystal reflection in the (n,n) position with perfect crystals is shown in Fig. 3. It is

bounded on the long wave side by a vertical discontinuity and falls off on the short wave side more gradually, meeting the axis of abscissae so as to have a base breadth $\Delta\lambda$ related to the maximum vertical divergence permitted by the system of lead stops limiting the x-ray beam. Referring to Fig. 4 let θ_0

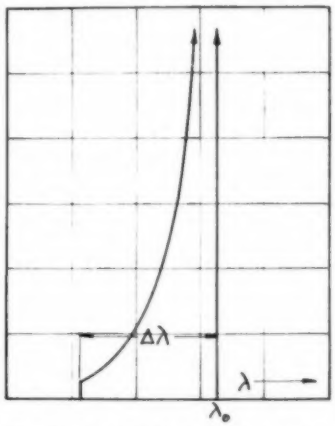

Fig. 3. Spectral intensity distribution selected by geometry of bicrystalline reflection *with crystals fixed*. This curve is not to be confused with the *shape of a spectral line* obtained by plotting reflected x-ray intensity against the dihedral angle between the crystals (or half of its supplement). Such line shapes are due to the overlapping of the "natural" line with the above curve as the latter is displaced spectrally with rotation of the crystals. The equation of the above curve is $y=k/[2(\lambda_0-\lambda_\alpha)\lambda_0]^{1/2}$; $\lambda_0(1-\frac{1}{2}\alpha^2)<\lambda_\alpha<\lambda_0$ calculated on the assumption that x-ray intensity is *uniformly distributed* over the permitted range of vertical divergences. The curve has a finite *area* in spite of the infinite *ordinate* at λ_0. In a spectral exploration as such a curve progressively overlaps a spectral line the intensity will therefore always remain finite.

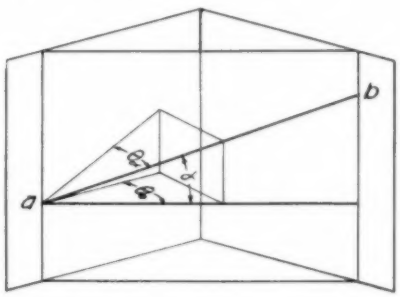

Fig. 4. Dependence of glancing angle on vertical divergence.

be the Bragg angle for a horizontally reflected ray, θ_α the Bragg angle for a ray of vertical divergence α. Then from the geometry of the case

$$\sin\theta_\alpha = \sin\theta_0 \cos\alpha$$

and since

$$n\lambda/2d = \sin\theta$$

we have

$$\lambda_\alpha = \lambda_0 \cos\alpha$$

$$\Delta\lambda = \lambda_0 - \lambda_\alpha = \lambda_0(1 - \cos\alpha)$$

and since in practice α is restricted to small values we have as a good approximation

$$\Delta\lambda = \tfrac{1}{2}\lambda_0\alpha^2.$$

Distortion of Lines by Vertical Divergences

The characteristic curve of Fig. 3 which may be regarded as the "frequency response curve" of the spectrograph for any given setting of the crystals displaces itself bodily toward longer wave-lengths as the dihedral angle between the crystal faces closes up. In this exploring process if a sharp line is encountered at some particular wave-length the ionization chamber will respond abruptly on the *short* wave side of the line and will diminish more gradually as the characteristic exploring curve moves to the *long* wave side of the lines. For this reason the distortion of spectral lines by the geometrical effect of vertical divergence alone is the *reverse* of Fig. 3, the discontinuous edge being on the *short* wave side. A good example of such distortions appears in Fig. 11 reproduced from a previous article[8] published by the authors. It is an easy matter however to so limit the vertical divergence that its effect in broadening spectral lines is negligble in comparison to the effects of crystal imperfections and natural x-ray line breadths combined.

Objections to Rocking Only One Crystal

The fact that the rays selected by the mechanism of the double reflection are symmetrically orientated with respect to the dihedral angle between the crystal faces immediately suggests that in exploring the spectrum *both* crystals should be simultaneously rotated in equal and opposite directions with respect to a plane through their axes of rotation.

As a matter of fact however most double spectrometers are built so that only one crystal is rotated in exploring the spectrum. This necessitates rotating the other crystal from time to time and also changing the relative position of the two crystals to prevent the beam from falling partly or wholly off the reflecting faces. As one crystal alone is rotated the selected beam must of necessity progress across the faces of the two crystals in order that it shall continue to make equal glancing angles with both crystal faces. The objections to this procedure are:

1. The crystals may present different reflecting powers in different parts of their surfaces so that spurious intensity fluctuations would be introduced in a spectral exploration. In particular all calcite cleavage faces have multitudinous small "steps" where the fracture changes abruptly from one plane to another one parallel to it. At glancing angles such steps obviously cast shadows in the reflected ray which will diminish its intensity in different degrees according to whether the beam falls on a part of the surface with high steps or a part in which steps are nearly absent. If the beam is obliged to migrate across the crystal face these steps will surely introduce undesirable spurious fluctuations. Even though the beam remains centered at one point of the crystal surface the area of crystal surface employed in reflection will

[8] DuMond and Hoyt, Phys. Rev. **36**, 799 (1930).

change with the glancing angle and some spurious fluctuations may thus be introduced by cleavage steps. These must however be regarded as an irreducible minimum.

2. If the source of radiation is not a point but has "horizontal" extension so as to permit reflection of one wave-length over a considerable area of the crystal a part of the beam which would otherwise be reflected may fall off one edge of the crystal introducing again spurious intensity fluctuations in a spectral exploration.

3. To avoid the above danger either very long crystals or a much reduced reflecting area must be used, both of which are rather serious difficulties.

4. The initial task of aligning the double spectrometer and locating a given spectral line is much harder in the instruments whose crystals do not rotate simultaneously.

As a corollary to what has just been said it is evidently desirable also to maintain the focal spot of the x-ray tube or other radiation source as well as the ionization chamber window always so situated with respect to the spectrometer that on one hand the selected beam from the tube will remain centered on the same reflecting region of the crystal faces for all glancing angles and on the other hand the selected radiation will always strike the ion chamber window at the same point. It is easy to see that large spurious fluctuations could be introduced by poor alignment of the beam entering a narrow ion chamber window and even with a broad window the transparancy of the window might not be uniform over its area.

It seemed desirable to divorce the design of the double spectrometer completely from the single spectrometer and produce an instrument suited to the requirements of a large group of problems likely to be attacked without aspiring to achieve one so universal in its applicability that it would perform none of its functions well.

Design of the Spectrometer

Fig. 5 is a general view of the spectrometer. Two circular tables A turning on conical pivots with accurately parallel axes support the crystals. The interpivotal distance is 5 inches. The pivot holes are bored in a single bed block of steel B, situated under the front end of the instrument. Two flat steel levers extending from the pivots to a similar steel bed block, C, under the rear end of the instrument can slide laterally, opening and closing like scissors, on top of this block so as to give equal and opposite rotations to the crystal tables. The levers are given their motion by a transverse shaft D, with right and left hand threads passing through nuts pivoted to the ends of the levers. The shaft is prevented from translating axially by a thrust bearing E half way between the levers. This bearing which has no axial play at all has sufficient lateral play to permit the screw shaft to translate in the direction of the crystal pivots as the levers spread apart. The action of the entire system is such that the crystal pivots and the driving nuts at the opposite ends of the two levers always stand at the four corners of a perfectly symmetrical isosceles trapezoid whose base is the screw shaft, whose sides are

the levers, and whose top is the line of centers of the crystal pivots. The top and sides are of constant length but the base and hence the altitude varies. It is for this reason that the thrust bearing on the screw provides for a slight lateral translation of the screw shaft. This same screw shaft carries a brass drum *F* on one projecting end on which the scale of glancing angles is engraved. The smallest divisions on this drum represent ten seconds of arc for the glancing x-ray reflection angles, and are separated by about three mm. A very important part of the design is a helical spring *G* running between two short posts on the under side of the two levers. The tension of this spring holds the levers together thus completely removing all backlash in the screw, nuts and pivots. The crystal tables are provided with angle scales engraved on their peripheries to facilitate setting. The levers can be clamped to and

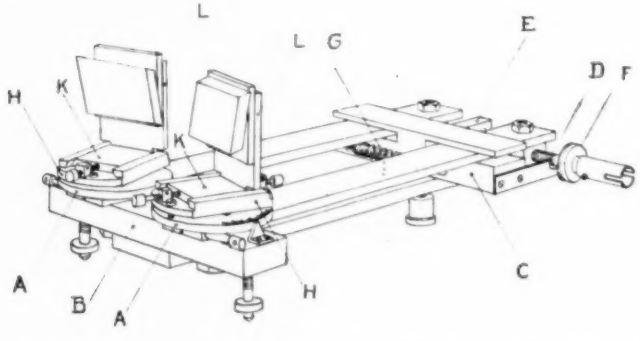

Fig. 5. Double spectrometer providing equal rotation of both crystals with respect to the line of pivot centers.

unclamped from the crystal tables in the same way as the tangent screws on a spectrometer or engineer's transit. The crystal tables are provided with removable false tops *H* which can rock about a horizontal axis. This is accomplished by two steel ball bearings lying between the crystal table disk and the false top in slight conical depressions provided for them and two opposing screws which clamp the false top to the crystal table with any desired slight inclination to the level. This adjustment is provided to permit of making the crystal faces accurately parallel to the axes of the pivots during the initial optical adjustment. A carriage *K* bearing the vertical crystal support slides in ways provided on each false top. This adjustment permits the crystal face to be brought in coincidence with the axis of rotation during the initial adjustment. The crystals are each fastened to a brass plate at three points with a very small quantity of beeswax. The brass plate can be fastened to the vertical crystal support *L* with two screws passing through holes large enough to permit of some adjustment in the position of the crystals. The vertical crystal support has a large hole bored through it at the point corresponding to the center of the crystal face. The reason for this hole is to permit sighting with a telescope and Gauss eyepiece at either side of a small interferometer plate which takes the place of the crystal during some of the initial adjustments. The entire spectrometer stands on leveling screws.

This instrument was very inexpensive to construct. The frame was built of pieces of cold rolled steel of rectangular section. No hand scraped surfaces were found necessary nor any precise circular divided scales. The one accurate requirement was that the pivot holes in the bed block *B* should have their axes as nearly parallel as possible. The spectrometer was built by one man in about five and one half days but in spite of its cheapness and simple construction a large amount of surprisingly precise work can be done with it.

The Subsidiary Rotating Mechanism

As before stated the quantities measured with the double spectrometer are: first, the angle between the crystals[9] and second, the intensity of the twice reflected x-rays. The spectrometer just described measures the first quantity with high precision and reproducibility. It is however an important refinement to provide motion of the ionization chamber and x-ray source relative to the spectrometer in order to avoid the errors caused by shifting of the beam across the crystal faces and kindred objections already mentioned. It should be understood however that the requirement of precision in the motion of source and ion chamber is not as exacting as it is in the angular motion of one crystal relative to the other since the precise wave-length selected by the double reflection does not depend on the position of source or ion chamber so long as these are so situated that some radiation can suffer the double reflection. The wave-length selected by the double reflection depends wholly and solely on the angle between the crystals and it is this quantity which must be and is measured precisely and reproducibly on the drum of the spectrometer.

The motion of x-ray source and ion chamber relative to the spectrometer in the instrument here described is accomplished in such a way that the ion chamber remains stationary relative to the room. This means that relative to the room the spectrometer rotates about a center in line with the axis of rotation of the second crystal and at twice the rate of the second crystal. At the same time relative to the spectrometer the x-ray source rotates about a center in line with the axis of rotation of the first crystal at twice its rate of rotation. The scheme of holding the ion chamber stationary was adopted in order to permit the use of a short unarticulated vacuum sleeve surrounding a short lead wire of low and perfectly constant capacity connecting the ion collector to the electrometer. The ion chamber could probably be permitted to move relative to the room by using a vacuum tube amplifier such as has recently been developed for The General Electric Company in a shielded housing attached to the ion chamber to replace the electrometer. There is some question as to whether the enormous sensitivity, stability and reproducibility attainable with the Hoffmann type vacuum electrometer can be matched with the amplifier tube, and work is now being started to investigate the possibilities of this method in connection with a vacuum double crystal spectrometer now in process of design at this Institute.

[9] The angles for which the drum is calculated are half the supplement of the dihedral angle between the crystals to facilitate their direct interpretation as glancing angles.

The above mentioned relative motions are obtained by means of two rotating false table tops of ply wood best shown in Figs. 6, 7. Ply wood was used instead of metal because the presence of the x-ray tube fed with high voltage made an insulating material convenient. The ply wood has proved to be quite free from warping and entirely satisfactory. The upper table top, *F*,

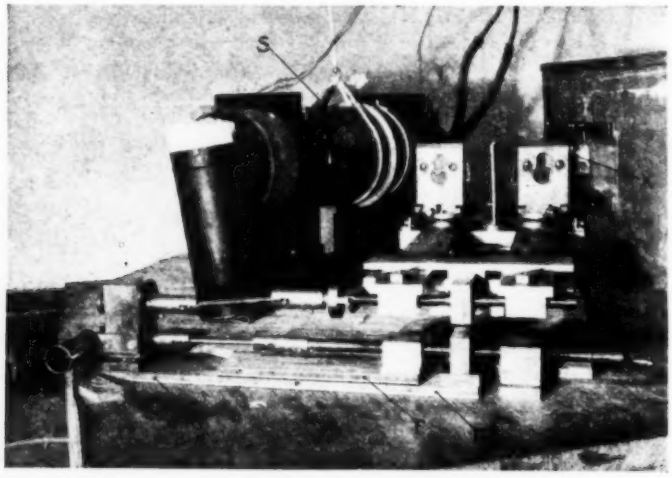

Fig. 6. General view of spectrometer, rotating table tops, rotating mechanism, and x-ray tube housing.

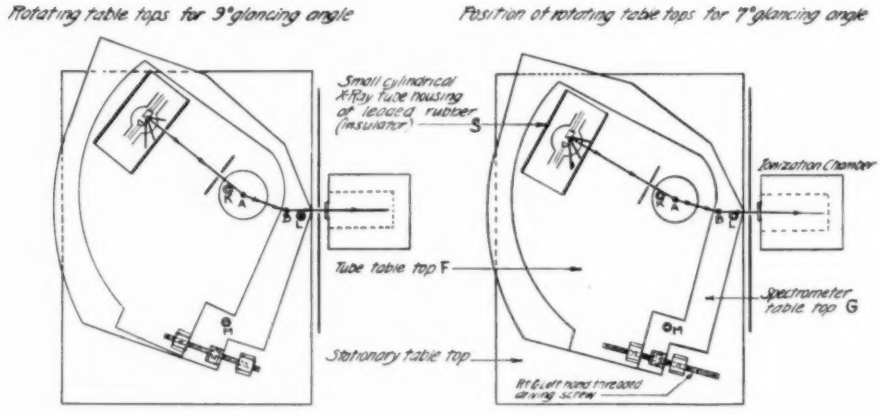
Rotating table tops for 9° glancing angle
Position of rotating table tops for 7° glancing angle
Small cylindrical X-Ray tube housing of leaded rubber (insulator)
S
Ionization Chamber
Tube table top F
Spectrometer table top G
Stationary table top
Right hand threaded driving screw

Fig. 7. Schematic diagram of table tops.

Figs. 6 and 7, carries the source of x-rays *S*. It rotates on a pivot centered at *A* consisting of a disk of ply wood 5 inches in diameter fixed to the second false table top *G*. This second table top in turn rotates on a stationary pivot centered at *B* and attached to the stationary table top. The centers *A* and *B* are separated by the same distance as the interpivotal distance on the spectrometer. The spectrometer rests entirely on the second table top *G*, the position of its three feet being at *K*, *L* and *M*. (The reason for the large diameter

pivot A is here obvious.) The pivots of the crystals are directly above and in line with the table top pivots A and B. The table tops are given the required angular rate of rotation by a second right and left hand screw with nuts and thrust bearing almost identical with the one on the spectrometer proper and having the same thread pitch. The two screws are connected through a simple type of universal joint transmission to gears having a ratio of two to one. The post supporting the gears is fastened to table top G and hence is stationary relative to the spectrometer. The entire mechanism is rotated by turning a shaft set at right angles to the screw shafts for accessibility the former driving the latter through bevel gears. This shaft terminates in a hollow brass tube T slotted axially on two diametrically opposite sides. A brass ball on the end of a long insulating handle can be inserted in this tube, and a rotary motion given to the tube by means of a diametral steel pin through the brass ball which engages in the slots of the tube. (The universal joints mentioned above are all of this simple ball and pin and slotted cylinder type and are very satisfactory.)

The kinematics of the table top drive is identical to that of the spectrometer. It is most easily grasped by taking as a reference, not the stationary table, but the false top G on which the spectrometer stands. The thrust bearing is attached to this top, and on turning the screw one nut causes the x-ray source on table F to rotate around the center A, relative to the spectrometer standing on G, at twice the rate of the crystal at A, while the other nut causes the table proper, and with it the room and the ion chamber, to rotate relative to the spectrometer standing on G around the center B, at twice the rate of the crystal at B. The same provision for lateral displacement of the shaft in the thrust bearing is provided for here as on the spectrometer. The whole device is of course open to the objection that it moves the source and ion chamber not accurately at twice the angular rate of the crystals, but rather at such a rate that the *sine* of one angle is twice the *sine* of the other angle. This however introduces far too small an error to cause trouble over the small rotations ordinarily required.

The lever arms of the spectrometer have each a range of motion of a little over one degree on each side of their position of mutual parallelism. The tables have each a range of two degrees on each side of their central position. A great deal of work can be done with even so small a range as this but slight modifications would suffice to increase the range. It is our practise to pick some definite angle setting near the midpoint of the range of glancing angles to be studied and then orient the crystals and other parts so that this angle corresponds to the zero position of the drum F (Fig. 5) with the levers in their central position. Details of this operation are described below.

Minor Spectrometer Details

The tube housing shown in Fig. 6 consists of a micarta tube large enough to contain the x-ray tube covered with a wrapping of two layers of the leaded rubber 1/16″ thick such as is used by Röntgenologists for protective aprons. This material which can be obtained from surgical supply houses has the

advantage of being opaque to x-rays, flexible, and a good insulator. Its uses are manifest to anyone who has worked in x-rays. Since it is an insulator one can construct small and therefore light boxes of it to contain x-ray tubes.

Fig. 6 was taken with a copper target tube in the lead rubber housing provided with a projecting goose-neck tube with a charcoal trap dipping into a liquid air container. The latter is plainly visable standing on table *F*. An investigation over a period of two months[10] was made with this copper target tube which had a mica window sealed on one side with DeKhotinsky cement. The liquid air and charcoal were found quite sufficient to maintain an excellent x-ray vacuum throughout the entire period.

The rotation required of the x-ray tube does not prevent the use of mercury pumps if necessary. These are installed under the table and are hung from table top *F* through holes bored in *G* and in the table top proper sufficiently large to permit the complete latitude of rotation. The pumps can be connected directly to the tube with an all-glass connection since no relative motion occurs between the two.

In order to insure smooth and easy operation of the table tops the bulk of the weight of the x-ray tube, housing, pumps and spectrometer is relieved by a simple system of lifting ropes going up to levers and counter weights hanging from the ceiling.

To give greater accessibility the entire table bearing all the parts so far described can be unclamped and moved away from the concrete wall shelf on which the detecting system consisting of electrometer and ion chamber stands.

Design of the Intensity Measuring System

The essential requirements are that the x-ray intensity measuring system shall have high sensitivity coupled with great stability and reproducibility. It is also convenient to have as large an x-ray window in the ion chamber as possible to make the task of alignment less arduous. Fig. 8 shows a cross section of the entire ion chamber-electrometer system. The chamber is a large cylindrical brass can *A* nickel plated inside and out. A disk shaped cover *B* fastens on to the end of the can with six screws, but is electrically insulated from the can with a gasket and insulating washers under the screws. The cover is made gas tight by pressing a fillet of red universal laboratory wax into the groove *C* provided for it. The $1'' \times 3''$ x-ray window in this cover is covered with a piece of paraffin impregnated Balsa wood—an extremely light yet stiff wood used in airplane model construction—with the grain running across the short dimension of the opening. The wood is attached to the cover with beeswax. The inner surface of the wood is coated with aluminum beryllium alloy 0.0002 inches thick making contact with the metal cover. The purpose of this coating is completely to define the potential all over the window so as to insure that the ions formed in this vicinity will not fail to be collected and also to prevent electrometer disturbances due to charges on the window inducing fluctuating charges on the collector.

[10] Dumond and Hoyt, Phys. Rev. **36**, 799–809 (1930).

A grid *D* of No. 36 nickel wire wound on and spot welded to a light nickel wire frame extends back from the window and surrounds the collector. This grid is supported on the brass cover *B* and by means of an external wire connected to the cover is brought to the potential of about 135 volts above ground, furnished by radio *B* batteries. The rest of the can which stands in contact with the electrometer housing is grounded.

The collector is led out of the can through a quartz insulator and as the can is itself grounded no guard ring is necessary. The collector of nickel wire can be fastened with a set screw into a brass cap on the top of the quartz

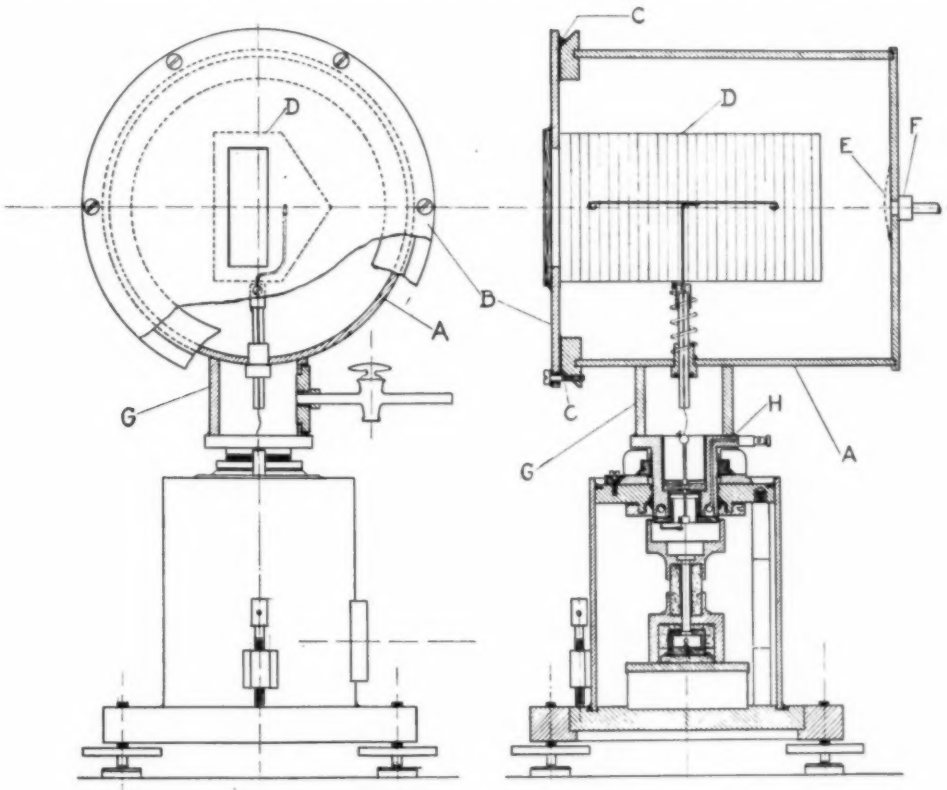

Fig. 8. Complete cross section of x-ray detecting system.

insulator. This collector is put in place through the x-ray tube window just before sealing on the Balsa wood cover. A small piece of fine mesh nickel screen *E* is welded over the inside opening of the gas connection *F*. This saves having to shield the glass tubes leading into the ion chamber by the usual method of covering them with tin foil.

The purpose of the internal grid is to minimize the fluctuations in the natural leak of the system caused by alpha-particles from the walls of the ion chamber. The space of about 5 cm from grid to chamber walls filled with about an atmosphere of methyl bromide accomplishes this very well.

The gas outlet from the ion chamber leads to a mercury manometer on

which any change in the methyl bromide pressure can be read. There is a glass cock for filling and a drying tube in constant connection with the chamber. It is important to keep the quartz insulator dry.

A fine No. 40 wire passing through the quartz insulator connects the collector to the highly insulated suspension of the Hoffman type electrometer. The connection is made through a short evacuated sleeve G which is made vacuum tight against the top flange of the electrometer with a fillet H of red universal wax.

Save for the flat flange just mentioned and for the use of universal wax instead of rubber gaskets to make the cylindrical case of the electrometer vacuum tight there are no changes in the design of the Hoffmann type vacuum electrometer. This remarkably satisfactory instrument has been completely described by its designer[11] and will not be given space in this article.

Sensitivities and Reproducibilities Obtained

The spontaneous fluctuations in readings with this x-ray measuring system correspond to about 5×10^{-16} amperes. These fluctuations are the limiting feature at present on the smallest currents readable. They are only due in part to alpha-particles from the walls of the chamber. Their source is being studied and it is hoped that they can still be very greatly reduced. With these fluctuations at the present value currents of 6×10^{-14} amperes can be read with a reproducibility of one percent in a single reading of the order of a minute's duration. Currents of 10^{-15} amperes can be read with fair accuracy by taking several somewhat longer readings and averaging. We have succeeded in detecting the satellite $K\alpha_{34}$ of copper at only 1.75 KV above its critical exitation voltage with this outfit. This satellite had spectral ordinates protruding above the background *only one four hundred and fiftieth* as high as the maximum ordinate of $K\alpha_1$ its parent line six X.U. away.

The electrometer has a very stable zero that will remain constant within a few millimeters for months. The instrument as now used has a rather stiff suspension. Mr. Julius Pearson of this institute has succeeded recently in producing Wollaston wire suspensions for the Hoffmann electrometer with much longer period than the one now in use. The present rather low volt sensitivity could then be increased to about 10000 mm per volt. The capacity of the whole insulated system of electrometer and ion chamber is about 12 electrostatic units. We therefore do not believe the possibilities of the above described system are exhausted with the results here reported.

Technique of Operation

Method of orientating the crystals initially.

The procedure about to be described accomplishes in practice the fulfillment of the following required conditions. (These conditions are not all equally exacting.)

1. The crystal reflecting planes must be parallel to the axes of rotation of the crystal table pivots.

[11] G. Hoffmann, Ann. d. Physik **52**, [7] 665–708 (1917).

2. The reflecting surfaces of each crystal must coincide with the axis of rotation of its pivot.

3. The two crystal reflecting planes must make equal angles with the plane through the axes of the pivots.

4. The dihedral angle between the two crystal planes must be set for some known value corresponding to the "zero" drum position of the screw and lever crystal turning mechanism to facilitate "finding" a spectral line.

The first condition is quite important since the accuracy with which the dihedral angle between the crystal faces can be determined and hence the accuracy to which the wave-length scale is known depends on this. Also if condition No. 1 is not fulfilled the so called "horizontal" plane i.e. the plane normal to the dihedral angle formed by the two crystals may be quite oblique to the pivot axes and the general line of the x-ray apertures causing an unsuspected vertical divergence of the rays from the "horizontal" plane. Requirement No. 1 evidently becomes more rigid due to both of these last named effects as the crystal planes approach parallelism.

The second condition cannot be fulfilled very rigidly since the plane of the face of the crystal is ill defined on account of the unavoidable cleavage steps. Its purpose is to minimize the gliding of the selected beam across the crystal face as the crystal rotates.

The third condition merely insures that the radiation from the first to the second crystal shall pass parallel to the line of centers of the two pivots thus facilitating the initial alignment of the apparatus. It need only be fulfilled to within a few minutes of arc.

The fourth condition is merely a convenience. We have however invariably succeeded by the technique about to be described in locating the crystals so closely that it was not necessary to *hunt* for a known spectral line over a region much greater than its own observed breadth.

A small optical spectrometer with collimator removed and with a Gauss eyepiece in the telescope is used. Calcite cleavage faces as Allison has noted are poor reflectors of visible light at normal incidence. It is however, possible to obtain a sufficiently intense image of the cross hairs for visibility if one employs a strong but small incandescent light, well shielded from directly striking the eye to illuminate the Gauss eyepiece. A small black disk of paper, say 0.5 mm in diameter, should be carefully attached with a little shellac to the intersection of the cross hairs. The period from a set of gummed letters such as are used to stick on drawings makes a good disk. This makes a spot large enough to see in the faint reflected image. Considerable patience is required in hunting for the faint image but the telescope and Gauss eyepiece furnish such an accurate method of alignment that it is worth while spending an hour or so, especially as it need not be done often.

A glancing angle θ_0 is first chosen as a setting for the crystals when the angle drum is set at zero and the levers and drum are then adjusted to that zero position. The optical spectrometer is then set on a bench in front of the x-ray spectrometer in such a position that in sighting the telescope alternately first at crystal one and then at crystal two the optical telescope must turn

through approximately the angle $2\theta_0$. The pivot axes of both spectrometers are then rendered accurately vertical with the leveling screws by taking reversed readings with a good level. A pair of light plumb lines of white silk thread are then adjusted so that they define a plane the perpendicular bisector of the plane through the two pivot axes. This can be done very precisely with a trammel which is engaged at one end in the conical center holes on which the crystal pivots were turned and is used as a "feeler" to strike four arcs in space centered each from a pivot and just making contact on either side with the plumb lines. The geometry is the simple Euclidian construction for a perpendicular bisector. The telescope is now adjusted to sight accurately down the line defined by the two plumb lines. The index of the divided circle on the optical spectrometer is then set on zero and clamped and the two spectrometers are rechecked for level and sealed to the bench with shellac or wax. The next step is to render the line of collimation of the telescope accurately normal to the pivot axes of the x-ray spectrometer. (Incidently when this is done the line of collimation of the telescope will be horizontal.) A small plane parallel glass interferometer plate is stuck on with wax over the hole in the vertical brass crystal support and trial reflections are made from both sides of this plate turning the crystal table through 180° each time and correcting half the error at the plate and half in the level adjustment of the telescope (not the spectrometer of course) until the Gauss cross hairs coincide with their reflected image equally well with the plate facing either way. This condition must be fulfilled for both crystal pivots. The telescope collimation line is now accurately normal to both the x-ray and optical spectrometer pivot axes and its level must not be subsequently disturbed. The plane parallel glass plate is now removed and the calcites ready mounted on their brass plates are attached to the vertical crystal supports with screws. Care should be taken to locate them symmetrically over their axes of rotation at the same height above the turntables. At zero reading on the divided circle of the optical spectrometer the telescope is now normal to the plane through the axes of the x-ray spectrometer pivots. Turn the telescope through the angle θ_0 to right or left of this point as read on the divided circle of the optical spectrometer and sight at the crystal face. The crystal table is then unclamped and orientated and the false top tilted until the cross hair image normally reflected from the calcite coincides with the cross hairs. The crystal reflecting face is brought into coincidence with its pivot axis by screwing the crystal support carriage diametrically across until a tangential view of the face with the crystal rotated to either side the stationary line of sight shows no displacement. This should be done after rendering the crystals vertical but before finally clamping them to the levers at the correct horizontal orientation defined by the telescope.

The entire procedure requires three or four hours and need only be performed once for each pair of crystals used unless some accident disturbs them. The divided circles on the crystal turn tables should be carefully read and recorded.[12] This gives a fiducial reference from which the proper

[12] A scale capable of being read to within a few minutes of arc is sufficiently accurate.

settings for other glancing angles can be made without having further recourse to the Gauss eyepiece reflection method.

Alignment of other parts

It is necessary also to align the source of x-rays in the proper position with respect to the spectrometer. Furthermore the entire system of source and spectrometer must be aligned with respect to the ion chamber so that the rays will enter its window. We have found that this can all be done very conveniently after the crystals have been aligned by cutting a templet out of Bristol board such as is shown in Fig. (9). The edge segments A, B, of this templet are fitted against the crystals and the edges C, D, then point respectively in the direction of the source and the ion chamber window when their locations are correct. If the templet is carefully laid out with a precision vernier protractor and accurately cut with a razor blade held against a steel

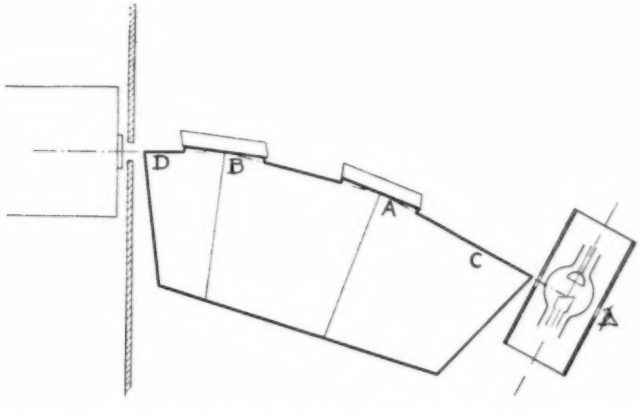

Fig. 9. Cardboard templet used in aligning table tops and x-ray tube.

straight edge the method is accurate to within a few minutes of arc. It is helpful to lay out the normals to the crystal faces on the cardboard. When the cardboard is properly orientated against the crystal faces the reflected image of these normals should line up straight with the normals themselves.

Needless to say the cardboard templet is laid out for the glancing angle θ_0 corresponding to the mid value of the spectral range chosen for the particular work to be done and the above described alignment procedure must be carried out with the spectrometer and the ply wood table tops set at the midpoint of their travel, i.e. at the point where the pivots of the nuts on the right and left hand screw shafts are separated by the same distance as the two crystal pivots.

Elimination of Background

The detection and accuracy of measurement of faint lines is limited by the intensity of the x-ray background. Also the shapes and positions of lines are distorted by background structure. It is therefore essential to consider means of reducing background. The causes of background are:

1. Selective reflection of continuous or "white" radiation from the source.

2. Natural leak of ion chamber and electrometer system.

3. Amorphous or non-selective crystal scattering and fluorescent radiation excited in the crystals.

4. Leakage of x-rays without suffering double reflection in the prescribed orders.

It is not always desirable to eliminate all of the above factors. For example if one is interested in studying either the continuous "white" radiation or diffuse lines partaking of the nature of a continuous distribution No. 1 should obviously be retained. Methods of controlling the above sources of background are in the above order as follows.

1. The intensity of white radiation adjacent to a spectral line as measured by the ionization chamber relative to the intensity when the crystals are set for the peak of a line can be very widely controlled by controlling the cross-fire or vertical divergence of the x-ray beam. As long as the band of wave-lengths selected by the bicrystal reflection is of larger order of magnitude than the natural line breadth, diminution of this band width reduces the background ordinates faster than the line ordinates. The vertical divergence angle is controlled by the height of defining lead openings and their distance apart. In the present instrument one such opening provided with adjustable jaws is arranged in the heavy lead wall dividing the spectrometer and x-ray source assembly from the electrometer and ion chamber.

2. Precautions for minimizing "natural leak" by means of the internal grid in the ion chamber have already been described as have also the use of quartz insulators kept dry with phosphorous pentoxide and the use of vacuum shields and a vacuum electrometer.

3. It is well known that scattering of x-rays is of two types namely modified and unmodified scattering. It is also well established that selective crystal reflection is solely of the unmodified type since this is the only type in which the incident and reflected beams are coherent. As regards modified scattering however the two calcite crystals might as well be two pieces of wood or graphite. All wave-lengths of radiation from the x-ray tube can be scattered into the ion chamber by the Compton modified scattering process independent of the angle setting of the crystals. The ratio of modified amorphous scattering to unmodified selective scattering increases with the hardness of the radiation. It is evident therefore that a great advantage in background reduction will be gained by filtering out all radiations from the source harder than those which are in the range being studied. This is especially true when the x-ray tube is being operated at voltages considerable higher than the critical voltage necessary to excite the radiation being studied. Thus in the study of the satellite $K\alpha_{34}$ of copper (parent, $K\alpha_1$) we have found that a filter made of a piece of nickel foil rolled out to 0.0005″ thickness was extremely effective in reducing the ratio of background ordinates to line ordinates.

The same procedure evidently reduces the background due to char-

acteristic fluorescent radiations excited in the crystals themselves by the harder regions of the continuous spectrum from the x-ray tube.

4. Finally a judicious disposition of lead shields will be found to reduce the background very materially. A vertical lead knife edge should be placed

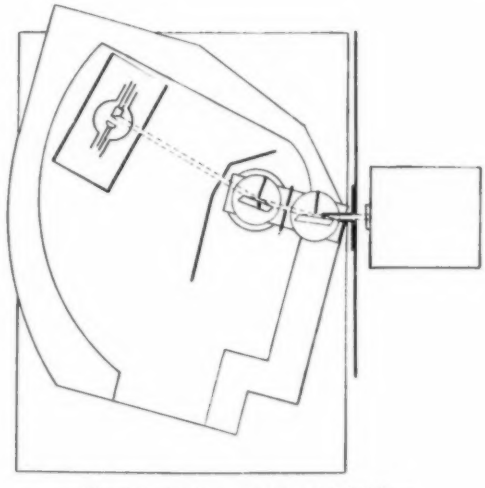

Fig. 10. Scheme of lead shielding.

normal to the reflecting face of each crystal, close enough to the face to prevent any radiation from reaching the ion chamber without suffering the double reflection. These knife edges if placed too close will cut down the

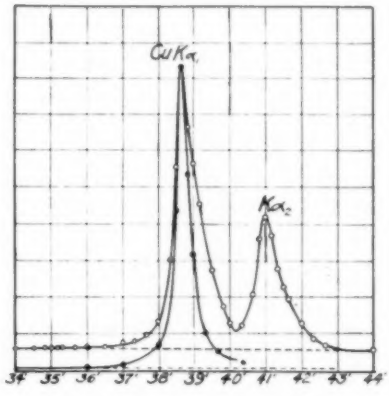

Fig. 11. Comparative curves of $\alpha_{1,2}$ before and after taking the precautions outlined in text for reducing relative background.

available intensity. A little experimentation is the best guide in this matter. A shield with a rectangular window of the proper dimensions placed symmetrically between both crystals is helpful as is also an extensive lead shield near the first crystal between it and the tube. Most effective of all is the use of a lead snout of rectangular cross section which hangs in front of the adjustable lead window in the lead partition between the spectrometer and

the detecting system and which projects forward to the second crystal. See X Fig. 6. The disposition of this snout if properly chosen will greatly reduce the solid angle from which stray radiation can enter the ionization chamber. Fig. 10 shows the system of lead shields.

The degree to which relative background can be reduced is shown in Fig. 11 by a comparison of the spectral curves of $K\alpha_1$ of copper before and

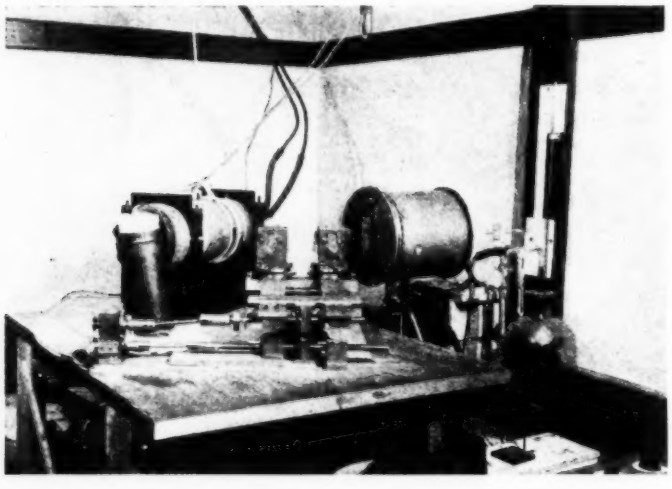

Fig. 12. General view of apparatus with lead shield between spectrometer and ionization chamber removed.

after taking the various precautions discussed above for reducing background. The ordinates of the curve with the low background have been plotted to a scale chosen so as to make both curves coincide at the maximum value of $K\alpha_1$. The relative reduction of background is very evident.

Fig. 12 is a general view of the apparatus with the lead shield removed from between ionization chamber and spectrometer.

THE VALUE OF e/m BY DEFLECTION EXPERIMENTS

By G. E. Uhlenbeck and L. A. Young
University of Michigan

(Received November 10, 1930)

Abstract

To clarify the discussion as to whether or not a quantum mechanical treatment of the motion of electrons in magnetic fields will lead to a formula for e/m, differing from that obtained by classical electro-dynamics the following problem was solved. A uniform magnetic field in the z-direction exists in the half-space $x>0$. A plane monochromatic de Broglie wave, travelling in the positive x-direction representing electrons of arbitrary energy, impinges normally on the plane $x=0$. Solutions of the wave equation were found fulfilling appropriate boundary conditions at the plane $x=0$. Currents are calculated quantum mechanically and compared with the corresponding classical expressions. It was found that for electrons possessing energies of the order of magnitude used in deflection experiments, no *observable* deviations from classical results are predicted. Another quantum mechanical effect is diffraction at slits. Simple approximate calculations show that this effect can produce a fractional error in e/m of the order of the de Broglie wave-length divided by the slit width. These results are opposite to the conclusions reached by Page. We may remark that he solved a problem of "stationary states" which does not represent the actual experiments.

IN A recent issue of the Physical Review Professor Leigh Page[1] tried to explain the difference in the value of e/m obtained from deflection experiments and from spectroscopic evidence on the basis of quantum mechanics. This was later criticized by Eckart,[2] first, he doubted certain approximate calculations of Page which may, however, be shown to be correct;[3] second, he referred to articles of Kennard[4] and Darwin[5] which prove quite conclusively that a wave packet representing an electron in a uniform magnetic field moves as in the classical theory. To this we may remark that in the deflection method the measurements are not made with a single particle but are statistical since we work with beams of electrons. However the work of Page does not seem conclusive because he considers the solutions of the wave equation corresponding to the completely quantized motion of isolated electrons in a magnetic field of infinite extension; whereas in the deflection experiments we have to deal with a problem of "streaming."

§2. In trying to decide the question as to whether or not quantum mechanics will lead to results appreciably different from those of the classical theory we have considered the following problem. A homogeneous magnetic field in the x-direction fills the half-space $x>0$. Free electrons moving in the

[1] L. Page, Phys. Rev. **36**, 444 (1930).
[2] C. Eckart, Phys. Rev. **36**, 1014 (1930).
[3] L. Page, Phys. Rev. **36**, 1418 (1930).
[4] E. H. Kennard, Zeits. f Physik **44**, 347 (1927).
[5] C. G. Darwin, Proc. Royal Soc. **A117**, 258 (1927).

x-direction impinge on the plane $x=0$ and penetrate the magnetic field. Classically they will describe half-circles with centers on the plane $x=0$ and radii

$$r = \frac{cp}{eH} \tag{1}$$

where p represents the momentum of the particles. We find easily that in the magnetic field the components of the current density S are

$$S_x = 0 \quad S_y = \frac{2Ix}{(r^2 - x^2)^{1/2}} \tag{2}$$

and the total current $\int_0^r S_y\,dx = 2Ir$ where I is the current density of the incoming electrons. Quantum mechanically we have for $x>0$ the wave equation

$$\left\{\Delta_2 + \frac{2\pi i}{\lambda r}\left(x\frac{\partial}{\partial y} - y\frac{\partial}{\partial x}\right) - \left(\frac{\pi}{\lambda r}\right)^2(x^2 + y^2) + \left(\frac{2\pi}{\lambda}\right)^2\right\}\psi_1 = 0 \tag{3}$$

where Δ_2 is the Laplace operator for two dimensions and $\lambda = h/p$ is the de Broglie wave-length of the incident electrons. The incoming electrons are represented by a wave function $\psi_i = A \exp(2\pi i/\lambda x)$ and the outgoing electrons by $\psi_o = B \exp(-2\pi i/\lambda x)$ so that for $x<0$ the total wave function $\psi_2 = \psi_i + \psi_o$. We must seek solutions of (3) which fulfill the boundary conditions at $x=0$:

$$\begin{aligned} \psi_1 &= \psi_2 && \text{(a)} \\ (mv_x)_1\psi_1 &= (mv_x)_2\psi_2 && \text{(b)} \\ (mv_y)_1\psi_1 &= (mv_y)_2\psi_2 && \text{(c)} \\ \psi_1(\infty) &= 0 && \text{(d)} \end{aligned} \tag{4}$$

where

$$mv_x = \frac{h}{2\pi i}\frac{\partial}{\partial x} + \frac{e}{c}A_x$$

and

$$mv_y = \frac{h}{2\pi i}\frac{\partial}{\partial y} + \frac{e}{c}A_y.$$

In our case the components of the vector potential A_x and A_y are given by $A_x = -\frac{1}{2}Hy$ and $A_y = \frac{1}{2}Hx$. Making use of results given in a recent paper by Landau[6] we find that

$$\psi_1 = \phi(x)e^{\pi i xy/\lambda r} \tag{5}$$

is a solution of (3) if $\phi(x)$ satisfies the equation

$$\phi''(x) + \left(\frac{2\pi}{\lambda}\right)^2\left(1 - \frac{x^2}{r^2}\right)\phi(x) = 0. \tag{6}$$

[6] L. Landau, Zeits. f. Physik **64**, 629 (1930).

We may therefore write our boundary conditions (4) (conditions 4c is identically fulfilled)

$$\phi(0) = A + B \qquad (a)$$

$$\phi'(0) = \frac{2\pi i}{\lambda}(A - B) \qquad (b) \quad (7)$$

$$\phi(\infty) = 0 \qquad (d)$$

It will be shown later that the condition $\phi(\infty)=0$ will, for a given λ determine $\phi'(0)/\phi(0)$ so that we may write for convenience

$$\frac{\lambda\phi'(0)}{2\pi\phi(0)} = q(\lambda) \qquad (8)$$

where $q(\lambda)$ is a real quantity.
The first and second of the relations (7) then give

$$q(A + B) = i(A - B)$$

or

$$B = \frac{i - q}{i + q}A = Ae^{\pi i\tau}. \qquad (9)$$

The phase of the outgoing electrons therefore differs from that of the incoming electrons by $\pi\tau$, where

$$\cos \pi\tau = \frac{1 - q^2}{1 + q^2}. \qquad (10)$$

Thus

$$\phi(0) = A(1 + e^{\pi i\tau}). \qquad (11)$$

§3. The current density is in general given by

$$S_x = \frac{eh}{4\pi im}\left(\psi\frac{\partial\bar{\psi}}{\partial x} - \bar{\psi}\frac{\partial\psi}{\partial x}\right) - \frac{e^2}{mc}A_x\psi\bar{\psi}$$

with a similar expression for S_y. Substituting equation (5) and the vector potentials we find immediately

$$(S_x)_1 = 0 \quad (S_x)_2 = \frac{e}{m}\frac{h}{\lambda}(B\bar{B} - A^2) = 0. \qquad (12)$$

This latter expression is zero due to the fact that A and B are equal in absolute value from (9). The intensities of the incoming and outgoing waves are equal. Further

$$(S_y)_1 = -\frac{e}{m}\frac{h}{\lambda r}x\phi\bar{\phi} \quad (S_y)_2 = 0. \qquad (13)$$

At $x=0$ $(S_y)_1=(S_y)_2=0$. Continuity of the currents is therefore a consequence of the boundary conditions (4). Finally we can calculate the total current

$$\int_0^\infty (S_y)_1 dx = -\frac{ch}{\lambda r m}\int_0^\infty x\phi\bar{\phi}dx.$$

By integrating partially and using the differential equation (6) for ϕ and the fact that $\phi(\infty)=0$ it is found that

$$\int_0^\infty x\phi\bar{\phi}dx = \frac{1}{2}r^2(1+q^2)\phi(0)\bar{\phi}(0).$$

Substituting (11) and noting that $I=chA^2/m\lambda$ we find that

$$\int_0^\infty (S_y)_1 dx = 2Ir$$

which is just the classical value.

§4. To get a clearer idea of $(S_y)_1$, a quantity which would be measured in a deflection experiment, we must study the solutions of (6) in more detail. Introducing $\xi=2x(\pi/\lambda r)^{1/2}$, $\nu+\frac{1}{2}=\pi r/\lambda$ (6) becomes

$$\frac{d^2\phi}{d\xi^2}+\left(\nu+\frac{1}{2}-\frac{1}{4}\xi^2\right)\phi=0.$$

This equation is treated extensively in Chapter 16, page 341 of Whittaker and Watson "Modern Analysis." In their notation we obtain for a solution vanishing at $\xi=\infty$:

$$\phi(\xi) = aD_\nu(\xi) = ae^{-\xi^2/4}\xi^\nu\left\{1-\frac{\nu(\nu-1)}{2\xi^2}+\frac{\nu(\nu-1)(\nu-2)(\nu-3)}{8\xi^4}-\cdots\right\}$$

for large ξ (a is a constant to be determined from $\phi(0)$. If ν is an integer the series breaks off and we obtain the well-known harmonic oscillator eigenfunctions. This solution "connects" with the following solution for small ξ:

$$\phi(\xi) = a\left\{\frac{\Gamma\left(\frac{1}{2}\right)2^{\nu/2+1/4}}{\Gamma\left(\frac{1}{2}-\frac{\nu}{2}\right)}\xi^{-1/2}M_{\nu/2+1/4,-1/4}\left(\frac{\xi^2}{2}\right)\right.$$
$$\left.+\frac{\Gamma\left(-\frac{1}{2}\right)2^{\nu/2+1/4}}{\Gamma\left(-\frac{\nu}{2}\right)}\xi^{-1/2}M_{\nu/2+1/4,1/4}\left(\frac{\xi^2}{2}\right)\right\}$$

where

$$M_{k,m}(\eta) = \eta^{1/2+m}e^{-\eta/2}\left\{1+\frac{\frac{1}{2}+m-k}{1!(2m+1)}\eta+\frac{(\frac{1}{2}+m-k)(\frac{3}{2}+m-k)}{2!(2m+1)(2m+2)}\eta^2+\cdots\right\}$$

From this solution one can show easily that

$$q = 2(2\nu + 1)^{-1/2} \frac{\Gamma\left(\frac{\nu}{2} + 1\right)}{\Gamma\left(\frac{\nu}{2} + \frac{1}{2}\right)} \tan \frac{\nu\pi}{2} \tag{14}$$

$$\leqq \tan \frac{\nu\pi}{2} \text{ for } \nu \gg 1$$

thus

$$\cos \pi\tau = \frac{1 - q^2}{1 + q^2} = \cos \nu\pi$$

or

$$\pi\tau = \pi\nu. \tag{15}$$

Thus the phase shift between the incoming and outgoing electrons is completely determined in terms of ν and therefore in terms of the energy of the incident electrons. It may be worth while to remark that ν is very simply related to the number N of de Broglie wave-lengths on the circumference of the classical half circle

$$\nu = N - \tfrac{1}{2} \text{ or } \pi\tau = (N - \tfrac{1}{2})\pi$$

or since λ is usually of the order of 10^{-8} cm, ν is of the order of magnitude 10^8 to 10^{10}. For quantum numbers of this order of magnitude one would hardly expect to find the differences between classical and quantum mechanical predictions to be measurable.

§5. To add weight to this belief we may consider the character of the function $\phi(x)$ in more detail. This is best done by considering the Wentzel-Brillouin-Kramers[7] approximation. For $x > r$ $\phi(x)$ behaves as an increasing or decreasing exponential and to satisfy the condition $\phi(\infty) = 0$ we must choose the latter. We obtain

$$\phi(x) \leqq \frac{a}{(x^2 - r^2)^{1/4}} \exp\left\{ -\frac{2\pi}{\lambda\tau} \int_r^x (x^2 - r^2)^{1/2} dx \right\}.$$

This "connects" according to Kramers with the oscillatory solution for $x < r$

$$\phi(x) \leqq \frac{2a}{(r^2 - x^2)^{1/4}} \cos\left\{ \frac{2\pi}{\lambda\tau} \int_z^r (r^2 - x^2)^{1/2} dx - \frac{\pi}{4} \right\}.$$

We see immediately that this approximate solution determines $q(\lambda) = \lambda\phi'(0)/2\pi\phi(0)$ and we find for it again

[7] G. Wentzel, Zeits. f. Physik **38**, 518 (1926); L. Brillouin, C. R., Juli, 1926; H. A. Kramers, Zeits. f. Physik **39**, 828 (1926); A. Zwaan, Utrecht Dissertation, 1929; L. A. Young and G. E. Uhlenbeck, Phys. Rev. **36**, 1154 (1930).

$$q = \tan \frac{\nu\pi}{2}.$$

The constant a has to be determined from the value $\phi(0)$. We find from (11)

$$a = \frac{A(1 + e^{\pi i\nu})r^{1/2}}{\cos \dfrac{\pi\nu}{2}}.$$

Calculation of the current gives then for $x < r$

$$(S_y)_1 = \frac{4Ix}{(r^2 - x^2)^{1/2}} \cos^2 \left\{ \frac{2\pi}{\lambda r} \int_x^r (r^2 - x^2)^{1/2} dx - \frac{\pi}{4} \right\}. \tag{16}$$

The current, therefore, is "oscillatory" with an amplitude just twice the classical current. The distance between the maxima is, for small x, just $\lambda/2$ but increases as x approaches r. The distance Δ of the last maximum from $x = r$ is given by

$$\frac{2\pi}{\lambda r} \int_{r-\Delta}^r (r^2 - x^2)^{1/2} dx = \frac{\pi}{4}$$

or

$$\Delta = \frac{3^{2/3}}{8} \lambda^{2/3} r^{7/3}. \tag{17}$$

For $x > r$ the current is given by

$$(S_y)_1 = \frac{2Ix}{(x^2 - r^2)^{1/2}} \exp \left\{ - \frac{4\pi}{\lambda r} \int_r^x (x^2 - r^2)^{1/2} dx \right\}. \tag{18}$$

This current falls off very rapidly with increasing x, in fact in going a distance $n\Delta$ beyond $x = r$ the ratio of the current to the current at $x = r - \Delta$ is given by

$$\frac{1}{2(n)^{1/2}} \exp (- 2n^{3/2}). \tag{19}$$

This ratio is equal to 0.001 for $n \geqq 2.1$.

§6. These last results are perhaps doubtful since in the neighborhood of $x = r$ the approximation from which they were derived becomes invalid. We can, however, derive them more rigorously by observing that near $x = r$,

$$1 - \frac{x^2}{r^2} \leqq 2\left(1 - \frac{x}{r}\right).$$

Instead of (6) we have then

$$\phi''(x) + 2\left(\frac{2\pi}{\lambda}\right)^2 \left(1 - \frac{x}{r}\right) \phi(x) = 0.$$

This equation has been thoroughly discussed by Kramers (reference 7) and the solution which "connects" properly with the exponential and oscillatory solutions of (6) is found immediately to be

$$\phi(x) = \omega\left\{2\left(\frac{\pi r}{\lambda}\right)^{2/3}\left(1 - \frac{x}{r}\right)\right\} \tag{20}$$

$\omega(z)$ has been tabulated by van der Held (see Kramers, reference 7) and we find from his table

$$\Delta = \tfrac{1}{2}\pi^{-2/3}\lambda^{2/3}r^{1/3} \tag{17'}$$

and in traveling a distance 2.5Δ the current drops to 0.001 of its maximum value.

§7. Returning now to the value of e/m we must distinguish between two quantum mechanical effects. The first is the one discussed above. If we observed the maximum current we would find it displaced a distance Δ from the classical position. If we calculated e/m from

$$\frac{e}{m} = \frac{cv}{H}\cdot\frac{1}{r}$$

we would obtain too *large* a value. This is in the right direction to explain the discrepancy between the deflection and spectroscopic values of e/m but quantitatively the relative error due to this is of the order $(\lambda/r)^{2/3}$ which is about 10^{-6}. The observed relative discrepancy is 4×10^{-3}.

A second quantum mechanical effect in an actual deflection experiment would be diffraction at the entrance slit. A rough calculation based on the uncertainty principle shows that this can give a relative error in e/m no larger than λ/d where d is the slit-width. For actual cases this is of the order 10^{-6}. We conclude therefore that the quantum mechanical analysis of the deflection experiments cannot explain the observed discrepancy. One might still think of relativistic or spin effects as a possible explanation of the e/m paradox, but we have a feeling that the resulting corrections will also be extremely small.

Note added in proof: We regret that, in preparing this manuscript we overlooked the article of Charlotte T. Perry and E. L. Chaffee (Phys. Rev. **36,** 904; 1930) which seems to show quite conclusively that the discrepancy between the two values of e/m is due to an error in the experimental determination of the velocity of the electrons in the deflection experiments.

RELATIVISTIC WAVE MECHANICS OF ELECTRONS DEFLECTED BY A MAGNETIC FIELD

By Milton S. Plesset*
Sloane Physics Laboratory, Yale University

(Received November 3, 1930)

Abstract

It is shown that the relativistic wave equation for electrons in a uniform magnetic field leads to the same wave function as that already deduced by Page from the non-relativistic equation. As in the latter case the motion at right angles to the field is quantized.

An expression is found for the current density from the relativistic wave equation. The relativistic expression differs from the non-relativistic only by a constant factor which does not affect the calculation of the mean radii of curvature of the electron current.

Hence, for the relativistic case, as for the non-relativistic, the mean radius of curvature is less than that expected on the classical theory. It follows that the classical relativistic relation between ϵ/μ and the mean radius of curvature upon deflection gives a value of ϵ/μ which is too large.

THE non-relativistic Schrödinger wave equation which governs the motion of electrons in a uniform magnetic field has been solved by Page.[1] The solution which he obtains shows that the mean radius of curvature of the electron current is less than that given by the classical theory. An appreciable error is thus introduced in applying the classical relation to the determination of ϵ/μ from deflection experiments.

Since the energies of the electrons used in deflection experiments are so large, it was thought that a treatment of the problem by the relativistic wave mechanics would be of interest.

The Relativistic Wave Equation

The relativistic wave equation[2] for electrons in a magnetic field is

$$\nabla\cdot\nabla\psi - \frac{1}{c^2}\frac{\partial^2\psi}{\partial t^2} - \frac{4\pi i\epsilon}{hc}A\cdot\nabla\psi - \frac{4\pi^2}{h^2}\left(\mu^2c^2 + \frac{\epsilon^2}{c^2}A^2\right)\psi = 0 \qquad (1)$$

where A is the vector potential and μ is the rest mass of the electron. For a uniform field H in the X direction

$$A = -j\frac{H}{2}z + k\frac{H}{2}y.$$

Eq. (1) then becomes in cylindrical coordinates r, θ, x,

* Charles A. Coffin Fellow.

[1] Leigh Page, Phys. Rev. **36**, 444 (1930).

[2] L. Brillouin, J. de Phys. et Le Radium **8**, 74 (1927).

$$\frac{1}{r}\frac{\partial}{\partial r}\left(r\frac{\partial\psi}{\partial r}\right)+\frac{1}{r^2}\frac{\partial^2\psi}{\partial\theta^2}+\frac{\partial^2\psi}{\partial x^2}-\frac{1}{c^2}\frac{\partial^2\psi}{\partial t^2}-\frac{2\pi i\epsilon H}{hc}\frac{\partial\psi}{\partial\theta}$$
$$-\frac{4\pi^2}{h^2}\left(\mu^2c^2+\frac{\epsilon^2H^2r^2}{4c^2}\right)\psi=0. \tag{2}$$

We put

$$\psi = R(r)X(x)e^{-im\theta}e^{-2\pi i(\mathcal{E}/h)t} \tag{3}$$

where $\mathcal{E}$ is the total energy, and m must be an integer for ψ to be single-valued. Eq. (2) then leads to the ordinary differential equations

$$\frac{d^2X}{dx^2}+\alpha X=0, \tag{4}$$

$$\frac{d^2R}{dr^2}+\frac{1}{r}\frac{dR}{dr}+\left\{\frac{4\pi^2\mathcal{E}^2}{h^2c^2}-\frac{4\pi^2\mu^2c^2}{h^2}-\frac{2\pi\epsilon Hm}{hc}\right.$$
$$\left.-\frac{\pi^2\epsilon^2H^2r^2}{h^2c^2}-\frac{m^2}{r^2}-\alpha\right\}R=0, \tag{5}$$

in which α is the constant of separation. Eq. (4) states that the electrons moving parallel to the field act like free particles. If we introduce the quanity

$$W\equiv\frac{1}{2\mu c^2}(\mathcal{E}^2-\mu^2c^4) \tag{6}$$

into Eq. (5), the differential equation for R becomes identical in form with that deduced by Page from the non-relativistic wave equation. We have therefore, as in Page's development,

$$W=\left(s+\frac{1}{2}\right)h\left(\frac{\epsilon H}{2\pi\mu c}\right),\quad s=m+k=0,1,2,\cdots. \tag{7}$$

The energy $\mathcal{E}$ is thus completely quantized.[3] We have also for the radius of curvature r of the deflected electrons[4]

$$r^2=\frac{2\mu c^2W}{\epsilon^2H^2}\frac{x}{2s+1} \tag{8}$$

in which $x\equiv(2\pi\epsilon H/hc)r^2$. Relativistic electrodynamics gives for the radius of curvature in terms of W as defined in Eq. (6)

$$r^2=\frac{2\mu c^2W}{\epsilon^2H^2} \tag{9}$$

so that the same correction is introduced here by the wave mechanics treatment as in the non-relativistic case.

[3] If the restriction of m to integral values is removed, the energy is no longer quantized. However, k remains integral in order that the series for R shall terminate, and the validity of subsequent calculations in both the non-relativistic and the relativistic case is not affected.

[4] Page, Eq. (33).

The Current

It is necessary to deduce from Eq. (1) an expression for the current density. If the differential equation satisfied by $\bar{\psi}$ is multiplied by ψ and the result subtracted from the product of Eq. (1) and $\bar{\psi}$, we get

$$\bar{\psi}\nabla\cdot\nabla\psi - \psi\nabla\cdot\nabla\bar{\psi} - \frac{1}{c^2}\left(\psi\frac{\partial^2\bar{\psi}}{\partial t^2} - \psi\frac{\partial^2\bar{\psi}}{\partial t^2}\right) - \frac{4\pi i\epsilon}{hc}\boldsymbol{A}\cdot(\bar{\psi}\nabla\psi + \psi\nabla\bar{\psi}) = 0. \quad (10)$$

Also

$$\bar{\psi}\nabla\cdot\nabla\psi - \psi\nabla\cdot\nabla\bar{\psi} = \nabla\cdot(\bar{\psi}\nabla\psi - \psi\nabla\bar{\psi}),$$

and

$$\boldsymbol{A}\cdot(\bar{\psi}\nabla\psi + \psi\nabla\bar{\psi}) = \nabla\cdot(\boldsymbol{A}\psi\bar{\psi}).$$

In addition we have

$$\bar{\psi}\frac{\partial^2\psi}{\partial t^2} - \psi\frac{\partial^2\bar{\psi}}{\partial t^2} = \frac{\partial}{\partial t}\left\{\psi\bar{\psi}\frac{\partial}{\partial t}\left(\log\frac{\psi}{\bar{\psi}}\right)\right\}$$
$$= -4\pi i\frac{\mathcal{E}}{h}\frac{\partial}{\partial t}(\psi\bar{\psi})$$

using Eq. (3). Eq. (10) may now be written

$$\frac{\epsilon hc^2}{4\pi i\mathcal{E}}\nabla\cdot\left(\bar{\psi}\nabla\psi - \psi\nabla\bar{\psi} - \frac{4\pi i\epsilon}{hc}\boldsymbol{A}\psi\bar{\psi}\right) + \frac{\partial}{\partial t}(\epsilon\psi\bar{\psi}) = 0. \quad (11)$$

We identify Eq. (11) with the equation of continuity so that the current density is

$$j = \frac{\epsilon hc^2}{4\pi i\mathcal{E}}\left(\bar{\psi}\nabla\psi - \psi\nabla\bar{\psi} - \frac{4\pi i\epsilon}{hc}\boldsymbol{A}\psi\bar{\psi}\right). \quad (12)$$

This result is to be compared with the non-relativistic expression[5]

$$j = \frac{\epsilon h}{4\pi\mu i}\left(\bar{\psi}\nabla\psi - \psi\nabla\bar{\psi} - \frac{4\pi i\epsilon}{hc}\boldsymbol{A}\psi\bar{\psi}\right). \quad (13)$$

The factor $\epsilon hc^2/4\pi i\mathcal{E}$ appearing in Eq. (12) is, like that in Eq. (13), constant in the coordinates so that it does not affect the calculation of the mean radii of curvature averaged with respect to the current density. Hence the relativistic wave equation gives the same values for the mean radii of curvature as those calculated by Page.[6]

Conclusion

The relativistic wave equation leads to the same wave function for electrons in a uniform magnetic field as that determined from the Schrödinger equation.

[5] Condon and Morse, Quantum Mechanics, p. 30.
[6] Page, Eqs. (45) and (48).

The electron motion at right angles to the field is found to be completely quantized as before. The relativistic expression for the current density differs from the non-relativistic only in that $\mathcal{E}/c^2$ replaces μ; this difference does not affect the calculation of the mean radii of curvature. We are led to a conclusion similar to that reached by the non-relativistic treatment: the classical relativistic relation between ϵ/μ and the mean radius of curvature upon deflection gives a value for ϵ/μ which is too large.

In conclusion the writer wishes to acknowledge his indebtedness to Professor Page for suggesting this problem and for his helpful criticism during its consideration.

THE HYPERFINE STRUCTURE OF S AND P TERMS OF TWO ELECTRON ATOMS WITH SPECIAL REFERENCE TO Li^+

By G. Breit and F. W. Doermann
Department of Physics, New York University

(Received October 28, 1930)

Abstract

The proper form of the interaction energy between the nuclear magnetic moment and the electronic system of a many electron atom is discussed. The results of the Dirac equation for a single electron are taken as the guiding principle. A form for the interaction energy is set up as an expression involving Pauli's spin matrices. No convergence difficulties occur in the form here given.

The interaction Hamiltonian is applied to the ^3S and ^3P terms of two electron atoms for the case of Russell-Saunder's coupling. An exact formula is derived for the resultant hyperfine structure of ^3S terms and corrections to the Goudsmit Bacher formulas for ^3P terms are given. It is shown that the Landé interval rule for ^3S hyperfine structure levels is exact, and that therefore the ratio of intervals can be used to determine nuclear spin moments.

The formulas are applied to the Li^+ 5485A line. Proper functions for S levels are worked out by the variational method and applied to the calculation of the magnetic moment of Li_7. With Schüler's wave-length data the nuclear g factor is 2.13 on the assumption that the nuclear spin is 3/2.

The accuracy of the calculation is discussed. It is likely to be good to at least 2% in g. As a by-product of the calculation the lowest energy level of ortholithium has been computed as $\leqq -1.1354$ in units of the ionization potential of Li^{++}. The empirical value is -1.1358.

Introduction

THE effect of nuclear spin on optical spectra has been treated mathematically by Casimir,[1] Fermi,[2] and Hargreaves.[3] A somewhat more qualitative discussion has been given by Goudsmit and Bacher.[4] In the first three of these discussions only one valence electron has been taken into account while in the last the more general problem of several valence electrons has been considered. Qualitatively the conclusions of Goudsmit and Bacher are doubtless correct. They do not pretend, however, to be exact quantitatively since the coupling between the nuclear spin and the electron system is supposed to be taking place only through one of the electrons—the most closely bound s electron. It is desirable to have a more exact quantitative theory taking into account the coupling of all electrons. This is particularly necessary if, say, two of them are s electrons. The desirability of having such a theory lies in its application to the absolute value of nuclear magnetic mo-

[1] See Goudsmit and Young, Nature, March 22, 1930.
[2] E. Fermi, Zeits. f. Physik **60**, 320 (1930).
[3] J. Hargreaves, Proc. Roy. Soc. **124**, 568 (1929); **127**, 141 (1930); **127**, 407 (1930).
[4] S. Goudsmit and R. F. Bacher, Phys. Rev. **34**, 1501 (1929).

ments. The observations of Schüler[5] and of Granath[6] show that the ^3S level of Li^+ is split into three components under the action of the nuclear magnetic field and the separation between the two extreme components can be said to be 1.03 cm.$^{-1}$. There seems to be no doubt that the three components in question are single. They are well and definitely resolved and so there is every reason to expect eventually a reliable determination of the nuclear magnetic moment from the determination of their frequency difference. The whole electron system consists in this case of only two electrons. The solution of the Schroedinger wave equation offers in this case a simpler problem than that of the heavy alkalies. An attempt at its approximate solution and its application to the calculation of the magnetic moment of the Li_7 nucleus is one of the objects of this paper. The other object is to formulate a theory for the interaction between the nucleus and the extranuclear electrons. A few words must be said as to why the formulation of such a theory is still subject to speculation.

For one electron an unambiguous result can be obtained by means of Dirac's equation. This has been done by Fermi and Casimir. The problem is not so clear when two or more electrons are discussed. There exists no satisfactory mathematical treatment of the relativistic two electron problem. It becomes necessary to use approximate equations. The simplest form for these is obtained through the introduction of Pauli's two row, two column spin matrices. It is known that interactions between electrons can be satisfactorily represented by means of these as long as the electronic velocities are not excessive. It might be expected that the interaction of nuclei and electrons can be reduced to the same basis. There is one important distinction between these two cases. The force between a nucleus and an electron is attractive while that between two electrons is repulsive. When an electron is close to the nucleus its velocity cannot be treated as small. For s electrons an important contribution to the interaction energy is due to the influence of the nucleus when the electron is very close to it. We have no reason to expect the interaction energy of the nucleus and the electron to be of the same form as that used for the approximate interaction energy of two electron spins. In fact it will be seen below that the two forms are different.

In order to derive the proper form of the interaction energy we consider first of all the one electron problem from the point of view of Dirac's equation, i.e. we write down the formulas found already in Fermi's paper. The two smaller Dirac wave-function components are then eliminated and an equation in the two large components is obtained. This equation involves Pauli's spin matrices and is equivalent to Dirac's for the discussion of the lighter nuclei. Having thus derived the proper interaction energy for one electron the result is generalized to the case of two or more. This forms the first section of the paper. In the second section the separations of spectral terms caused

[5] H. Schüler, Zeits. f. Physik **42**, 487; (1927).

[6] L. P. Granath, Phys. Rev. **36**, 1018, (1930), (letter). See also the forthcoming paper by P. Güttinger in the Zeits. f. Physik in which the feasibility of $i=3/2$ is explained and an approximate g value for the nucleus is derived.

by nuclear interactions are worked out. In the third the results of the second section are applied to Li.+

(I). The Interaction Energy for One Electron

We consider one electron of charge $-e$ under the influence of a single nucleus. The electrostatic potential due to the nucleus is A_0. The electrostatic field due to the nucleus is central so that A_0 is a function only of r, the distance from the nucleus. The vector potential due to the nucleus is A. In special applications we take

$$\boldsymbol{A} = \frac{[\boldsymbol{\mu} \times \boldsymbol{r}]}{r^3}. \tag{1}$$

With the abbreviations

$$\boldsymbol{p} = \boldsymbol{P} + (e/c)\boldsymbol{A}, \quad \boldsymbol{P} = (h/2\pi i)\nabla, \quad p_0 = E/c + (e/c)A_0 \tag{2}$$

Dirac's equation for a stationary state is

$$(p_0 + \alpha_1 p_1 + \alpha_2 p_2 + \alpha_3 p_3 + \alpha_4 mc)\psi = 0. \tag{3}$$

We suppose the α_s to be those given in Dirac's original paper. Equation (3) is, of course, a set of four equations in four ψ_s. It is convenient to eliminate ψ_1, ψ_2 as has been done by Darwin.[7] The reader will verify that without approximations

$$\left\{ p_0 - mc - (\boldsymbol{p}\boldsymbol{\sigma})\frac{1}{p_0 + mc}(\boldsymbol{p}\boldsymbol{\sigma}) \right\}\psi = 0 \tag{4}$$

where now the $\sigma_k (k = 1, 2, 3)$ are Pauli's matrices and the column matrix ψ contains only two rows: ψ_3, ψ_4. Equation (4) must be satisfied for any solution of (3). It is not altogether equivalent to (3) if it is used for the determination of the eigenwerte E. In (3) it is required that $\psi_1^*\psi_1+\psi_2^*\psi_2+\psi_3^*\psi_3+\psi_4^*\psi_4$ be integrable. Equation (4) is equivalent to (3) only if this last condition is added. If ordinary perturbation methods of quantum theory are applied to (4) it is more convenient to use the integrability of $\psi_3^*\psi_3+\psi_4^*\psi_4$ as the restricting condition. As will be seen presently this circumstance is only of secondary importance. For the present we use (4) and derive its consequences as though $\psi_3^*\psi_3+\psi_4^*\psi_4$ were integrable. Performing the operations indicated in the second term, using (2) and introducing the electric and magnetic fields by means of

$$\mathcal{E} = -\operatorname{grad} A_0, \quad \mathfrak{H} = \operatorname{curl} \boldsymbol{A} \tag{5}$$

we obtain

$$\begin{aligned} E = mc^2 - eA_0 + \frac{c^2}{E + mc^2 + eA_0}\left[\boldsymbol{P}^2 + \frac{e}{c}(\boldsymbol{P}\boldsymbol{A} + \boldsymbol{A}\boldsymbol{P}) + \frac{e^2}{c^2}\boldsymbol{A}^2 + \frac{he}{2\pi c}(\mathfrak{H}\boldsymbol{\sigma}) \right] \\ + \frac{h}{2\pi i}\frac{c^2 e}{(E + mc^2 + eA_0)^2}\left[(\mathcal{E}\boldsymbol{P}) + \frac{e}{c}(\mathcal{E}\boldsymbol{A}) + i[\mathcal{E} \times \boldsymbol{P}]\boldsymbol{\sigma} \right. \\ \left. + i\frac{e}{c}[\mathcal{E} \times \boldsymbol{A}]\boldsymbol{\sigma} \right] \end{aligned} \tag{6}$$

[7] C. G. Darwin, Proc. Roy. Soc. **118**, 654 (1928).

this is still an exact consequence of (2). At this point we make an approximation. The magnetic moment μ enters (6) only through A. It is sufficient to consider first order effects in μ and therefore in A. Quadratic terms in A are disregarded from here on. The perturbation energy may therefore be taken to be

$$H' = \frac{c^2}{E + mc^2 + eA_0}\left[\frac{e}{c}(\boldsymbol{PA} + \boldsymbol{AP}) + \frac{he}{2\pi c}(\mathfrak{K}\mathfrak{d})\right] + \frac{hc^2e}{2\pi(E + mc^2 + eA_0)^2}\left[\frac{e}{c}[\mathcal{E} \times \boldsymbol{A}]\mathfrak{d} - i\frac{e}{c}(\mathcal{E}\boldsymbol{A})\right]. \tag{7}$$

In this expression the first bracketed term corresponds to the ordinary interaction energy which is used in the ordinary discussions of two electrons. In the major portion of the configuration space eA_0 is negligible in comparison with $E+mc^2$ which itself is very nearly $2mc^2$. In this region the first bracketed term of (7) is on using (1)

$$H'' = \frac{e}{mc}\frac{\boldsymbol{M}\mathfrak{\mu}}{r^3} + \frac{eh}{4\pi mc}\left\langle (\nabla\mathfrak{d})(\nabla\mathfrak{\mu})\frac{1}{r}\right\rangle \tag{8}$$

where

$$\boldsymbol{M} = [\boldsymbol{r} \times \boldsymbol{P}] \tag{8'}$$

is the angular momentum operator and ∇ operates only on r^{-1} in the $\langle\rangle$. Only the expression (8) can be derived from the analogy of the electron and the nucleus to little magnets. For s terms the second term of (8) becomes indeterminate. A definite theory can be formulated by means of (8) if $\mathfrak{\mu}$ is defined as the limit of a spatial distribution of magnetic moment of very small extension in the limiting case of the extension approaching zero. It will be seen that the result of this limiting process is different from the application of the complete expression (7). For s electrons the result of (7) is (-2) times the result of (8). Hargreaves obtains zero for the perturbing effect of (8) in the case of s terms. He could have obtained any desired result since he has not defined the limiting process for the definition of the divergent integrals. Nevertheless his conclusion is correct. The exact effect of the first bracketed term of (7) is zero for s terms, the presence of eA_0 in the denominator making the radial integrals convergent. We see that the picture of the nucleus and electron as little magnets can be applied in this instance only with extreme caution.

If the field is central $\mathcal{E}$ is perpendicular to $\boldsymbol{A}$ and the imaginary part of the second bracketed term of (7) disappears. Its real part containing $[\mathcal{E}\times\boldsymbol{A}]$ is then combined advantageously with the second part of the first bracketed term containing $(\mathfrak{K}\mathfrak{d})$. The perturbation energy becomes

$$H' = \frac{(e/mc)(\boldsymbol{M}\mathfrak{y})}{1+(E-mc^2+eA_0)/2mc^2}\cdot\frac{1}{r^3}$$
$$+\frac{hec/2\pi}{E+mc^2+eA_0}\left\{-\frac{(\mathfrak{y}\mathfrak{d})}{r^3}+\frac{3(\mathfrak{r}\mathfrak{d})(\mathfrak{r}\mathfrak{y})}{r^5}\right\}$$
$$+\frac{(hec/2\pi)(e|\mathcal{E}|)}{(E+mc^2+eA_0)^2}\left\{\frac{(\mathfrak{y}\mathfrak{d})}{r^2}-\frac{(\mathfrak{r}\mathfrak{d})(\mathfrak{r}\mathfrak{y})}{r^4}\right\} \tag{9}$$

The perturbation energy (9) can now be applied to the calculation of the splitting of an s term. The first term of (9) can be disregarded because $\boldsymbol{M}\psi=0$ for s terms and because the radial integration gives a finite result on account of eA_0 in the denominator. It is well known that the conservation of angular momentum makes it sufficient to calculate the average value of the coefficient of $\mu_z\sigma_z$ in the second line of (9). If this average be w and the nuclear spin k the s level is split into two components displaced by the amounts w, $(-1-k^{-1})w$ from the normal position.[8] The first component is the one of higher fine quantum number $f=k+\frac{1}{2}$. The first term of the second line of (9) contributes nothing to the average, again on account of the presence of eA_0 in the denominator which makes the integration over r give a finite result. Using (5) we have on partial integration

$$w = -\int_0^\infty \frac{8\pi\mu}{3}\,\frac{hec}{2\pi}\,\frac{2\psi\psi'}{E+mc^2+eA_0}dr \cong \frac{8\pi\mu}{3}\left(\frac{he}{4\pi mc}\right)\psi^2(0) \tag{10}$$

in agreement with Fermi.

The final result is not quite correct, but is very nearly so as long as the region in which $eA_0<<mc^2$ is negligible in comparison with the spatial extention of $\psi\psi'$ and as long as $E-mc^2<<mc^2$. Both of these conditions are satisfied by light nuclei. The difference between (10) and the correct result is of the order of the square of the fine structure constant.[8] This example shows that the substitution of the integrability of $\psi_3^*\psi_3+\psi_4^*\psi_4$ for the integrability of $\psi_1^*\psi_1+\psi_2^*\psi_2+\psi_3^*\psi_3+\psi_4^*\psi_4$ is safe for the present purpose. We see also that the "empirical terms" used by Hargreaves are essentially the same as the terms derived above from Dirac's equation.

If instead of using Dirac's equation we were to use the perturbation energy (8) we should run into convergence difficulties. These may be avoided by endowing the magnetization of the nucleus with a finite spatial extension, say, by supposing that the magnetization is spread uniformly through the volume of a very small sphere. The first term then has no effect. The second gives rise to

$$w = \frac{\mu eh}{4\pi mc}\int\frac{\psi^2(P)}{3}\int f(P')\Delta_P\left(\frac{1}{r_{PP'}}\right)dV_{P'}dV_P$$

[8] See e.g. G. Breit, Phys. Rev. **35**, 1447 Equations (2), (3) (1930).

where P' refers to a point of the magnetization distribution, and $f(P')\mu dV_{P'}$ is the amount of magnetization in the element of volume $dV_{P'}$. The above double integral is easily evaluated if $I=\int f(P')(1/r_{PP'})dV_{P'}$ is interpreted as the electrostatic potential at the point P due to a charge distribution of density $f(P')$. The total charge is $1=\int f(P')dV_{P'}$. Outside the nucleus $\Delta_P I=0$. Inside the nucleus Poisson's equation gives

$$\Delta_P I + 4\pi f(P) = 0,$$

and therefore

$$\int (\Delta_P I) dV_P = -4\pi.$$

In the limit of a very concentrated distribution $f(P')$ we may set therefore

$$\Delta_P \int f(P') \frac{1}{r_{PP'}} dV_{P'} = -4\pi\delta(P) \tag{11}$$

and we obtain then

$$w = -\frac{4\pi\mu}{3}\frac{eh}{4\pi mc}\psi^2(0). \tag{12}$$

This result must be multiplied by (-2) in order to give Fermi's result (10). The magnetic doublet model and Dirac's equation give in this case widely different results. The present evidence is that Dirac's equation is to be preferred so that (10) is the correct result.

The perturbation energy (9) must now be generalized to include the case of two or more electrons. As has been explained in the introduction we are unable to start with a relativistic treatment of two electrons and we must instead use (9) as an indication for the proper generalization. A number of possible generalizations could be made. Thus one could go back to (7) and use the field quantities $\mathcal{E}$, $\mathfrak{H}$ taking $\mathcal{E}_1$ to be the electric intensity at x_1, y_1, z_1, due to the nucleus and also due to electron 2. Or else one may take $\mathcal{E}_1$, $\mathfrak{H}_1$ to be due only to the nucleus. For the first choice we would have to prove that the imaginary term in (7) contributes nothing to the result. Also some generalization of A_0 would have to be made. Having no basis for forming such a generalization we make instead

$$H' = H_1' + H_2' \tag{13}$$

where H_1' is the result of using x_1, y_1, z_1, $\mathfrak{d}_1$, instead of x,y,z, $\mathfrak{d}$ in all of the terms of (9). The coupling between the nucleus and each electron is thus represented by a term in the Hamiltonian which depends only on the coordinates of that electron.

It may also be shown that for ^3S terms the alternative generalization based on (7) leads to the same final result as (13) provided $\mathcal{E}_i=-\text{grad}\, A_{0i}$ $(i=1, 2)$. The proof is not of sufficient interest to be quoted.

II. Calculation of Perturbations in Terms of Schroedinger ψ in Configuration Space

We use the method of sums.[9] Consider first the ^3S terms. It is convenient to define the following spin functions

$$S_1 = S_\alpha{}^1 S_\alpha{}^2,\ S_0 = 2^{-1/2}(S_\alpha{}^1 S_\beta{}^2 + S_\alpha{}^2 S_\beta{}^1),\ S_{-1} = S_\beta{}^1 S_\beta{}^2. \tag{14}$$

The upper indices refer to electrons 1 and 2. The functions S_α, S_β are as usual the column matrices $\binom{1}{0}, \binom{0}{1}$. The upper row corresponds to the spin being in the positive direction of the z axis. In the case of Russell-Saunders coupling there are three unperturbed functions for the ^3S state. Each of these is the product of a coordinate function and of one of the three functions (14). The coordinate function ψ depends only on the shape and size of the electronic triangle and not on its orientation.[10] The wave-function of the coupled system nucleus+electrons contains also the angular momentum specification of the nucleus. Denoting the angular momentum of the nucleus by k there are $2k+1$ nuclear functions

$$N_k = \begin{pmatrix} 1 \\ 0 \\ 0 \\ \cdot \\ \cdot \\ \cdot \\ 0 \end{pmatrix}, \quad N_{k-1} = \begin{pmatrix} 0 \\ 1 \\ 0 \\ \cdot \\ \cdot \\ \cdot \\ 0 \end{pmatrix}, \cdots \quad N_{-k} = \begin{pmatrix} 0 \\ 0 \\ \cdot \\ \cdot \\ \cdot \\ 0 \\ 1 \end{pmatrix} \tag{15}$$

The vector matrix $\mathfrak{y}$ operates on these. The matrices for the components of $\mathfrak{y}$ we take to be the same as Fermi's. Among these the only matrix having diagonal elements is μ_z. It is a diagonal matrix with elements $\mu(1, k-1/k, \cdots -1)$. The complete system of $3(2k+1)$ unperturbed eigenfunctions can be represented by means of

$$u_i{}^m = S_i N^m \psi \begin{pmatrix} i = 1, 0, -1 \\ m = k, k-1, \cdots -k \end{pmatrix} \tag{16}$$

It is most conveniently arranged in a table:

Angular momentum:	$k+1$	k	$k-1$	-------	$-k+1$	$-k$	$-k-1$
	$u_1{}^k$	$u_1{}^{k-1}$ $u_0{}^k$	$u_1{}^{k-2}$ $u_0{}^{k-1}$ $u_{-1}{}^k$	------- ------- -------	$u_1{}^{-k}$ $u_0{}^{-k+1}$ $u_{-1}{}^{-k+2}$	$u_0{}^{-k}$ $u_{-1}{}^{-k+1}$	$u_{-1}{}^{-k}$

In Slater's method we are concerned only with diagonal elements of the perturbation energy matrix. The functions N^m are normal orthogonal and so are the S_i. We are therefore concerned only with coefficients of μ_z. This shows that the combined effect of the perturbations due to $\boldsymbol{M}_1\mathfrak{y}$ and $\boldsymbol{M}_2\mathfrak{y}$ is zero. In fact this perturbation is of the form $(\boldsymbol{B}_1+\boldsymbol{B}_2)\mathfrak{y}$. It, by itself, commutes with the total angular momentum. When it operates on $u_1{}^k$ it gives $(B_{1z}+B_{2z})\mu u_1{}^k$ as well as other terms which do not count in the calculation

[9] J. C. Slater, Phys. Rev. **34**, 1293 (1929).
[10] E. Wigner, Zeits. f. Physik **43**, 624 (1927).

of the diagonal element $\int u_1^{*k} H' u_1^k$. The operation on u_{-1}^{-k} gives $-(B_{1z}+B_{2z})\mu u_{-1}^{-k}$. Thus $\int u_1^{*k} H' u_1^k = -\int u_1^{*k} H' u_1^k = 0$. The term of highest fine structure quantum number is therefore undisturbed. Considering the other functions in turn we see that there is no splitting due to terms not involving $\mathfrak{d}_1$, $\mathfrak{d}_2$. This may also be verified by a short calculation of the average value of $A(r_1)\partial/\partial\phi_1 + A(r_2)\partial/\partial\phi_2$ in the six dimensional configuration space $x_1 \cdots z_2'$ for the case of $\psi = \psi(r_1, r_2, \cos\theta_{12})$. The terms in $\mathfrak{d}_1$, $\mathfrak{d}_2$ are easily treated if it is observed that, so far as the calculation of diagonal matrix elements is concerned, the symmetric operator $\boldsymbol{A}_1\mathfrak{d}_1 + \boldsymbol{A}_2\mathfrak{d}_2$ gives rise only to the following terms

$$(\boldsymbol{A}_1\mathfrak{d}_1 + \boldsymbol{A}_2\mathfrak{d}_2)(S_1, S_0, S_{-1}) \rightarrow (A_{1z} + A_{2z})(S_1, 0, -S_{-1}). \tag{17}$$

Letting now the energy perturbations of the three levels be w_1, w_2, w_3, in the order of decreasing fine quantum numbers, we have from the first three columns of the table

$$w_1 = \int \psi^*(A_{1z} + A_{2z})\psi, \quad w_1 + w_2 = \frac{k-1}{k} w_1, \quad w_1 + w_2 + w_3$$

$$= \left(-1 + \frac{k-2}{k}\right) w_1$$

$$w = w_1\left(1, \quad -\frac{1}{k}, \quad -\frac{k+1}{k}\right). \tag{18}$$

Here

$$A_{1z} = \frac{hec}{2\pi(2mc^2 + Ze^2/r_1)^2}\left\{2mc^2\left(\frac{3z_1^2}{r_1^5} - \frac{1}{r_1^3}\right) + \frac{2Ze^2}{r_1^6} z_1^2\right\}.$$

Performing one of the integrations over 1 for A_{1z} and over 2 for A_{2z} and then using the symmetry of ψ^2 in 1 and 2 we have

$$w_1 = 16\pi/3\,\mu\mu_0 \int \psi^2(0, 0, 0; x, y, z)dx \quad dydz$$

$$(\mu_0 = eh/4\pi mc > 0). \tag{19}$$

The only approximations made in deriving (19) are: (1) a definite case of Russell-Saunders coupling, (2) neglect of the square of the fine structure constant. The integral in (19) represents the probability of one electron being in a unit volume near the nucleus. The connection of this result with Goudsmit and Bacher is seen if one writes

$$\psi = (1/2^{1/2})[\phi_n(q_1)\phi_m(q_2) - \phi_n(q_2)\phi_m(q_1)]. \tag{20}$$

If n refers to the inner electron state

$$\int \psi^2(0, q)dq \cong \tfrac{1}{2}\phi_n^2(0), \text{ and}$$

$$w_1 = (8\pi/3)\mu\mu_0\phi_n^2(0). \tag{21}$$

In this approximation (19) (18) are identical with the corresponding formulas of Goudsmit and Bacher. A discussion of the difference between (19) and (21) will be given in the third section.

If $k=1/2$ formula (18) remains correct if it is read from left to right and the last term is omitted. This is obvious from the order in which w_1, w_2, w_3 have been derived.

We may now consider ^3P terms. There are three linearly independent coordinate eigenfunctions, each of these combining with the three spin functions (14) and thus forming a set of nine functions. The coordinate functions may be called $\psi_1, \psi_0, \psi_{-1}$ corresponding to components 1, 0, -1 of the orbital angular momentum in the z direction. The functions $\psi_i S_k$ do not themselves correspond to definite parts of the ^3P term but certain linear combinations of them do. These linear combinations are

$$\begin{aligned}
&^3P_0 : 3^{-1/2}(\psi_1 S_1 - \psi_0 S_0 + \psi_{-1} S_{-1}) \\
&^3P_1 : 2^{-1/2}(\psi_1 S_0 - \psi_0 S_1),\ 2^{-1/2}(\psi_1 S_{-1} - \psi_{-1} S_1),\ 2^{-1/2}(-\psi_{-1} S_0 + \psi_0 S_{-1}) \quad (22) \\
&^3P_2 : \psi_1 S_1,\ 2^{-1/2}(\psi_0 S_1 + \psi_1 S_0),\ 6^{-1/2}(\psi_1 S_{-1} + 2\psi_0 S_0 + \psi_{-1} S_1), \\
&\qquad 2^{-1/2}(\psi_0 S_{-1} + \psi_{-1} S_0),\ \psi_{-1} S_{-1}.
\end{aligned}$$

The functions $\psi_1, \psi_0, \psi_{-1}$ are supposed to be chosen so as to transform themselves under rotations as $2^{-1/2}(x+iy), -z, 2^{-1/2}(-x+iy)$. The set of functions (22) is convenient because each one of them corresponds to a definite value of the angular momentum in the direction of the z axis. There is no splitting for the $^3P_0$ and we consider first the $^3P_1$ term. The nucleus is brought in by means of the N_k just as in the case of ^3S terms. The table which led to (18) is still correct, though now the functions $u_l{}^m$ are different. Equation (18) still is valid although (19) is different. The validity of (18) is of course a consequence of the "cosine" law of interaction with the nucleus. It is very easy to prove this by writing $u_l{}^m = v_l N^m$. Denoting the coefficient of μ_z in the interaction energy by a_z we have on applying the diagonal sum theorem from both ends of the table $w_1 = I_1 = -I_{-1}$; $w_2 + w_1 = (k-1)/k I_1 + I_0 = -((k-1)/k) I_{-1} - I_0$ where $I_l = \mu \int v_l{}^* a_z v_l$. This shows that $I_0 = 0$ and (18) follows at once. It remains to determine w_1. We may omit the correction in the denominator of the first term of (9). The second two terms are easily combined and we have

$$w_1 = (e\mu/mc) \int v_1{}^* (r_1{}^{-3} M_{1z} + r_2{}^{-3} M_{2z}) v_1 + \mu \int v_1{}^* (\boldsymbol{B}_1 \boldsymbol{\delta}_1 + \boldsymbol{B}_2 \boldsymbol{\delta}_2) v_1 \quad (23)$$

where

$$\boldsymbol{B}_1 = \frac{hec}{2\pi \{2mc^2 + (Ze^2/r_1)\}^2} \left\{ 2mc^2 \left(3 z_1 \frac{\boldsymbol{r}_1}{r_1{}^5} - \frac{\boldsymbol{\zeta}}{r_1{}^3} \right) + \frac{2Ze^2}{r_1{}^6} z_1 \boldsymbol{r}_1 \right\}. \quad (24)$$

Here $\boldsymbol{\zeta}$ is a unit vector along the z axis. $\mathcal{B}_2$ is obtained from $\mathcal{B}_1$ on substituting z_2, r_2 everywhere for z_1, r_1. Performing the operations $\boldsymbol{\delta}_1$, $\boldsymbol{\delta}_2$ in (23) we have on letting

$$\boldsymbol{B} = \boldsymbol{B}_1 + \boldsymbol{B}_2 \tag{25}$$

$$w_1 = \frac{e\mu}{2mc}\int \psi_1^*(r_1^{-3}M_{1z} + r_2^{-3}M_{2z})\psi_1 + \frac{e\mu}{2mc}\int \psi_0^*(r_1^{-3}M_{1z} + r_2^{-3}M_{2z})\psi_0$$
$$+ (\mu/2)\int \{\psi_0^* B_z\psi_0 - \psi_1^* 2^{-1/2}(B_x + iB_y)\psi_0 - \psi_0^* 2^{-1/2}(B_x - iB_y)\psi_1\} \tag{26}$$

This form for w_1 is correct quite regardless of any approximations which may be made as to the representation of the coordinate wave-functions $\psi_1, \psi_0, \psi_{-1}$. The most general forms of these functions are known and formula (26) is capable of giving exact results as long as the hypothesis of Russell-Saunders coupling applies.[11] In practical applications it appears to be unnecessary to use the general expressions for $\psi_1, \psi_0, \psi_{-1}$ and it will usually be sufficient to use the approximate representation of these coordinate functions as antisymmetric combinations of products of functions involving the coordinates of only one particle. We may then write

$$\begin{aligned}
\psi_1 &= (3^{1/2}/4\pi)(F\sin\theta_1 e^{i\phi_1} - \tilde{F}\sin\theta_2 e^{i\phi_2}) \\
\psi_0 &= -(6^{1/2}/4\pi)(F\cos\theta_1 - \tilde{F}\cos\theta_2) \\
\psi_{-1} &= -(3^{1/2}/4\pi)(F\sin\theta_1 e^{-i\phi_1} - \tilde{F}\sin\theta_2 e^{-i\phi_2})
\end{aligned} \tag{27}$$

with

$$\begin{aligned}
F &= f_1(r_1)f_2(r_2); \quad 4\int F^2 r_1^2 r_2^2 dr_1 dr_2 = 1 \\
\tilde{F} &= f_1(r_2)f_2(r_1).
\end{aligned} \tag{27'}$$

The functions in (27) are chosen so as to give (22). The radial function f_1 is characteristic of the p state while f_2 describes the s state. If a single electron were in that s state it would be described by a normalized function ψ_s. Clearly

$$4\pi\psi_s(0)^2 = f_2(0)^2 \Big/ \left(\int f_2(r_2)^2 r_2^2 dr_2\right). \tag{28}$$

It is now found on substitution of (27) (27′)

$$(e/2mc)\int \psi_1^*(r_1^{-3}M_{1z} + r_2^{-3}M_{2z})\psi_1 = (eh/4\pi mc)\overline{(r_1^{-3})} \tag{29}$$

where

$$\overline{(r_1^{-3})} = 4\int F^2 r_1^{-3} r_1^2 r_2^2 dr_1 dr_2 \tag{29'}$$

is the average of r^{-3} for a p electron described by a radial function f_1. Also in

$$\tfrac{1}{2}\int \psi_0^* B_z \psi_0$$

[11] E. Wigner, reference 10; G. Breit, Phys. Rev. **35**, 569 (1930).

we need

$$(3/16\pi^2)\int F^2\cos^2\theta_1 B_{1z} = (1/5)\mu_0\overline{(r_1^{-3})} - (1/20)\mu_0\overline{(r_1^{-4})}\,(Ze^2/mc^2).$$

A numerical estimate shows that the term in $\overline{r_1^{-4}}$ is much too small ordinarily to be worried about and this as well as similar terms will be neglected here. The most important contribution to (26) comes from terms of the type

$$(3/16\pi^2)\int F^2\cos^2\theta_1 B_{2z} = (2\pi/3)\mu_0\psi_s(0)^2$$

using (28). The remaining contributions are from

$$-\tfrac{1}{2}\int\{\psi_1^*2^{-1/2}(B_x+iB_y)\psi_0+\psi_0^*2^{-1/2}(B_x-iB_y)\psi_1\} = (3/5)\mu_0\overline{(r_1^{-3})}.$$

It is thus found on substituting all the integrals into (26) that

$$w_1 = \mu\mu_0\{(4\pi/3)\psi_s(0)^2 + 2\overline{(r^{-3})}_p\}. \tag{30}$$

This completes the calculation for the $^3P_1$ level.

For the $^3P_2$ term we have five electronic functions given by the last row of (22). These may be designated as v_l and the complete specification of the system is given by $u_l^m = v_l N^m$. Only now $l=(2,\ 1,\ 0,\ -1,\ -2)$ and the v_1, v_0, v_{-1} are, of course, now different from those just used for the $^3P_1$ term. In this case the table following equation (16) must be extended so as to have five rows. The method of sums does not suffice now to give all of the separation ratios. Denoting as before the coefficient of μ_z by a_z and letting $Il = \mu\int v_l^* a_z v_l$ the method of sums shows directly that $I_2=-I_{-2}$, $I_1=-I_{-1}$, $I_0=0$ but it does not establish a relation between I_1 and I_2. A calculation is easily made however for both I_1 and I_2. We have:

$$I_2 = \frac{\mu e}{mc}\int\psi_1^*(r_1^{-3}M_{1z}+r_2^{-3}M_{2z})\psi_1 + \mu\int\psi_1^*B_z\psi_1. \tag{31}$$

Substitution of the integrals used in deriving (30) gives

$$I_2 = \mu\mu_0[(8\pi/3)\psi_s(0)^2 + (8/5)\overline{(r^{-3})}_p]. \tag{32}$$

Also

$$\begin{aligned} I_1 &= (\mu e/2mc)\int\psi_1^*(r_1^{-3}M_{1z}+r_2^{-3}M_{2z})\psi_1 \\ &+ (\mu/2)\int\{\psi_0^*B_z\psi_0+\psi_1^*2^{-1/2}(B_x+iB_y)\psi_0+\psi_0^*2^{-1/2}(B_x-iB_y)\psi_1\} \end{aligned} \tag{33}$$

so that I_1 can be obtained directly from (30) by subtracting $(6/5)\ \overline{(r^{-3})}_p$ inside the parenthesis. We have

$$I_1 = \mu\mu_0[(4\pi/3)\psi_s(0)^2 + (4/5)\overline{(r^{-3})}_p] = I_2/2. \tag{35}$$

Using the sum theorem we obtain for the first order energy perturbations

$$^3P_2 = \mu\mu_0[(4\pi/3)\psi_s(0)^2 + (4/5)\overline{(r^{-3})}_p]$$
$$\left(2,\ \frac{k-2}{k},\ -\frac{3}{k},\ -\frac{k+3}{k},\ -2\frac{(k+1)}{k}\right) \tag{36}$$

which may be compared with

$$^3P_1 = \mu\mu_0[(4\pi/3)\psi_s(0)^2 + 2\overline{(r^{-3})}_p]\left(1,\ -\frac{1}{k},\ -\frac{k+1}{k}\right) \tag{36'}$$

$$^3S_1 = \mu\mu_0(8\pi/3)(1+\epsilon)\psi_s(0)^2\left(1,\ -\frac{1}{k},\ -\frac{k+1}{k}\right). \tag{36''}$$

Here ϵ is a fractional correction due to the difference between (19) and (21).

III. Application to the Spectrum of Li^+

The pattern of the $^3S-{}^3P$ line of Li^+ which has been observed by Schüler and Granath will now be considered using formulas (36) (36′) (36″). The quantities $\overline{(r^{-3})}_p$ and ϵ are of the nature of correction terms and neglecting them these formulas become identical with those of Goudsmit and Young. The $\psi_s(0)^2$ for a hydrogenic s electron is related to the fine structure constant by

$$2\pi\psi_s(0)^2\mu_0^2 = R\alpha^2Z^3/n^3 \tag{37'}$$

which is convenient for calculation. For $Z=3$ and $n=1$ we have in agreement with Goudsmit and Young $(8/3)R\alpha^2Z^3/1840n^3 = 0.228\ \text{cm}^{-1}$. Letting $(1840\mu/\mu_0) = g(k)$ we have therefore the approximate formulas:

$$^3P_2 = 0.228(g(k)/4)\left(2,\ \frac{k-2}{k},\ -\frac{3}{k},\ -\frac{k+3}{k},\ -\frac{2(k+1)}{k}\right)$$
$$^3P_1 = 0.228(g(k)/4)\left(1,\ -\frac{1}{k},\ -\frac{k+1}{k}\right) \tag{37}$$
$$^3S_1 = 0.228(g(k)/2)\left(1,\ -\frac{1}{k},\ -\frac{k+1}{k}\right)$$

which are essentially the same as those of Goudsmit and Bacher. An application of (37) and the calculation of relative intensities of the different components of the pattern can be made for different values of k. As has been pointed out by Granath the experimental pattern seems to agree best with $k=3/2$. Most of the pattern appears to have a complicated structure which is due to unresolved components. Only the group of lines due to transitions from $^3P_0$ to $^3S_1$ is simple and consists of three fairly well resolved lines. It seems difficult at present to draw any definite conclusions from the other parts of the pattern on account of lack of resolution. We consider it more im-

portant therefore to have an accurate calculation of the correction factor $1+\epsilon$ in (36'') than the exact evaluation of (36) (36'). There is, of course, no difficulty in evaluating $(\overline{r^{-3}})_p$. In the present instance the correction due to $(\overline{r^{-3}})_p$ amounts to about 1 percent change of scale for $^3P_2$ and 2 percent for $^3P_1$.

In order to calculate the factor $1+\epsilon$ in formula (36'') we must use the exact formula (19) which differs from (37) by the correction factor

$$1+\epsilon = 2\int \psi^2(0, q)dq/\psi_{1s}(0)^2. \tag{38}$$

The integral in the numerator is here the same as the integral in (19) the letter q having been written collectively for (x, y, z). The denominator of (38) is the $\psi_s(0)^2$ of (37') for $n=1$, $Z=3$.

We have tried a number of approximate forms for $\psi(q_1, q_2)$ using the variational method for the calculation of the term value of the ^3S state and then, having adjusted the constants to satisfy the minimizing requirement, calculated by means of the minimized functions the corresponding value of $1+\epsilon$. In all cases ϵ is a small quantity. Some of the functions give eigenwerte in good agreement with the spectroscopic term value while others give considerably too small absolute values of the eigenwert. It is of interest to see the results of the bad as well as the good functions. A very rough approximation to the solution can be obtained by tentatively expressing ψ as an antisymmetric combination of products of hydrogenic functions in the field of a certain nuclear charge. This charge is deliberately taken to be the same for both functions. The two functions entering are orthogonal and the calculation is very easy, only the common scale of the two functions being varied. In terms of the ionizing potential of Li^{++} the energy of the 2^3S state is known to be $\lambda=-1.1358$. In the same units the above function gives $\lambda=-1.1279$ and $1+\epsilon=0.96$. This is a deliberately poor function, possessing only one adjustable constant and giving a relatively poor agreement with the experimental λ. Hylleraas[12] has considered the ^3S terms of two electron spectra particularly for He. In his paper functions are tried for the ortho state of He which may be called the one and the two term approximations. These give for He $\lambda=-1.0855$ and $\lambda=-1.0871$. The values of $1+\epsilon$ for He would be 1.009 and 1.04 respectively. For Li^+ we have used only the one term function of Hylleraas giving $\lambda=-1.1337$, $1+\epsilon=1.02(6)$. From the analogy to He one would suppose that the two term function of Hylleraas would give an appreciably larger ϵ. The calculations with the two term function of Hylleraas are complicated, however, and we have found it more convenient to use another three constant function. It has also been possible to correct the first function of Hylleraas by a numerical method. In the latter case there is no definite way of using the eigenwert agreement as a check on the calculations and the procedure itself is somewhat arbitrary. Nevertheless it appears to be definite enough to show that $1+\epsilon>1.02$ and

[12] Hylleraas, Zeits. f. Physik **54**, 347 (1929).

that $1+\epsilon \leqq 1.06$. The numerical method is based on the following consideration. In the units of length ($h^2/8\pi^2 mZe^2$) and energy ($RhcZ^2$) used by Hylleraas the differential equation to be satisfied by ψ is

$$\left[\frac{\partial^2}{\partial r_1^2}+\frac{2}{r_1}\frac{\partial}{\partial r_1}+\frac{\partial^2}{\partial r_2^2}+\frac{2}{r_2}\frac{\partial}{\partial r_2}+\left(\frac{1}{r_1^2}+\frac{1}{r_2^2}\right)\frac{1}{\sin\theta}\frac{\partial}{\partial\theta}\left(\sin\theta\frac{\partial}{\partial\theta}\right)+\frac{\lambda}{4}+\frac{1}{r_1}+\frac{1}{r_2}-\frac{1}{Zr_{12}}\right]\psi=0. \tag{39}$$

The angle θ is the angle between the radii r_1, r_2 and r_{12} is the distance between electrons 1 and 2. A certain approximation to the exact solution can be obtained by supposing that ψ is a function only of r_1 and r_2 the angle θ being not very important for this particular state. The one term function of Hylleraas does not involve θ or r_{12} and is therefore an approximation of the above type. A systematic neglect of the dependence on θ leads of course to a definite eigenwert and to a definite eigenfunction if the variational method of solution is used. Substituting a general function $\psi(r_1, r_2)$ into the variational equation it is easy to obtain a differential equation for this ψ. This equation is

$$\left[\frac{\partial^2}{\partial r_1^2}+\frac{2}{r_1}\frac{\partial}{\partial r_1}+\frac{\partial^2}{\partial r_2^2}+\frac{2}{r_2}\frac{\partial}{\partial r_2}+\frac{\lambda}{4}+\frac{1}{r_1}+\frac{1}{r_2}-\frac{1}{Z\rho}\right]\psi=0$$
$$\rho=r_1 \text{ if } r_1>r_2$$
$$\rho=r_2 \text{ if } r_1<r_2. \tag{39'}$$

We assume for the present that the eigenvalue of λ and the function ψ of (39′) is a sufficient approximation to λ and ψ of (39). For the ^3S state ψ is antisymmetric in r_1, r_2 and vanishes therefore at $r_1=r_2$. It may be represented in two dimensions. Along the axis of $r_2=0, \rho=r_1$. The last three terms behave as $1/r_2$. If ψ and its first and second derivatives are finite on this axis we must require in order to satisfy (39′) that the term $2/r_2\,\partial\psi/\partial r_2+\psi/r_2$ should be finite i.e.

$$\left(\frac{\partial \log\psi}{\partial r_2}\right)_{r_2=0}=-\frac{1}{2}. \tag{40}$$

Any trial ψ can be checked qualitatively by means of (40) and it is important to require that (40) be satisfied in the region of large numerical values of ψ. This is especially advisable in the present instance because the result we wish to obtain is proportional to $\int\psi(r_1, 0)^2 r_1^2 dr_1$ and depends primarily on the relative values of ψ^2 at $r_2=0$ as compared with its value at other points of the r_1, r_2 plane.

The one term function of Hylleraas was tested by means of (40) and it was found that although the logarithmic derivative was fairly close to its correct value the differences were greater than could be desired. At a certain point of the r_1 axis (40) is satisfied exactly. This point lies at a higher value of $r_1=r_{10}$ than that which corresponds to the maximum of $r_1^2\psi^2$. At the maxi-

mum ψ does not decrease rapidly enough in absolute value with increasing r_2. The dependence of ψ on r_2 has therefore been corrected by a numerical procedure so as to satisfy (40) in most of the important region. For values of $r_1 < r_{10}$ this was done by fitting the exponential curve $Ce^{-r_1/2}$ to the curve of ψ against r_2. The fit was made quite accurate by calculating logarithmic derivatives $\partial \log \psi/\partial r_2$ of the Hylleraas function and choosing such an r_2 for every r_1 that $\partial \log \psi/\partial r_2 = -\frac{1}{2}$. This procedure is of course somewhat arbitrary because $e^{-r_1/2}$ is not an exact solution of the wave equation and because $\partial \log \psi/\partial r_2 = -\frac{1}{2}$ only at $r_2 = 0$. Nevertheless, as long as the correction applies only to a small region in the neighborhood of $r_2 = 0$ it is essentially correct. For values of $r_1 > r_{10}$ it is impossible to correct the function

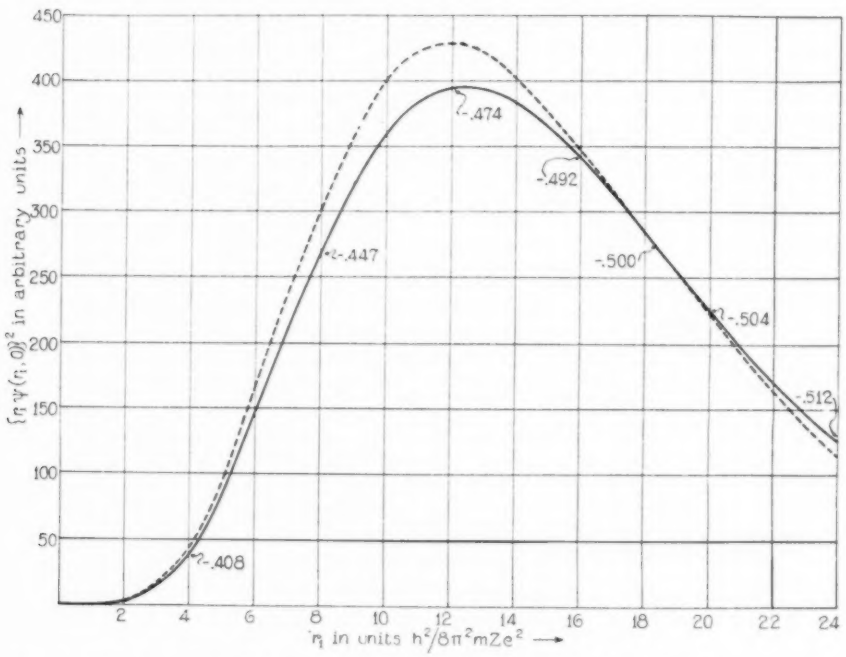

Fig. 1. The dotted curve is computed from the corrected, the full drawn curve from the uncorrected Hylleraas function. The values of $\partial \log \psi/\partial r_2$ are indicated along the curve.

by means of an exponential curve. The correction was made, therefore, by choosing for a given $r_1 = r_1'' > r_{10}$ a corresponding value of $r_1 = r_1' < r_{10}$ for which $\partial \log \psi/\partial r_2$ deviates from $-1/2$ by a numerically equal amount. The known corrections to ψ for $r_1 = r_1'$ and different values of r_2 were now applied to $r_1 = r_1''$ for the same values of r_2. This means that the deviation of $\partial \log \psi/\partial r_2$ was taken as the criterion of the magnitude of the correction to ψ. The whole procedure has of course a meaning only as long as the corrections are small and can be applied therefore only in the region around the maximum of $r_1\psi(r_1, 0)$. This maximum is at $r_1 = 12.5$ in the units of length used by Hylleraas. The correction becomes zero at $r_1 = 18.5$. The values of $(r_1\psi(r_1, 0))^2$ at these points are 397.5 and 270 on an arbitrary scale. The relation of the corrected and the uncorrected $(r_1\psi(r_1, 0))^2$ curves is shown in the Fig. 1.

Using these corrections the changes in $\int r_1^2\psi^2(r_1, 0)\, dr_1$ and $\iint r_1^2 r_2^2\psi^2(r_1, r_2)\, dr_1 dr_2$ were calculated. The corrections were taken into account only from $r_1=0$ to $r_1=24$. The resultant change in

$$\int r_1^2\psi^2(r_1, 0)dr_1 \Big/ \int\int r_1^2 r_2^2\psi^2(r_1, r_2)dr_1 dr_2$$

came out to be 4 per cent. The value of $1+\epsilon$ for the one term Hylleraas function is 1.02; the corrected value of $1+\epsilon$ is *1.06*.

Our correction procedure may of course be criticized on account of its arbitrariness. It must be remarked however that the sign and the order of magnitude of the result depend primarily on the fact that an increase in the absolute value of ψ is required at the maximum by the logarithmic derivative condition. Thus even though mathematically the procedure lacks rigor we believe that for the present problem it is essentially correct.

Finally we have calculated the result by the variational method using the following trial function.

$$\psi = \phi(kr_1, kr_2);\ \phi = (r_1 - c)e^{-(a/2)r_1-(b/2)r_2} - (r_2 - c)e^{-(a/2)r_2-(b/2)r_1}.$$

This function is easily adapted to the variational procedure. It contains three constants a, b, c. The constants c and k can be treated algebraically in the variational procedure. Extensive arithmetic need be done only in connection with different values of a. The reason for this simplification is that the minimized value of k is always close to $k=1$ if $b=1$, the difference from 1 being usually of the order of 1 percent or less. The first step is to choose a value of a and to take $b=1$. Supposing that $k=1$ the minimizing is done for c analytically. Taking this value of c the result is minimized for k analytically. It is then usually unnecessary to minimize for c again because $k \cong 1$. The procedure is repeated for different values of a and the absolute minimum of λ is fixed by interpolation.[13] We reproduce the final formulas for the minimizing procedure because they may be found useful in other connections. For $k=1$

$$\lambda/4 = (M - L_0 + L_1)/N \tag{41}$$

where

$$\begin{aligned} M = {} & 8a^{-3}b^{-3} + 24b^{-1}a^{-5} - 12a^{-1}b^{-1}\beta^{-7}(3\beta^{-1} - 2a^{-1}) \\ & - c[4a^{-2}b^{-3} + 12a^{-4}b^{-1} - 8ab\beta^{-6}(3\beta^{-1} - a^{-1})] \\ & + c^2[2a^{-1}b^{-3} + 2a^{-3}b^{-1} - 4ab\beta^{-6}];\ \beta = (a+b)/2 \end{aligned} \tag{42}$$

$$\begin{aligned} L_0 = {} & 24a^{-4}b^{-3} + 48a^{-5}b^{-2} - 48\beta^{-7} - c[16a^{-3}b^{-3} + 24a^{-4}b^{-2} - 40\beta^{-6}] \\ & + c^2[4a^{-2}b^{-3} + 4a^{-3}b^{-2} - 8\beta^{-5}] \end{aligned} \tag{42'}$$

[13] The trick of minimizing for k is the same as that used by Hylleraas, ref. 12, and amounts physically to satisfying the requirement of having the kinetic energy $= -(1/2)$ times the potential energy in a system with Coulomb forces.

$$\begin{aligned} ZL_1 = {} & 24[a^{-4}b^{-2}(a+b)^{-1} + a^{-3}b^{-2}(a+b)^{-2} + a^{-2}b^{-1}(a+b)^{-4} \\ & + 2a^{-1}b^{-1}(a+b)^{-5}] - (33/2)\beta^{-7} - c\{8[2a^{-3}b^{-2}(a+b)^{-1} \\ & + a^{-2}b^{-2}(a+b)^{-2} + a^{-2}b^{-1}(a+b)^{-3} + 3a^{-1}b^{-1}(a+b)^{-4}] \\ & - (25/2)\beta^{-6}\} + c^2\{4[a^{-2}b^{-2}(a+b)^{-1} + a^{-1}b^{-1}(a+b)^{-3}] - (5/2)\beta^{-7}\}. \end{aligned} \tag{42''}$$

Z = nuclear charge.

$$N/4 = 24a^{-5}b^{-3} - 18\beta^{-8} - 12c(a^{-4}b^{-3} - \beta^{-7}) + 2c^2(a^{-3}b^{-3} - \beta^{-6}) \tag{42'''}$$

With $L = L_0 - L_1$ the minimum for k comes at

$$k = L/2M, \quad \lambda/4 = L^2/(MN).$$

The correction factor $1+\epsilon$ is obtained as

$$1 + \epsilon = k^3 I/(N/4) \tag{43}$$

where

$$I = 24a^{-5} - 12c(a^{-4} - \beta^{-4}) + 2c^2(a^{-3} + b^{-3} - 2\beta^{-3}). \tag{43'}$$

Using these formulas we obtain for $a = 1/3$; the minimized values $c = 1.446$, $k = 1.0057$, $-\lambda/4 = 1.1344$; $1+\epsilon = 1.082$. The minimized value of a is 0.380 giving $-\lambda/4 = 1.1354$; $1+\epsilon = 1.063$. On the other side of the best value of a say at $a = 0.395$, $1+\epsilon = 1.055$ and $-\lambda/4 = 1.1353$. The calculations have been carried out to several more significant places and for several more values of a than given here. It is seen that $1+\epsilon$ varies slowly for the functions minimized for changes in c and k. We believe therefore that 1.063 is a fairly accurate result. It will be noted that this result is in agreement with that obtained by correcting Hylleraas' one term function, and that the agreement between the empirical value of $-\lambda/4 = 1.1358$ and the theoretical $-\lambda/4 = 1.1354$ indicates that the trial function used by us is good.

It is of course usually said that an eigenfunction may be quite inaccurate even if a good eignwert is obtained. We must consider this in somewhat more detail. Eckart[14] has already given a criterion for the accuracy of eigenfunctions. His reasoning may be extended so as to apply to the specific calculation of a given quantity.

With Eckart we let the solution obtained by the variational method with a given trial function be ϕ and the true eigenfunctions (in this case of the ^3S system) we denote in order of decreasing term values by $\psi_1, \psi_2, \cdots$; the corresponding negatives of the energy we write as $W_1, W_2, \cdots$ The functions $\psi_1, \psi_2, \cdots$ are supposed to be normalized and $\phi = a_1\psi_1 + a_2\chi_2 + \cdots$ where $a_1^2 + a_2^2 + \cdots = 1$. Eckart shows that if the trial function ϕ leads to

[14] Carl Eckart, Phys. Rev. **36,** 878 (1930). In this very useful and interesting paper will be found also many other eigenfunctions. The one used for ^3S states of two electron systems is very similar to ours. The eigenwert for Li^+ obtained by Eckart is almost as good as the one obtained by us. For our work we considered it important to minimize for c as well as the other constants because the result is fairly sensitive to c. See also D. S. Hughes and C. Eckart, Phys. Rev. **34,** 694 (1930) for the calculation of the isotope effect in the Li^+ spectrum.

an energy value of absolute amount W then $1-a_1^2<(W_1-W)/(W_1-W_2)$. We wish to calculate the average of some quantity $f(q)$ over the configuration space q. The function ϕ gives the approximate result $\bar{f}_0=\int f(q)\phi^2(q)dq$ while the correct result is $\bar{f}=\int f(q)\psi_1^2(q)dq$. The error is

$$\bar{f}_0-\bar{f}=(a_1^2-1)f_{11}+a_2^2f_{22}+a_3^2f_{33}+\cdots+2a_1a_2f_{12}+\cdots$$

where $f_{ik}=\int\psi_i\psi_k f dq$. The terms in f_{ii} are of the order of $1-a_1^2$ which in the present instance is of the order of 4×10^{-3}. The relative error due to these terms can be therefore neglected. The only important terms are those containing $f_{1i}(i\neq1)$. Thus

$$\bar{f}_0-\bar{f}\leqq 2a_1\sum_{i=2}^{\infty}a_if_{1i}\leqq 2\sum_{i=2}^{\infty}a_if_{1i}. \tag{44}$$

Any a_i^2 for $i>1$ is $<1-a_1^2<(W_1-W)/W_1-W_2)$ and the general order of magnitude of (44) is that of $(\ (W_1-W)/(W_1-W_2)\ )^{.1/2}$. The numbers f_{1i} are however also of influence. In order to estimate their order of magnitude we must use the special form of f. In our problem

$$f=\tfrac{1}{2}(\delta(0,q_2)+\delta(0,q_1))$$

q_1 and q_2 being the collective coordinates of electrons 1 and 2. We have then

$$f_{12}=\int\psi_1(0,q)\psi_2(0,q)dq. \tag{45}$$

Approximately

$$\psi_1\leqq 2^{-1/2}[\phi_{1s}(q_1)\phi_{2s}(q_2)-\phi_{1s}(q_2)\phi_{2s}(q_1)]$$
$$\psi_2\leqq 2^{-1/2}[\phi_{1s}(q_1)\phi_{3s}(q_2)-\phi_{1s}(q_2)\phi_{3s}(q_1)]$$

where the ϕ_{1s} is a hydrogenic function in a central field of nuclear charge Z and ϕ_{2s}, ϕ_{3s} are hydrogenic functions in a central field of nuclear charge $Z-1$. The hydrogenic functions ϕ_{2s}, ϕ_{3s} are orthogonal to each other. In this approximation $f_{12}\leqq(1/2)\phi_{2s}(0)\phi_{3s}(0)$. It will now be remembered that $\phi_{ns}(0)^2$ in a field of charge Z is proportional to Z^3/n^3. Thus $\phi_{2s}(0)^2/\phi_{1s}(0)^2\leqq(2/3)^3(1/2)^3=1/27$ in the present instance. We may take $f_{12}<(1/30)f$. It is now seen that we are likely to over-estimate the error by setting $a_3=a_4\cdots=0$, and attributing all the error to a_2. Doing this, $\bar{f}_0-\bar{f}=2a_2f_{12}\leqq(a_2/15)f$ and a_2 itself is of the order of $1/15$. Thus the accuracy is likely to be about $(1/2)$ percent.

This estimate of the probable error together with the agreement of this calculation with the numerically corrected Hylleraas one term function makes us think that the value 1.06 which we calculated by both methods is probably correct to 1 percent. We thus conclude

$$1+\epsilon=1.06. \tag{46}$$

Using this value in (36″) (37) and the separation between components (1) and (3) observed by Schüler we can derive the value of μ. According to Gran-

ath[6] a slight correction must be applied to Schüler's value of v_{vac} for component (3). Applying this correction and supposing that the nulear spin is $k=3/2$ we get

$$1840\mu/k = g = 2.13. \tag{46'}$$

Thus Schüler's and Granath's present data and the present calculation indicate that the magnetic moment of the Li_7 nucleus is approximately equal to three times the theoretical magnetic moment of a proton. If the magnetic moment were exactly three times the theoretical protonic moment the g value in (46') would be $g=2$. We have at present no explanation to offer for the result $g=2.13$. It appears that the difference of 2 and 2.13 is a greater one than can be accounted for by experimental errors or by errors in our calculation. It must be remembered however that the measured position of component (1) may be slightly affected by the proximity of component (2) and that the whole separation between (1) and (3) is of the order of 1 cm^{-1}.

Note added in proof: If the coupling of the electronic orbits and spins is of the Russell-Saunders type and if the electronic interactions are not too large and yet considerably larger than the interactions with the nucleus it is possible to give general and simple formulas applying to the case of one electron being in an s state. The other electron is then supposed to be in an L state of azimuthal number l. We may write the energy perturbation as:

$$w = (\mu/k)(b/2)[f(f+1) - k(k+1) - j(j+1)] \tag{47}$$

where the perturbation Hamiltonian is taken to be $H' = (\boldsymbol{B}\boldsymbol{\mu}) = (\mu/k)(\boldsymbol{B}\boldsymbol{k})$ and $\boldsymbol{k}$ denotes the angular momentum matrix vector of the nucleus in units $h/2\pi$. If the electronic angular momentum $\boldsymbol{J}$ is made diagonal in the sense of containing $\delta(j', j'')$ as a factor for every matrix element and if for a given j the matrix J_z is also diagonal then the diagonal elements of B_z for that j mb; $m=(j, j-1, \cdots, -j)$. The proof of this for B_z is exactly similar to the proof for σ_z in the usual derivation of Lande's g factor. The momentum J_z remains conserved under the perturbation B_z. We now imagine the coupling between the electron spins and between the two orbital momenta to be removed. The matrix elements may be referred to pairs of states such as $(^2S_{1/2})_{m_1}$ and $(^2L_{l+1/2})_{m_2}$. A canonical transformation does not change the sum of diagonal matrix elements belonging to a given $m=m_1+m_2$. The values of b for ^3L and ^1L are thus related to the values for ^2S, ^2L by sum rule equations:

$$(l+1)b(^3L_{l+1}) = (\tfrac{1}{2})b(^2S) + (l+\tfrac{1}{2})b(^2L_{l+1/2})$$

$$l\{b(^3L_{l+1}) + b(^3L_l) + b(^1L_l)\}$$

$$= (\tfrac{1}{2})b(^2S) + 2lb(^2L_{l+1/2}) + (l-\tfrac{1}{2})b(^2L_{l-1/2}) \text{ etc.}$$

The values of b for the one electron terms are known:

$$b(^2L_j) = 2\mu_0\, l(l+1)/j(j+1)\cdot(\overline{r^{-3}});\ b(^2S) = (16\pi/3)\mu_0\, \psi_S^2(0).$$

The value of $b(^1L_l)$ is easily computed directly and the remaining b are determined by the above relations. Thus:

$$
\begin{aligned}
b(^3L_{l+1})/\mu_0 &= (8\pi/3)\psi_S^2(0)/(l+1) + 4l(\overline{r^{-3}})/(2l+3) \\
b(^3L_l)/\mu_0 &= (8\pi/3)\psi_S^2(0)/(l^2+l) + 2(\overline{r^{-3}}) \\
b(^3L_{l-1})/\mu_0 &= -(8\pi/3)\psi_S^2(0)/l + 4(l+1)(\overline{r^{-3}})/(2l-1) \qquad (47') \\
b(^1L_l)/\mu_0 &= 2(\overline{r^{-3}}).
\end{aligned}
$$

Formulas (36), (36′) are special cases of (47), (47′). The fact that sum relations such as used here exist has already been mentioned on p. 210 of Pauling and Goudsmit, Structure of Line Spectra. According to an informal communication of Professor Goudsmit these sum rules have been used by him in the derivation of the general formula in Phys. Rev. **35,** 440 (1930). Formulas (47), (47′) apply only to the case of Russell-Saunders coupling but have the advantage of simplicity.

THE THERMOANALYSIS OF METAL SINGLE CRYSTALS AND A NEW THERMOELECTRIC EFFECT OF BISMUTH CRYSTALS GROWN IN MAGNETIC FIELDS

By Alexander Goetz and Maurice F. Hasler
California Institute of Technology, Pasadena

(Received September 29, 1930)

Abstract

Part I. The Thermoanalysis of Bi Single Crystals

Production of crystals.—Crystals of Bi of any desired orientation were grown by the method of Goetz, one half of each normally, the other half within a transversal magnetic field. The orientations, predetermined by a seed crystal, were not affected by this process. Two methods of growth—the continuous and the discontinuous—were used.

The thermoanalysis of a crystal.—A method and its experimental realization—the thermoanalyzer—were developed to measure and to localize any changes of the thermoelectric properties along the lengths of crystals without applying mechanical stresses to them, by progressive local heating of the specimens. Thus very small distortions and imperfections were detectable due to their thermoelectric asymmetry.

Types of thermoanalytic diagrams.—The types of diagrams to be expected in the cases of a perfect single crystal, a double-, and a triple-crystal are discussed and a method is developed to analyze simple diagrams by means of the theory of heat-conduction.

Part II. Experimental Results Obtained for Normal and Magnetic Crystals with a Discussion of the Same

The thermoanalysis of normal crystals.—The application of the thermoanalysis to normal single crystals leads to the discovery of very small (0.1 mm²) regions within a crystal which are distorted due to very slight variations of the cooling conditions during the growth of the crystal. It is however possible to avoid these faults and to produce comparatively perfect specimens. Hence it was possible to test the results of different methods of crystal production and thus to refine the method used as well as to measure quantitatively the influence of a magnetic field applied to the crystal during the time of its formation.

The thermoanalysis of "magnetic" crystals.—It was found that the normal half of a crystal has a thermoelectric e.m.f. against the "magnetic" half. The sign and size of this e.m.f. depend on many circumstances, though mainly on the orientation the growing crystal has with regard to the direction of the field lines.

The effect as a function of the orientation.—The effect is a maximum if the principal axis of the crystal grows normal to the lines of force and it is very small (probably zero) if the axis grows parallel. It depends furthermore on the orientation of the crystal with regard to the direction of the thermoelectric current, since the two orientations in which the principal axis is normal to the field show different effects: a small one if the axis is normal to the current, and a very large one if it is parallel. —The thermal e.m.f. obtained for the latter case is 4.3 microvolts/degree which would correspond to a change in orientation of ca. 21° though no actual change could be observed.

The effect as a function of the method of growth.—The thermal e.m.f. depends largely upon the method of growth, i.e., whether the crystal is grown by the continuous or the discontinuous method.

The effect as a function of impurities.—The thermal e.m.f. for one and the same method of growth depends also on the amount of chemical impurities. Four kinds of purest Bi of different provenience were used in which the total amount of other substances was less than 0.2%. The metals were spectroscopically examined and it appeared that the purest (electrolytic) metal showed the smallest effect. It was *ca.* 40 times smaller than the effect of another metal. Traces of Ag and Pb seem to affect the "magnetic" sensibility of Bi most whereas Sb is rather ineffectual.

The effect as function of the field strength.—The effect is influenced by the strength of the applied field through this problem is not yet settled quantitatively. The influence of a small field (10^2 Gauss) is comparatively large, whereas fields of more than 13000 Gauss seem to decrease the effect. The maximum seems to depend largely on the kind of the impurity.

The effect as a function of temperature.—The Peltier-effect (extrapolated from the $E-f(\theta)$ curve) shows a sharp discontinuity between 75° and 90°C, indicating a different relation with regard to the transformation of Bi in this region. No indication could be found that annealing above this point (16 hours) and aging (1 month) destroys the difference between the normal and the "magnetic" half of a crystal.

Discussion.—The results obtained are brought into relation with the diamagnetic anisotropy of Bi. They are discussed with regard to the investigations of other authors and it appears possible to describe the effect as due to a change in the secondary (mosaic) lattice of the Bi crystal.

Part I. The Thermoanalysis of Bi Single Crystals

Introduction

IN A previous paper,[1] one of the authors (G) described a method of producing Bi-single crystals which permits the application of strong, transverse, magnetic fields at the zone of crystallization. The influence of the field with regard to the orientation of the growing crystal was studied. It was stated that the orientation frequently obtained was such that the trigonal axis of the growing crystal was parallel to the lines of force, in case the crystal formed its first center of crystallization within the field. This result was partly to be expected if one considers the anisotropic nature of the diamagnetic susceptibility in Bi-crystals. Since this susceptibility is at a minimum along the trigonal axis and at a maximum in a direction normal to it, the crystal assumes an orientation which corresponds to a minimum of free energy. This result is in agreement with the early observations of Plücker[2] and Leduc.[3] It was, however, unexpected that the orienting forces of the strongest magnetic fields (*ca.* 22000 Gauss) did not show any effect as soon as the orientation of the growing crystal was already predetermined before entering the field. Yet for several reasons, it seemed to be interesting to investigate whether or not a crystal, one half of which was grown without, the other half within a strong transverse magnetic field showed any differences at all between portions, despite the fact that the orientation remained unchanged.

Such differences were to be expected when, for instance, one considers

[1] A. Goetz, Phys. Rev. **35,** 193 (1930).
[2] S. Plücker, Pogg. Ann. **76,** 583 (1849).
[3] M. A. Leduc, C. R. **140,** 1022 (1905).

such observations as those by Tieri[4] concerning the Hall-coefficient of Bi specimens crystallized within a strong magnetic field. A large difference of the Hall-e.m.f. was found with regard to different directions of the field lines crossing the solidifying specimen, but no interpretation was possible as these experiments were only of a qualitative kind and made on polycrystals.

Production of crystals. Since the method of producing bismuth single crystals introducing a minimum of mechanical stresses has already been described[1,5] as well as the way the magnetic field was applied to the growing crystal only a few additional details need be mentioned.

The orientation of the crystal was as usual predetermined by a seed. Three main orientations were grown, which represent the possible primary relations between trigonal axis, the (111) plane, and the lines of force (see below). Two methods of growth were employed which differ principally both in the forces applied to the growing crystal at the moment when the field was energized and in the results obtained.

The first, entitled the *discontinuous method*, consisted of two distinct processes. A crystal was first grown completely without any magnetic field present (the residual field of the magnet was eliminated by removing the pole pieces). It was then removed from the growing trough, etched, and carefully examined with regard to irregularities. In case none could be detected, the crystal was put back into the trough, which in turn was put back into the furnace so far that only one half of the crystal melted again, the temperature of the furnace being regulated so as to bring the border between solid and liquid-crystal exactly in the middle of the pole-pieces of the magnet. This process had to be done very carefully in order to avoid irregularities along the molten part of the crystal. As soon as thermal equilibrium was reached, which condition could easily be recognized since the progress of the molten region into the space between the pole-pieces stopped as soon as the heat distribution along the crystal became stable, then the magnetic field was excited and the driving mechanism of the crystal apparatus started, thus the second half of the crystal recrystallized within a magnetic field.

The second, entitled the *continuous method*, allowed the growth of the unmagnetic and magnetic portion of the crystal in one operation. This was done by growing the crystals in the usual manner but with the pole-pieces in position, a precaution that was essential as pole-piece moving with its attendent jarring was prohibitive during crystal growth. This method had the advantage over the other process in that the growing forces remained undisturbed when the magnetic field was applied. In the early work, however, it had the disadvantage in that the residual field of the magnet (200–300 gauss) was present while the first portion of the crystal, the so-called "unmagnetic" half, was growing. Later this was eliminated by providing a magnetic by-pass of soft iron across the pole-pieces and above the trough, which was removed just before the magnet was energized. All these crystals

[4] L. Tieri and E. Persico, Linc. Rend. **30**, 464 (1921).

[5] A. Goetz and M. F. Hasler, Proc. Nat. Acad. **15**, 646 (1929).

were grown in an atmosphere of CO_2 to prevent oxidation so that in this respect they also differ from those grown by the discontinuous method.

The first observation which was made on crystals produced by the discontinuous method with fairly high fields was the difference in reflectivity of light between the two halves. This was most noticeable in the P_1 orientation, i.e. where (111) plane is parallel to the lines of force. It seems improbable that this difference was due entirely to the second recrystallisation, as etching off a layer one mm or more thick does not destroy the phenomenon. This effect must indicate a change of the structure of the crystal-faces within the magnitude of the wave-length of visible light and it thus seems possible that it concerns the mosaic lattice as described by Zwicky[7] and Goetz[8]. This possibility will be treated at length in another paper.

The thermoanalysis of a crystal. Concerning a sensitive and effective method for determining possible differences between these two halves of one and the same crystal, it seemed that the measurement of the thermoelectric effect fulfilled the requirements the most easily. Nevertheless, it was experimentally rather difficult to perform, since it was not only necessary to measure the thermal e.m.f., but also, to localize it as exactly as possible. Several methods had to be tried until it was possible to obtain reliable results and since such methods, allowing one to measure as well as to localize a thermal e.m.f. within a metal rod, are excellent indicators of inhomogeneities undetectable by other means, their applicability is not limited to this special problem. Thus it seems worth while to give a more detailed description of them. (A similar idea has been put into realization independently by Terada and his collaborators.[9,10,11] Their experiments had been started for testing the reality of the Benedix effect and the method used was fundamentally the same as ours, though quite different in its experimental procedure. It is excellent for the detection of the "residual" thermal e.m.f.'s. but its sensitivity and reproducibility does not meet the requirements of the thermoanalysis of single crystals).

A simple method first tried was as follows: The crystal was first protected by a coat of Duco paint. Leads from the ends were connected to a galvanometer, the contacts with the crystal being kept at constant temperature. The crystal held horizontally, had a small portion heated locally by the touch of a mercury meniscus which topped a column of that metal heated by an electric furnace. If the meniscus was moved slowly along the crystal and the deflections of the galvanometer were observed with relation to the position of the heated point on the crystal, then a thermoelectric analysis of each increment of length could be made. As soon as the heated region came near the border between the "magnetic" and the normal part of the crystal, an

[6] A. B. Focke, Phys. Rev. **36,** 319 (1930).
[7] F. Zwicky, Proc. Nat. Acad. **15,** 253, 816 (1929); **16,** 211 (1930).
[8] A. Goetz, Proc. Nat. Acad. **16,** 99 (1930).
[9] T. Terada and T. Tsutsui, Proc. Imp. Acad. Tokio. **5,** 132 (1929).
[10] T. Terada, T. Tsutsui and M. Tamano, Sc. Pap. Inst. Res. Tokio, **7,** 201 (1927).
[11] T. Terada, T. Tsutsui and M. Tamano, Proc. Imp. Acad. Tokoi, **3,** 507 (1927).

e.m.f. was indicated, but its size could not be measured accurately enough inasmuch as it depended on the contact conditions of the meniscus which could not be made reproducible. This method was therefore soon abandoned.

The next method that was tried was to heat the crystal locally by focusing radiation of a powerful incandescant lamp upon it. This method had the advantage over the previous one in that it was not necessary to protect the surface of the crystal against amalgamation, with a covering that was necessarily a poor heat conductor. A large number of observations were made with this apparatus, but due to certain inherent difficulties of the method, it was abandoned. These difficulties were, for instance, providing air cooling

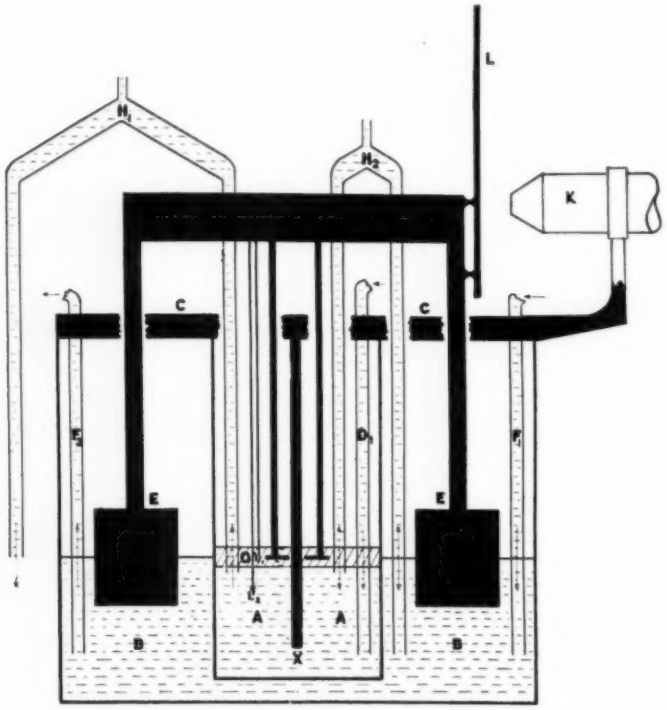

Fig. 1. Diagram of the thermoanalyzer.

of the crystal as a whole while preventing local convection currents at the point of heating, measuring the temperature at the heated point, and preventing surface irregularities of the crystal from nullifying results.

The final arrangement which avoided the above difficulties and made possible quantitative measurements is sketched in principle in Fig. 1. A cylindrical glass-container A, 18 cm long and 9 cm wide is held in the center of a large glass-container B, 24 cm wide, 22 cm long, by means of the bridge C. The glass tube D_1 is fixed in A and brings water at a definite temperature and under constant pressure into A. The vessel B is also filled partially with water, the level of which determines the position of a ring-shaped float E. Two tubes F_1 and F_2 fixed in B permit the raising or lowering

of the water level of B, which in turn changes the position of the float E. Fixed to this float E is a frame arrangement which carried several devices among which are the syphons H_1 and H_2 and the scale L. The latter serves to measure the position of the float (incl. oil-layer, furnace, etc). with regard to the crystal by means of the reading microscope K attached to the frame C. The syphons H_1 and H_2 have one end in A just underneath the water level, the other end of H_1 going outside of B, the corresponding end of H_2 ending beneath the water level in B. The horizontal part of both syphons is shaped to separate air bubbles from the flowing water, while adjustments for bringing the tubes into correct positions with regard to the water levels are provided. Beside the syphons, the float carries an electric heater consisting of a horseshoe-shaped thin mica sheet around which chromel wire is coiled. Other mica sheets above and below insulate this heater from two thin copper plates which bind the whole, making for equal heat-distribution and rigidity. This whole heater is only 1 mm thick. Its position with regard to the frame is so adjusted that it is slightly above the water level in A when the ends of H_1 and H_2 are just beneath that level. On top of the water in A, an oil layer of 5–10 mm thickness is put in order to surround the heater completely.

The arrangement works as follows: A constant flow of water is sent into A filling it up to a certain point, any surplus being syphoned off. The water level in A is therefore determined by the position of the syphons H_1 and H_2 or what amounts to the same thing, by the position of the float E in B. Thus a permanent circulation of the water underneath the heated oil layer results and consequently a constant temperature. If a certain amount of water is added through F_1, the water in B rises and with it the float E holding the syphons and the heater. The oil layer in turn maintains its relative position with regard to the heater since its supporting water column rises as the syphons rise. It follows that the water has to be added into B at a rate sufficiently slow to permit hydrostatic equilibrium in A. Therefore, the cross sections of H_1 and H_2 are large compared with the cross-sections of F_1, F_2 and D_1. As an indicator of this equilibrium, a differential thermocouple is also attached to the frame of E. It consists of two copper wires L_1 and L_2 the ends of which, ending one in the middle of the oil-layer, the other within the water flow, are connected by a very thin constantan wire. This arrangement is extremely sensitive because the smallest displacement of the heater with respect to the oil and water level changes the temperature of the L_1-junction and thus produces a change in the thermal e.m.f.

The reason the syphon H_2 is used in addition to H_1 is first, to tie the water systems of B and A together so that no appreciable differences in levels can result, though when everything is properly adjusted this link is largely static, and second to minimize the irregularities of the flow in H_1 caused by small differences in the surface tension of the water at the outside opening of H_1, since H_2 allows the large volume of B to be used as a "shock-absorber."

Thus an arrangement is obtained which permits the production of a constant gradient of temperature which can progress regularly along a crystal X hung perpendicularly in the vessel A as indicated in Fig. 1. To com-

plete the ensemble, it is only necessary to mount the crystal in a holder which keeps it in a fixed position with regard to A, to provide connections at both ends with a galvanometer, and to keep the upper contact at a constant temperature, a temperature as nearly as possible equal to that of the water in A. All this was conveniently done with the so-called "crystal holder."

The bakelite tube J in Fig. 2 carries at one end the adjustable fork K, while close to the other, the clamp L. Through J sealed in, runs a copper wire, the upper end of which is connected directly with the galvanometer. The other end, bent, has a silver wire (0.1 mm) soldered to it. Furthermore, J carries an adjustable clamping device M which permits one, with the aid of a similar one on the bridge C (Fig. 1), to fix the holder into any position desired with respect to A. To cool the upper end of the crystal, a copper cylinder N is used, provided with two small side-tubings N_1 and N_2, N_1 being

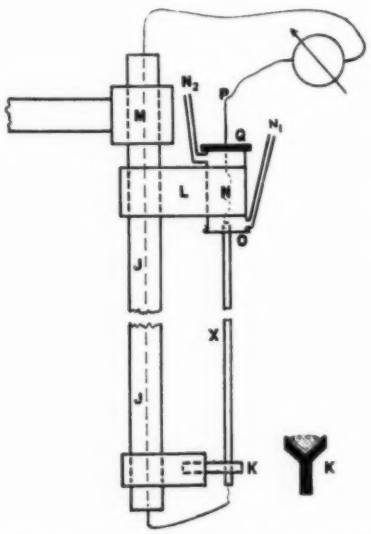

Fig. 2. Diagram of the crystal-holder of the thermoanalyzer.

connected with a water reservoir of constant temperature and hydrostatic pressure. In this way, a water flow is sent into N_1 and leaves by N_2. To fix the upper end of the crystal X in a position within the water flow without applying any fatal strain to it, a thin rubber membrane O (toy balloon), with a small central hole burned into it is stretched over one end of N. After a silver wire similar to the one previously mentioned is spark-welded to the crystal, the hole in O is momentarily widened, the crystal is introduced and the membrane released, thus forming a tight sleeve around X able to withstand the water pressure in N. The silver wire protruding now from the other side of N is soldered onto the copper wire P which is fixed in the bakelite plate Q. After a contact is thus made between P and X the plate Q is sealed tight onto N, thereby closing the water chamber. N and X are fixed into the clamps L and K respectively and the silver wire at the lower end is also spark-welded onto X. The whole arrangement is then put

vertically into A in such a way as to bring X exactly through the central opening of the heater. The wire P is connected through a resistance box to the galvanometer, thus completing the circuit. Fig. 3 shows a photograph of the apparatus for thermoelectric analysis and Fig. 4 a picture of a crystal in its holder. It is necessary to mention that the task of mounting crystals without distortion is a very difficult one and requires a special apparatus which avoids critical stresses by facilitating manipulation.

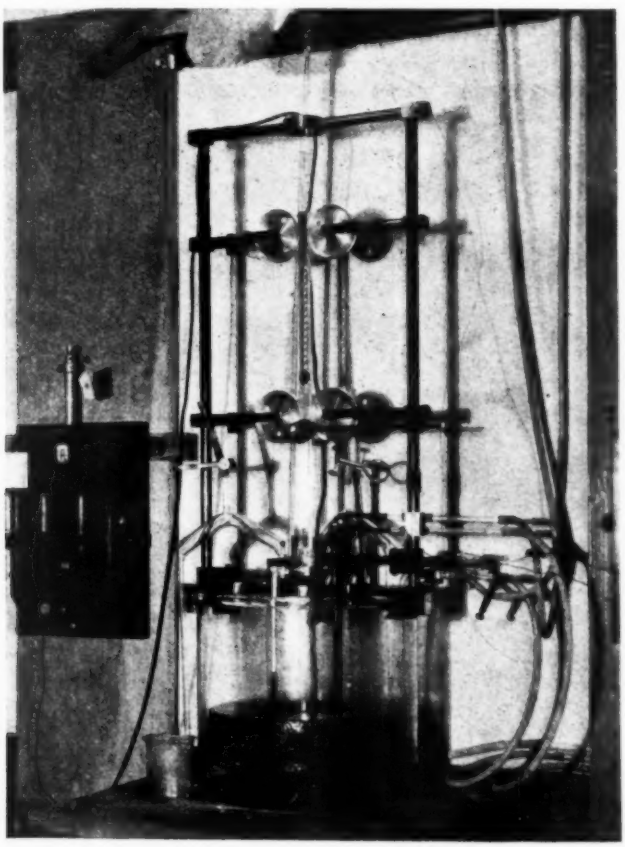

Fig. 3. Photographic view of the thermoanalyzer.

After the crystal, mounted in its holder, is fixed in the vessel A, the different water flows are started and the furnace-plate is heated, in general to a temperature 18° above the temperature of the running water. After thermal equilibrium is reached measurements are taken, i.e. the deflections of the galvanometer are measured as a function of the position of the oil-layer relative to the crystal. Simultaneously the e.m.f. of the differential-thermocouple is measured to assure the maintenance of thermal equilibrium. Schematically, this is shown in Fig. 5 where X is the crystal, W_1 is the water cooling the lower end of the crystal and W_2 that cooling the upper end, G_1 is the galvanometer measuring the thermal e.m.f. of the crystal, and G_2 one

measuring the difference of temperature between the heated oil layer O and the water W_1.

Types of thermoanalytic diagrams. First it will be considered what type of curve one would expect to obtain with this kind of an arrangement. The obvious way of plotting the diagrams is to represent the thermal e.m.f. indicated by G_1 (Fig. 5) as ordinates and the position X of the heated oil layer with respect to the crystal as abscissas. If one considers first, the diagram that would be obtained by the thermoanalysis of a perfectly homogeneous crystal, one realizes immediately that it should not show any thermo-

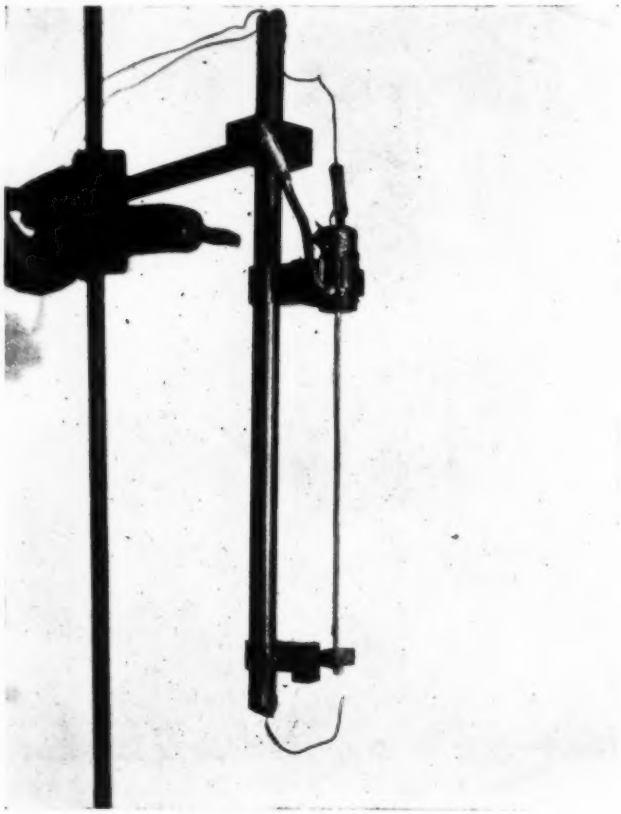

Fig. 4. Photographic view of the crystal-holder.

electric potential (Magnus' Law). However, certain deviations from this purely theoretical concept would be expected as a result of imperfect cooling conditions and the heat-conductivity of the crystal. Hence, a curve of the type (Fig. 6a) should be expected where the dotted line would represent a constant thermal e.m.f. (τ) due to a slight difference of temperature between the two different end cooling systems; while the curve drawn in full with its deviations from linearity would be obtained under normal conditions, where the cooling of the ends of the crystal is not sufficient to prevent a slight heating by conductivity through the metal. To make this "end-effect" as small as possible, the crystal used has to have a small cross-section.

The second case to be considered is shown in Fig. 6b, which represents an unhomogeneous crystal consisting of two halves (I and II) which have a thermal e.m.f. against each other. In this case, a curve as shown would be obtained, where a maximum would permit the exact localization of the junc-

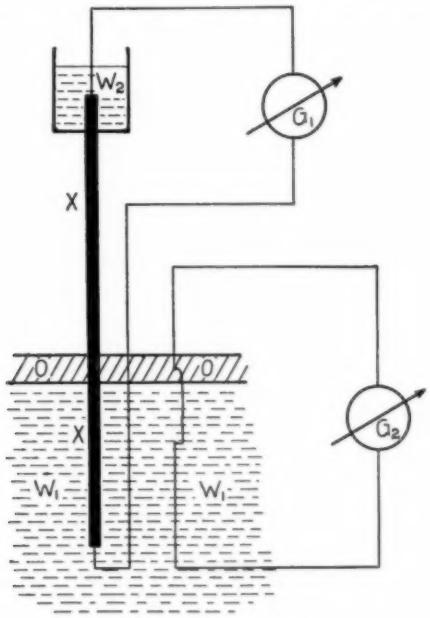

Fig. 5. The electrical connections of the thermoanalyzer.

tion of the two halves. Superimposed upon this would be the effects previously mentioned (Fig. 6a) though the constant thermal e.m.f. due to unequal end cooling would have a different value since the thermoelectric

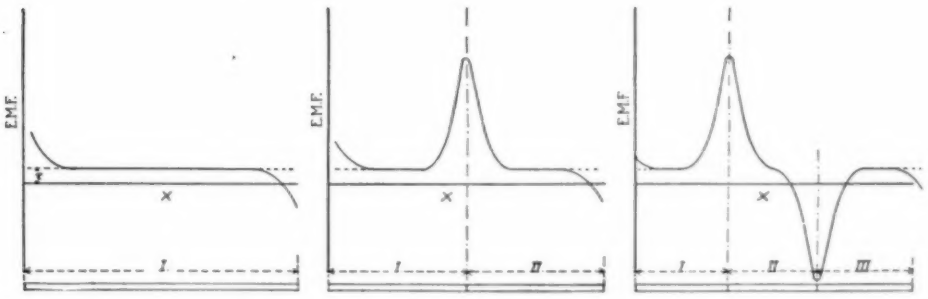

Fig. 6. a. b. c. Ideal thermoanalytic diagrams of a perfect single-crystal (a), a perfect double-crystal (b), and a perfect triple-crystal (c).

power of the two halves against the contact metal would be different from that in the case of a single crystal. Also, the end effects due to heat conduction would be slightly asymmetrical since the two different halves are involved. The sharpness of the maximum would depend on the gradient of

temperature along the crystal and the extension of the heated zone, thus the former should be as large while the latter as small as possible.

The third case in which the crystal consists of three sections, the second of which has the same thermal e.m.f. against the first and third (I: III, Fig. 6c) would result in a curve which is more complicated. With the heated oil layer at the junction of part I and II, there would be a maximum similar to that of Fig. 6b. Furthermore, on reaching the transition from II to III, the same thing would happen but in the opposite direction. Of course, the shape of the whole curve would depend very much on the relative sizes of the three sections. For a given thermoelectric difference of II against III, and a given difference of temperature in the analyzing apparatus, the maximum and minimum would not change their size as long as II is large enough to contain the whole drop of temperature given by the analyser. If II is smaller, the maxima would decrease and finally there is a size below which no effect whatsoever would be observed. This threshold determines the resolving power of the arrangement and depends on the construction of the analyser and the cross-section, thermal conductivity, etc., of the crystal as follows: The thermal conditions along the crystal within the thermo-analyser are easily treated by the general equation of the temporal and local distribution of temperature in a linear conductor:[12]

$$\frac{\partial\theta}{\partial t} = \frac{\sigma}{\rho\, c}\frac{\partial^2\theta}{\partial x^2} - \frac{h}{\rho\, c}\frac{U}{S}\theta \tag{1}$$

where: θ is the temperature for (x) and (t); r the radius of the crystal; U the circumference of a cross-section of the crystal; S the cross-section of the crystal; x the length-coordinate of the crystal; h, the thermal emissivity of the crystal surface; c the specific heat; ρ the density; and σ the specific heat-conductivity.

Since the movement of the oil-layer along the crystal within the thermoanalyser is very slow we assume stationary condition, i.e. $\partial\theta/\partial t = 0$. Thus Eq. (1) becomes:

$$\frac{\partial^2\theta}{\partial x^2} = \frac{U}{S}\frac{h}{\sigma}\theta = \frac{2\,h}{r\,\sigma}\theta \tag{2}$$

and:

$$\theta = A\exp\left[-(2h/r\sigma)^{1/2}x\right] + B\exp\left[(2h/r\sigma)^{1/2}x\right]. \tag{3}$$

For the assumption of $x = \infty$, i.e. in case the crystal cools down so fast that the gradient is zero before the end of the crystal (which fact is indicated by the absence of the end-effects mentioned above), B and therewith the second term of Eq. (3) equals zero; hence we obtain:

$$\theta = A\exp\left[-(2h/r\sigma)^{1/2}x\right] \tag{4}$$

where A equals $\theta_{\max}$, the temperature of the oil layer, if one assumes the absence of any gradient across the crystal as was already done for the entire crystal implicitly in Eq. (1).

[12] Enzyklopädie d. Math. Wiss. **5**, I, 181.

The graphical interpretation of the records of the thermoanalyzer is more convenient if Eq. (4) is transformed into a logarithmic system:

$$\ln \theta = \ln A - (\alpha h)^{1/2} x \tag{5}$$

where $\alpha = 2/r\sigma$. If $\ln\theta$ is chosen as ordinate and $(h^{\frac{1}{2}}x)^{-1}$ as abscissa, the cooling curve becomes a straight line as shown in Fig. 7a, its inclination ($tg\ \phi$)

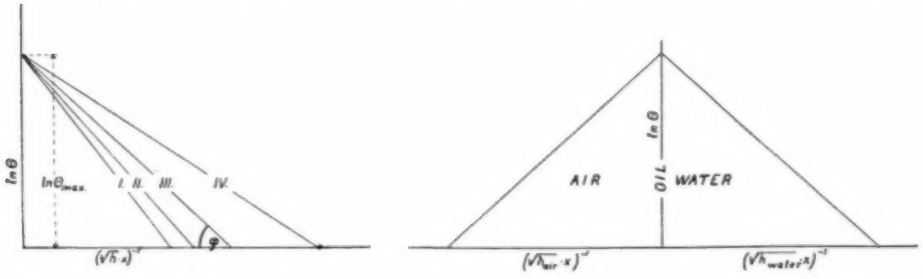

Fig. 7. a. b. Ideal logarithmical diagrams of a perfect double-crystal. The difference between the thermal "emissivity" for water (h_{water}) and air (h_{air}) of the crystal surface is compensated to obtain a symmetrical diagram. (Read +1 for −1 as abscissa-exponent!)

is for the same crystal directly proportional to $\ln\theta_{max}$ and $h^{-\frac{1}{2}}$, since r as well as σ is constant for a perfect single crystal over its whole length. However h differs with the surrounding medium, for instance is $h_{air} < h_{water}$. Hence the diagram is simplified if the abscissa indicates $\xi = (h^{\frac{1}{2}}x)$ instead of x, since in this case $tg\ \phi$ is the same for the cooling curve above and below the oil layer (Fig. 7b).

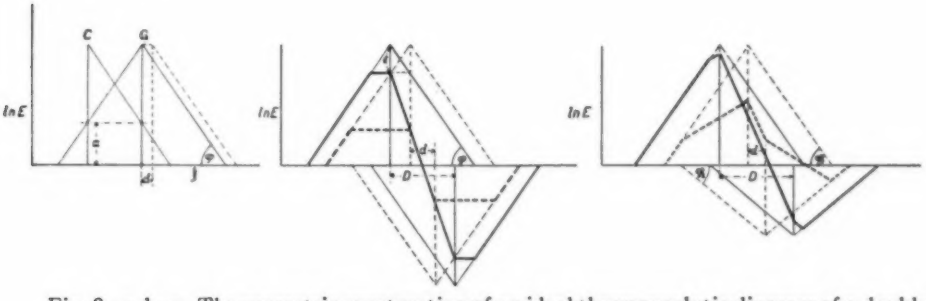

Fig. 8. a. b. c. The geometric construction of an ideal thermoanalytic diagram of a double crystal (a), a symmetrical triple-crystal (b), and an asymmetrical triple-crystal (c). 8b and 8c show each two different cases, the diagram of a large intersection (D; full-drawn lines) and of a narrow one (d; dotted lines).

If the rather valid assumption be made that E, the thermoelectric force is directly proportional to the (small) difference of temperature between oil and water (resp. air), then equation (5) may be written:

$$\ln E + \ln E_{max} - \alpha^{1/2}\xi \tag{6}$$

where E_{max} represents the value of E for $\theta = \theta_{max}$.

The e.m.f. produced at the ends of a double crystal (Fig. 6b) in a certain position (G) of the oil layer (C) (Fig. 8a) is given by the intersection with

the ln E- ξ line (a). Hence it is evident that the thermoanalytic curve $E = f(x)$ will follow that line in the coordination used if one moves the intersection gradually through the oil layer; i.e. the diagram (Fig. 8a) thus obtained is identical with the measured curve to be expected from an ideal double crystal if one considers (according to the medium surrounding the intersection) the two different values of h which are easy to find empirically.

It goes without saying that the assumption of a two-dimensional oil layer is not justified by the actual conditions, since the oil layer is of considerable thickness (d), its temperature is not uniform, and $d\theta/dx$ has a definite value as well as being a function of x_{oil}.

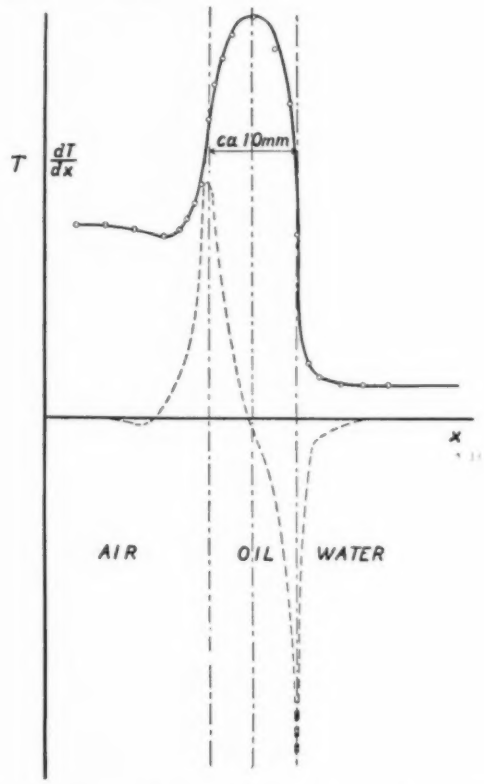

Fig. 9. The temperature diagram of the thermoanalyzer. The full drawn curve shows $T=f(x)$, the dotted lines show $dT/dx=f(x)$.

However the real curves are not fundamentally different from the constructed ones as soon as the oil layer is comparatively thin and the thermal conductivity of the crystal is large. If those conditions are fullfilled one can account for the oil layer by moving the starting point of the second half of the diagram the distance d (dotted in Fig. 8a). This also is only a first approximation on account of the neglection of $\partial^2\theta/\partial x^2 \neq$ const.

Fig. 9 shows the measured temperature-curve within the thermoanalyzer (full line). The latter can be found readily by putting a very thin thermocouple into the thermoanalyzer instead of the crystal. The dotted line in Fig. 9.

indicates the temperature gradient obtained by graphical differentiation of the first curve. It shows that very large gradients could be obtained at the boundary layer of oil and water and furthermore that the theoretical assumptions are not very far from the facts.

In the case of a triple-crystal (Fig. 6c) the construction of the curve is more complicated though fundamentally the same. Here it is necessary to subtract the intersections of the ln E-ξ lines crossing one transition from those crossing the other. The diagram obtained thus has ordinates ($\ln E_1 - \ln E_2$), while what is actually desired is $\ln (E_1 - E_2)$. Since the latter, however, give curves it was considered advisable from the view-point of a convenient graphical synthesis of the analytic curves to plot the former, which give the correct position of the maxima though not the correct amplitudes. The ordinates of the two elementary curves have to be plotted into the opposite direction since the sign of the e.m.f. is negative in one case. Fig. 8b. shows the diagrams of two different triple-crystals, one with a large II-section (full lines) (distance D) the other with a small section (dotted lines) (distance d). The thermal e.m.f. between I and II, and II and III is the same in both cases.

It is apparent that the size of the maxima depends on the length of the heterogeneous section II as soon as $d < x_0$; (x_0 means the distance from the heated intersection to where θ is so small that the thermal e.m.f. cannot be measured anymore).

The decrease of E_{max} is then simply given by:

$$E_{max} = (\xi_0 - d)\ tg\phi \text{ for } d < (h^{1/2} \cdot x_0) = \xi_0. \tag{7}$$

Moreover it is evident that the width of the maxima increases with the decrease of their sharpness.

Fig. 8c. shows another case of a triple crystal, for different lengths of section II. Hence where all three sections are thermoelectrically different, one obtains asymmetrical curves as well as an asymmetrical decrease of the maxima with the length of section II.

The dependence of the size of the maxima indicated by the thermoanalyzer on the length of the straight section II determines the resolving power of the analyser in each case since it is related to the indicated e.m.f. in the limit by the relation:

$$de = - E_{max} \left(\frac{2h}{r\ \sigma}\right)^{1/2} \exp\left[-(2h/r\sigma)^{1/2}x\right]dx \tag{8}$$

which, if the oil layer is at section II reduces to:

$$de = - E_{max} \left(\frac{2h}{r\ \sigma}\right)^{1/2} dx. \tag{8a}$$

The resolving limit of the analyzer is then given by a value dx which cannot produce a measurable de.

The above considerations show that the analyzer, since it does not necessitate the slightest stress to the specimen, is a very useful instrument

for the detection of all kinds of invisible imperfections and inhomogenities in a metal rod, especially in a delicate single crystal. The size of the smallest imperfection still resolved distinctively was *ca.* 0.1 mm. It is evident that thin rodes (2 mm diameter in the present case) give better results than those of large diameter since the method integrates necessarily over the whole cross-section.

Part II. Experimental Results Obtained for Normal and Magnetic Crystals with a Discussion of the Same

The Thermo-analysis of normal crystals. It is obvious that the described method of thermoanalysis can serve the purpose of detecting and locating imperfections within a crystal only when the size of these imperfections is above the resolving power of the analyzer. Furthermore, it is only possible to detect imperfections which cause a thermoelectric force, though it seems

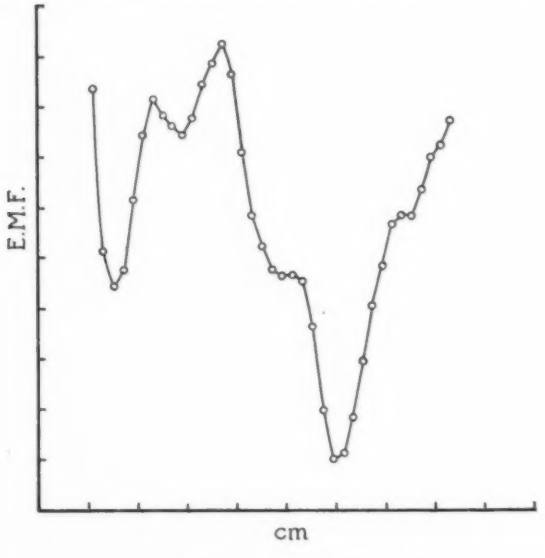

Fig. 10. The thermoanalytic curve of a Bi crystal grown in a glass tube.

very probable that any imperfection due to a distortion or change in the orientation within the crystal causes one, the detection of which depends only on the sensitivity of the galvanometer used. Thus this method is an excellent one to detect and locate heterogeneous inclosures and local plastic deformations. The latter became particularly evident in the case of bismuth since they result in the production of twin lamellae, a phenomenon treated at length in other papers.[1,8]

Because of the effectiveness of this method, the different means used for the production of single-crystals were examined as to their results, and the development of a method of crystal growth—a method to be used in the final experiments—was guided step by step by this kind of an analysis. First crystals grown in glass tubes by the ordinary method (Tammann, Bridgman) were analysed. The deviations of the thermoanalysis curves from

linearity were to be expected especially as the taking off of the glass cover caused many twin lamellae. Fig. 10 shows a diagram of such a crystal.

The lower curve in Fig. 11 shows a crystal with one maximum (M) due to a magnetic effect (see later). After the analysis had been taken, the crystal was plastically deformed just enough to produce two small sets of twin lamellae visible under the magnifying glass. The diagram taken afterwards

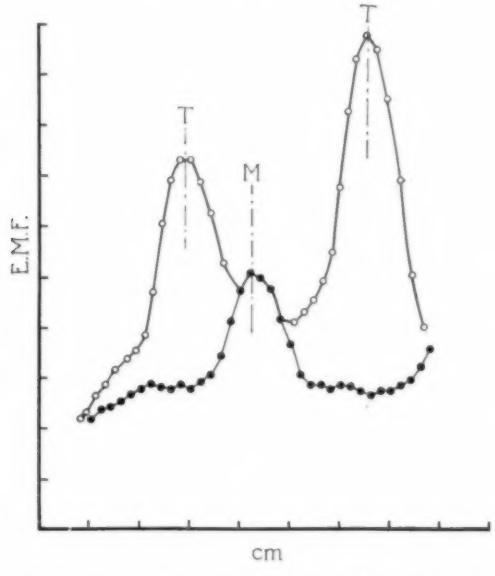

Fig. 11. The thermoanalytic curve of a crystal before (black points) and after artificial deformations at the points $T-T$ (white points). M is the starting point of the magnetic field.

is shown as the upper curve where now two new maxima (T, T) occur, the position of which coincided exactly with the location of the twin-sets.

Fig. 12 shows the diagram of a crystal of the same orientation (P_3) as Fig. 11 as homogenous as it could be produced by means of the graphite

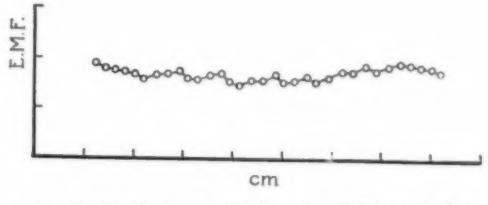

Fig. 12. Thermoanalytic diagram of a "perfect" Bi cyrstal grown after the method of Goetz. Orientation: P_3; Kind "B."

trough, protecting atmosphere, etc., as previously described.[1] Since the scale of this diagram is the same as that of the previous ones it is quite evident that the method used for the production of the crystals gave quite uniform results.

Among the large number of diagrams which have been taken, it occurred very often that an apparently perfect crystal (as far as its examination after

etching was concerned) showed one or more distinct maxima. If the crystal then was cleaved at the point where a maximum had occurred, a microscopic investigation led always to the detection of the inclusion of a crystal of different orientation, which orientation was usually that of a twin. Fig. 13 is a microphotograph of an inclosure of that kind which shows distinctly a twinned region within a normal (111) plane characterized by an alternating penetration of $(11\bar{1})$ planes through the original (111) plane bordered by (110) planes. The cause of these imperfections was, in general, a disturbance

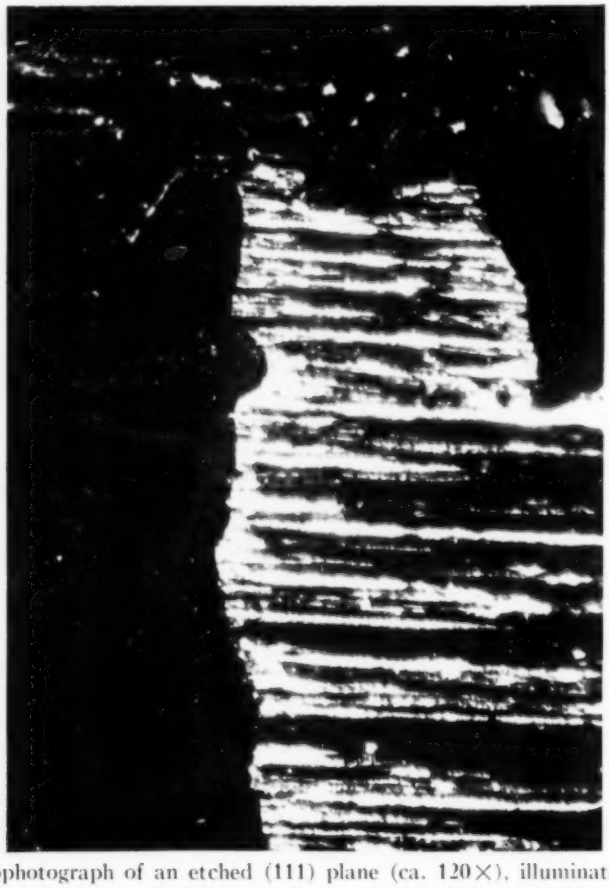

Fig. 13. Microphotograph of an etched (111) plane (ca. 120×), illuminated by polarized light, showing the inclosure of a region of periodical twinning.

(vibration, shock, etc.) happening at the time when this section of the crystal was forming.

The Thermoanalysis of "magnetic" crystals. The described method of thermoanalysis was applied to crystals, one half of which was grown without, the other half within a magnetic field. *It was found that the border between the magnetic and the normal half of the same crystal was the origin of a thermoelectric force.* Furthermore, the thermoanalysis gave evidence that *the origin of this force is exactly at the point where the magnetic field was applied.*

Nevertheless, it proved to be very difficult to measure this force quantita-

tively and not even the sign of the force could at first be reproduced although each curve showed a maximum if it was not fogged by other maxima due to distortions of the kind mentioned in the previous chapter.

To obtain a higher degree of reproducibility, certain definite conditions were imposed, both on the growth and on the analysis of the crystals. In the case of the former, four factors were considered in detail; orientation, method of growth, impurities in the metal, and field strength. For the latter, two were considered: temperature of the analyser, and annealing.

The actual results obtained indicate that at least for the first group of factors the thermoelectric effect is a very complicated function. Despite this complexity, however, duplication of results, for any given set of conditions, with less than ten percent deviation was always possible which indicates that all the principal variants were being controlled.

In presenting the results, the effect of each of the factors on the thermoelectric e.m.f. will be considered separately, the stationary values of the

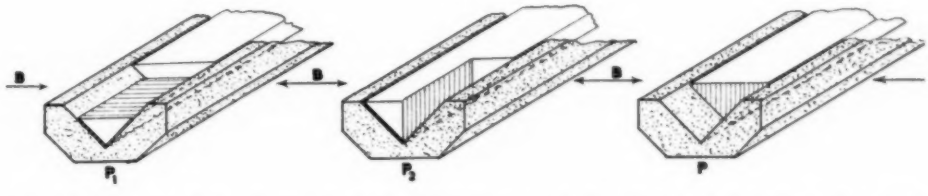

Fig. 14. Scheme of the three principal orientations used. The hatched plane indicates (111), the arrow shows the direction of the field lines.

other factors being given in each case. Up to date, no attempt has been made systematically to evaluate the effect for a large number of values of each of the factors involved, thus the results given can be considered as merely illustrating the type of variation to be expected.

For all the curves to be presented unless specifically stated, the temperature difference in the analyzer was 18°C measured above tap water temperature of 19° to 21°C.

TABLE I. *The three orientations of the crystal.* The third column entitled "vector" shows the direction of the heat flow and the electric current during the thermoanalysis.

Name	Trigonal axis to rod	Trigonal axis to field	Trigonal axis to vector	(111) plane to rod	(111) plane to field	(111) plane to vector
P_1	$\perp$	$\perp$	$\perp$	$\parallel$	$\parallel$	$\parallel$
P_2	$\perp$	$\parallel$	$\perp$	$\parallel$	$\perp$	$\parallel$
P_3	$\parallel$	$\perp$	$\parallel$	$\perp$	$\parallel$	$\perp$

The ordinate scale for the curves unless designated otherwise is 7.8×10^{-6} volts per division. It indicates positive volts for increasing values. The units of the abscissa (length of the crystal) are centimeters.

The solid line, mid-way along the abscissa scale on the curves, indicates the position of the furnace at the intersection between magnetic and normal

portions of the crystal.* The dotted lines indicate the extent of the oil layer to each side of the furnace.

The Effect as a function of the orientation. As stated already in a previous paper,[1] there are three different orientations the crystal can have with regard to the rod, or to the direction of the lines of force, which are essentially different from each other.** Fig. 14 shows the trough *G* dotted, and the crystal white, the latter cut parallel to its main cleavage plane. These three orientations are given in Table I.

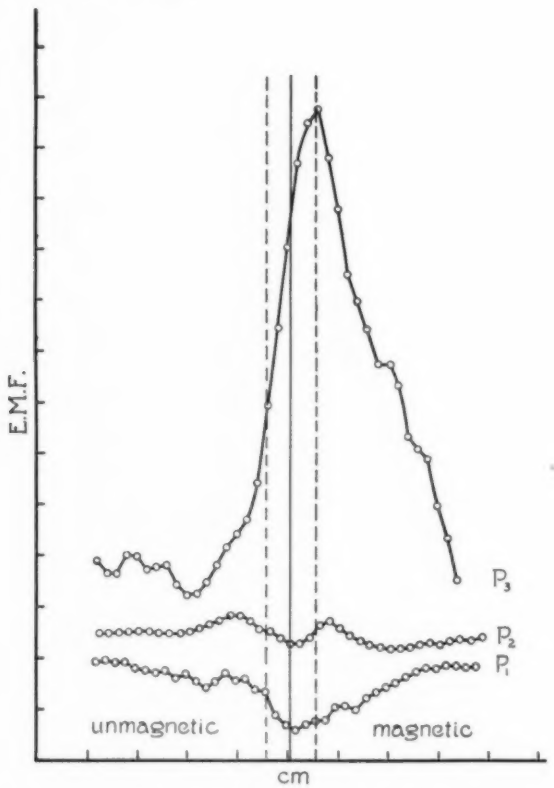

Fig. 15. The thermoanalytic curves of three principal orientations of crystals (kind "*B*") grown discontinuously. Field: 21,000 Gauss.

Fig. 15 shows analysis curves typical for crystals of these three orientations. The method of growth employed was the discontinuous (see Part I), the metal of purity "*B*" (see later), and the field strength 21,000 Gauss.

* The thickness of the center line is misleading in so far as the furnace plate was 1 mm thick and since it was impossible to measure exactly its location within the oil layer.

** The possibilities of azimuthal variation were neglected in these experiments. There are:

two for P_1 with regard to field and vector;
two for P_2 with regard to vector;
two for P_3 with regard to field;

which differ essentially from each other.

The diagram shows that the thermal e.m.f. depends very much on the orientation of the principal axis of the crystal to the field lines. The effect is very large for P_3 and very small for P_2; it is even very probable that the latter effect does not exist at all, and that the deviations of the P_2-diagram are due to inaccuracies in orientation.

The thermal e.m.f. is positive for P_3 and negative for P_1.*** Furthermore it is apparent from Fig. 15 that the thermal e.m.f. is different from what should be expected, (see Part I) since the maximum of the P_3-curve is not at the intersection with the center line, i.e. within the region where θ is largest (see Fig. 9), but at the border between oil and water, where $d\theta/dx$ is a maximum, a fact which seems to be of fundamental importance.

The size of the thermal e.m.f. of the P_3 curve seems remarkable (7.8×10^{-5} volt or 4.33×10^{-6} volt. degree^{-1}), if one calculates the change in orientation of the crystal necessary to produce this e.m.f. due to the thermoelectric anisotropy of the Bi crystal. Taking the data from Bridgman's last paper[13] one finds that change would have to be 21°**** though it is certain that there is no larger change of orientation at the intersection than 0.5°, which fact makes it quite impossible that the thermal e.m.f. is just caused by a change of orientation at the intersection.

The Effect as a Function of the method of growth. The methods of growth employed have been described in detail in Part I of this paper. They were the so-called continuous and discontinuous methods. Fig. 16 shows curves obtained from crystals of P_3 orientation produced in these different ways. "1" represents the former, "3" the latter; in both these cases, no appreciable residual field was present over the so-called unmagnetic portion of the crystal. "2" on the other hand, represents a crystal of continuous growth with the residual field present during the growth of the first portion of the crystal.

It was entirely unexpected to find that the thermal e.m.f. depended on the method of growth to such an extent as shown in Fig. 16. The fundamental difference between "3" and "1" is that there exists only one maximum in the former (the small second maximum at "*b*" has a different cause and will be discussed later) and a maximum and a minimum in the latter. The sign of these maxima is opposite in "1" and "3" but their positions coincide again with the extreme values of $d\theta/dx$ in the thermoanalyzer, for "1" the thermoanalytic curve is even an exact repetition of the $d\theta/dx$ curve in Fig. 9. The case of "2" shows the large effect of a small field strength which seems to suppress entirely the first maximum.

*** The thermal e.m.f. is called positive, if the end of the "magnetic" part of the crystal had a potential positive with regard to the end of the normal half, if the temperature of the intersection was higher than the temperature of the ends.

**** This diagram (Fig. 16, page 384) shows the thermal e.m.f. as a function of $\cos^2\phi$ (angle of orientation). The units of the ordinate are 3.10×10^{-4} volt for a difference of temperature of 68°. Since the curve is no straight line it is necessary to measure at an orientation corresponding to P_3, i.e., starting from $\cos^2\phi=1.0$. Since the e.m.f. unit in that diagram equals $3.10\times 10^{-4}/68°=4.56\times 10^{-6}$ volt. degree^{-1} our e.m.f. corresponds to $4.33/4.56=.95$ units. For the P_3-orientation ($\cos\phi=1$) .95 ordinate-units correspond to 1.3 units of the abscissa, i.e. $\cos\phi=(0.87)^{1/2}$, $\phi-21°$.

The effect as a function of the impurities. It became evident that the magnitude of the effect depended on the purity of metal used to a very large extent. The crystals were therefore prepared from four kinds of Bi, obtained

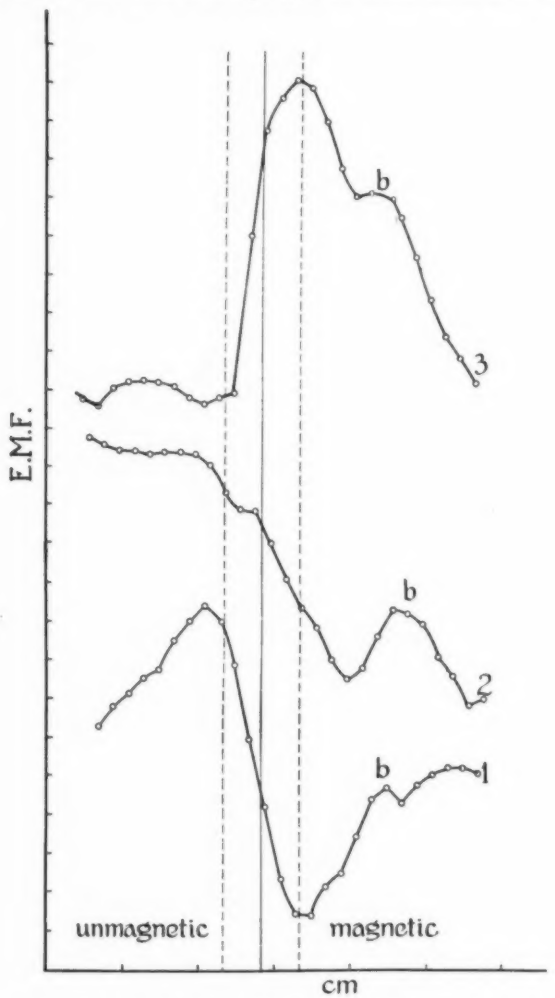

Fig. 16. The thermoanalytic curves of three different types of growth:
1. represents the continuous method without residual field. Field: 13,800 Gauss; kind "*B*;" orientation: P_3.
2. represents the continuous method with residual field.
3. represents the discontinuous method.

from different sources which were designated as "A", "B", "C", and "D" as shown in the following table:

TABLE III. *Sources of the bismuth used.*

Designation	Characterization	Source
"A"	Bismuth C. P.	Brown Corp., Philadelphia, Pa.
"B"	Bismuth purissimum	Hartmann & Braun, Frankfurt a, M.
"C"	Electrolytic bismuth	" "
"D"	Bismuth "Kahlbaum"	Kahlbaum A. G., Adlershof.

Fig. 17 shows curves of the P_3 orientation made from these four different kinds of Bi by the discontinuous method, whereas Fig. 18 represents the corresponding crystals of continuous growth.

Since from this work as well from papers of Bridgman[13] and Kapitza[14] it was well-known how large the influence of small impurities on the electric effects of Bi can be, an accurate chemical analysis of the different kinds of bismuth was made. The results obtained showed that a very small trace of

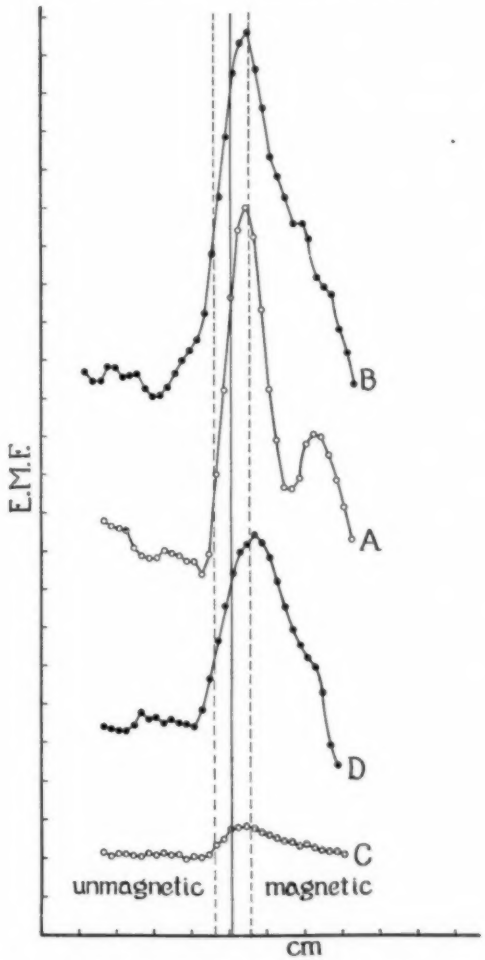

Fig. 17. The thermoanalytic curves for P_3 crystals of four different degrees of chemical purity, grown discontinuously; field: 21,000 Gauss.

silver was present in "A" and "B" though the amount was too small to measure accurately. Since this indicated that the impurities involved were only present in extremely small amounts, a spectral analysis seemed necessary. Dr. R. M. Badger was kind enough to perform this type of analysis

[13] P. W. Bridgman, Proc. Am. Acad. **63,** 351 (1929).
[14] P. Kapitza, Proc. Roy. Soc. **A119,** 358 (1929).

on our different metals. The amount of any impurity was measured by comparing the intensities of its different lines as observed for the specimen, with the intensity of the lines obtained from these metals by themselves in a spark. The bismuth electrodes were prepared by putting the metal into Pryex tubes after it had been ascertained that the glass did not contain any of the metals

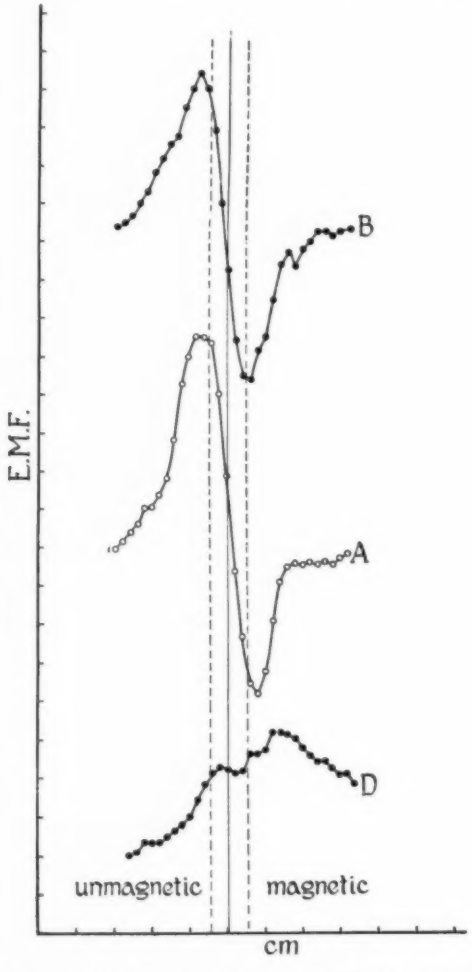

Fig. 18. The thermoanalytic curves for P_3 crystals of three different degrees chemical purity, grown continuously; field: 13,800 Gauss.

involved in the analysis. The results are given in the following table, where the numbers give the approximate relative intensities of the indicated lines of the different impurities.

In general, it can be said that the amount of impurity is probably on the whole, smaller than 0.2 percent in the worst case which is "B". It is smaller for "A" which contains less Pb. "D" differs from "B" in its smaller content of Pb, though in its Ag content, it compares badly whereas "C" is by far the purest metal.

TABLE IV. *Spectroscopic analysis of Bi samples.*

Sample	Ag		Cu		Sn	Pb						Zn			Sb			
	3281	3383	3247	3274	3262	2863	4058	3683	3639	3275	2802	2613	4810	4722	3345	3267	3232	2598	2528.5
A	4	1	1		?		5	1			?								?
B_1	5	2	1		?		10	4	3										
B_2	5	2	1		?		10	4	2										
C_1	1		5	3	?		1						?						?
C_2	1		5	3			1	?					?						?
D_1	7	3	1–0			1	6	1											
D_2	7	4				1	5												?

Thus it is apparent from the diagrams that the purest metal shows the smallest effect and also that the shape of the curve is but little affected. However the secondary maximum ("b" in Fig. 16) depends apparently on certain impurities, since it is very large for "A" (Fig. 17) and extremly small for "C". The method of continuous growth shows very little difference between "A" and "B" and a large one for "D". It is however doubtful whether the latter measurement is a correct one, since it is based only on a few crystals.

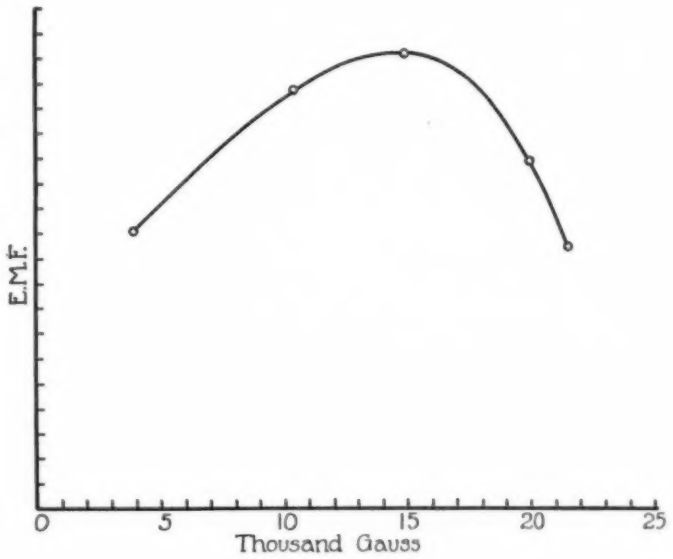

Fig. 19. The size of the maximum thermal e.m.f. as a function of the field strength for P_3 crystals, kind "*B*," grown discontinuously.

The effect as function of the field strength. Although it is very important to investigate what influence the strength of the applied field has upon the thermoelectric effect, it appeared very difficult to obtain reliable results, since the effect does not depend merely on the orientation of the crystal but also on the method of growth, the degree of impurity, etc. Thus

it has not yet been possible to obtain results of sufficient generality in spite of a great number of experiments. It seems however quite safe to state that there exists a large influence of the field strength upon the effect for crystals of the P_3-orientation. (Other orientations have not yet been investigated.) The influence of weak fields is very large whereas strong fields (20,000 Gauss) decrease the effect considerably in the case of the discontinuous method of growth.

Fig. 19 shows the variation with field strength obtained for crystals grown with the P_3 orientation, composed from a series of curves of the type of Fig. 15.

The field which produces the maximum thermoelectric effect seems to depend on the degree of impurity.

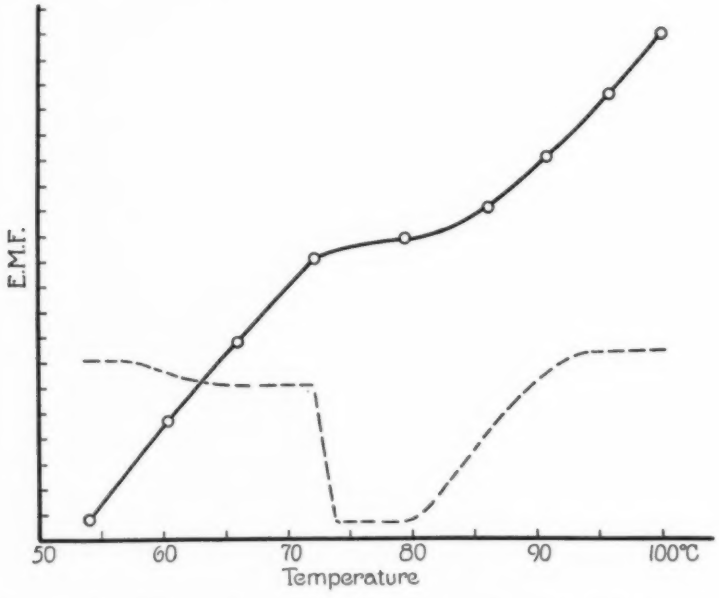

Fig. 20. The size of the maximum thermal e.m.f. as a function of the temperature (The hypothetical transformation of α into β-bismuth.) P_3-crystal, grown discontinuously, kind "B," field: 21,000 Gauss. The dotted curve gives $dE/dT=f(T)$.

The effect as a function of the temperature. Fig. 20 shows the thermoelectric effect between the magnetic and the normal half of a crystal as a function of the temperature of the analyzer and its differential curve (dotted). The curve was taken by first finding the exact position of the maximum e.m.f. with regard to the crystal (crystal of the type shown in Fig. 15) and then keeping the oil layer in this position while its temperature was gradually increased.

This experiment performed on many crystals of different types showed that the temperature function is independent of the impurity as far as the general shape of the curve is concerned. It seems quite interesting that the differential curve $dE/d\theta$ shows a large discontinuity between 75° and 90°C.

Since it is well known that this type of curve is obtained in case of an allotropic transformation (as for instance typically represented by the thermoelectric effects of pure iron[15]) the shape of the curve obtained indicates that the discontinuity in that region of temperature affects the magnetic half of the crystal in a different way than the normal.*

In order to decide whether or not the magnetic state is just a more or less unstable allotropic state caused by strains, such as magnetostriction for instance, specimens showing large effects were reinvestigated after being annealed. The temperature of annealing was chosen sufficiently high, above 90°C, to see whether the transition into the normal state would occur at all. Since this annealing temperature lies above the point of the mentioned "allotropic" transformation, it is probable that the instability of the magnetic state should increase, or the transformation speed into the normal state should be larger.

Hence a crystal (P_3 of "B") was analyzed the day it had been grown, it was then annealed for 16 hours at 100°C and analyzed again a month later. No change of any kind could be detected which indicates that the magnetic state is either perfectly stable or that it has an extremly slow speed of transformation. It is certainly not affected by passing the critical temperature of normal Bi. (75°–90°C)

This experiment shows also that the effect of "aging" Bi crystals does not occur in specimens of good crystallographic perfection, either for normal or for magnetic crystals.

* The question of the existence of an allotropic state of Bi is still unsettled; Cohen[16] and Cohen and Moesveld[17] concluded from their pyknometric and dilatometric measurements the existence of an α and a β modification, of which the α-state is stable below 75°C having a larger density than the β-state. However those authors found other transformations at 81° and 90° where the volume of the metal changed suddenly according to its thermal history. Würschmidt[18] found also the transformation point at 75° indicated by a large contraction, whereas the temperature coefficient of the conductivity of Bi as investigated by Bridgman[19] and Holborn[20] does not indicate such transformation at all.—Furthermore the thermoelectric effects as a function of temperature of Bi single crystals were investigated by Boydston;[21] his $E=f(\theta)$ curves show a slight indication of an irregularity in this region of temperature which becomes much more evident in the case of the Peltier effect curve: $\Pi=T\ dE/d\theta=f(\theta)$. A recent investigation of the Peltier and Thomson effect by Fagan and Collins[22] would have cleared this question, if the authors had extended their measurements into this region of temperature. The exact coincidence of the critical temperatures in our measurements with the transformation-point of Cohen, Moesveld, and Würschmidt seem to render the existence more probable. It may be however another example of "pseudo-allotropy" due to traces of impurities as shown recently in the case of extremely pure Zn by Guertler and Anastasiadis.[23]

[15] A. Goetz, Phys. Zeits. **25,** 562 (1924); **26,** 260 (1925).

[16] E. Cohen, Akad. Amsterdam Verls. **23,** 1224 (1914/15).

[17] E. Cohen and A. L. Th. Moesveld, Zeits. f. Phys. Chem. **85,** 420 (1913).

[18] J. Würschmidt, Verh. d. Dt. Phys. Ges. **16,** 799 (1914).

[19] P. W. Bridgman, Proc. Am. Acad. **52,** 636 (1916/17).

[20] L. Holborn, Ann. d. Physik (4) **59,** 152 (1919).

[21] R. W. Boydston, Phys. Rev. **30,** 911 (1927).

[22] H. D. Fagan and T. R. D. Collins, Phys. Rev. **35,** 421 (1930).

[23] W. Guertler and L. Anastasiadis, Zeits. f. Metallkd. **21,** 338 (1929).

Discussion

Generally speaking the above results are far from sufficient to start an explanation of the effect on a theoretical basis. However the results seem to us complete enough to describe the phenomenology of the new effect approximately.

In the first place, it becomes quite apparent that the forces acting at the moment of crystallization affect the physical properties of the final crystal, though neither orientation nor any other macroscopic quality of the crystal is changed.

The effect as a function of the orientation of the crystal with regard to the field seems the most obvious of all the different variations of the experimental conditions. Here we obtain the largest thermal e.m.f. if the principal axis is normal to the field lines and parallel to the heat flow, i.e. the direction of the thermoelectric current (P_3); whereas the effect is extremly small if the axis is parallel to the lines of force and normal to the flow (P_2).

If one considers the anisotropy of the diamagnetic susceptibility of Bi crystals as measured recently by Focke[6] a relation between the two effects is quite evident, since in case of P_3 the crystal is in a position where the direction of the largest diamagnetism is parallel to the lines of force, and in the case of P_2 the most "paramagnetic" direction is parallel to the field. Hence there is a difference between the content of free energy in these cases, for the stability of the latter orientation is larger than of the former. If thus a crystal is grown first under normal conditions and then in a field the stability does not change in case of P_2 but is does considerably in case of P_3. One knows from other observations that a crystal prefers the P_2 orientation when forming its first center of crystallization in a transverse field and also that the field does not even change the opposite orientation if the latter is enforced on it by inoculation with a seed crystal. The fact that the point where the field (i.e. the instability) started is indicated by a thermal e.m.f. shows that the crystal undergoes a change in spite of the constancy of the orientation. Thus the question about the nature of this change becomes quite interesting.

Regarding the shape of the thermoanalytic curves it seems as if the curves of discontinuous growth (Fig. 15) were due to a double-crystal, and the curves of continuous growth (Fig. 18) represent a triple crystal, as has been discussed in Part I of this paper. The interpretation however of the latter diagram as being produced by a triple-crystal seems to be inadequate in view of the fact that the length of sandwiched section (d in Fig. 8b and 8c) would have to coincide with the thickness of the oil layer to produce the maxima and minima at the borders of the layer, which coincidence would seem highly improbable; i.e. the maxima and minima of the diagrams are too close together to be sufficiently resolved if caused by a section smaller than the thickness of the oil layer. Furthermore those points are not situated at the hottest part of the oil layer of the thermoanalyzer (Fig. 9), which means that the e.m.f. does not reach its maximum if the intersection of the crystal passes θ_{max}. This concerns also the simpler curves of discontinuously grown crystals.

It is very remarkable that the maximum of the thermoanalytic curves of P_3 crystals of that kind does not coincide with the position of the maximum of temperature, it does however with the maximum of the $d\theta/dx$ curve (Fig. 9), i.e. at the border of water and oil. *The only simple interpretation is thus that the thermal e.m.f. must depend on the temperature gradient or the density of the heat flow crossing the intersection between the normal and the magnetic half of the crystal.*

It is apparent that such effect cannot be caused simply by a double or a triple crystal, since the normal thermoelectric effect between two different metals or orientations of a crystal depends on the difference of the temperature and is quite independent of the gradient.

Although the assumption of such a type of a thermoelectric effect seems to be quite uncertain in view of the fact that the passing of the opposite gradient (air-oil, see Fig. 9) is much less expressed by the thermoanalytic curves of discontinuously grown crystals, such interpretation gains some probability in the case of continuously grown crystals (Fig. 18). Here we have curves which are the exact duplicates of the $d\theta/dx$-curve in Fig. 9. The sign of the effect is opposite in these two cases as follows: If the heat flow passes the intersection *from* the magnetic *to* the unmagnetic half of the crystal, the magnetic half is *positive* for *continuous* growth and *negative* for discontinuous growth, it is opposite if the heat flows the other way. In case of the discontinuous kind of growth the flow in the latter direction seems to be quite uneffective.

It is apparent that the influence of the impurities makes the effect very complex since the amount as well as the kind of impurity affects the thermal e.m.f. considerably as is to be expected from a consideration of the dependence of the anisotropy of the electric qualities of the crystal on the impurities present. Hence the mentioned instability of a growing crystal for certain orientations to the field should increase with an increasing anisotropy due to impurities and one should expect a kind of proportionality of the thermal e.m.f. with the impurity. This however is misleading, since it seems highly probable from the behavior of the metal "C" that an ideally pure Bi would not show any effect at all though the electric anisotropy still exists. Thus one is forced to assume that the whole effect is due to disturbances of the odd atoms in the Bi lattice, which disturbance is the more distinct the better the crystal is grown. The disturbance for a given amount and kind of odd atoms depends apparently on their arrangement and is easily affected by external influences during the act of crystallization.

Very little can be said as yet about the actual nature of the disturbance though the fact that an extremely small amount of impurities has such a large influence seems to indicate a surface effect, i.e. an effect due to a formation of mono- or bimolecular layers of odd atoms sandwiched between perfect sections of the crystal. Such arrangement similar to the "Π-planes" of the mosaic structure of Zwicky[7,24] would require an extremely small amount of impurity to affect the electronic relations inside the lattice. In case of such an interpretation one has to assume that the arrangement of the odd atoms is changed under the influence of the magnetic field. It is quite plausible that such a

change differs with different crystallographic planes as well as that its effect works differently upon an electric current, which might explain the difference between the thermoanalytic curves of P_1 and P_3. (As has been mentioned already, these two orientations do not differ with regard to the field though they do with regard to the direction of the thermoelectric current and the heat flow.)

The arrangement of the odd atoms within the crystal must depend furthermore on the growth of the crystal, since any disturbance during the formation will affect the structure of the impurity layers to a certain extent and therewith the final influence of the magnetic field. This would explain the difference between the thermoanalytic curves of continuous and discontinuous growth. The highly metastable state of the configuration of the odd atoms within the Π-planes during the formation of the mosaic structure is probably the cause of the extreme experimental difficulties in obtaining reproducable results.

Before closing, some comparisons with Kapitza's work[14] may be made. Concerning his observations of the change of the resistance of Bi crystals in a strong magnetic field, it is to be expected from the above hypothesis that the Bi which produced an extremly small effect (K.'s crystal "B" in his Fig. 13, p. 407, l.c.) would produce in our case one of medium magnitude, since his metal corresponds to our "D" whereas his crystal "A" which produced large effects was of metal of the same source as our "C" giving—for our work—the smallest values. Since the influence of an external field upon the change of the resistance depends on the size of the disturbances within the lattice, our experience with "D" and "C" compares very well with Kapitza's result, his effect being fogged by impurities and ours depending apparently wholly on their presence.

With regard to the orientation effects, a few comparisons can also be made. Being limited to only one direction of both the field to the rod, and the thermoelectric current to the rod, only one kind of Kapitza's experiments can be considered for comparison, i.e. where the field is normal to the current. Neglecting the azimuthal effects which seem in our case small, at best, comparison shows that the largest values obtained of the ratio R/R_0 is for our so-called P_3 orientation, while the value obtained for P_1 was only a fractional part of that for P_3, both facts being analogous to our results. In the case of P_2 however, a larger value of R/R_0 than the P_1 case was obtained which might be interpreted as suggested above, because our effect shows no appreciable influence of the odd atoms upon this orientation.

Conclusion

Although these experiments were begun several years ago during which time a very large number of measurements have been taken, it is not yet possible to give more than a rather vague hypothetical explanation as outlined above. Since the experimental difficulties proved to be very large the

[14] F. Zwicky, Helv. Phys. Acta **3**, 269 (1930).

actual progress has been slow and the present paper cannot be more than a first report about the new effect.

Systematic measurements concerning the electrical conductivity, the specific gravity, and the magnetic susceptibility were performed and are still going on, as well as a detailed x-ray analysis of the "magnetic" crystals. Papers concerning these subjects will be published in near future.

In conclusion, the authors wish to express their great obligation to Dr. R. A. Millikan for the interest he has taken in the work, to Dr. R. M. Badger to whom they owe the spectroscopical analysis of the bismuths, to Mr. J. Pearson for his helpful technical advice and to Mr. A. Focke for his general assistance.

THE SECOND VIRIAL COEFFICIENT FOR GASES: A CRITICAL COMPARISON BETWEEN THEORETICAL AND EXPERIMENTAL RESULTS

By Henry Margenau
Sloane Physics Laboratory, Yale University

(Received November 5, 1930)

Abstract

On the basis of a recent theory developed by London the second virial coefficient of the following gases is computed: He, Ne, A, H_2, N_2, O_2, CO_2, NH_3 H_2O. For the latter two, which have a dipole moment, the contribution of the dipole interaction is also calculated. The results are compared graphically with experimental values. Except in the case of He and H_2, where the disagreement can be accounted for by the presence of zero point energy, the accordance is as good as is compatible with the inaccuracies involved in the calculation.

IN CLASSICAL mechanics it was necessary to attribute the attractive forces between molecules, demanded by the empirical equation of state, to the action of permanent or induced electric poles. Quadrupoles of considerable moment had to be assigned to molecules such as H_2 and the rare gases, which were known to carry no permanent dipoles. On the basis of the old atomic models the required assumption of quadrupoles was entirely reasonable, but it is inconsistent with the more uniform distribution of molecular charges calculated by wave mechanics. Moreover, molecular quadrupoles are not yet accessible to measurement, so that a theory based on their presence is unsatisfactory for its lack of verification. This difficulty was very successfully removed when Eisenschitz and London[1] recognized the significance of attractive forces appearing in the second order perturbation in the interaction problem of two H atoms. They showed that Van der Waals' constant a derived from these forces had the correct order of magnitude. In a recent paper London[2] made a more comprehensive study of these forces (arising from what he terms the "dispersion effect") and discussed in particular their relation to two other types of attractive forces existing between molecules having electric moments (resulting from Keesom's effect of "alignment" and Debye's induction effect).[3] He also calculates the contribution to the molecular interaction energy of the dispersion effect and finds that this is for many gases the dominant constituent of the interaction, resulting in a van der Waals' a which is in good agreement with the value for a computed from critical data. This is indeed a most interesting and significant observation which goes far in confirming the validity of the theory. Now it is well known that van der Waals' equation with a independent of the

[1] R. Eisenschitz and F. London, Zeits. f. Physik **60**, 491 (1930).
[2] F. London, Zeits. f. Physik **63**, 245 (1930).
[3] Cf.[2] for literature.

temperature does not represent the empirical equation of state, nor does the a value computed from critical data coincide of necessity with the factor of $1/T$ in the equation of state. It is the purpose of this communication to make a closer comparison between the predictions of London's theory and experimental data, and also to include in this comparison the results of a recent paper[4] dealing with forces between dipole molecules. We shall express the second virial coefficient, B, as a function of the temperature and examine its correspondence to the empirically known values of B for various temperatures. The results can best be shown by graphs.

It will appear that the calculation of B is of necessity very crude because idealized assumptions and lack of accurate knowledge of certain quantities involved; hence one is justified to look for qualitative agreement only. The method used is essentially the same as that employed by London to compute a and is subject to the same errors.

Non-Polar Gases

It may be recalled that B is the coefficient of $1/V$ in an expansion of pV/RT as a power series in $1/V$. It measures the deviation from Boyle's law for small concentrations (large V) and is given analytically by:

$$B = 2\pi N \int_0^\infty (\varepsilon^{-\epsilon/kT} - 1) r^2 dr, \tag{1}$$

where ϵ is the interaction energy of two molecules expressed as a function of r, the distance between the molecules. If N is Avogadro's number, B is in cc per mole. The result of London's[5] investigation concerning the dispersion effect is:

$$\frac{3}{4}\frac{\alpha^2 V_a}{r^6} \leqq -\epsilon \leqq \frac{3}{4}\frac{\alpha^2 V_i}{r^6} \tag{2}$$

where α is the polarizability, V_a the excitation potential, and V_i the ionization potential of the substance. An accurate theoretical expression for ϵ involves the energy values and matrix elements of the molecules and is, therefore, in general difficult to evaluate. At $r<d$ the interaction energy ceases to be given by (2), ϵ merges into the rapidly rising exponential curve characteristic of the valence forces.[6] Here the assumption will be made that

$$\epsilon = +\infty \text{ for } r < d \tag{3}$$

corresponding essentially to the supposition that the molecules have a diameter d and are impenetrable. Refinements, such as introducing a dependence of d on T, as would be necessary to take account of the finite slope of the exponential curve at $r=d$ are possible but can be omitted in view of the general lack of precision of the premises on which we are compelled to make

[4] H. Margenau, Zeits. f. Physik **64**, 584 (1930).
[5] Reference 2, p. 256.
[6] See Fig. 1 in the paper by Eisenschitz and London.

the calculation. We shall therefore assume an empirical value for d, independent of T. Moreover we shall put

$$\epsilon = -\frac{3}{4}\frac{\alpha^2 V_i}{r^6} \tag{4}$$

introducing thereby a considerable error. (There is reason to suppose that in general ϵ is nearer the upper limit in (2).)[7] Expanding the exponential in (1) and performing the integration using (3) and (4) we obtain

$$B = \frac{2\pi Nd^3}{3}\left\{1 - 0.75\frac{\theta_1}{T} - 9.4\times 10^{-2}\left(\frac{\theta_1}{T}\right)^2 - 1.4\times 10^{-2}\left(\frac{\theta_1}{T}\right)^3 - 1.9\times 10^{-3}\left(\frac{\theta_1}{T}\right)^4 - 2.2\times 10^{-4}\left(\frac{\theta_1}{T}\right)^5 - 2.2\times 10^{-5}\left(\frac{\theta_1}{T}\right)^6 - \cdots\right\}, \tag{5}$$

where

$$\theta_1 = \frac{\alpha^2}{d^6}\frac{V_i}{k}.$$

If we put

$$\frac{2\pi Nd^3}{3} = B_0$$

we have

$$\theta_1 = \frac{4\pi^2 N^2}{9k}\frac{\alpha^2 V_i}{B_0^2}.$$

B_0 can be determined from the empirical B curve and is essentially the same as van der Waals' b. The values of B_0 used in the computation of B are taken from Beattie and Bridgeman's[8] work, except for O_2 and CO_2. For these two gases the experimental and the theoretical B obtained from the data listed by the latter authors proved to be peculiarly discrepant, more so than could be explained by the crudeness of the calculation. It may be observed, however, that while for all other gases listed here Beattie and Bridgeman's B_0 is in the neighborhood of the usual b-values (as computed from critical data), it is considerably higher for O_2 and CO_2 (46 and 105). Also, in the case of He, Ne, A, N_2 their constants are derived from isothermals up to 400°C, whereas for the two gases in question only temperatures up to 100°C were used. If now it is remembered that B_0 is the limit of B for high temperatures one could be led to suppose that though Beattie-Bridgeman's B_0, together with their other constants, describe the behavior of O_2 and CO_2 very well over the range of lower temperatures, it may not actually be the limit which is here required.[9]

[7] See reference (1), action of the continuous spectrum.

[8] Cf. for instance Zeits. f. Physik **62**, 95 (1930).

[9] At 258° Beattie and Bridgeman's constants for CO_2 give a value of B which is, compared to Amagat's measurements, about 50 percent too small.

If this supposition is erroneous the discrepancy spoken of would have to be admitted as unexplained. We have in the following assumed B_0 values for O_2 and CO_2 equal to the b-values from critical data, which are in agreement with our knowledge about the size of molecules derived from other sources (viscosity). If they are chosen the experimental and the theoretical B-curves agree quite well.

Table I contains the experimental data on the basis of which the computation of B was made. The ionization potentials of some of the gases may be in considerable doubt, but in view of the other uncertainty concerning the

TABLE I.

	$\alpha\times10^{24}$	B_0	V_i (volts)	θ_1
He	0.20	14	24.5	92
Ne	0.39	20	21.5	150
A	1.63	39	15.4	500
H_2	0.81	21	16.4	440
N_2	1.74	50	17	385
O_2	1.57	32 (46)	13	580 (280)
CO_2	2.9	42 (105)	10	880 (180)

value of V to be used (Eq. (2)) this need not disturb us particularly. It is interesting to observe the magnitude of θ_1. The calculation of van der Waals' a[10] neglects higher powers of θ_1/T than the first, which seems unsatisfactory, even if due consideration is given to the large errors in our assumptions. CO_2, though having a small dipole moment ($\mu=0.06\times10^{-18}$) is included in the list of non-polar gases.

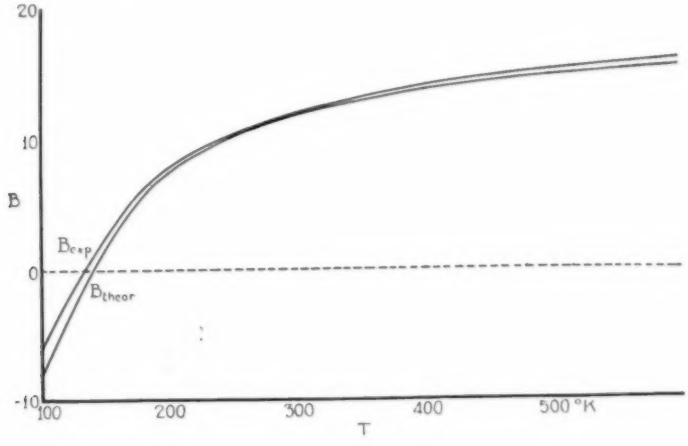

Fig. 1. Neon.

The curves in Figs. 1–7 show the results, the ordinates being in cc per mole, the abscissae in absolute degrees. Except for CO_2 (where the experimental B-values were taken from Amagat's diagram) the experimental points were computed from Beattie and Bridgeman's constants. The broken curves

[10] F. London, reference 2.

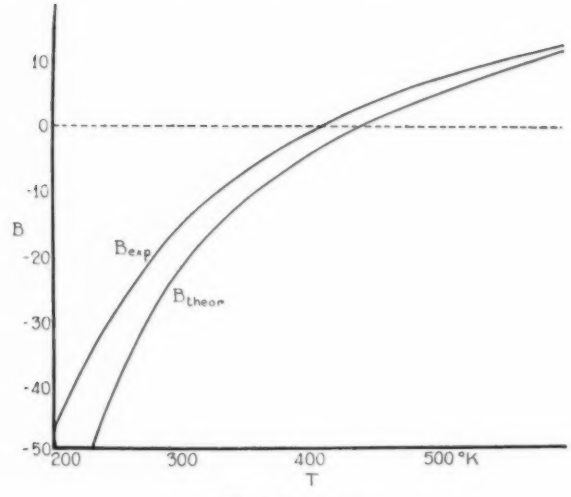

Fig. 2. Argon.

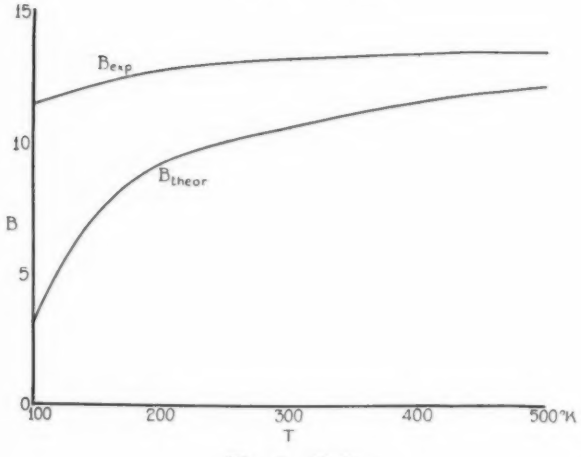

Fig. 3. Helium.

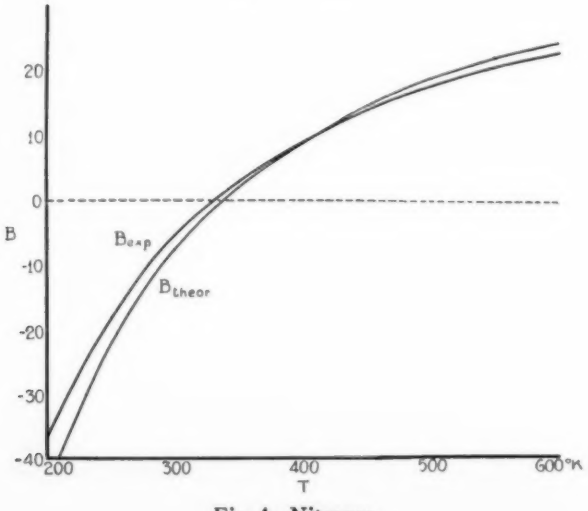

Fig. 4. Nitrogen.

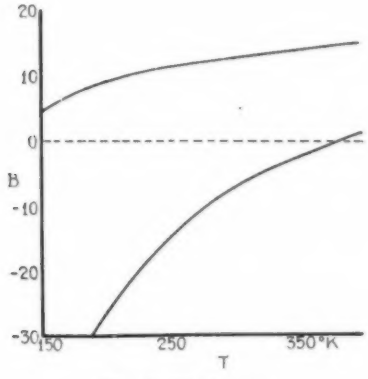

Fig. 5. Hydrogen.

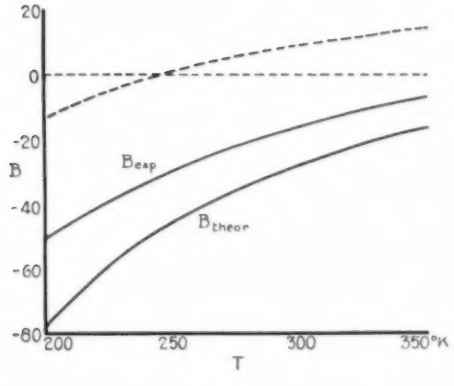

Fig. 6. Oxygen. The broken curve was computed on the assumption $B_0 = 46$.

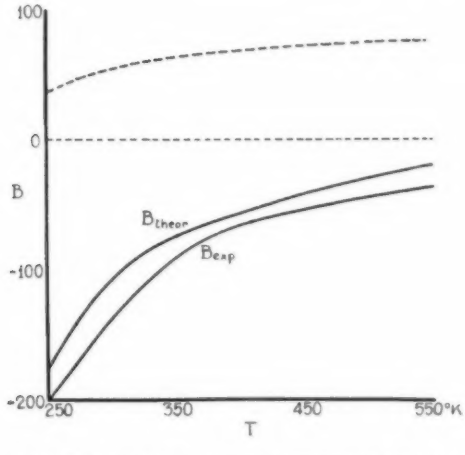

Fig. 7. Carbon dioxide. The broken curve was computed on the assumption $B = 105$.

in Figs. 6 and 7 represent the values obtained by using $B_0 = 46$ and 105 respectively. The agreement is seen to be good for all substances with the exception of He and H_2, where the large deviation can be accounted for qualitatively by the zero point energy of the interacting molecules. As London has pointed out, this is negligible for molecules of larger mass, but would, in the case of He and H_2, cause the theoretical curves to be displaced toward the experimental ones.

Polar Gases

It has been shown[11] that for sufficiently high temperatures ($kT \gg h^2/8\pi^2 A$) the virial coefficient of polar molecules is given by

$$B = \frac{N^2}{8\pi} \int_\Omega \int_0^\infty (e^{-V/kT} - 1) r^2 dr d\Omega \tag{6}$$

where the first integration is extended over all orientations of the two molecules and V is their classical potential energy in terms of r and the angles. For dipole molecules capable of polarization we find, if μ is the dipole moment,

$$V = \frac{\mu^2}{r^3}[- 2 \cos\theta_1 \cos\theta_2 + \sin\theta_1 \sin\theta_2 \cos(\phi_1 - \phi_2)]$$

$$- \frac{\mu^2 \alpha}{2r^6}(3\cos^2\theta_1 + 3\cos^2\theta_2 + 2) \text{ neglecting small terms.} \tag{7}$$

The B computed from (6) will have to be added to the B resulting from the dispersion effect, but in doing so it must be remembered that the integration over r from 0 to d has already been counted, and the relevant part of (6) results from $\int_d^\infty$. Expression (6) has been calculated by Falkenhagen.[12] He finds for several dipole gases, among them NH_3 and H_2O, good agreement between experimental data and the results of (6). This is very surprising from our present point of view, for it would seem to indicate that, if the dispersion effect also were taken into consideration the total B would be much too large. This difficulty, we feel, resolves itself on closer examination. It is impossible to check Falkenhagen's calculations in detail because the numerical values used in them are not all stated. (If we use the values of d derived from the B_0 of Table II, the agreement found by him is considerably disturbed.) We also note that his potential energy expression contains a polarization term (the second term in the brackets of (7)) twice as large as ours, which circumstance we are inclined to attribute to a numerical error in his G_2. This tends to enlarge the contribution of (6) to B.

[11] H. Margenau, Zeits. f. Physik **64**, 584 (1930). In Eq. (1) of this paper a bar was omitted. It should read, of course,

$$B = 2\pi N^2 \int_0^\infty (\overline{e^{-V(R,\omega)/kT}} - 1) R^2 dR.$$

[12] H. Falkenhagen, Phys. Zeits. **23**, 87 (1922).

In evaluating (6) we remember that

$$\int_{d\Omega} d\Omega = \int\int\int\int \sin\theta_1 d\theta_1 \sin\theta_2 d\theta_2 d\phi_1 d\phi_2,$$

and obtain, after expanding the exponential, for the dipole contribution to the total B,

$$B' = -\frac{2\pi Nd^3}{3}\left\{ 2z\frac{\theta_2}{T} + [0.33 + 0.73z^2]\left(\frac{\theta_2}{T}\right)^2 + [0.27z + 0.35z^3]\left(\frac{\theta_2}{T}\right)^3 + [1.3\times 10^{-2} + 0.21z^2]\left(\frac{\theta_2}{T}\right)^4 + 2.3\times 10^{-2}z\left(\frac{\theta_2}{T}\right)^5 + 5.2\times 10^{-4}\left(\frac{\theta_2}{T}\right)^6 \right\}. \quad (8)$$

Here

$$\theta_2 = \frac{\mu^2}{kd^3} = \frac{2\pi N}{3k}\cdot\frac{\mu^2}{B_0}$$

$$z = \frac{\alpha}{d^3} = \frac{2\pi N}{3B_0}\alpha.$$

There is but little sense in using more terms since (1) would probably lose its validity for temperatures in which these terms become significant. The only dipole gases for which a comparison can be made at present are NH_3 and H_2O on account of the lack of experimental data for others. Table II shows the data from which the B values of these two gases were computed.

TABLE II.

	$\alpha\times 10^{24}$	B_0	V_i	$\mu\times 10^{18}$	θ_1	θ_2	z
NH_3	2.21	34	11	1.50	880	610	0.085
H_2O	1.48	34	13	1.84	470	920	0.055

B_0 for NH_3 was taken from Beattie and Bridgeman's work and the experimental B computed from their constants, while for H_2O it was necessary to take the critical data b, using for comparison experimental data by M. Jacob[13] from which Falkenhagen[14] has calculated the second virial coefficient.

In Figs. 8 and 9 the experimental curves are plotted together with values obtained from (a) (5), (b) (5) + (8). It is seen in both cases that the dipole effect is a very essential part of the interaction causing B. For NH_3 the agreement between B_{exp} and $B_{disp+dipole}$ is quite good, showing that the two effects here considered suffice to explain the molecular interaction. For H_2O, however, it is evident that they do not suffice, and that we must look, for quad-

[13] M. Jacob, Zeits. f. Ing. 1912, p. 1980.
[14] Reference 12.

rupole interaction to fill the space between the two lower curves of Fig. 9. It is plausible to assume that water molecules have a quadrupole moment, and one can without difficulty compute it from the last figure, for Keesom's

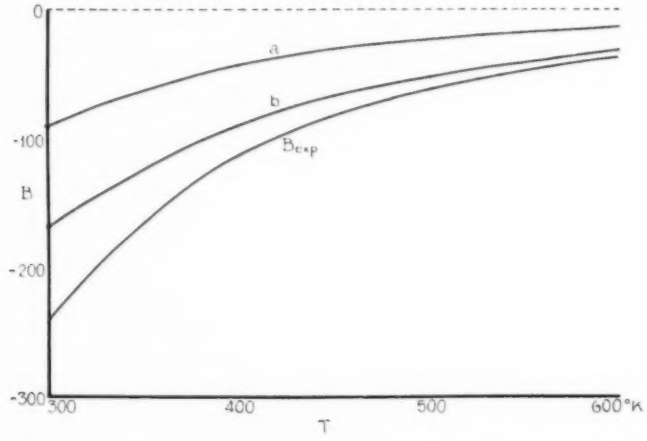

Fig. 8. Ammonia. Curve *a* represents values of *B* due to the disperson effect, curve *b* those due to dispersion plus dipole effect.

theory, and the formulae he developed,[15] have been shown to be applicable from the point of view of wave mechanics provided that the temperatures

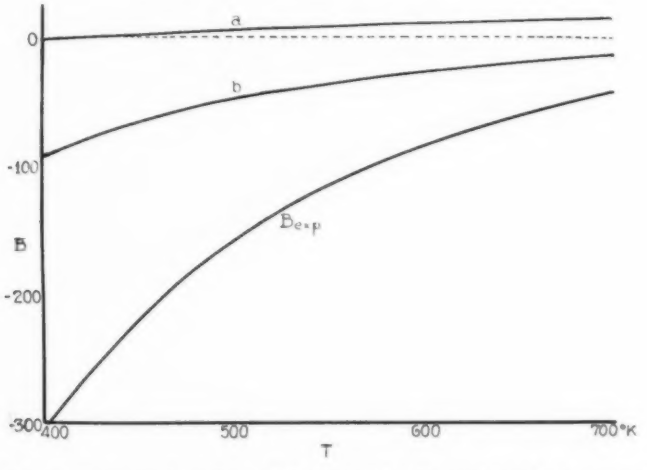

Fig. 9. H_2O. Curve *a* represents values of *B* due to the dispersion effect, curve *b* those due to dispersion plus dipole effect.

are sufficiently high.[16] The result is about 5×10^{-26} for the quadrupole moment. But there appears to be no way at present of checking this value by independent experiments.

[15] W. H. Keesom, Phys. Zeits. **22**, 129 (1921).
[16] H. Margenau, reference 11.

TEMPERATURE EQUILIBRIUM IN A STATIC GRAVITATIONAL FIELD

By Richard C. Tolman and Paul Ehrenfest

Norman Bridge Laboratory of Physics, Pasadena, California

(Received October 27, 1930)

Abstract

In the case of a gravitating mass of perfect fluid which has come to thermodynamic equilibrium, it has previously been shown that the proper temperature T_0 as measured by a local observer would depend in a definite manner on the gravitational potential at the point where the measurement is made. In the present article the conditions of thermal equilibrium are investigated in the case of a general static gravitational field which could correspond to a system containing solid as well as fluid parts. Writing the line element for the general static field in the form

$$ds^2 = g_{ij}dx_i dx_j + g_{44}dt^2 \qquad i, j = 1, 2, 3,$$

where the g_{ij} and g_{44} are independent of the time t, it is shown that the dependence of proper temperature on position at thermal equilibrium is such as to make the quantity $T_0\sqrt{g_{44}}$ a constant throughout the system.

§ I. Introduction

IN SEVERAL previous articles the principles of relativistic thermodynamics have been discussed[1] and then applied[2] to determine the conditions for thermodynamic equilibrium in the presence of gravitational fields. In the case of a gravitating mass of perfect fluid which has come to thermodynamic equilibrium, it was shown in the course of the work[3] that the proper temperature as measured by a local observer would depend in a definite manner on the gravitational potential at the point where the measurement is made. Thus if we write the line element, for a spherical mass of fluid which has come to equilibrium, in the form

$$ds^2 = -e^{\mu}(dr^2 + r^2 d\theta^2 + r^2 \sin^2\theta d\phi^2) + e^{\nu}dt^2 \tag{1}$$

where μ and ν are functions of the coordinate r, the dependence of the proper temperature T_0 on position was found to be given by the equation

$$\frac{d \log T_0}{dr} = -\frac{1}{2}\frac{d\nu}{dr}. \tag{2}$$

This result is a very interesting one since uniform temperature throughout a system which has come to thermodynamic equilibrium has hitherto been regarded as an inescapable part of thermodynamic theory. In accordance with this equation, however, the proper temperature is found to

[1] Tolman, Proc. Nat. Acad. **14**, 268 (1928); ibid. **14**, 701 (1928); Phys. Rev. **35**, 875 (1930); ibid. **35**, 896 (1930).

[2] Tolman, Proc. Nat. Acad. **14**, 348 (1928); ibid. **14**, 353 (1928); Phys. Rev. **35**, 904(1930).

[3] See reference 2, last article.

increase as we move inwards towards the center of the sphere, and this can be qualitatively interpreted by ascribing to heat the property of weight and regarding the increase in temperature as we move inwards as necessary in order to prevent the flow of heat from higher to lower gravitational levels.

Integrating equation (2) we obtain the result

$$\log T_0 + \frac{\nu}{2} = \text{const.}$$

or

$$T_0 e^{\nu/2} = T_0 \sqrt{g_{44}} = \text{const.} \tag{3}$$

and have thus obtained a quantity which has a constant value throughout the fluid even though the proper temperature itself does not. This result, however has so far only been proved for the equilibrium condition of a perfect fluid, and the question naturally arises whether the quantity $T_0\sqrt{g_{44}}$ would also have a constant value in the case of a more complicated system containing solid parts. In the present article we shall investigate temperature equilibrium in the case of a general static gravitational field by considering that the parts of the system whose temperatures are to be compared are in thermal contact with a small connecting tube containing radiation. Such a tube may be called a *radiation thermometer*, and by calculating the change in pressure as we go from one portion of the tube to another it will be easy to show that the radiation has the same value of $T_0\sqrt{g_{44}}$ throughout the thermometer.

§ 2. The Energy-Momentum Tensor for Black-Body Radiation

In order to solve our problem by the method suggested, we shall need an expression for the energy-momentum tensor for black-body radiation and shall take this as given by the equation

$$T^{\mu\nu} = (\rho_{00} + p_0)\frac{dx_\mu}{ds}\frac{dx_\nu}{ds} - g^{\mu\nu}p_0 \tag{4}$$

with

$$\rho_{00} = 3p_0 \tag{5}$$

where ρ_{00} is the proper macroscopic density of the radiation at the point of interest, p_0 its proper pressure, and the velocities dx_μ/ds correspond to the macroscopic motion of the radiation; i.e., to the motion, in the coordinate system which is being used, of an observer who finds on the average no net flow of energy in the radiation field.

Equation (4) is well known in general relativity as being an expression for the energy-momentum tensor of a perfect fluid,[4] and the primary justification for adopting it as applying to black body radiation resides in its

[4] See for example Eddington, "The Mathematical Theory of Relativity," Cambridge1923, equations (54.81) and (54.82).

general applicability in studying the relativistic mechanics of any system whose local properties can be specified by the two scalars, proper density ρ_{00} and pressure p_0. And such is evidently the case for black-body radiation, with the additional simplification $\rho_{00} = 3p_0$.

In addition to this primary justification, however, it will also be of interest to start with the usual relativistic generalization of the Maxwell-Lorentz electromagnetic equations and derive the above expression for the energy-momentum tensor by treating black-body radiation as an electromagnetic phenomenon.

In accordance with this relativistic generalization, the electromagnetic field at any point can be specified by a certain antisymmetric tensor $F_{\mu\nu}$ whose components are directly related in Galilean coordinates to the classical components of electric field strength X, Y, Z and magnetic field strength α, β, γ. And the energy-momentum tensor is given in terms of the $F_{\mu\nu}$ by the equation[5]

$$T^{\mu\nu} = -g^{\mu\gamma}F^{\nu\alpha}F_{\gamma\alpha} + \tfrac{1}{4}g^{\mu\nu}F^{\alpha\beta}F_{\alpha\beta}. \tag{6}$$

Using Galilean coordinates at the point of interest and substituting for the components of $F_{\mu\nu}$ the values which they then have, it is found that the components of $T^{\mu\nu}$ assume the values indicated by the following typical examples[6]

$$\begin{aligned} T^{11} &= -\tfrac{1}{2}(X^2 - Y^2 - Z^2) - \tfrac{1}{2}(\alpha^2 - \beta^2 - \gamma^2) \\ T^{12} &= -\alpha\beta - XY \\ T^{14} &= -\beta Z + \gamma Y \\ T^{44} &= \tfrac{1}{2}(X^2 + Y^2 + Z^2) + \tfrac{1}{2}(\alpha^2 + \beta^2 + \gamma^2) \end{aligned} \tag{7}$$

Thus in Galilean coordinates T^{11}, T^{22}, T^{33}, T^{12}, T^{13}, and T^{23} become the classical components of the stress in the field, T^{14}, T^{24}, and T^{34} become the classical components of the Poynting vector, and T^{44} becomes the classical density of energy.

If now we consider that the electromagnetic field in question corresponds to black-body radiation, and take a proper system of Galilean coordinates in which the radiation as a whole is at rest, it is evident that we shall have *on the average*

$$X^2 = Y^2 = Z^2 \quad \text{and} \quad \alpha^2 = \beta^2 = \gamma^2 \tag{8}$$

since the average field strength will be independent of direction,

$$XY = YZ = ZX = 0 \quad \text{and} \quad \alpha\beta = \beta\gamma = \gamma\alpha = 0 \tag{9}$$

since the lack of phase relations between waves will make it equally probable that the instantaneous values of these products will have positive or negative magnitude, and

[5] See Eddington, reference 4, equation (77.2).

[6] See Eddington, reference 4, equations (77.41–2–3–4).

$$-\beta Z + \gamma Y = -\gamma X + \alpha Z = -\alpha Y + \beta X = 0 \tag{10}$$

since there will be no net flow of energy in the proper system of coordinates that we are now using. Hence, introducing these results into equations 7, it is evident that in proper coordinates the averaged energy-momentum tensor for black-body radiation will have as its only surviving components

$$T^{11} = T^{22} = T^{33} = p_0 \quad \text{and} \quad T^{44} = \rho_{00} \tag{11}$$

with

$$\rho_{00} = 3p_0 \tag{12}$$

where ρ_{00} is the proper macroscopic density at the point of interest and the three surviving components of the stress are each equal to the pressure p_0.

This expression for the energy-momentum tensor of black-body radiation holds, however, only for a set of proper coordinates x, y, z, t, in which there is no net flow of energy, and to pass to a general set of coordinates x_1', x_2', x_3', x_4' we shall have to substitute the above values into the general transformation equation

$$T'^{\mu\nu} = \frac{\partial x'_\mu}{\partial x_\alpha}\frac{\partial x'_\nu}{\partial x_\beta}T^{\alpha\beta}.$$

Doing so we at once obtain

$$T'^{\mu\nu} = (\rho_{00} + p_0)\frac{\partial x_\mu'}{\partial t}\frac{\partial x_\nu'}{\partial t} + p_0\left(\frac{\partial x_\mu'}{\partial x}\frac{\partial x_\nu'}{\partial x}+\frac{\partial x_\mu'}{\partial y}\frac{\partial x_\nu}{\partial y}+\frac{\partial x_\mu'}{\partial z}\frac{\partial x_\nu'}{\partial z}-\frac{\partial x_\mu'}{\partial t}\frac{\partial x_\nu'}{\partial t}\right) \tag{13}$$

For the macroscopic velocity of the radiation in our new set of coordinates, however, we can evidently write

$$\frac{dx_\mu'}{ds} = \frac{\partial x_\mu'}{\partial x}\frac{dx}{ds} + \frac{\partial x_\mu'}{\partial y}\frac{dy}{ds} + \frac{\partial x_\mu'}{\partial z}\frac{dz}{ds} + \frac{\partial x_\mu'}{\partial t}\frac{dt}{ds} = \frac{\partial x_\mu'}{\partial t} \tag{14}$$

owing to the null value for the components dx/ds, dy/ds and dz/ds and the equality of dt and ds in proper coordinates. And from the transformation equation

$$g'^{\mu\nu} = \frac{\partial x_\mu'}{\partial x_\alpha}\frac{\partial x_\nu'}{\partial x_\beta}g^{\alpha\beta}$$

we obtain

$$g'^{\mu\nu} = -\frac{dx_\mu'}{\partial x}\frac{\partial x_\nu'}{\partial x} - \frac{\partial x_\mu'}{\partial y}\frac{\partial x_\nu'}{\partial y} - \frac{\partial x_\mu'}{\partial z}\frac{\partial x_\nu'}{\partial z} + \frac{\partial x_\mu'}{\partial t}\frac{\partial x_\nu'}{\partial t}. \tag{15}$$

Hence, substituting (14) and (15) into (13) and dropping primes we at once obtain the result which was to be proved

$$T^{\mu\nu} = (\rho_{00} + p_0)\frac{dx_\mu}{ds}\frac{dx_\nu}{ds} - g^{\mu\nu}p_0$$

with

$$\rho_{00} = 3p_0.$$

The second justification which we have thus presented for our expression for the energy-momentum tensor for black-body radiation suffers from the fact that it makes our final expression, which contains none but macroscopically measurable quantities, a consequence of the relativistic generalization of the Maxwell-Lorentz equations, which assume possibilities of microscopic measurement in conflict with the modern ideas of quantum mechanics. Nevertheless, in view of the primary justification which we presented, it is evident that our expression for the energy-momentum tensor for black-body radiation may be used with reasonable confidence at the present time, and may actually be regarded as more certain than the basis of the second justification. At some future time, the expression might have to be modified in the light of a successful unified field theory if that should ever be achieved.

§ 3. The Line Element

Having justified the expression which we shall use for the energy-momentum tensor of radiation, we are now ready to proceed to our problem of determining the distribution of radiation in a static gravitational field.

For the case of a general static system which may contain solid parts we can not assume spherical symmetry as a necessary accompaniment of equilibrium, and must take the line element in the *general static* form

$$ds^2 = g_{ij}dx_i dx_j + g_{44}dt^2 \qquad i, j = 1, 2, 3 \tag{16}$$

where $g_{ij}dx_i dx_j$ is a negative quadratic form.

We adopt the convention of using Latin indices i, j, etc. to correspond with the spatial coordinates x_1, x_2 and x_3, and shall reserve Greek indices α, β etc. to correspond with all four coordinates x_1, x_2, x_3 and t. In accordance with the usual definition of a static system we take the potentials g_{14}, g_{24} and g_{34} equal to zero, and take the other potentials g_{ij} and g_{44} as independent of the time t, although depending in any arbitrary way desired on the spatial coordinates x_1, x_2 and x_3.

For the potential g_{44}, we note from the form of the line element that we have the simple relation

$$g^{44} = \frac{1}{g_{44}}. \tag{17}$$

§ 4. Energy-Momentum Tensor for Black-Body Radiation in a Static Field

We must now consider the form taken by the energy-momentum tensor for black-body radiation in the field defined by the above line element. Returning to our general Eq. (4) for the energy-momentum tensor

$$T^{\mu\nu} = (\rho_{00} + p_0)\frac{dx_\mu}{ds}\frac{dx_\nu}{ds} - g^{\mu\nu}p_0 \tag{18}$$

we note that in a static system the macroscopic velocities dx_μ/ds will evidently be zero for $\mu = 1, 2, 3$

$$\frac{dx_i}{ds} = 0 \tag{19}$$

and taking account of Eq. (17) will reduce for the case $\mu = 4$ to

$$\frac{dx_4}{ds} = \frac{dt}{ds} = \frac{1}{\sqrt{g_{44}}} = \sqrt{g^{44}}. \tag{20}$$

Substituting in (18), the energy-momentum tensor degenerates into

$$\begin{aligned} T^{ij} &= -\, g^{ij} p_0 \\ T^{44} &= g^{44} \rho_{00} \end{aligned} \tag{21}$$

And on lowering suffixes we have

$$\begin{aligned} T^i_j &= g_{j\alpha} T^{i\alpha} = -\, g_{j\alpha} g^{i\alpha} p_0 = -\, g^i_j p_0 \\ T^4_4 &= g_{44} g^{44} \rho_{00} = \rho_{00} \end{aligned}$$

so that the only surviving components become

$$T^1_1 = T^2_2 = T^3_3 = -\, p_0 \qquad T^4_4 = \rho_{00}. \tag{22}$$

§ 5. Application of the Principles of Mechanics

We can now investigate the pressure of radiation in our thermometer by applying the principles of relativistic mechanics in the form of the well-known equation

$$\frac{\partial \mathfrak{T}^\nu_\mu}{\partial x_\nu} - \frac{1}{2} \mathfrak{T}^{\alpha\beta} \frac{\partial g_{\alpha\beta}}{\partial x_\mu} = 0. \tag{23}$$

Taking the case $\mu = 1$ and substituting Eqs. (21) and (22), we obtain

$$\frac{\partial}{\partial x_1}(-\, p_0 \sqrt{-g}) - \frac{1}{2}(-\, g^{ij} p_0 \sqrt{-g}) \frac{\partial g_{ij}}{\partial x_1} - \frac{1}{2}(g^{44} \rho_{00} \sqrt{-g}) \frac{\partial g_{44}}{\partial x_1} = 0$$

which can evidently be rewritten in the form

$$\sqrt{-g} \frac{\partial p_0}{\partial x_1} + p_0 \frac{\partial \sqrt{-g}}{\partial x_1} - \frac{1}{2} p_0 \sqrt{-g} \left(g^{ij} \frac{\partial g_{ij}}{\partial x_1} + g^{44} \frac{\partial g_{44}}{\partial x_1} \right) + \frac{1}{2} (\rho_{00} + p_0) \sqrt{-g}\, g^{44} \frac{\partial g_{44}}{\partial x_1} = 0 \tag{24}$$

This equation can easily be simplified, however, since we are permitted to write in accordance with a well-known result of tensor analysis

$$g^{ij} \frac{\partial g_{ij}}{\partial x_1} + g^{44} \frac{\partial g_{44}}{\partial x_1} = g^{\alpha\beta} \frac{\partial g_{\alpha\beta}}{\partial x_1} = \frac{1}{g} \frac{\partial g}{\partial x_1} \tag{25}$$

and if this is substituted in Eq. (24), it is found that the second and third terms will cancel. Making other obvious simplifications, we then obtain for the dependence of pressure on position the simple expression

$$\frac{\partial p_0}{\partial x_1} + \frac{\rho_{00} + p_0}{2} \frac{\partial \log g_{44}}{\partial x_1} = 0 \tag{26}$$

and similar relations will hold with respect to the other spatial coordinates x_1 and x_2.

For the case of radiation, moreover, we have the additional simplification

$$\rho_{00} = 3p_0$$

so that equation (26) further reduces to

$$\frac{\partial \log p_0}{\partial x_1} + 2\frac{\partial \log g_{44}}{\partial x_1} = 0 \tag{27}$$

and since similar relations hold for the other spatial coordinates, we can express the dependence of radiation pressure on position in our gravitational field by the remarkably simple equation

$$p_0(g_{44})^2 = \text{const.} \tag{28}$$

§ 6. Dependence of Temperature on Position

Finally, however, in the case of radiation we can connect proper pressure and proper temperature by the well-known result of Boltzmann

$$p_0 = \frac{a}{3} T_0^4 \tag{29}$$

where a is the Stefan Boltzmann constant, and substituting this into Eq. (28) we at once obtain the desired conclusion for the dependence of proper temperature on position in the case of a general static gravitational field

$$T_0\sqrt{g_{44}} = \text{const.} \tag{30}$$

§ 7. Discussion

In conclusion several remarks may be made with respect to the above result which will be of interest.

In the first place it should be noted from the method of derivation that the constancy of $T_0\sqrt{g_{44}}$ has been proven in the first instance sole'y for points inside the radiation thermometer. Nevertheless since we shall expect T_0 and g_{44} to be continuous functions of position, we shall feel justified in concluding that $T_0\sqrt{g_{44}}$ is also constant in the system itself where it comes in thermal contact with the thermometer.

In the second place it should be noted that the derivation was carried out on the assumption that the system had already been provided with a radiation thermometer connecting the parts whose temperatures were to be compared. Hence in the case of a given system of interest the question arises

whether a thermometer can be inserted to connect the desired points without thereby seriously altering the system itself. Thus if we had a gravitating system containing solid parts it would be necessary to make a hole into the solid and insert a radiation thermometer if we wished to obtain information as to the temperature of the interior by the method that we have suggested. This procedure, however, would certainly affect the gravitational potentials $g_{\mu\nu}$ which are themselves completely determined by the distribution of the matter and energy in the system. Nevertheless since the equation of connection

$$-8\pi\rho_0\frac{dx_\mu}{ds}\frac{dx_\nu}{ds} = -8\pi T^{\mu\nu} = G^{\mu\nu} - \frac{1}{2}Gg^{\mu\nu} + \Lambda g^{\mu\nu} \tag{31}$$

is a differential one giving the distribution of matter and energy in terms of the $g_{\mu\nu}$ *and* their first and second differential coefficients, it seems correct to assume that the insertion of a thermometer of small dimensions can be made without appreciably affecting the values of the $g_{\mu\nu}$ themselves. This question might bear further investigation, however, since singular cases of interest might be found.

Finally, it might be emphasized that although the proper temperature itself, T_0, varies from point to point in a gravitational system which has come to equilibrium, nevertheless the constancy of the combined quantity $T_0\sqrt{g_{44}}$ provides many of the advantages of the older principle of constant temperature throughout as necessary for equilibrium. Indeed it would be possible to label $T_0\sqrt{g_{44}}$ as *the* temperature of a system, except for the undesirability of multiplying the different things that are signified by that word. In this connection it is also interesting to recall that Einstein himself was led in his early speculations on the nature of gravitation[7] to distinguish between a quantity, called "wahre Temperatur," which would be constant throughout a system in thermal equilibrium and a second quantity, called at the suggestion of Ehrenfest "Taschentemperatur," which would vary with gravitational potential. The considerations were of only a limited applicability since this was at a time before Einstein's complete development of the general theory of relativity; the quantities in question, however, were quite analogous to our present $T_0\sqrt{g_{44}}$ and T_0.

[7] Einstein, Ann. d. Physik **38**, 443 (1912).

LETTERS TO THE EDITOR

Prompt publication of brief reports of important discoveries in physics may be secured by addressing them to this department. Closing dates for this department are, for the first issue of the month, the twenty-eighth of the preceding month; for the second issue, the thirteenth of the month. The Board of Editors does not hold itself responsible for the opinions expressed by the correspondents.

The Inner Potential of a Copper Crystal

From electron diffraction experiments Rupp (Ann. d. Physik **5**, 453, 1930) obtains values for the inner potentials of several metals. His value of the inner potential for any one metal is approximately constant and independent of the electron wave-length. In some results for a copper crystal obtained by the writer (Phys. Rev. **34**, 679, 1929) it appears that the inner potential decreases with increase of wave-length or decrease of voltage. It is to be noted that, in his calculation for copper, Rupp uses the distance between adjacent (100) planes as 3.59A. This is the value for the edge-length of an elementary cube, but since the copper crystal is a face-centered cube, the distance between adjacent (100) planes is one-half the above value. With a gas-free Cu crystal Rupp obtains maxima at 54 and 134 volts for which he chooses the values 3 and 4, respectively, for n. If the distance 1.8A between adjacent planes is used, the above values of n must be divided by two to give the same values for the inner potential. This, however, requires the use of a half-integer. If only whole integers are used then equal values for the inner potential from the observed two maxima are not obtained.

H. E. FARNSWORTH
Brown University
Providence, R. I.
November 15, 1930

Differences in the Absorption Spectrum of Benzene in the Liquid and Vapor State

The absorption spectra of benzene, liquid and vapor, in the 1.1μ and 1.6μ regions have been recorded with an effective slit width of 6A. Four meters of saturated vapor and two millimeters of liquid were used, both at room temperature and pressure. Several interesting differences between the liquid and vapor absorptions appear when this resolution is attained. The vapor spectrum is shifted towards higher frequencies. The 1.1μ band is shifted 28 cm^{-1}. Two shifts appear in the 1.6μ region, 18 cm^{-1} and 28 cm^{-1}, due to the fact that the 1.6μ absorption is a combination of overtones of two fundamentals. The absorption in the 1.6μ region is similar in intensity for the two phases while the vapor absorbs only 4–6 percent as much as the liquid in the 1.1μ region.

These preliminary results yield information as to the distribution of energy in the vibrational states of the molecule in the two phases, and show the effect of the proximity of the molecules in the liquid state. The two shifts in the 1.6μ region are about equally divided between the twenty lines observed. This enables a separation of the overtones of the two fundamentals that overlap in this region. An extensive investigation of this general problem is now under way and a comprehensive report will be published in the near future.

E. D. MCALISTER
H. J. UNGER
Division of Radiation & Organisms
Smithsonian Institution
Physics Department.
University of Oregon
November 25, 1930.

Relative Intensities in Hyperfine Structure Multiplets

The extension of the Landé interval rule to hyperfine structure energy levels was first made by Bach and Goudsmit[1] from observations of hyperfine patterns in bismuth. Since the observed intervals followed very closely the interval rule, the nuclear spin, I, was calculated to be $(9/2)(h/2\pi)$. This was later verified by them[2] in the Zeeman splitting up of each line into ten components, in a paper which is now considered a classic.

The interval rule has since been shown by the author to hold for over a hundred hyperfine patterns in praeseodymium. With the partially resolved patterns of three lines in manganese, the patterns or graphs of many lines were predicted for Mn I by making the assumption that the intensity rules as well as the interval rule were, in general, valid. These predictions fit the observed patterns so beautifully that the interval rule was used in computing all of the hyperfine levels.[3] The interval rule, as pointed out in a short note by Goudsmit and Fisher,[4] should hold in general and is therefore a powerful tool that may be used in analysing hyperfine-structure patterns.

Since each tiny hyperfine multiplet in Mn I has not been completely resolved the intensities of several lines were qualitatively given by the authors[3] in diagrams or graphs. With intensity rules[5] similar to those for ordinary multiplets, relative intensities have been calculated for quite a number of the hyperfine multiplets already published. The qualitative agreement with the observed patterns is so remarkable for all patterns studied that accurate measurements are now contemplated. A comparison of the two figures, here shown, with the graphs and microphotometer curves of the same lines[3] strongly confirms their interpretation. It is now clear why the *off-diagonal* or faint components are rarely observed.

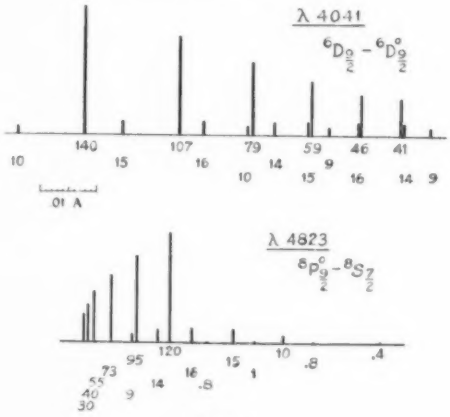

Fig. 1.

While very few accurate intensity measurements are known for hyperfine lines, qualitative measures indicate that in general the intensity rules hold as well as the interval rule. This should be true even though the ordinary multiplet to which the hyperfine pattern belongs does not follow *LS* coupling or the intensity rules.

H. E. White

University of California,
Berkeley, California
November 22, 1930.

[1] Bach and Goudsmit, Zeits. f. Physik **43**, 321 (1927).

[2] Bach and Goudsmit, Zeits. f. Physik **47**, 174 (1928).

[3] White and Ritschl, Phys. Rev. **35**, 1146 (1930).

[4] Goudsmit and Fisher, Paper presented at the Amer. Phys. Soc. November 29, 1930.

[5] For hyperfine intensity rules see Hill, Nat. Acad. Sci. **15**, 779 (1929).

The Vibrational and Rotational Analysis of the S_2 Bands.

The absorption and emission spectrum of S_2 has been photographed from λ5300 to λ2400 withgreater dispersion than that used byother investigators. The absorption spectrum was obtained by means of a quartz cell which contained pure sulphur and could be heated electrically up to about 700°C. A hydrogen continuous source was used. The absorption photographs were taken with an E_1 Hilger quartz spectrograph, and also in the first order of a 21-foot Rowland grating. For the rotational analysis we have used emission plates taken in the third order of the Rowland grating.

Our work confirms essentially the vibrational analysis as given by Rosen (Zeits. f. Physik **43**, 69, 1927). However, the assignment of quantum numbers to some of the bands has been changed and several other

band heads have been measured. Numerous perturbations have been found mainly among the levels of the upper electronic state. $v'=10$ is the first level showing diffuseness due to predissociation (c.f. V. Henri, Structures des Molecules, Paris, 1925). This is shown definitely in both our emission and absorption plates. In absorption all bands with $v'=10$ are diffuse, while in emission no bands are obtained with $v'=10$. The 9–0 band does not appear in our emission plates. This can be attributed to the small probability in the Franck-Condon parabola rather than to predissociation. From $v'=10$ to $v'=15$ the diffuseness decreases and for $v'=16$ it increases greatly. Our interpretation of the predissociation differs somewhat from that of Herzberg (Zeits. f. Physik **61,** 604, 1930).

We have used for the fine structure analysis the bands 9–1, 7–0, 8–1, 9–2, and 7–1. These were photographed in emission in the third order of a 21-foot Rowland grating with a dispersion of 0.8A per mm. The overlapping is such that even with this dispersion a considerable number of lines are not clearly separated. The lines can be arranged in two P and two R branches, one series of each kind being considerably stronger than the other. Each of the stronger branches, however, split into two series of equal intensity for high quantum numbers. This structure (three P and three R branches of approximately equal intensity) is that of a $^3\Sigma \rightarrow {}^3\Sigma$ transition, and the bands are presumably analogous to the Schumann-Runge bands of O_2 ($^3\Sigma_g^- \rightarrow {}^3\Sigma_u^-$). The rotational constants B_e' (extrapolated) and B_e'' are 0.319 and 0.414 cm^{-1}. These give $r_e'=0.573$ and $r_e''=0.503$A. The upper rotational states belonging to $v'=9$ are irregular in that their spacing corresponds to a larger value of B than that for the lower rotational states. This is thought to be due to perturbations in the rotational states, since these levels are close to the predissociation limit. Just as in the case of O_2, alternate rotational levels, hence alternate band lines, are missing in each series, showing that the sulphur atom S^{32} has zero nuclear spin. In the lower $^3\Sigma$ state, the levels with even K values are missing, in the upper state the odd K values, as in the Schumann-Runge bands of O_2.

Our analysis does not agree with that given recently by Rompe (Zeits. f. Physik **65,** 404, 1930), according to which the bands are due to a $^1\Pi \rightarrow {}^1\Sigma$ transition. Rompe's analysis was based on flourescence spectra of sulphur excited by various lines of the mercury arc and were photographed with relatively low dispersion. He did not use single line excitation, and although flourescence spectra in general facilitates the analysis of complex bands, the use of several exciting lines simultaneously, the proximity of the sulphur levels as well as the dispersion used makes it difficult to interpret the results.

The analysis is complete except for a number of weak satellite heads found mainly in absorption which are probably due to a different electronic transition.

Gilles (C.R. **188,** 1607, 1929) and Van Iddekinge (Nature **51,** 858, 1930) have reported a new system due to S_2 in the ultra-violet. These bands, however, are due to CS and not to S_2, and the vibrational analysis of this system has been given by Jevons (Proc. Roy. Soc. **A117,** 351, 1927–1928). They are very intense and a small impurity of carbon in the discharge tube is sufficient to bring them out prominently.

A detailed discussion of both the rotational and vibrational analyses will appear shortly. The authors wish to express their appreciation to Professor Mulliken for his interest and assistance.

S. Meiring Naudé
Andrew Christy

Ryerson Physical Laboratory,
University of Chicago,
December 12, 1930.

Erratum

I note in my letter concerning efficiency of emission of oxide-coated filaments published in the October 15th issue of the Physical Review that the value of A has been printed as 0.3 ampere per cm^2 degree^2. This is a typographical error and should be 0.03 ampere per cm^2 degree^2.

B. J. Thompson
Vacuum Tube Engineering Department
General Electric Company,
November 5, 1930.

AUTHOR INDEX TO VOLUME 36

References marked (A) are to abstracts of papers presented at meetings of the Physical Society, those marked with (L) refer to Letters to the Editor.

Adams, E. Q. Penetration of radiation—1020(L)

Adams, J. M. Polar properties of single crystals of ice—788(A)

Albright, C. L. Hyperfine structures of some cadmium lines and the hypothesis of nuclear spin—847

Allison F. and E. J. Murphy. Probable number of isotopes of eight metals as determined by a new method—1097(L)

Anderson, W. A remark on the paper of R. C. Tolman: "Mechanical treatment of temperature distribution in the case of radiation"—365(L)

Andrews, D. H. (see Kettering, C. F.)—531

——— Relation between the Raman spectra and the structure of organic molecules—544

Arnott, E. G. F. (see Smyth, H. D.)—1023

Atanasoff, J. V. Dielectric constant of helium—1232

Babcock, H. D. Classification of iron lines—784(A)

Bainbridge, K. T. Simple isotopic constitution of Cs—1668(L)

Baker, E. B. Application of the Fermi-Thomas statistical model to the calculation of potential distribution in positive ions—630

Band, W. A new relativity theory of the unified physical field—1405

Bardeen, J. Diffraction of a circularly symmetrical electromagnetic wave by a co-axial circular disc of infinite conductivity—1482

Barnes, R. B. Infrared absorption of some organic liquids under high resolution—296

Barnes, B. T. Spectral distribution of energy radiated from a new type of tungsten mercury arc—1468

Barnes, S. W. (see Richtmyer, F. K.)—1017(L)

Barnett, S. J. Discovery and rough measurement of a new electron inertia effect—786(A)

——— Further work on the rotation of soft iron and permalloy by magnetization and the gyromagnetic anomaly—789(A)

Bartlett, J. H., Jr. Orbital valency—1096(L)

Beams, J. W. Propagation of luminosity in discharge tubes—997

Bearden, J. A. A double crystal study of scattered x-rays—791

Beattie, J. A. A rational basis for the thermodynamic treatment of real gases and mixtures of real gases—132

——— (see Gillespie, L. J.)—743, 1008

Bedell, F. and J. Kuhn. Linear correction for cathode ray oscillograph—993

Beese, N. C. Thermionic emission of oxide coated cathodes containing a Ni-Ba alloy core—1309

Bender, P. I. Effect of gases on the optically excited cadmium I spectrum—1535

——— II. Optical excitation of cadmium hydride and zinc hydride bands—1543

Bennett, R. D. A search for the source of dielectric polarization—65, 1670 (L)

Bergstein, M., J. F. Rinke, and C. M. Gutheil. Studies in contact rectification. II. Cupric sulfide-magnesium junction—587; errata—1022

Bingham, E. C. and H. J. Fornwalt. Chemical constitution and association—381(A)

Bitter, F. On the magnetic properties of metals—978

——— Magnetic susceptibility of gases. II. Temperature dependence—1648

Blair, H. A. Spark spectra of silver and palladium (Ag II and Pd II)—an extension—173

——— Correction and extension of the series of the silver arc spectrum Ag I—1531

Bleakney, W. Ionization potentials and probabilities for the formation of multiply charged ions in helium, neon and argon—1303

Bouma, T. (see Ornstein, L. S.)—679

Bowen, I. S. Presence of neutral oxygen in the gaseous nebulae—600(L)

Boyce, J. C. (see MacInnes, J. M.)—368(L)

Boynton, W. P. Equations of state and thermodynamic functions for a substance with variable specific heat—787(A)

Bradbury, N. E. (see Luhr, O.)—1394

Braun, M. L. Current, pressure, and frequency relationships for the initiation and maintenance of the electrodeless glow discharge—1195

Breit, G. Fine structure of He as a test of the spin interactions of two electrons—383

——— **and F. W. Doermann.** Magnetic moment of the Li_7 nucleus—1262(L)

——— **and F. W. Doermann.** Hyperfine structure of S and P terms of two electron atoms with special reference to Li^+—1732

Breit, G. and E. O. Salant. Note on frequency shifts in dispersing media—871
Bridgman, P. W. Book review—155, 781
Browne, T. E., Jr. and F. C. Todd. Extinction of short a.c. arcs between brass electrodes—726
——— (see Todd, F. C.)—732
Bryan, A. B. (see Heaps, C. W.)—326
Buchta, J. W. Book reviews—1420, 1517, 1594
Busang, P. F. (see Smith, W. O.)—524
Campbell, J. S. (see Frerichs, R.)—151(L), 1460
Cassen, B. (see Lauritsen, C. C.)—988
Caswell, A. E. A note on the quantization of the solar system—787(A)
Chaffee, E. L. (see Perry, C. T.)—904
Chaffee, M. A. (see Lawrence, E. O.)—1099(L)
Chao, C. Y. Scattering of hard γ rays—1519
Chapman, S. Wind mixing and diffusion in the upper atmosphere—1014(L)
Chase, C. T. Scattering of fast electrons by metals. I. Sensitivity of the Geiger point-discharge counter—984
——— Scattering of fast electrons by metals. II. Polarization by double scattering at right angles —1060
Christy, A. (see Crane, W. O.)—421
——— (see Naudé, S. M.) 1801 (L)
Clark, J. C. (see Ross, P. A.)—378(A)
Coade, E. N. X-ray scattering coefficient as a function of wave-length and atomic number—778(L), 1109
Cohn, B. E. (see Nyswander, R. E.)—1257
Collins, J. R. Effect of high pressure on the near infrared absorption spectrum of certain liquids—305
Colvert, W. W. X-ray absorption in gases—1619
Compton, K. T. An interpretation of pressure and high velocity vapor jets at cathodes of vacuum arcs—706
——— (see Van Voorhis, C. C.)—1435
Condon, E. U. Theory of complex spectra—1121.
——— Book reviews—156, 369, 1594
Constant, F. W. Magnetic properties of dilute cobalt alloys—786(A)
——— Magnetic properties of certain Pt-Co and Pd-Co alloys—1654
Cook, R. V. Formation of striae in a Kundt's tube —1098(L)
Cook, S. R. On an electromagnetic theory of sight and color vision—790(A)
Cooksey, C. D. (see Cooksey, D.)—80
——— **and D. Cooksey.** Precision measurements of the glancing-angle of reflection from calcite for silver ($K\alpha_1$) x-rays by the "method of displacement"—85
Cooksey, D. and C. D. Cooksey. Unreliability of photographic emulsions on glass for recording distances and a method of minimizing this defect—80
Cooksey, D. (see Cooksey, C. D.)—85
Copeland, L. C. Heat of formation of molecular oxygen—1221
Cork, J. M. False lines in x-ray grating spectra—665
Cotton, J. C. (see Knauss, H. P.)—1099(L)
Crane, W. O. and A. Christy. Vibrational quantum analysis of the potassium infrared absorption bands—421
Cravath, A. M. Rate at which ions lose energy in elastic collisions—248
——— Behavior of a mercury vapor arc with a jet of liquid mercury as cathode—1480
Crump, C. C. Book review—1419
Dahl, O. (see Tuve, M. A.)—1261(L)
Dasannacharya, B. Polarization of the continuous x-rays from single electron impacts—1675
Davisson, C. J. Book review—782
Dennison, D. M. Book review—608
——— **and S. B. Ingram.** A new band in the absorption spectrum of methane gas—1451
Dershem, E. and M. Schein. Apparatus for measuring absorption coefficients of soft x-rays in gases and the absorption in air of the $K\alpha$ line of carbon —378(A)
Doermann, F. W. (see Breit, G.)—1262(L), 1732
Donal, J. S., Jr. Abnormal shot effect of ions of tungstous and tungstic oxide—1172
Dooley, D. General Electric type *S*-1 lamp as a spectroscopic source—1476
Dumond, J. W. M. Breadth of Compton modified line—146(L)
——— Evidence for the Richtmyer double jump hypothesis of x-ray satellites—1015(L)
——— Multiple scattering in the Compton effect—1685
——— **and A. Hoyt.** Energy of $K\alpha_2$ of copper as a function of applied voltage with the double crystal spectrometer—799
——— **and A. Hoyt.** Design and technique of operation of a double crystal spectrometer—1702
Dunham, J. L. Isotope effect on band spectrum intensities—1553
Easley, M. A. (see Forsythe, W. E.)—150(L)
Eckart, C. Calculation of energy values—149(L)
——— Theory and calculation of screening constants—878
——— Wave mechanics of deflected electrons—1014(L), 1514(L)
——— (see Hughes, D. S.)—694
Ehrenfest, P. (see Tolman, R. C.)—1791
Eldridge, J. A. Book review—1516
Ellis, J. W. (see Kinsey, E. L.)—603(L)
Ellwood, W. B. An experimental determination of the change in temperature accompanying change in magnetization of iron—1066

Evans, H. P. A two dimensional boundary value problem for the transmission of alternating currents through a semi-infinite heterogeneous conducting medium—1579

Ewing, M. An x-ray study of the structure of electrets—378(A)

Farnsworth, H. E. and V. H. Goerke. Distinction between contact-potential effects and true reflection coefficients for low-velocity electrons—1190

——— Inner potential of a copper crystal—1799(L)

Faust, L. Y. Fine structure of the *K*-radiation of the lighter elements—161

Ffolliott, C. F. Raman spectra of geometric isomers —367(L)

Findlay, J. H. Spark spectrum of cobalt, Co II—5

Focke, A. B. Principal magnetic susceptibilities of bismuth single crystals—319

Foote, P. D. (see Smith, W. O.)—524

Fornwalt, H. J. (see Bingham, E. C.)—381(A)

Forsythe, W. E. and M. A. Easley. Some peculiarities of the spectrum of the tungsten mercury arc —150(L)

Found, C. G. (see Langmuir, I.)—604(L)

Franklin, D. and E. R. Laird. Raman effect in trimethylethylene—147(L)

Freed, S. and C. Kasper. A simple accurate method for measuring the diamagnetic susceptibility of dissolved substances—1002

Frenkel, J. On the electrical resistance of contacts between solid conductors—1604

Frerichs, R. and J. S. Campbell. Experimental evidence for the existence of quadrupole radiation —151(L), 1460

——— Singlet system of the oxygen arc spectrum and the origin of the green auroral line—398

Froman, D. K. A photographic method of determining atomic structure factors—1330

——— A note on the extrapolation of atomic structure factor curves—1339

Geer, W. (see Utterback, C. L.)—785(A)

Gessner, G. S. Luminescence of zinc sulphide under the action of alpha, beta and gamma-rays—207

Giauque, W. F. and H. L. Johnston. On the entropy of hydrogen—1592(L)

Gillespie, L. J. Gibbs-Dalton law of partial pressures—121

——— **and J. A. Beattie.** Thermodynamic treatment of chemical equilibria in systems composed of real gases. I. An approximate equation for the mass action function applied to the existing data on the Haber equilibrium—743

——— **and J. A. Beattie.** Thermodynamic treatment of chemical equilibria in systems composed of real gases. II. A relation for the heat of reaction applied to the ammonia synthesis reaction. Energy and entropy constants for ammonia—1008

Gingrich, N. S. Double crystal analysis of scattered x-rays—364(L)

——— An analysis of scattered x-rays with the double crystal spectrometer—1050

Goerke, V. H. (see Farnsworth, H. E.)—1190

Goetz, A. and M. F. Hasler. Thermoanalysis of metal single crystals and a new thermoelectric effect of bismuth crystals grown in magnetic fields —1752

Goucher, F. S. Contact resistance and microphonic action—375(A)

Granath, L. P. Angular momentum of the Li_7 nucleus—1018(L)

Gray, F. Contact resistance and microphonic action —375(A)

Green, J. B. Incomplete Paschen-Back effect—157; 379(A)

Green, M. C. Effect of small angle scattering on the electron absorption coefficient—239

——— Scattering of electrons in small angles by gas molecules and its effect on the electron absorption coefficient—786(A)

Gronwall, T. H. A diaphantine equation connected with the hydrogen spectrum—1671(L)

Gunn, R. Origin of the variations in the sun's rotational velocity—1251

Gutheil, C. M. (see Bergstein, M.)—587; 1022

Hafstad, L. R. (see Tuve, M. A.)—1261(L)

Ham, W. R. (see LeGalley, D. P.)—379(A)

Hartig, H. E. Book review—156

Hasler, M. F. (see Goetz, A.)—1752

Harrington, M. C. (see Uyterhoeven, W.)—709

Harrison, G. R. and P. A. Leighton. Fluorescent dry plates for photographic photometry—779(L)

Harvey, A. and F. A. Jenkins. Interpretation of the spectra of CaF and SrF—1413(L)

Heaps, C. W. and A. B. Bryan. Discontinuous changes in length accompanying the Barkhausen effect in nickel—326

Henderson, G. H. and J. L. Nickerson. Range of the α-particles from thorium—1344

Henderson, J. E. and E. B. Jordan. Reflection of x-rays from thin metallic films—785(A)

Hershberger, W. D. (see Klein, E.)—1262(L)

Hicks, V. Experiments on the relative intensities of x-ray lines in the *L*-spectrum of tantalum— 785(A), 1273

Hidnert, P. and W. T. Sweeney. Thermal expansion of M-M-M alloy—787(A)

Hilberry, N. (see Smith, H.)—374(A)

Hoffmann, B. (see Veblen, O.)—810

Holzer, R. E. Absorption of slow hydrogen positive rays in hydrogen—788(A), 1204

Hopfield, J. J. Continuous spectrum in the region 500–1100A—784(A)

———— Newoxygenspectraintheultraviolet—789(A)

Hopfield, J. J. New spectra in nitrogen—789(A)
Hoxton L. G. Note on the pressure variation of specific heats of gases derived from compressibility data—1091
Houston, W. V. Book review—1674
——— (see Huff, L. D.)—842
Hoyt, A. (see Dumond, J. W. M.)—799, 1702
Hoyt, F. C. Structure of emission lines—380(A), 860
Hubbard, J. C. Problems in acoustic interferometry in gases—1668(L)
Huff, L. D. and W. V. Houston. Appearance of "forbidden lines" in spectra—842
Hughes, A. L. and G. E. M. Jauncey. An attempt to detect collisions of photons—773
——— **and C. M. Van Atta.** A second ionization potential in potassium vapor—214
Hughes, D. S. and C. Eckart. Effect of the motion of the nucleus on the spectra of Li I and Li II—694
Hulburt, E. O. Spectra of gases lighted with strong electrical discharges—13
——— Wind mixing and diffusion in the upper atmosphere—1264(L)
——— Ultraviolet light theory of aurorae and magnetic storms (continued)—1560
Hull, A. W. Book review—369
Humphreys, C. J. Interference measurements in the first spectra of krypton and xenon—380(A)
Hutchisson, E. Band spectra intensities for symmetrical diatomic molecules—410
Huxford, W. S. (see Stowell, E. Z.)—1348
Hyatt, J. M. (see Wold, P. I.)—375(A)
Hyman, H. H. Resonance (*B-A*) band system of the hydrogen molecule—187
Ingram, S. B. (see Dennison, D. M.)—1451
Jauncey, G. E. M. (see Hughes, A. L.)—773
Jenkins, F. A. (see Harvey, A.)—1413(L)
Johnson, T. H. Diffraction of hydrogen atoms—381(A)
Johnston, H. L. (see Giauque, W. F.)—1592(L)
Jordan, E. B. (see Henderson, J. E.)—785(A)
Kabakjian, D. H. Luminescence due to radioactivity—379(A)
Kaplan, J. Band intensities—778(L)
——— Some properties of the third positive carbon and associated bands—784(A)
——— Quenching of mercury resonance radiation by nitrogen and carbon monoxide—788(A)
Kasper, C. (see Freed, S.)—1002
Kemble, E. C. and F. F. Rieke. Interaction between excited and unexcited hydrogen atoms at large distances—153(L)
Kennard, E. H. Wave mechanics of deflected electrons—1667(L)
Kettering, C. F., L. W. Shutts and D. H. Andrews. A representation of the dynamic properties of molecules by mechanical models—531
Keyes, F. G. and J. G. Kirkwood. Dielectric constant of carbon dioxide as a function of temperature and density—754
——— **and J. G. Kirkwood.** Dielectric constant of ammonia as a function of temperature and density—1570
Kievit, B. and G. A. Lindsay. Fine structure in the x-ray absorption spectra of the *K* series of the elements calcium to gallium—648
Kimball, W. S. Entropy, elastic strain and the second law of thermodynamics, the principles of least work and of maximum probability—377(A)
Kinsey, E. L. and J. W. Ellis. Electrolytic dissociation of nitric acid as revealed by its infrared absorption spectrum—603(L)
Kirkwood, J. G. (see Keyes, F.)—754, 1570
Klein, E. and W. D. Hershberger. Use of the Pierce acoustic interferometer for the determination of absorption in gases for high frequency sound waves—1262(L)
Knauss, H. P. and J. C. Cotton. Intensity changes of Cameron bands in the electrodeless discharge—1099(L)
Kobel, E. Pressure and high velocity vapour jets at cathodes of a mercury vacuum arc—1636
Koller, L. R. Photoelectric emission from thin films of caesium—1639
Kozanowski, H. N. and N. H. Williams. Shot effect of the emission from oxide cathodes—1314
Kruger, P. G. New lines in the arc and spark spectrum of helium—855
Kuhn, J. (see Bedell, F.)—993
Kurth, E. H. On the recombination of electrons with caesium ions—374(A)
Laird, E. R. (see Franklin, D.)—147(L)
——— (see Sterling, V.)—148(L)
Langmuir, I. and C. G. Found. Metastable atoms and electrons produced by resonance radiation in neon—604(L)
Lauritsen, C. C. and B. Cassen. High potential x-ray tube—988
——— Spectrum of the radiation from a high potential x-ray tube—1680
Lawrence, E. O. and L. B. Linford. Effect of intense electric fields on the photoelectric properties of metals—482
——— **and M. A. Chaffee.** On the direction of emission of photoelectrons from potassium vapor by ultraviolet light—1099(L)
LeGalley, D. P., W. R. Ham, and M. W. White. Some measurements of currents through the walls of x-ray tubes—379(A)
Lewis, A. B. Coupled vibrations with applications to the specific heat and infrared spectra of crystals—568

Lewis, G. N. Principle of identity and the exclusion of quantum states—1144
Leighton, P. A. (see Harrison, G. R.)—779(L)
Lille, H. R. Margules method of measuring viscosities modified to give absolute values—347
Linder, E. G. Organic reactions in gaseous electrical discharge. I. Normal paraffin hydrocarbons—374(A), 1375
Lindsay, G. A. (see Kievit, B.)—648
Linford, L. B. (see Lawrence, E. O.)—482
——— Electrostatic surface fields near thoriated tungsten filaments by a photoelectric method—1100(L)
Livingood, J. J. (see Shenstone, A. G.)—380(A)
Loeb, L. B. Mobility of Na^+ ions in H_2—152(L) 790(A)
Lozier, W. W. A study of the velocities of H^+ ions formed in hydrogen by dissociation following electron impact—1285
——— Negative ions in hydrogen and water vapor—1417(L)
Lucy, A. A method offered as a means of computing Planck's constant without involving the charge on the electron—367(L)
Luhr, O. Recombination of ions in argon, nitrogen and hydrogen—24, 788(A)
——— Recombination of ions in air and oxygen in relation to the nature of gaseous ions—787(A)
——— **and N. E. Bradbury.** Mobility of aged ions in air—1394
Lynch, W. A. (see Smith, H.)—374(A)
MacDougall, F. H. Book review—371
MacGillavry, D. On the entropy of hydrogen—1398
MacInnes, J. M. and J. C. Boyce. Gas discharge wave-length list in extreme ultraviolet—368(L)
McAlister, E. D. High resolution in the near infrared—784(A)
——— **and H. J. Unger.** Differences in the absorption spectrum of benzene in the liquid and vapor state—1799(L)
McKeehan, L. W. Book review—608
——— Electrical resistance of nickel and permalloy wires as affected by longitudinal magnetization and tension—948
——— Magnetostriction in nickel—1014(L)
——— Molecular field and atomic order in ferromagnetic crystals and in hydrogenized iron—1512(L)
——— Magnetostriction and magnetic hysteresis—1670(L)
McMillen, J. H. Angle and energy distribution of electrons scattered by helium, argon and hydrogen—1034
Mack, J. Book review—609
Manning, K. V. (see Richtmyer, F. K.)—1017(L)
Margenau, H. Second virial coefficient for gases: a critical comparison between theoretical and experimental results—1782
Maxwell, L. R. Average life for ionized helium—379(A)
Mazumder, K. C. Absorption of x-rays by lithium—457
Merritt, E. and D. R. Morey. Polarized fluorescence of solutions of rhodamine-B and uranine—1386
Metcalf, G. F. and B. J. Thompson. A low grid current vacuum tube—1489
Michels, W. C. Optical excitation function of helium—604(L), 1362
Millikan R. A. On the question of the constancy of the cosmic radiation and the relation of these rays to meteorology—1595
Milne, W. E. Book review—1673
Mitchell, A. C. G. Behavior of positive ions in hydrogen—381(A)
——— Polarization of mercury lines in stepwise radiation—1589(L)
Montgomery, C. G. Magnetic isotropy of copper crystals—498
——— Magnetic isotropy of a paramagnetic alum—1661
Morey, D. R. (see Merritt, E.)—1386
Morse, P. M. (see Stueckelberg, E. C. G.)—16
——— (see Robertson, H. P.)—375(A)
Mrozowski, S. On the origin of the bands in the spectrum of mercury vapor—1168
——— On the incomplete polarization of the mercury resonance radiation—1591(L)
Mulliken, R. S. Interpretation of the visible halogen bands—364(L)
——— Report on notation for spectra of diatomic molecules—611
——— Electronic states in the visible halogen bands—699
——— Correlation of atomic J values and molecular quantum numbers with applications to halogen, alkaline earth hydride, and alkali molecules—1440
Murnaghan, F. D. Book review—609
Murphy, E. J. (see Allison, F.)—1097(L)
Muskat, M. Dispersion formula and Raman effect for the symmetrical top, an erratum—363
Muzzey, D. S. Jr. Some measurements of the longitudinal elastic frequencies of cylinders using a magnetostriction oscillator—935
Nadai, A. Some applications of the theory of plastic deformations of ductile metals—762
——— **and A. Christy.** Vibrational and rotational analysis of the S_2 bands—1801(L)
Naudé, S. M. Isotopes of nitrogen, mass 15, and oxygen, mass 18 and 17, and their abundances—333

Nickerson, J. L. (see Henderson, G. H.)—1344
Nottingham, W. B. Work functions and thermionic constant "A" determined for toriated tungsten —376(A)
Nutting, F. L. Position and structure of the modified line of the spectrum of scattered x-rays—1267
Nyswander, R. E. and B. E. Cohn. Tribothermoluminescence—1257
O'Brien, B. Energy distribution in the ultraviolet spectrum of skylight—381(A)
Olpin, A. R. Method of enhancing the sensitiveness of alkali metal photoelectric cells—251
——— Inhibition of photoelectric emission by near infrared light—376(A)
Ornstein, L. S. and T. Bouma. Intensity measurements in the spectrum of nickel and cobalt—679
——— (see Uhlenbeck, G. E.)—823
Osgood, T. H. Book reviews—781, 782
Page, L. Deflection of electrons by a magnetic field on the wave mechanics—444
——— Effect of the earth's electric and magnetic fields on ions in the atmosphere—601(L)
——— Wave mechanics of deflected electrons—1418(L)
——— Book reviews—369, 610
Pauling, L. Rotational motion of molecules in crystals—430
Perry, C. T. and E. L. Chaffee. A determination of e/m for an electron by direct measurement of the velocity of cathode rays—904
Peters, H. On the fluorescence of quartz under the influence of cathode rays of low voltage—1631
Pfund, A. H. Infrared filters of controllable transmission—71
Pielemeier, W. H. Ultrasonic velocity and absorption in oxygen—1005
——— Use of the Pierce acoustic interferometer—1667(L)
Plesset, M. S. (see Weigle, J. J.)—373(A)
——— Relativistic wave mechanics of electrons deflected by a magnetic field—1728
Pugh, E. M. Hall effect and the magnetic properties of some ferromagnetic materials—1503
——— **and C. A. Swartz.** Cataphoresis in rotating electric fields—787(A), 1495
Rashevsky, N. On chain reactions caused by physical structure—376(A)
Reich, H. J. A new type of glow-discharge tube—373(A)
Richtmyer, F. K., S. W. Barnes, and K. V. Manning. Hyperfine structure of x-ray lines—1017(L)
——— **and L. S. Taylor.** Intensity of x-ray satellites —1044
——— Book review—1673
Rieke, F. F. (see Kemble, E. C.)—153(L)
Rinke, J. F. (see Bergstein, M.)—587; 1022
Robertson, H. P. and P. M. Morse. Effect of collisions on potential distribution in positive ion sheaths—375(A)
Roller, D. Photoelectric behavior of solid and liquid mercury—738
Rolnick, H. Tension coefficient of resistance of metals—506
Rosen, N. and M. S. Vallarta. Spherically symmetrical field in the unified theory—110
Ross, P. A. and J. C. Clark. Modified line in scattered x-rays—378(A)
Rossi, B. On the magnetic deflection of cosmic rays —606(L)
Ruark, A. E. Book review—155
Russell, H. N. A note on Zeeman patterns—1590(L)
Salant, E. O. (see Breit, G.)—871
——— **and A. Sandow.** Raman effect of HBr and HI—1591(L)
Sandow, A. (see Salant, E. O.)—1591(L)
Sawyer, R. A. Excitation processes in the hollow cathode discharge—44
Schein, M. (see Dershem, E.)—378(A)
Shenstone, A. G. and J. J. Livingood. Spark spectrum of rhodium—380(A)
——— Note on wave-lengths in the vacuum copper arc—603(L)
——— Arc spectrum of palladium—669
——— Book review—607
Shereshefsky, J. L. Corresponding state of maximum surface tension of saturated vapors—377(A)
Shutts, L. W. (see Kettering, C. F.)—531
Silverman, S. Adsorption of methyl alcohol films on rock-salt—311
Skinner, E. W. Diffraction of x-rays in liquids: effect of temperature—1625
Slater, J. C. Atomic shielding constants—57
——— Book review—1516
Smith, H., W. A. Lynch and N. Hilberry. Electrodeless discharge in mercury vapor—374(A)
Smith, P. T. Ionization of helium, neon, and argon by electron impact—1293
Smith, S. A note on the spectra of doubly and trebly ionized lead—1
Smith, W. O., P. D. Foote and P. F. Busang. Capillary retention of liquids in assemblages of homogeneous spheres—524
Smyth, H. D. and E. C. G. Stueckelberg. Ionization of carbon dioxide by electron impact—472
——— **and E. G. F. Arnott.** Canal ray and electron excitation of the band spectrum of nitrogen—1023
——— (see Stueckelberg, E. C. G.)—478
Soderman, M. Structure of K-radiation from C, B, and Be—1414(L)
Soh, H. P Non-statical solution of Einstein's law

of gravitation in a spatially symmetrical field—1515(L)

Soller, T. Velocity distribution of secondary electrons from molybdenum—1212

Stauffer, L. H. Electro-optical modification of light waves—1352

Stauss, H. E. Use of the refraction of x-rays for the determination of the specific charge of the electron—1101

Steadman, L. T. Wave-length measurements of gamma-rays from radium and its products—460

Sterling, V. and E. R. Laird. Raman effect in solutions of sodium nitrate of varying concentration—148(L)

Stewart, G. W. Effect of electric field upon x-ray diffraction pattern of a liquid—1413(L)

——— Book review—1265

Stewart, J. Q. Fundamental correspondences between geometry and thermodynamics—377(A)

Stibitz, G. R. Vibrations of a non-planar membrane—513

Stowell, E. Z. and W. S. Huxford. Possibilities of the oscillating arc in spectrochemical analysis—1348

Strong, J. A method for growing large crystals of the alkali halides—1663

Stueckelberg, E. C. G. and P. M. Morse. Computation of the effective cross section for the recombination of electrons with hydrogen ions—16

——— **and H. D. Smyth.** Ionization of nitrous oxide and nitrogen dioxide by electron impact—478

——— (see Smyth, H. D.)—472

Swann, W. F. G. Book review—1265

Swartz, C. A. (see Pugh, E. M.)—787(A), 1495

Sweeney, W. T. (see Hidnert, P.)—787(A)

Taylor, L. S. (see Richtmyer, F. K.)—1044

Terenin, A. Photoionization of salt vapors—147(L)

Thomas, C. H. Potential drop-current relations of a Geissler discharge from a hollow cathode—374(A)

Thompson, B. J. High efficiencies of emission from oxide-coated filaments—1415(L); erratum—1802

——— (see Metcalf, G. F.)—1489

Thompson G. E. Velocity of ultrasonic waves in water vapor—77

Tiedeman, J. A. Relation between the number of electrons ejected photoelectrically from the cathode and the time lag of the spark—376(A)

Todd, F. C. (see Browne, T. E. Jr.)—726

——— **and T. E. Browne, Jr.** Restriking of short a.c. arcs—732

Tolman, R. C. A remark on the letter of W. Anderson—365(L)

——— Book review—370

——— **and P. Ehrenfest.** Temperature equilibrium in a static gravitational field—1791

Tuve, M. A., L. R. Hafstad, and O. Dahl. High-voltage tubes—1261(L)

——— Note on the production of extremely high voltages—1576

Uhlenbeck, G. E. and L. S. Ornstein. On the theory of the Brownian motion—823

——— (see Young, L. A.)—1154

——— **and L. A. Young.** The value of e/m by deflection experiments—1721

Unger, H. J. Near infrared spectrum of Hg—784(A)

——— (see McAlister, E. D.)—1799(L)

Utterback, C. L. and W. Geer. Electronic emission from a metal target bombarded with positive ions—785(A)

Uyterhoeven, W. and M. C. Harrington. Secondary emission from metals by impact of metastable atoms and positive ions—709

Valasek, J. Fine structure of certain x-ray emission lines—1523

Vallarta, M. S. (see Rosen, N.)—110

Van Atta, C. M. (see Hughes, A. L.)—214

Van Voorhis, C. C. and K. T. Compton. Heats of condensation of electrons on several metals in several ionized gases—1435

Vavilov, S. On the attempt to detect collisions of photons—1590(L)

Veblen, O. and B. Hoffmann. Projective relativity—810

Wall, C. N. Potential and potential energy of space lattices—1243

Watson, W. W. Evidence for Be isotope of mass 8 in the BeH band spectrum—1019(L)

——— Zeeman effect in the ZnH and CdH bands—1134

Weigle, J. J. and M. S. Plesset. Preliminary measurements of the mean free path of potassium atoms in nitrogen—373(A)

Werth, M. Relative efficiency of the Hg-arc lines in exciting the Raman spectrum of benzol—1096(L)

White, H. E. Relative intensities in hyperfine structure multiplets—1800(L)

White, M. W. (see LeGalley, D. P.)—397(A)

Williams, N. H. (see Kozanowski, H. N.)—1314

Winans, J. G. New bands in the absorption spectrum of mercury—1020(L)

Winch, R. P. Photoelectric outgassing—601(L)

Wold, P. I. and J. M. Hyatt. Hall effect in tellurium amalgams—375(A)

Wood, R. W. Improved technique for the Raman effect—1421

——— Raman spectra of benzene and diphenyl—1431

Workman, E. J. A new method of measuring the variation of the specific heats (c_p) of gases with pressure—1083

Wyckoff, R. W. G. Atomic scattering powers of nickel, copper and iron for various wave-lengths —1116

Yates, R. C. Elastic character of the homopolar chemical bond—555

——— Study of the small vibrations of six particles in a system analogous to the benzene ring—563

Young, L. A. and G. E. Uhlenbeck. On the Wentzel-Brillouin-Kramers approximate solution of the wave equation—1154

——— (see Uhlenbeck, G. E.)— 1721

Zahl, H. A. Reflection of cadmium and zinc atoms from sodium chloride crystals—893

Zeleny, J. Mobilities of ions in dry and moist air—35

——— Book review—156

Zemansky, M. W. Absorption and collision broadening of the mercury resonance line—219, 380(A)

——— New experimental determination of effective cross-sections for the quenching of mercury resonance radiation—919

——— Absorption and collision broadening of resonance radiation—1591(L)

Zener, C. Analytic atomic wave functions—51

Zwicky, F. Energy changes related to the secondary structure of crystals—378(A)

ANALYTIC SUBJECT INDEX TO VOLUME 36

References marked (A) are to abstracts of papers presented at meetings of the American Physical Society, those marked with (L) refer to letters to the Editor.

Absorption of light (see also **X-Rays, absorption**)
Hg 2537 in Hg vapor, broadening, M. W. Zemansky—219, 380(A), 1591(L)
Liquids, infrared, effect of pressure, J. R. Collins—305
Organic liquids in infrared, high resolution, R. B. Barnes—296

Acoustics
Absorption of high frequency sound, E. Klein, W. D. Hershberger—1262(L)
Kundt's tube, striae, R. V. Cook—1098(L)
Ultrasonic velocity and absorption in oxygen, W. H. Pielemeier—1005, 1667(L); J. C. Hubbard—1668(L)
Ultrasonic waves, velocity in water vapor, G. E. Thompson—77

Adsorption
Methyl alcohol on rock salt, S. Silverman—311

Alloys
Electrical resistance, magnetization and tension of Ni and permalloy, L. W. McKeehan—948
Gyromagnetic anomaly and rotation by magnetization of permalloy, S. J. Barnett—789(A)
Magnetic properties of Pt-Co and Pd-Co, F. W. Constant—786(A), 1654
Thermal expansion of M-M-M, P. Hidnert, W. T. Sweeney—787(A)
Thermionic emission from oxide-coated Ni-Ba alloy, N. C. Beese—1309

Alpha particles
Range from Th, G. H. Henderson, J. L. Nickerson—1344

Arcs (see also **Discharge of electricity in gases, Sparks**)
Extinction of short a.c. arcs between brass electrodes, T. E. Browne, Jr., F. C. Todd—726
General Electric type S-1 lamp, spectrum, D. Dooley—1476
Hg arc, moving jet cathode, A. M. Cravath—1480
Oscillating arc in spectrochemical analysis, E. Z. Stowell, W. S. Huxford—1348
Pressure and vapor jets at cathode, K. T. Compton—706; E. Kobel—1636
Restriking of short a.c. arcs, F. C. Todd, T. E. Browne, Jr.—732
Tungsten mercury arc, spectral energy, B. T. Barnes—1468
Tungsten mercury, peculiarities in spectrum, W. E. Forsythe, M. A. Easley—150(L)

Astrophysics
Quantization of solar system, A. E. Caswell—787(A)
Variations in the sun's rotational velocity, R. Gunn—1251

Atmospheric electricity
Aurorae and magnetic storms, theory of, E. O. Hulburt—1560
Ionization of cosmic rays, R. A. Millikan—1595
Ions in upper atmosphere, motion of, L. Page—601(L)

Atomic beams
Cs^+ in H_2, pressure changes, A. C. G. Mitchell—381(A)
Diffraction of H atoms, T. H. Johnson—381(A)
Hydrogen ions in H_2, absorption of, R. E. Holzer—788(A), 1204
Potassium atoms in nitrogen, mean free path, J. J. Weigle, M. S. Plesset—373(A)
Reflection of Cd and Zn atoms from NaCl crystals, H. A. Zahl—893

Atomic radii (see also **Collision diameter**)
Absorption of H ions in H_2, R. E. Holzer—788(A), 1204

Atomic and molecular radii (see **Collision diameter**)

Atomic structure factors
Electron distribution in atoms of KCl and MgO, D. K. Froman—1330, extrapolation of factors, D. K. Froman—1339

Atoms
Wave functions, approximate, for any atom, J. C. Slater—57
Wave functions for Be, B, C, N, O, F, Ne, C. Zener—51

Aurora
Green line, Zeeman effect, R. Frerichs, J. S. Campbell—151(L)
Origin of auroral green line, R. Frerichs—398
Transverse Zeeman effect of green auroral line, quadrupole radiation, R. Frerichs, J. S. Campbell—1460

Barkhausen effect
Discontinuous changes in length of Ni, C. W. Heaps, A. B. Bryan—326

Book reviews
Baker, Robert H., Astronomy, An Introduction —1419
Brillouin, Leon, Les Statistiques Quantiques—1674
deBroglie, L., Einführung in die Wellenmechanik —369
Campbell, J. W., An Introduction to Mechanics —1517
Castelfranchi, Gaetano. Physique Moderne—155
Emeléus, K. G. The conduction of Electricity through Gases—156
Grube, Georg., Grundzuge der Theoretischen und Angewandten Elektrochemie—371
Haas, A., Einfuhrung in die Theoretische Physik —610
Halpern, O. and H. Thirring. Die Grundgedanken der neueren Quantentheorie—156
Heisenberg, W., The Physical Principle of the Quantum Theory—1516
Hoag, J. Barton., Electron Physics—1420
Jackson, D., The Theory of Approximation —1673
Jäger, Gustav. Theoretische Physik—610
Jahrbuch des Forschungs, Instituts der Allgemeinen Elektricitäts-Gesselschaft, Erster Band, 1928-1929—782
Handbuch der Experimentalphysik, Volume 24, 1 Teil, Kirchner, F. Allgemeine Physik der Röntgenstrahlen—1673; 2 Teil, Lindh, Axel, Röntgenspek troskopie—609
Kiebitz, F. Radio Technic. VI. Die electrischen Wellen—156
Lichtenstein, L., Grundlagen der Hydromechanik —609
Longinescu, I.-N. Essai sur les Principes de la Thermodynamique—155
Millikan, Gale and Edwards. A Manual of Experiments, to accompany A First Course in Physics for Colleges—1594
Moulton, F. R., Differential Equations—1265
Newman, F. H. and V. H. L. Searle. The General Properties of Matter—1517
Pauling and Goudsmit. Structure of Line Spectra—607
Peek, F. W. Jr., Dielectric Phenomena in High Voltage Engineering—369
Planck, Max, Einführung in die Theorie der Wärme, Volume V—781
Pohl, R. W., Einführung in die Mechanik and Akustik—1265
Schaefer, Cl. and F. Matossi, Das Ultrarote Spektrum—608
Silberstein, Ludwig, The Size of the Universe—370
Sommerfeld, Arnold, Wave Mechanics—1594
Thibaud, J., Les Rayons X—781
Worsnop, B. L., X-Rays—782
Wulf, Theodor, Modern Physics—1516
Wyckoff, Ralph W. G., The Analytical Expression of the Results of the Theory of Space Groups—608
Zeleny, Anthony, Elements of Electricity—369
Brownian motion
Theory of, G. E. Uhlenbeck, L. S. Ornstein—823.
Canal rays
Spectra in N_2 excited by, H. D. Smyth, E. G. F. Arnott—1023
Capillary action (see **Surface tension**)
Cataphoresis
In rotating electric fields, E. M. Pugh, C. A. Swartz—787(A), 1495
Cathode rays (see **Electrons, Electrons in gases**)
Chemical bonds
Elastic character of the homopolar, R. C. Yates —555
Vibration of system analogous to benzene ring, R. C. Yates—563
Chemical constitution
And association of homologous compounds, E. C. Bingham, H. J. Fornwalt—381(A)
Chemical reaction
Chain reactions caused by physical structure, N. Rashevsky—376(A)
Organic reactions in gaseous electrical discharge, E. G. Linder—374(A), 1375
Thermodynamic treatment of chemical equilibria in systems composed of real gases, ammonia synthesis, I. Mass action function, L. J. Gillespie, J. A. Beattie—743; Heat of reaction, entropy, L. J. Gillespie, J. A. Beattie—1008
Collision diameter (see also **Electrons in gases, Electron scattering**)
Calculated values, Fermi-Thomas statistics, E. B. Baker—630
From scattering of electrons, M. C. Green—239, 786(A)
Colloids
Cataphoresis in rotating electric fields, E. M. Pugh, C. A. Swartz—787(A), 1495
Compton effect (see **X-Rays, diffraction, scattering**)
Constants, physical
Planck's constant, h, method of computing, A. Lucy—367(L)
Contact potential
Effect on reflection coefficients, H. E. Farnsworth, V. H. Goerke—1190
Contact resistance
Microphonic action, F. Gray—375(A); F. S. Goucher—375(A)
Wave mechanical theory, J. Frenkel—1604
Cosmic rays

Constancy and relation to meteorology, R. A. Millikan—1595
Magnetic deflection, B. Rossi—606(L)
Crystals and crystal structure
Calcite, glancing angle for Ag $K\alpha_1$ rays, C. D. Cooksey, D. Cooksey—85
Cu, magnetic susceptibility, C. G. Montgomery—498
Growing large crystals of the alkali halides, J. Strong—1663
Ice, polar properties of single crystals, J. M. Adams—788(A)
Inner potential of a copper crystal, H. E. Farnsworth—1799(L)
Potential and potential energy of space lattices, C. N. Wall—1243
Properties of metal crystals grown in magnetic fields, A. Goetz, M. F. Hasler—1752
Rotational motion of molecules in crystals, L. Pauling—430
Secondary structure, energy changes, F. Zwicky—378(A)
Cybotactic state
Organic liquids, temperature effect, E. W. Skinner—1625
Dielectric constant
CO_2, temperature and density variations, F. G. Keyes, J. G. Kirkwood—754
H_2, calculated, J. V. Atanasoff—1232
NH_3, temperature and density variations, F. G. Keyes, J. G. Kirkwood—1570
Dielectric properties
Polarization, search for source, R. D. Bennett—65, 1670(L)
Diffraction of atoms (see **Atomic beams**)
Diffraction of electrons (see **Electrons, diffraction**)
Diffraction of corpuscles
H atoms, T. H. Johnson—381(A)
Diffraction of radiation (see **X-Rays, diffraction**)
Discharge of electricity in gases (see also **Arc, spark**)
A.c. arcs, extinction of, T. E. Browne, Jr., F. C. Todd—726
A.c. arcs, restriking of, F. C. Todd, T. E. Browne, Jr.—732
Electrodeless discharge, current, pressure, and frequency relations—M. L. Braun—1195
Electrodeless, Hg vapor, characteristics, H. Smith, W. A. Lynch, N. Hilberry—374(A)
Geissler, hollow cathode, characteristics, C. H. Thomas—374(A)
Heats of condensation of electrons on Mo, Pt and W-K, C. C. Van Voorhis, K. T. Compton—1435
Hollow cathode, excitation processes, spectra, R. A. Sawyer—44
Luminosity, propagation of, J. W. Beams—997
Ne arc, metastable atom and resonance radiation, I. Langmuir, C. G. Found—604(L)
New type of glow-discharge tube, H. J. Reich—373(A)
Organic reactions in gaseous electrical discharge, E. G. Linder—374(A), 1375
Positive ion sheaths, effect of collisions on potential distribution, H. P. Robertson, P. M. Morse—375(A)
Secondary electrons produced by metastable atom and positive ions, W. Uyterhoeven, M. C. Harrington—709
Spectra, variation with discharge, characteristics, E. O. Hulburt—13
Vapor jets in Hg arc, E. Kobel—1636
Dissociation
Nitric acid from absorption spectra, E. L. Kinsey, J. W. Ellis—603(L)
H_2 velocities of H^+ ions formed, W. W. Lozier—1285 H_2O and formation of negative ions in H_2 and H_2O, W. W. Lozier—1417(L)
Dissociation, heat of (see also **Molecular structure and constants**)
O_2, heat of formation, L. C. Copeland—1221
Elasticity
Longitudinal vibration of rods, D. S. Muzzey, Jr.—935
Plastic deformations of ductile metals, A. Nadai—762
Electrets
X-ray study of structure, M. Ewing—378(A)
Electrical conductivity and resistance
Contact between carbon spheres, microphonic action, F. Gray—375(A); F. S. Goucher,—375(A)
Contact resistance, wave-mechanical theory, J. Frenkel—1604
Electrical discharge in gases (see **Discharge of electricity in gases**)
Electromagnetic theory
Diffraction of a circularly symmetrical electromagnetic wave by a co-axial circular disc, J. Bardeen—1482
Transmission of alternating currents through a semi-infinite heterogeneous conducting medium, H. P. Evans—1579
Unified theory, spherically symmetrical field, N. Rosen, M. S. Vallarta—110
Electrons
Deflection in magnetic field on wave mechanics and value of e/m, L. Page—444; criticism, C. Eckart—1014(L), 1514(L); reply, L. Page—1418(L); G. E. Uhlenbeck, L. A. Young—1721; M. S. Plesset—1728; E. H. Kennard—1667(L)
e, by x-ray refraction, H. E. Stauss—1101

e/m from velocity measurements, C. T. Perry, E. L. Chaffee—904
e/m measurements from inertia effects, S. J. Barnett—786(A)
Heat of condensation of electrons on Mo, Pt and W-K, C. C. Van Voorhis, K. T. Compton—1435
Polarization by double scattering, C. T. Chase—1060
Recombination with Cs^+, E. H. Kurth—374(A)
Recombination with protons, theory, E. C. G. Stueckelberg, P. M. Morse—16
Reflection coefficients and contact potentials, H. E. Farnsworth, V. H. Goerke—1190
Scattering by gas molecules, M. C. Green—239, 786(A)
Scattering and operation of Geiger counter, C. T. Chase—984
Electrons, diffraction
Inner potential of a copper crystal, H. E. Farnsworth—1799(L)
Electrons in gases
Formation of, W. Bleakney—1303
Ionization of helium, neon, and argon by electron impact, efficiency, P. T. Smith—1293
Scattering in He, A and H_2, angular and energy distribution, J. H. McMillen—1034
Electrons, photoelectric (see **Photoelectric effect**)
Electrons, scattering (see also **Electrons in gases**)
Effect of small angle scattering on absorption coefficient, M. C. Green—239, 786(A)
Electrons, secondary
From metals bombarded by positive ions, C. L. Utterback, W. Geer—785(A)
Metastable atoms and positive ions, produced by, W. Uyterhoeven, M. C. Harrington—709
Velocity distribution of secondary electrons from molybdenum, T. Soller—1212
Electron tubes
Cathode ray oscillograph, F. Bedell, J. Kuhn—993
High potential x-ray tube, C. C. Lauritsen, B. Cassen—988
Energy states of atoms
Average life of ionized helium, L. R. Maxwell—379(A)
Method of calculation, C. Eckart—149(L)
Energy states of molecules
As effected by interaction, E. C. Kemble, F. F. Rieke—153(L)
Excitation function
He, spectra, W. C. Michels—604(L), 1362
Filters, light
Infrared, controllable transmission, A. H. Pfund—71
Fine structure (see also **Hyperfine structure**)
He 2^3P level, test of spin interaction, G. Breit—383
K radiation of lighter elements, L. Y. Faust—161; M. Soderman—1414(L)
K series, Ca to Ga, B. Kievit, G. A. Lindsay—648
$K\alpha$ of Fe, Co, Ni, Cu, Mo and Ag, $K\beta$ of Mo, J. Valasek—1523
Mo$K\alpha$ lines, double crystal spectrometer, N. S. Gingrich—1050
Unmodified scattered x-rays, J. A. Bearden—791
Fluorescence
Polarized, of rhodamine-B and uranine, E. Merritt, D. R. Morey—1386
Quartz, under low voltage cathode rays, H. Peters—1631
ZnS, under α, β, γ rays, decay characteristics, G. S. Gessner—207
Gamma rays
Wave-length in spectrum of Ra, RaB, RaC, and RaD, including intensity measurements of line and continuous spectra, L. T. Steadman—460
Geiger-counters
Sensitivity, C. T. Chase—984
Geophysics
Wind mixing and diffusion in the upper atmosphere, S. Chapman—1014(L); reply, E. O. Hulburt—1264(L)
Hall effect
Te amalgams, P. I. Wold, J. M. Hyatt—375(A)
Heat of dissociation (see **Dissociation**)
High voltages
Production, M. A. Tuve—1576; M. A. Tuve, L. R. Hafstad and O. Dahl—1261(L)
Hyperfine structure
Cd lines and nuclear spin, C. L. Albright—847
Hyperfine structure and interval rule, H. E. White—1800(L)
S and P terms of Li^+, G. Breit, F. W. Doermann—1732
W$K\alpha$, F. K. Richtmyer, S. W. Barnes, K. V. Manning—1017(L)
Infrared spectra :see also **Spectra, molecular;**
Hg, arc, H. J. Unger—784(A)
High resolution in near infrared, E. D. McAlister—784(A)
Instruments (see **Methods and instruments**)
Intensities in spectra
Bands of diatomic molecules, theory, E. Hutchisson—410
Cameron bands, intensity changes, H. P. Knauss, J. C. Cotton—1099(L)
Ni I, Ni II, Co I multiplets, L. S. Ornstein, T. Bouma—679
X-ray lines in the tantalum L-spectrum, V. Hicks—785(A), 1273

X-ray satellites, intensity ratios, F. K. Richtmyer, L. S. Taylor—1044

Ionization by impact

CO_2 by electrons, H. D. Smyth, E. C. G. Stueckelberg—472

He, Ne, and A, efficiency by electrons 0–4500 volts, P. T. Smith—1293

K and Hg vapors, extra ionization potentials, A. L. Hughes, C. M. Van Atta—214

Multiply charged ions, He, Ne and A, W. Bleakney—1303

NO_2 and N_2O, by electrons, E. C. G. Stueckelberg, H. D. Smyth—478

Velocities of H^+ ions formed, W. W. Lozier—1285

Ions

Cs^+ in H_2, pressure changes, A. C. G. Mitchell—381(A)

Negative ions in hydrogen and water vapor, W. W. Lozier—1417(L)

Recombination of H^+ with electron, theory, E. C. G. Stueckelberg, P. M. Morse—16

Ions in gases

Energy losses at elastic collisions, A. M. Cravath—248

Recombination in A, N_2 and H_2, O. Luhr—24, 788(A); in air and O_2—787(A)

Ions, mobility

Aged ions in air, O. Luhr, N. E. Bradbury—1394

In dry and moist air, J. Zeleny—35

Na^+ in H_2, L. B. Loeb—152(L), 790(A)

Isotopes

Be^8, band spectrum of BeH, W. W. Watson—1019(L)

Cs, K. T. Bainbridge—1668(L)

Effect on band spectrum intensities, J. L. Dunham—1553

N_{15}, O_{18}, O_{17}, abundances, from band spectra, S. M. Naudé—333

Number of isotopes of eight metals, F. Allison, E. J. Murphy—1097(L)

Kinetic theory of gases

Second virial coefficient, experimental and theoretical, H. Margenau—1782

Light waves

Electro-optical modification of, electric oscillations on Kerr cell, L. H. Stauffer—1352

Frequency shifts in dispersing media, G. Breit, E. O. Salant—871

Luminescence

Due to α, β, γ rays, mechanism, D. H. Kabakjian—379(A)

ZnS under α, β, γ rays, decay characteristics, G. S. Gessner—207

Magnetic properties

Barkhausen effect in Ni, discontinuous changes in length, C. W. Heaps, A. B. Bryan—326, criticism, L. W. McKeehan—1014(L)

Cu and Ag, susceptibilities of and structure sensitivity, F. Bitter—978

Electrical resistance, tension and magnetization of Ni and permalloy, bibliography included, L. W. McKeehan—948

Gyromagnetic anomaly and rotation by magnetization, S. J. Barnett—789(A)

Hall effect in ferromagnetic materials, E. M. Pugh—1503

Hall effect of Te amalgams, P. I. Wold, J. M. Hyatt—375(A)

Isotropy of a paramagnetic alum, C. G. Montgomery—1661

Li_7 nucleus, momentum of, L. P. Granath—1018(L); see also G. Breit, F. W. Doermann—1262(L)

Molecular field and atomic order in ferromagnetic crystals, L. W. McKeehan—1512(L), 1670(L)

Pt-Co and Pd-Co alloys, F. W. Constant—786(A), 1654

Susceptibility measurements, S. Freed, C. Kasper—1002

Susceptibilities of Bi single crystal, A. B. Focke—319

Susceptibility of Cu crystals, C. G. Montgomery—498

Susceptibility of gases, temperature dependence, F. Bitter—1648

Temperature change on magnetization, W. B. Ellwood—1066

Magnetostriction oscillator

For elastic studies, D. S. Muzzey, Jr.—935

Mechanics

Coupled systems of linear oscillators, A. B. Lewis—568

Solar system, quantization and inverse square law, A. E. Caswell—787(A)

Vibrations of mechanical systems representing organic molecules, R. C. Yates—555

Vibrations of non-planar membrane, G. R. Stibitz—513

Vibration of system representing benzene ring, R. C. Yates—563

Mechanics, quantum

Complex spectra, theory, E. U. Condon—1121

Calculation of energy values, C. Eckart—149(L)

Deflection of electrons in magnetic field and value of e/m, L. Page—444; criticism, C. Eckart—1014(L); 1514(L); reply, L. Page—1418(L); G. E. Uhlenbeck, L. A. Young—1721; M. S. Plesset—1728; E. H. Kennard—1667(L)

Dielectric constant H_2, J. V. Atanasoff—1232

Electrical resistance of contacts, J. Frenkel—1604
Energy states of molecules as affected by interaction, E. C. Kemble, F. F. Rieke—153(L)
Extrapolation of atomic structure factor curves, D. K. Froman—1339
Frequency shifts in dispersing media, G. Breit, E. O. Salant—871
Intensities in band spectra, E. Hutchisson—410
Isotope effect on intensities, J. L. Dunham—1553
Magnetic moment of Li_7 nucleus, G. Breit, F. W. Doermann—1262(L)
Motion of nucleus, effect on spectra, D. S. Hughes, C. Eckart—694
Orbital valency, J. H. Bartlett, Jr.—1096(L)
Paschen-Back effect, incomplete, J. B. Green—157, 379(A)
Principle of identity and the exclusion of quantum states, G. N. Lewis—1144
Recombination of electron and H^+, E. C. G. Stueckelberg, P. M. Morse—16
Relativity, unified field, W. Band—1405
Rotational motion of molecules in crystals, L. Pauling—430
Screening constants, calculation of, C. Eckart—878
Spin interactions as tested by fine structure of He, G. Breit—383
Structure of emission line, theory, F. C. Hoyt—380(A), 860
Symmetrical top, dispersion formula, Raman effect—an erratum, M. Muskat—363
Wave equation, solution, L. A. Young, G. E. Uhlenbeck—1154
Wave functions, approximate, for any atom, J. C. Slater—57
Wave functions for Be, B, C, N, O, F, Ne, C. Zener—51

Mechanics, statistical
Brownian motion, theory of, G. E. Uhlenbeck, L. S. Ornstein—823
Entropy of H_2, D. MacGillavry—1398, W. F. Giauque, H. L. Johnston—1592(L)
Fermi-Thomas method applied to positive ions, E. B. Baker—630

Metastable atoms
Ne, in arc by resonance radiation, I. Langmuir, C. G. Found—604(L)

Meteorology (see also **Atmospheric electricity**)
Cosmic rays and meteorology, R. A. Millikan—1595

Methods and instruments
Calorimeter to measure small heat changes, W. B. Ellwood—1066
Cathode ray oscillograph, correction, F. Bedell, J. Kuhn—993
Diamagnetic susceptibility measurements, S. Freed, C. Kasper—1002
False x-ray lines, J. M. Cork—665
Filters, infrared, controllable transmission, A. H. Pfund—71
Fluorescent dry plates for photographic photometry, G. R. Harrison, P. A. Leighton—779(L)
Geiger counter, voltage effects, C. T. Chase—984
Glow discharge tube—new type, H. J. Reich—373(A)
High potential x-ray tubes, C. C. Lauritsen, B. Cassen—988
High voltage tubes, M. A. Tuve, L. R. Hafstad and O. Dahl—1261(L)
Infrared, high resolution in, E. D. McAlister—784(A)
Low grid-current vacuum tube for current measurements, G. F. Metcalf, B. J. Thompson—1489
Mass spectrograph, H. D. Smyth, E. C. G. Stueckelberg—472
Mechanical models to represent dynamic properties of molecules, C. F. Kettering, L. W. Shutts, D. H. Andrews—531
Minimizing errors in reading distance on photographic plates, D. Cooksey, C. D. Cooksey—80
Optically excited radiation, P. Bender—1535
Photoelectric cells, methods of enhancing sensitiveness, O. R. Olpin—251
Photographic method of determining atomic structure factors, D. K. Froman—1330
Pierce acoustic interferometer, high frequencies, E. Klein, W. D. Hershberger—1262(L)
Rectifier, cupric sulfide-magnesium junction, M. Bergstein, J. F. Rinke, C. M. Gutheil—587; 1022
Refraction of x-rays, H. E. Stauss—1101
Shot-circuit impedence measurements, H. N. Kozanowski, N. H. Williams—1314
Specific heat variation with pressure, E. J. Workman—1083
Velocity Measurement of electrons, C. T. Perry, E. L. Chaffee—904
Viscosimeter, Margules method for absolute values, H. R. Lille—347
X-ray spectrometer, double crystal, J. W. M. Dumond, A. Hoyt—1702

Microphone
Microphonic action of contact resistance, F. Gray—375(A); F. S. Goucher—375(A)

Mobility of ions (see **Ions, mobility**)

Molecular structure and constants (see also **Spectra, molecular**)
Atomic J values and molecular quantum numbers, R. S. Mulliken—1440
Benzene ring model and Raman spectra, R. C. Yates—563

Homopolar chemical bond and Raman spectra, R. C. Yates—555
K_2, heat of dissociation, vibrational constants, W. O. Crane, A. Christy—421
Mechanical models to represent dynamic properties, C. F. Kettering, L. W. Shutts, D. H. Andrews—531
Methane gas, new absorption band, D. M. Dennison, S. B. Ingram—1451
O_2, heat of formation, L. C. Copeland—1221
Orbital valency, J. H. Bartlett, Jr.—1096(L)

Multiplets
Intensity ratios Ni I, Ni II, Co I, L. S. Ornstein, T. Bouma—679

Packing effect
Cs, K. T. Bainbridge—1668(L)

Paschen-Back effect
For intermediate fields, theory, J. B. Green—157, 379(A)

Photoelectric cells
Methods of enhancing sensitiveness, O. R. Olpin—251

Photoelectric effect
Cs thin films on O, L. R. Koller—1639
Direction of emission of photoelectrons, E. O. Lawrence, M. A. Chaffee—1099(L)
Effect of intense electric fields, E. O. Lawrence, L. B. Linford—482; see also L. B. Linford—1100(L)
Inhibition by infrared light, A. R. Olpin—376(A)
Outgassing, action of photoelectrons, R. P. Winch—601(L)
Photoionization of salt vapors, A. Terenin—147(L)
Threshold and current variation with temperature (Hg), D. Roller—738

Photography
Fluorescent dry plates for photographic photometry, G. R. Harrison, P. A. Leighton—779(L)
Unreliability of photographic emulsions for recording distances, improvements, D. Cooksey, C. D. Cooksey—80

Photons
Collisions of, A. L. Hughes, G. E. M. Jauncey—773; S. Vavilov—1590(L)

Planck's constant, h
Method of computing not involving e, A. Lucy—367(L)

Polarization, electrical (see **Dielectric properties**)

Potentials, critical (see also **Spectra**)
Ag I, ionization, spectra, H. A. Blair—1531
CO_2, ionization by electrons, H. D. Smyth, E. C. G. Stueckelberg—472
CO II, ionization, spectra, J. H. Findlay—5
Ionization potentials, successive, calculated, E. B. Baker—630
Ionization of He, Ne and A, W. Bleakney—1303
K and Hg vapor, extra ionization potentials, A. L. Hughes, C. M. Van Atta—214
NO_2 and N_2O, ionization by electrons, E. C. G. Stueckelberg, H. D. Smyth—478

Proceedings of the American Physical Society
Ithaca Meeting, June 19 to 21, 1930—372
Eugene Meeting, June 19 to 21, 1930—783

Quadrupole radiation
Experimental evidence, R. Frerichs, J. S. Campbell—151(L); 1460

Quantum mechanics (see **Mechanics, quantum**)

Radiation
Penetration, therapeutic use, E. Q. Adams—1020(L)
Quenching of resonance radiation (Hg), M. W. Zemansky—919

Radio
Diffraction of a circularly symmetrical electromagnetic wave by a co-axial circular disc, J. Bardeen—1482

Radioactivity
Range of α particles from Th, G. H. Henderson, J. L. Nickerson—1344
γ-ray scattering, ThC, C. Y. Chao—1519
Wave-length measurements of gamma rays for Ra, RaB, RaC, and RaD, L. T. Steadman—460

Raman effect
Benzene and diphenyl, anti-Stokes lines, R. W. Wood—1431
Excitation efficiency, relative, of Hg lines, M. Werth—1096(L)
Geometric isomers, C. F. Ffolliott—367(L)
HBr and NI, E. O. Salant, A. Sandow—1591(L)
Hg and He arc excitation, filters and improved technique, R. W. Wood—1421
Solutions of $NaNO_3$, V. Sterling, E. R. Laird—148(L)
Structure of organic molecules, D. H. Andrews—544
Trimethylethylene, D. Franklin, E. R. Laird—147(L)

Recombination
Electron and H^+, theory, E. C. G. Stueckelberg, P. M. Morse—16
Of ions in A, N_2 and H_2, O. Luhr—24, 788(A)
Electrons with Cs^+, E. H. Kurth—374(A)

Rectifiers
Cupric sulfide-magnesium junction, M. Bergstein, J. F. Rinke, C. M. Gutheil—587; errata—1022

Relativity
Mechanical treatment of temperature distribution in case of radiation W. Anderson—365(L); reply, R. C. Tolman—365(L)
Non-statical solution of Einstein's law of gravitation, H. P. Soh—1515(L)

Projective relativity, O. Veblen, B. Hoffmann—810
Relativistic wave mechanics, of deflected electrons, M. S. Plesset—1728
Temperature equilibrium in a static gravitational field, R. C. Tolman, P. Ehrenfest—1791
Unified physical field, W. Band—1405
Unified theory, spherically symmetrical field, N. Rosen, M. S. Vallarta—110
Resistance of metals (see **Electrical conductivity and resistance**)
Tension coefficient of, H. Rolnick—506
Resonance radiation
Width of line as function of geometry of tube and vapor density, M. W. Zemansky—219, 380(A), 1591(L)
Screening constants
Theory and calculation of, C. Eckart—878
Shielding constants
For any atom, approximate, J. C. Slater—57
Shot effect
Abnormal effect of ions, J. S. Donal, Jr.—1172
Oxide coated filaments, H. N. Kozanowski, N. H. Williams—1314
Skylight
Energy distribution in ultraviolet, B. O'Brien—381(A)
Spark
Time lag, relation to photoelectrons from cathode, J. A. Tiedeman—376(A)
Specific heats
Gases, variation with pressure, calculated values, L. G. Hoxton—1091
Gases, variation with pressure, experimental values, E. J. Workman—1083
Organic crystals, calculated from mechanical models, A. B. Lewis—568
Spectra, absorption
Benzene in the liquid and vapor state, E. D. McAlister, H. J. Unger—1799(L)
Nitric acid dissociation, by absorption spectra, E. L. Kinsey, J. W. Ellis—603(L)
Spectra, atomic
Ag II and Pd II, extension, H. A. Blair—173
Ag I, classification and new lines, H. A. Blair—1531
Atomic *J* values and molecular quantum numbers, R. S. Mulliken—1440
Auroral green line, Zeeman effect, quadrupole radiation, R. Frerichs, J. S. Campbell—151(L), 1460
Co II, classification, J. H. Findlay—5
Cu arc, correction to published list, A. G. Shenstone—603(L)
Diaphantine equation, hydrogen spectrum, T. H. Gronwall—1671(L)
Energy states, calculation, C. Eckart—149(L)
Excitation function of helium, W. C. Michels—604 (L); 1362
Excited in hollow cathode discharge, R. A. Sawyer—44
Fe lines, classification, H. D. Babcock—784(A)
Forbidden lines and quadrupole terms, L. D. Huff, W. V. Houston—842
He, new lines in arc and spark, P. G. Kruger—855
Hg lines, fluorescence, polarization of, A. C. G. Mitchell—1589(L)
Hg 2537, ratio of emission to absorption line width, M. W. Zemansky—219, 380(A), 1591(L)
Hyperfine structure Cd lines, C. L. Albright—847
Hyperfine structure of *S* and *P* terms of two electron atoms, G. Breit, F. W. Doermann—1732
Kr and Xe, wave-lengths, C. J. Humphreys—380(A)
Li I and Li II, calculated effect of motion of nucleus, D. S. Hughes, C. Eckart—694
Nitrogen atomic, resonance series, J. J. Hopfield—789(A)
Ni I, Ni II, Co I, intensity measurements, multiplet intensity ratios, L. S. Ornstein, T. Bouma—679
O, singlet system, origin of auroral line, R. Frerichs—398
Oxygen, atomic, resonance series, J. J. Hopfield—789(A)
Pb III and Pb IV, classification, S. Smith—1
Pd I analysis, A. G. Shenstone—669
Polarization of Hg resonance line, S. Mrozowski—1591(L)
Quenching of Cd lines by gases, P. Bender—1535
Rh, term values, A. G. Shenstone, J. J. Livingood—380(A)
Structure of emission line, theory, F. C. Hoyt—380(A), 860
Theory of complex spectra, E. U. Condon—1121
Wave equation, application to hydrogenic atoms, L. A. Young, G. E. Uhlenbeck—1154
Wave-length list for extreme ultraviolet, J. M. MacInnes, J. C. Boyce—368(L)
Spectra, continuous
From gases lighted by strong discharge, E. O. Hulburt—13
Spectra, general
Excitation function of helium, W. C. Michels—604(4); 1362
Fluorescence of quartz, H. Peters—1631
Fluorescence, polarization of, E. Merritt, D. R. Morey—1386
From gases lighted by strong discharge, E. O. Hulburt—13
General Electric type S-1, spectrum, D. Dooley—1476

He, continuous spectrum in condensed discharge 500–1100A, J. J. Hopfield—784(A)
Hg vapor absorption bands, origin of, S. Mrozowski—1168
Optical excitation, P. Bender—1543
Oscillating arc in spectrochemical analysis, E. Z. Stowell, W. S. Huxford—1348
Oxygen, auroral and nebular lines, I. S. Bowen—600(L)
Quenching of mercury resonance radiation by nitrogen and carbon monoxide, J. Kaplan—788(A)
Radiation from a high potential x-ray tube, C. C. Lauritsen—1680
Tungsten mercury arc, peculiarities, W. E. Forsythe, M. A. Easley—150(L)
Tungsten mercury arc, spectral energy, B. T. Barnes—1468

Spectra, molecular
Absorption bands of K_2, W. O. Crane, A. Christy—421
Atomic J values and molecular quantum numbers, R. S. Mulliken—1440
Band in Be^9H spectra, W. W. Watson—1019(L)
Bands in the absorption spectrum of mercury, J. G. Winans—1020(L)
CaF and SrF, interpretation of, A. Harvey, F. A. Jenkins—1413(L)
Cameron bands in CO intensities, H. P. Knauss, J. C. Cotton—1099(L)
CO third positive group, J. Kaplan—784(A)
Electronic states in halogen bands, R. S. Mulliken—699
Energy states, effect of interaction, E. C. Kemble, F. F. Rieke—153(L)
Halogen bands, interpretation, R. S. Mulliken—364(L)
H_2, B-A resonance bands, quantum assignments, H. H. Hyman—187
Intensities in bands, J. Kaplan—778(L)
Isotope effect on intensities, J. L. Dunham—1553
Liquids, absorption in infrared, effect of pressure, J. R. Collins—305
Methane gas, new absorption band, theory of overtones, D. M. Dennison, S. B. Ingram—1451
N_2, absorption bands, J. J. Hopfield—789(A)
N_2 and O_2, abundances of N_{15}, O_{18} and O_{17}, S. M. Naudé—333
N_2 band spectra, by canal ray excitation, H. D. Smyth, E. G. F. Arnott—1023
Notation, report on, R. S. Mulliken—611
O_2 bands, new, J. J. Hopfield—789(A)
Optical excitation of CdH and ZnH bands, P. Bender—1543
Organic liquids, absorption in infrared, high resolution, R. B. Barnes—296
S_2, vibrational and rotational analysis—S. M Naudé, A. Christy—1801(L)
Symmetrical diatomic molecules, intensities, theory, E. Hutchisson—410
ZnH and CdH bands, Zeeman effect, W. W. Watson—1134

Spectrograph, spectrometer
X-ray, double crystal, J. W. M. Dumond, A. Hoyt—1702

Spectroscopic technique
Unreliability of photographic emulsions for recording distances, improvements, D. Cooksey, C. D. Cooksey—80

Sun (see **Astrophysics**)

Surface tension
Of saturated vapors, maximum, J. L. Shereshefsky—377(A)
Retention of liquids between homogeneous spheres, W. O. Smith, P. D. Foote, P. F. Busang—524

Susceptibility, magnetic (see **Magnetic properties**)

Thermal expansion
M-M-M alloy, P. Hidnert, W. T. Sweeney—787(A)

Thermionic emission of electrons
Efficiency of emission from oxide coated filaments, B. J. Thompson—1415(L); erratum—1802(L)
Oxide coated filaments, shot effect, H. N. Kozanowski, N. H. Williams—1314
Oxide coated Ni-Ba alloy, N. C. Beese—1309
Shot effect, abnormal, of ions, J. S. Donal Jr.—1172
Work function and constant A for thoriated tungsten, W. B. Nottingham—376(A)

Thermodynamics
c_p variation, calculated from p-v-t data, L. G. Hoxton—1091
Entropy, elastic strain, W. S. Kimball—377(A)
Entropy of crystalline hydrogen, L. Pauling—430
Entropy of H_2, D. MacGillavry—1398; W. F. Giauque, H. L. Johnston—1592(L)
Equations of state and thermodynamic functions for a substance with variable specific heat, W. P. Boynton—787(A)
Equilibrium, ammonia synthesis reaction. I. Mass action function, L. J. Gillespie, J. A. Beattie—743. II. Heat of reaction entropy, L. J. Gillespie, J. A. Beattie—1008
Fundamental correspondence to geometry, J. Q. Stewart—377(A)
Gibbs-Dalton law of partial pressures, L. J. Gillespie—121
Mechanical treatment of temperature distribution of radiation, W. Anderson—365(L); reply, R. C. Tolman—365(L)
Real gases and mixtures, J. A. Beattie—132

Surface tension of saturated vapors, J. L. Shereshefsky—377(A)
Temperature equilibrium in a static gravitational field, R. C. Tolman, P. Ehrenfest—1791
Thermoelectric effect
In crystals grown in magnetic fields, A. Goetz, M. F. Hasler—1752
Tribothermoluminescence
In crystals, glass and frits, R. E. Nyswander, B. E. Cohn—1257
Ultrasonic waves
Velocity and absorption in O_2, W. H. Pielemeier—1005, 1667(L); J. C. Hubbard—1668(L)
Velocity in water vapor, G. E. Thompson—77
Vacuum tubes
High voltage, M. A. Tuve, L. R. Hafstad, O. Dahl—1261(L)
Low grid-current tube, type F. P.-54, G. F. Metcalf, B. J. Thompson—1489
Viscosity
Margules method, absolute values, H. R. Lille—347
Vision theory of
Electromagnetic theory of sight and color vision, S. R. Cook—790(A)
Wave functions
For any atoms, approximate, J. C. Slater—57
For Be, B, C, N, O, F, Ne, C. Zener—51
Work function (see **Thermionic emission**)
X-rays, absorption
By Li, K. C. Mazumder—457
Elements Ca to Ga, fine structure, B. Kievit, G. A. Lindsay—648
In gases, W. W. Colvert—161
Penetration, therapeutic use, E. Q. Adams—1020(L)
Soft rays in gases, C $K\alpha$ in air, E. Dershem, M. Schein—378(A)
X-rays, diffraction, reflection and scattering
Compton effect, position and structure of modified line, F. L. Nutting—1267
Compton shift, accurate measure, N. S. Gingrich—364(L)
Electric fields and diffraction pattern of a liquid, G. W. Stewart—1413(L)
Fine structure lines, with double crystal spectrometer, N. S. Gingrich—1050
Fine structure of unmodified line, J. A. Bearden—791
Liquids, effect of temperature, E. W. Skinner—1625
Multiple scattering in the Compton effect, J. W. M. Dumond—1685
Scattering coefficient as a function of wave-length and atomic number, E. N. Coade—778(L), 1109
Scattering power of Ni, Cu, Fe, for various wavelengths, R. W. G. Wyckoff—1116
Thin metallic films, reflection from, J. E. Henderson, E. B. Jordan—785(A)
Width and structure of modified $K\alpha_1$, $K\alpha_2$, P. A. Ross, J. C. Clark—378(A)
X-rays, emission
Fine structure, $K\alpha$ of Fe, Co, Ni, Cu, Mo and Ag, $K\beta$ of Mo, J. Valasek—1523
Hyperfine structure W $K\alpha$, F. K. Richtmyer, S. W. Barnes, K. V. Manning—1017(L)
$K\alpha_2$ of Cu, origin of, and Richtmyer double group hypothesis, J. W. M. Dumond, A. Hoyt—799; J. W. Dumond—1015(L)
Ta, L-spectrum relative intensities of lines, V. Hicks—785(A), 1273
X-rays, polarization
Continuous x-rays from single electron impacts, B. Dasannacharya—1675
X-rays, reflection and refraction
Glancing angle of calcite for Ag $K\alpha_1$ C. D. Cooksey, D. Cooksey—85
X-rays, scattering
Breadth of modified line, J. W. M. Dumond—146(L)
X-rays, spectra
Fine structure in K-radiation of lighter elements, L. Y. Faust—161; M. Soderman—1414(L)
X-rays, spectra and spectroscopy
False lines in x-ray grating spectra, J. M. Cork—665
Intensity ratios of satellites, F. K. Richtmyer, L. S. Taylor—1044
Radiation from a high potential x-ray tube, C. C. Lauritsen—1680
X-rays, tubes
Currents through walls, D. P. LeGalley, W. R. Ham, M. W. White—379(A)
Zeeman effect
Auroral green line. R. Frerichs, J. S. Campbell—1460
Incomplete Paschen-Back effect, calculation, J. B. Green—157, 379(A)
In Co II spectrum, J. H. Findlay—5
In quadrupole radiation, R. Frerichs, J. S. Campbell—151(L)
Misplacements and g values, H. N. Russell—1590(L)
ZnH and CdH bands, W. W. Watson—1134

Back Numbers Wanted

of the

PHYSICAL REVIEW

We will pay $2.00 each for copies of the January, February, April and May issues of Volume 7, 1916; also $1.00 for copies of the January, 1927, issue.

Send to the Physical Review, University of Minnesota, Minneapolis, Minnesota,

A New Math. Tool

EDGAR DEHN

ALGEBRAIC CHARTS

for solving quadratic, cubic and biquadratic equations. Price in special folder $1.00, library edition $1.50 bound.

Patents Pending

NOMOGRAPHIC PRESS
509 Fifth Ave., New York

Handy Reference Cards

of the most probable values of the GENERAL PHYSICAL CONSTANTS as estimated by Raymond T. Birge in the July issue of

THE PHYSICAL REVIEW SUPPLEMENT

Tables of the values of the general physical constants taken from Birge's article are printed on two stiff cards, 8½ x 11", bound together with linen tape.

Price 50 cents

The Physical Review Supplement

University of Minnesota
Minneapolis, Minnesota

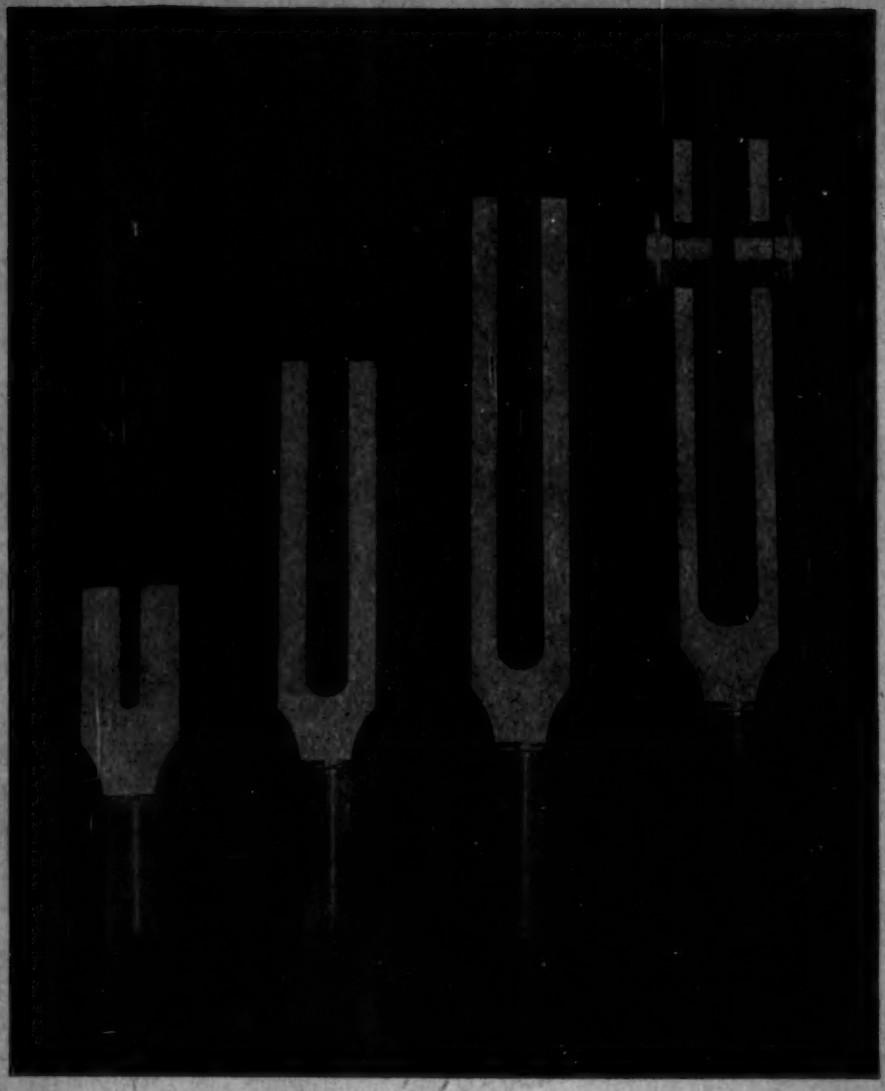

DURATONE TUNING FORKS

A new line of fine physics forks made of a special long vibrating alloy, calibrated to extreme pitch precision, with improved retention of pitch accuracy and having an extremely small temperature coefficient. Prices from $7.50 to $36.00. Ask for circular 75P.

CENTRAL SCIENTIFIC COMPANY
LABORATORY SUPPLIES
Apparatus CSC Chemicals
NEW YORK - BOSTON - CHICAGO - TORONTO - LOS ANGELES

GEORGE BANTA PUBLISHING COMPANY, MENASHA, WISCONSIN